Museu de Zoologia
Universidade de São Paulo

Paulo Presti

Phylogenetic relationships and evolution of the musculoskeletal system of Polynemidae (Teleostei: Percomorphacea: Perciformes).

Relações filogenéticas e evolução do sistema musculoesquelético de Polynemidae (Teleostei: Percomorphacea: Perciformes)

São Paulo
2019

Paulo Presti

Phylogenetic relationships and evolution of the musculoskeletal system of Polynemidae (Teleostei: Percomorphacea: Perciformes)

Relações filogenéticas e evolução do sistema musculoesquelético de Polynemidae (Teleostei: Percomorphacea: Perciformes)

Original Version

Dissertation submitted to the Graduate Program of the Museu de Zoologia da Universidade de São Paulo in partial fulfillment of the requirements for the degree of Master of Science (Systematics, Animal Taxonomy and Biodiversity).

Advisor: Prof. Dr. Aléssio Datovo

São Paulo
2019

Serviço de Biblioteca e Documentação

Museu de Zoologia da Universidade de São Paulo

Cataloging in Publication

Presti, Paulo
Phylogenetic relationships and evolution of the musculoskeletal Polynemidae (Teleostei: Percomorphacea: Perciformes).= Relações filogenéticas e evolução do sistema musculoesquelético de Polynemidae (Teleostei: Percomorphacea: Perciformes/ Paulo Presti; orientador Aléssio Datovo. São Paulo, 2019.
265p.
Dissertação (Mestrado) – Programa de Pós-Graduação em Sistemática, Taxonomia e Biodiversidade, Museu de Zoologia, Universidade de São Paulo, 2019.
Versão original

1. Filogenia – Polynemidae (Teleostei: Percomorphacea: Perciformes). 2. Teleostei . I. Datovo, Aléssio, orient. II.Título.

CDU 597.556

CRB 8-3805

PRESTI, Paulo

Phylogenetic relationships and evolution of the musculoskeletal system of Polynemidae (Teleostei: Percomorphacea: Perciformes).

Relações filogenéticas e evolução do sistema musculoesquelético de Polynemidae (Teleostei: Percomorphacea: Perciformes)

Dissertation submitted to the Graduate Program of the Museu de Zoologia da Universidade de São Paulo in partial fulfillment of the requirements for the degree of Master of Science (Systematics, Animal Taxonomy and Biodiversity).

Date approved: _____/_____/_____

COMMITTEE MEMBERS

Prof. Dr._____ Institution: _____

Decision: _____ Signature: _____

Prof. Dr._____ Institution: _____

Decision: _____ Signature: _____

Prof. Dr._____ Institution: _____

Decision: _____ Signature: _____

para Mariana,

ACKNOWLEDGMENTS

Gostaria de deixar aqui todos os meus mais sinceros agradecimentos a todos que me ajudaram, direta ou indiretamente, ao longo desses últimos anos.

Em primeiro lugar agradeço ao meu orientador e amigo, Prof. Dr. Aléssio Datovo, que desde o começo da minha jornada ictiológica me apoiou e me deu confiança para seguir na área. Antes do mestrado eu nunca havia trabalhado com peixes e não possuía muito conhecimento nessa nova área. Agradeço a ele também por sua imensa paciência ao longo do processo de orientação, sempre me transmitindo o seu conhecimento e experiência. Logo de início acredito que houve uma afinidade mútua, tanto pela área de sistemática filogenética e anatomia comparada quanto pela ilustração científica. Foram diversos momentos compartilhados que não se restringiram apenas ao laboratório. Pudemos compartilhar almoços, confraternizações e até uma viagem para Praga.

Também não posso deixar de agradecer à Profa. Dra. Mônica Toledo-Piza, quem, não só me indicou o Aléssio, mas quem me apresentou ao mundo da ictiologia, com a sua disciplina "Ictiologia básica". Ao longo da graduação tive bastante contato com a Mônica durante as monitorias na disciplina de "Vertebrados", do Instituto de Biociências da USP e posso dizer que, de uma forma ou de outra, teve bastante influência na minha graduação. É engraçado me lembrar de uma passagem logo no meu primeiro ano de graduação, em 2009 (a Mônica provavelmente nem deva se lembrar) Havia uma bolsa aberta para curadoria do museu seco do IB e eu logo de cara me interessei. Mandei um email para ela e marcamos uma reunião. Eu, calouro, não sabia de nada e não li nada sobre a tal vaga. Chegando à reunião, a Mônica me deu uma bronca, pois não havia feito nada do que era exigido no edital (acho que precisava fazer um cadastro na reitoria ou algo do gênero). Sai de lá sem nada, apenas com a bronca dada. Claro que não guardo mágoas! Foi interessante e um bom "puxão de orelha" que me fez ficar mais esperto ao longo da graduação. Espero que agora na defesa do Mestrado venham poucos "puxões de orelha" deste tipo.

Deixo aqui também os meus agradecimentos a toda equipe do Museu de Zoologia da USP, começando com os professores Mario C. C. de Pinna, Naércio A. Menezes, Heraldo A. Britski e José L. de Figueiredo pela receptividade dentro do laboratório. Agradeço também a

todos os amigos feitos dentro do laboratório e pelos folhados de ameixa compartilhados em diversas tardes. Muito obrigado Murilo Pastana, Gustavo Ballen, Guilherme Dutra, Henrique Varella, Arthur de Lima, João Genova, Luiz Peixoto, Manoela Marinho, Marina Loeb, Michel Gianeti, Vitor Abrahão, Fábio Pupo, Priscila Camelier, Verônica Slobodian, Vinícius Espíndola, Vinícius Reis, George Vita, Luz Eneida, Ilana Fichberg, Péricles Gentile, Karol Reis, Victor Tagliacollo, Roberto Mansani. Agradeço em especial aos técnicos da seção Michel Gianeti e Osvaldo Oyakawa pelo apoio com todo o material analisado e recebido em doações. Agradeço também ao pessoal técnico do laboratório de Micro Tomografia, Alberto e Vanessa por terem escaneado todos os meus bichos e contribuindo significativamente com o presente trabalho. Agradeço em especial ao Murilo Pastana, que além de sempre me ajudar nas questões biológicas que trazia a ele, foi (e é) um grande amigo dentro da seção de peixes. Muito obrigado por tudo e pelos seus ensinamentos. Também deixo minha gratidão em especial ao Guilherme Dutra que leu e comentou diversos pontos do presente trabalho. Suas considerações foram de grande valia para mim, muito obrigado. Agradeço também em especial ao Luiz Peixoto e à Manoela Marinho, pelos diversos conselhos e ajudas ao longo do mestrado. O meu obrigado também se estende a todos os funcionários do MZUSP e aos coordenadores do programa de pós-graduação em Sistemática, Taxonomia Animal, e Biodiversidade do museu. Deixo também meu obrigado a outros colegas de profissão: Karla Soares, Kleber Mathubara, João Paulo Capretz e Victor Giovannetti.

Gostaria de agradecer também a toda a equipe do *National Museum of Natural History*, *Smithsonian Institution*, em Washington, DC, local no qual passei três meses realizando parte do meu mestrado. Agradeço em especial ao Dr. Dave Johnson que me recebeu de braços abertos e foi de uma hospitalidade imensa. Além trocar informações com uma das maiores referências dentro da ictiologia, pude compartilhar diversos momentos agradáveis juntos ao longo desses meses, desde reuniões, almoços e confraternizações na sua casa. Nesses eventos sempre esteve presente sua esposa, Ai Nonaka, que, também de uma forma incrivelmente hospitaleira, me acolheu durante minha estadia em DC e me ajudou muito com a obtenção de fotografias das larvas que estava trabalhando. Muito obrigado por tudo. Agradeço também à fiel turma do almoço, os quais pude ter um vislumbre de suas grandezas: Bruce Colette, Victor Springer, Carole Baldwin, Lynne Parenti,

Roy McDiarmid, Rayna Bell, Kevin De Queiroz, Daniel Mulcahy. Expresso ainda meus sinceros agradecimentos ao trabalho de curadoria de Jeff Clayton, Sandra Raredom, Kris Murphy e Jeff Williams. Não posso deixar de agradecer também aos meus companheiros de estadia em DC, Vinícius Espíndola, João Pedro Trevisan, Bill Ludt, David Santana e Thaisi Andia. Sem vocês DC certamente seria muito menos engraçado e proveitoso. Muito obrigado.

Expresso também meus profundos agradecimentos aos curadores das instituições que carecidamente me emprestaram ou doaram os materiais necessários para este trabalho: *National Museum of Natural History* (NMNH), *Smithsonian Institution*; *Natural History Museum of Los Angeles County*; *Southeast Area Monitoring and Assessment Program* (SEAMAP) *Archiving Center*; *Fish and Wildlife Research Institute* (FWRI), St. Petersburg, Florida (Laura Habbeger); *Academy of Natural Sciences of Drexel University* (ANSP); *California Academy of Sciences* (CAS); *Museum and Art Gallery of the Northern Territory*, Australia; *Tunghai University*, Taiwan (Wen Collin).

Por fim, gostaria de agradecer a toda a minha família pelo suporte ao longo da minha vida. Sou muito grato a vocês por tudo. Especialmente aos meus pais, Elder e Sylvana, aos meus irmãos, Gabi e Léo e aos meus avós, Vinício e Lourdes. Agradeço também a todos os meus amigos que contribuírem para que eu chegasse até aqui. Deixo também os meus profundos agradecimentos à Mariana, minha companheira de vida e aproveito para expressar o meu mais sincero amor por você. Sem você este trabalho certamente ficaria com menos brilho. Muito obrigado.

Agradeço a Pró-Reitoria de Pós-Graduação da Universidade de São Paulo pelo apoio concedido no início do meu mestrado. Do mesmo modo, sou grato a toda equipe da seção acadêmica do museu, por toda ajuda com os auxílios burocráticos ao longo do mestrado.

Este projeto foi financiado pela Fundação de Amparo à Pesquisa do Estado de São Paulo (FAPESP #2017/16192-7 e #2018/19399-4) e sou muito grato a esta agência de fomento. O presente trabalho foi realizado com o apoio da Coordenação de Aperfeiçoamento de Pessoal de Nível Superior – Brasil (CAPES) – Código de Financiamento 001, a qual agradeço por todo o suporte.

ABSTRACT

Polynemidae is a family of primarily marine fishes with eight genera and 42 extant species. The phylogenetic allocation of polynemids within Percomorphacea as well as its internal relationships are uncertain as highly conflicting hypotheses has been proposed in the literature. Many aspects of the polynemid morphology are largely unknown, with little reports in the literature about their osteology, barely any information on their myology, and no studies on the ontogeny of their skeleton. This project aimed to study different aspects of the musculoskeletal system of Polynemidae and understand its internal relationships. The most remarkable feature of polynemids is their pectoral fin divided into an upper, unmodified fin and a lower portion with rays highly modified into specialized filaments. The present analysis reveals that the main *adductor* and *abductor* muscles masses of the pectoral fin involved in such intricate structure are completely divided into two muscle segments that serve separately the pectoral-fin rays, dorsally, and pectoral filaments, ventrally. Interestingly, it is herein demonstrated that the pectoral filaments receive massive nerves specialized in gustatory reception, indicating that the polynemid pectoral filament have not only tactile but also tasting functions. Several unique specializations in the mandibular, hyopalatine and branchial musculature of polynemids are herein reported for the first time. A comprehensive cladistic analysis based on 162 morphological characters and all valid polynemid genera was performed and resulted in fully resolved new hypothesis of relationships. All genera were recovered as monophyletic except *Polydactylus*, which is polyphyletic. Lastly, a survey of the skeletogenesis of polynemids reveals remarkable changes during their ontogeny, such as the shifting in pectoral radial 3 and the expansion of pectoral radial 4, both transformations associated with the differentiation of the pectoral filaments. The saddle-like ossification pattern of vertebral centra 1-4 of polynemids is only shared with sciaenids and additionally supports the hypothesis of a closer relationship between these families.

Keywords: Musculature. Ontogeny. Polynemids. Systematic. Threadfins.

RESUMO

Polynemidae é uma família de peixes primariamente marinhos, com oito gêneros e 42 espécies existentes. Sua posição filogenética dentro de Percomorphacea, bem como suas relações internas, são incertas visto que hipóteses altamente conflitantes foram propostas na literatura. Muitos aspectos da morfologia dos polinemídeos são amplamente desconhecidos, com poucos relatos na literatura sobre sua osteologia, quase nenhuma informação sobre sua miologia e nenhum estudo sobre a ontogenia de seu esqueleto. Este projeto teve como objetivo estudar diferentes aspectos do sistema musculoesquelético de Polynemidae e entender suas relações internas. A característica mais notável destes animais é a presença de uma nadadeira peitoral dividida em uma porção superior não modificada e uma porção inferior composta por raios altamente modificados em filamentos especializados. O presente estudo revelou que as principais massas musculares adutoras e abdutoras envolvidas nesta complexa arquitetura peitoral são completamente divididas em dois segmentos musculares, que servem separadamente os raios da nadadeira peitoral, dorsalmente, e os filamentos peitorais, ventralmente. Curiosamente, é aqui demonstrado que os filamentos peitorais recebem nervos maciços especializados em recepção gustativa, indicando que tais filamentos possuem não somente funções táteis, mas também gustativas. Diversas especializações únicas na musculatura mandibular, hiopalatina e branquial dos polinemídeos são relatadas pela primeira vez. Uma análise cladística abrangente, baseada em 162 caracteres morfológicos e em todos os gêneros de polinemídeos válidos, foi realizada e resultou em uma nova hipótese de relacionamento totalmente resolvida. Todos os gêneros foram recuperados como monofiléticos, exceto *Polydactylus*, que foi recuperado como polifilético. Por fim, um levantamento da esqueletogênese dos polinemídeos revela mudanças notáveis durante sua ontogenia, como o deslocamento do terceiro radial e a expansão do quarto radial, ambas transformações associadas à diferenciação dos filamentos peitorais. O padrão de ossificação *"saddle-like"* dos centros vertebrais 1-4 de polinemídeos é compartilhado apenas com os scianídeos, suportando a hipótese de um relacionamento mais próximo entre essas famílias.

Palavras-chave: Musculatura. Nariz-de-vidro. Ontogenia. Polinemídeos. Sistemática.

CONTENT

GENERAL INTRODUCTION

The division Percomorphacea (Wiley and Johnson, 2010; Betancur-R *et al.*, 2013) is one of the most diverse lineages of Teleostei, comprising about 17,000 species (Near *et al.*, 2013) and representing over half of bony fishes species and almost a quarter of all living vertebrates (Nelson, 2006). This richness of species is distributed among 30 different orders, 23 of which have contentious phylogenetic allocation, turning Percomorphacea in one of the most daunting challenges of fish systematics (Johnson, 1993; Nelson, 2006; Wiley and Johnson, 2010; Near *et al.*, 2013; Datovo *et al.*, 2014).

The monophyletic status of Percomorphacea has been corroborated by recent literature and, in the past decades, some hypotheses of internal relationships had been proposed for its orders on grounds of molecular (Chen *et al.*, 2003; Miya *et al.*, 2003; Li *et al.*, 2009; Near *et al.*, 2012; Betancur-R *et al.*, 2013; Near *et al.*, 2013; Sanciangco *et al.*, 2015; Hughes *et al.*, 2018) and morphological evidence (Johnson and Patterson, 1993; Springer and Johnson, 2004; Springer and Orrell, 2004; Wiley and Johnson, 2010; Datovo *et al.*, 2014). Nevertheless, morphological- and molecular-based hypotheses are often highly conflicting. Most recent papers regarding percomorphacean systematic are solely based on molecular data and disassociate widely known monophyletic clusters grouped together by anatomical characters (Chen *et al.*, 2003; Miya *et al.*, 2003; Li *et al.*, 2009; Betancur-R *et al.*, 2013). There are only a few morphological studies attempting to address the uncertainties amongst the major lineages of Percomorphacea and, most of them, employ only osteological data. Such analyses hardly dedicate any effort in investigating soft anatomy, despite the demonstrable phylogenetic importance of these systems (Winterbottom, 1974a; b; 1993; Springer and Johnson, 2004; Datovo and Bockmann, 2010; Datovo *et al.*, 2014).

Historically, the most diverse and challenging group within Percomorphacea is the Perciformes, an order that considerably varied along the past decades both in terms of its definition and composition. According to traditional classifications, Perciformes were a non-monophyletic group including many suborders and families with uncertain phylogenetic position, so that the order was the most diverse amongst vertebrates, with around 1500 genera and approximately ten thousand species (Rosen, 1973; Johnson, 1993; Johnson and Patterson, 1993; Nelson, 2006). Later classifications have substantially reduced those

numbers by erecting to the ordinal rank several noticeably monophyletic suborders placed within Perciformes (e.g., Blennioidei, Gobioidei, Carangoidei, etc.; Wiley & Johnson, 2010; Betancur-R et al., 2013). In spite of these changes, in most classification Perciformes remains as a non-monophyletic assemblage that is still one of the largest fish orders that contains a considerable amount of possibly unrelated families.

Polynemidae is one of the dozens families surrounded by systematic uncertainties that is usually allocated within Perciformes. This family is globally distributed and has around 42 species distributed in eight genera: *Eleutheronema, Filimanus, Galeoides, Leptomelanosoma, Parapolynemus, Pentanemus, Polydactylus,* and *Polynemus* (Feltes, 1991; Motomura, 2004; Wiley and Johnson, 2010; Fricke *et al.*, 2019). Polynemids are marine epibenthic animals, inhabiting sandy or muddy bottoms of turbid shallow waters (not exceeding 150 meters of depth). Some species may occur in brackish waters and some might even enter into rivers. These animals have economic value and certain species can reach up to two meters long (De Sylva, 1984; Feltes, 1991; Motomura, 2004; Nelson, 2006).

Polynemids are easily identifiable as a natural group due to their external morphological features, mainly by their distinct pectoral fin which is divided into a dorsal part, with 12 to 19 soft rays united by a membrane, and a ventral portion with around 3 to 16 isolated rays that are usually elongated forming a filament with tactile functions. There are several others characteristics that additionally help to diagnose the family, such as a conic snout with a ventral mouth; adipose eyelid covering the eye; superior lip absent or not well developed; possession of seven branchiostegal rays, where only one ray articulates with the posterior ceratohyal; presence of two well-separated dorsal fins, which the first one has VII to VIII spines and the second one has I spine and around 11 to 18 soft rays; and caudal fin deeply forked (Motomura, 2004; Nelson, 2006).

Polynemidae lacks a consensual phylogenetic position within Percomorphacea and different papers have advanced alternative hypotheses of relationships. Gosline (1962) proposed that polynemids were closely related to Mugilidae and Sphyraenidae due to their sharing of similar vertebral counts, postcleithrum supporting the pelvic girdle, and presence of non-adhesive eggs. The author additionally states that Polynemidae, Mugilidae, Sphyraenidae, Atherinidae and Phallostethoidei were closely related and might be clustered into a newly defined order Mugiliformes. Rosen (1964) defended that Polynemidae,

Mugilidae and Sphyraenidae should not be apart from Perciformes and, in addition, removed Atheriniformes from Mugiloidei. Nevertheless, Gosline (1968; 1971) continued to support the hypothesis of a closer relationship amongst polynemids, sphyraenids, mugilids and atherinoids, based on their lacking of attachment between cleithrum and pelvic girdle.

On the other hand, Johnson (1993) concluded that the characters proposed to support the closer relationship of polynemids with sphyraenids and mugilids were most likely homoplastic. The author suggested that Polynemidae is actually closely related to Sciaenidae due to their shared similarities during larval development, evidence also reported by De Sylva (1984) but that was not considered by most prior systematics in the formulation of hypotheses relationships among perciforms. The phylogeny of the Sciaenidae was the subject of a morphological analysis by Sasaki (1989). In that study, the author proposed 21 synapomorphies for the family, but is inconclusive about the sister group of Sciaenidae. However, Johnson (1993) noticed that, from the 21 synapomorphies for Sciaenidae provided by Sasaki (1989), five are shared by Polynemidae, which are the extension of *epaxialis* onto the frontals, absence of trisegmental pterygiophores, absence of supramaxilla, insertion of a single branchiostegal ray on the posterior ceratohyal, and a medial interdigitation between the quadrate and metapterygoid. Johnson (1993) and also drew attention to the fact that Freihofer (1978) had already pointed out that the two families share a deep and complex membranous prenasal canal extension. Considering all these evidences, Johnson (1993) recognized that more research were necessary to settle these relationships, but believed that Polynemidae and Sciaenidae are indeed sister groups and recommended that both families should be included in a superfamily Polynemoidea. That hypothesis of relationships was contested by Grove and Lavenberg (1997) and by Gusmao-Pompiani *et al.* (2005) based on the otolith structure and on the spermatozoid morphology, respectively.

Molecular analyses, in turn, allocate Polynemidae in positions that are quite contrasting with all prior hypotheses based on morphological evidence. In the study of Betancur-R *et al.* (2013) the family was removed from Perciformes and appeared as sister group of Menidae that, in turn, formed the sister group of Sphyraenidae. Those three families were clustered within Carangimorphariae, one of the nine major lineages of Percomorphacea proposed in that study). Mugilidae, was allocated within Ovalentariae as the sister group of Ambassidae, whereas Sciaenidae was placed in Percomorpharia (yet

outside Perciformes) as sister the group of Emmelichthyidae. In the molecular analysis of Near *et al.* (2013) the authors proposed an alternative hypothesis of placement of polynemids. In that scheme, Polynemidae appears as the sister group of the large lineage that holds Pleuronectiformes and Carangiformes. Also based on molecular data, Polynemidae was placed as the sister group of Menidae and Lactariidae in the study of Sanciangco *et al.* (2015). The analysis of ultraconserved elements recently published by Harrington *et al.* (2016) and Hughes *et al.* (2018) show a different proposal: Polynemidae as the sister group of Pleuronectiformes, only. In conclusion, the phylogenetic position of Polynemidae lack consensual agreement in both molecular morphology-based hypotheses and the family proved to be one of the most recalcitrant groups within the percomorphacean tree.

The intrarelationships of Polynemidae are comparably unclear. Although the polynemid taxonomy had been discussed in important studies (e.g. Motomura, 2004), the relationships among their eight genera have been the subject of only two explicit phylogenetic analyses until now: the unpublished thesis of Feltes (1986) and Kang (2017). The first one did not included all recent genera (*Leptomelanosoma* is lacking) and was based on 55 characters mostly from skeleton, whereas the second phylogeny was proposed based on 64 morphological characters.

It is also surprising the generalized lack of anatomical studies on polynemids, especially considering their highly modified and greatly sophisticated pectoral fins. The ontogeny and evolution of their pectoral filaments is still enigmatic and details of their structural components remains almost completely unknown. The morphological studies about Polynemidae are typically focused in superficial analyses of specific structures, such as vertebrae and pectoral-filament counts (De Sylva, 1984; Motomura, 2002; 2004), caudal fin anatomy (Feltes, 1991) and some cephalic structures (Feltes, 1993; Gosline, 1993). Osteological reports with more detailed analysis (for instance, jaws, neurocranium and shoulder girdle) are found only in a few descriptions of new genera and/or species (Feltes, 1993; Motomura and Iwatsuki, 2000; 2001; Motomura *et al.*, 2002). Knowledge on polynemid myology is even scarcer. There is only one paper superficially reporting the *adductor mandibulae* in *Polydactylus octonemus* (Gosline, 1993) and another that describes the dorsal gill-arch musculature in *Polydactylus oligodon* and *Filimanus xanthonema*

(Springer and Johnson, 2004). More recently, Kang *et al.* (2017) assembled several characteristics for the family, most of which are from osteological nature.

The present study is the major assessment of polynemid morphology done so far, ranging from muscles morphology never surveyed, cladistic analysis to test the family monophyly and to resolve internal relations, and a descriptive osteological study about polynemid development.

GENERAL REFERENCES

BETANCUR-R, R. et al. The tree of life and a new classification of bony fishes. **PLOS Currents Tree of Life**, 2013. ISSN 2157-3999.

CHEN, W.-J.; BONILLO, C.; LECOINTRE, G. Repeatability of clades as a criterion of reliability: a case study for molecular phylogeny of Acanthomorpha (Teleostei) with larger number of taxa. **Molecular phylogenetics and evolution,** v. 26, n. 2, p. 262-288, 2003. ISSN 1055-7903.

DATOVO, A.; BOCKMANN, F. A. Dorsolateral head muscles of the catfish families Nematogenyidae and Trichomycteridae (Siluriformes: Loricarioidei): comparative anatomy and phylogenetic analysis. **Neotropical Ichthyology,** v. 8, n. 2, p. 193-246, 2010. ISSN 1679-6225.

DATOVO, A.; DE PINNA, M. C. C.; JOHNSON, G. D. The infrabranchial musculature and its bearing on the phylogeny of percomorph fishes (Osteichthyes: Teleostei). **PloS one,** v. 9, n. 10, p. e110129, 2014. ISSN 1932-6203.

DE SYLVA, D. Polynemoidei: development and relationships. In: MOSER, H. G.;RICHARDS, W. J.*, et al* (Ed.). **Ontogeny and systematics of fishes**. Lawrence, Kansas: American Society of Ichthyologists and Herpetologists, v.Special Publication 1, 1984. p.540-541.

FELTES, R. M. **A systematic revision of the Polynemidae (pisces)**. 1986. The Ohio State University

FELTES, R. M. Revision of the polynemid fish genus Filimanus, with the description of two new species. **Copeia**, p. 302-322, 1991. ISSN 0045-8511.

FELTES, R. M. Parapolynemus, a new genus for the polynemid fish previously known as Polynemus verekeri. **Copeia**, p. 207-215, 1993. ISSN 0045-8511.

FREIHOFER, W. C. **Cranial nerves of a percoid fish, Polycentus schomburgkii (Family Nandidae), a contribution to the morphology and classification of the order perciformes**. 1978

FRICKE, R.; ESCHMEYER, W.; FONG, J. Species by family/subfamily in the Catalog of Fishes. [Electronic version]. **San Francisco (CA): California Academy of Sciences**, 2019.

GOSLINE, W. A. Systematic position and relationships of the percesocine fishes. **Pacific Science,** v. 16, p. 207-217, 1962.

GOSLINE, W. A. The suborders of perciform fishes. **Proceedings of the United States National Museum,** v. 124, 1968.

GOSLINE, W. A. **Functional morphology and classification of teleostean fishes**. Honolulu: University of Hawaii Press, 1971. 208.

GOSLINE, W. A. A survey of upper jaw musculature in higher teleostean fishes. **Occasional Papers of the Museum of Zoology University of Michigan** v. 724, p. 1-26, 1993.

GROVE, J.; LAVENBERG, R. **The fishes of the Galápagos islands**. Stanford University Press, 1997. ISBN 0804722897.

GUSMAO-POMPIANI, P.; OLIVEIRA, C.; QUAGIO-GRASSIOTTO, I. Spermatozoa ultrastructure in Sciaenidae and Polynemidae (Teleostei: Perciformes) with some consideration on Percoidei spermatozoa ultrastructure. **Tissue and Cell,** v. 37, n. 3, p. 177-191, 2005. ISSN 0040-8166.

HARRINGTON, R. C. et al. Phylogenomic analysis of carangimorph fishes reveals flatfish asymmetry arose in a blink of the evolutionary eye. **BMC evolutionary biology,** v. 16, n. 1, p. 224, 2016. ISSN 1471-2148.

HUGHES, L. C. et al. Comprehensive phylogeny of ray-finned fishes (Actinopterygii) based on transcriptomic and genomic data. **Proceedings of the National Academy of Sciences,** v. 115, n. 24, p. 6249-6254, 2018. ISSN 0027-8424.

JOHNSON, D. G. Percomorph phylogeny: progress and problems. **Bulletin of marine Science,** v. 52, n. 1, p. 3-28, 1993. ISSN 0007-4977.

JOHNSON, D. G.; PATTERSON, C. Percomorph phylogeny: a survey of acanthomorphs and a new proposal. **Bulletin of Marine Science,** v. 52, n. 1, p. 554-626, 1993. ISSN 0007-4977.

KANG, S. **Comparative morphology and phylogenetic relationships of the family Polynemidae (Pisces: Perciformes)**. 2017. Hokkaido University

KANG, S.; IMAMURA, H.; KAWAI, T. Morphological evidence supporting the monophyly of the family Polynemidae (Teleostei: Perciformes) and its sister relationship with Sciaenidae. **Ichthyological Research,** v. 65, n. 1, p. 29-41, 2017. ISSN 1341-8998.

LI, B. et al. RNF213, a new nuclear marker for acanthomorph phylogeny. **Molecular phylogenetics and evolution,** v. 50, n. 2, p. 345-363, 2009. ISSN 1055-7903.

MIYA, M. et al. Major patterns of higher teleostean phylogenies: a new perspective based on 100 complete mitochondrial DNA sequences. **Molecular phylogenetics and evolution,** v. 26, n. 1, p. 121-138, 2003. ISSN 1055-7903.

MOTOMURA, H. Revision of the Indo-Pacific threadfin genus Polydactylus (Perciformes: Polynemidae) with a key to the species. **Bulletin of the National Science Museum, Tokyo, Series A (Zoology),** v. 28, n. 3, p. 171-194, 2002.

MOTOMURA, H. **Threadfins of the world (Family Polynemidae): An annotated and illustrated catalogue of polynemid species known to date**. Food & Agriculture Org., 2004. ISBN 9251051283.

MOTOMURA, H.; IWATSUKI, Y. A new genus, Leptomelanosoma, for the polynemid fish previously known as Polydactylus indicus (Shaw, 1804) and a redescription of the species. **Ichthyological research,** v. 48, n. 1, p. 13-21, 2000. ISSN 1341-8998.

MOTOMURA, H.; IWATSUKI, Y. Review of Polydactylus species (Perciformes: Polynemidae) characterized by a large black anterior lateral line spot, with descriptions of two new species. **Ichthyological research,** v. 48, n. 4, p. 337-354, 2001. ISSN 1341-8998.

MOTOMURA, H. et al. Review of seven-spined Polynemus species (Perciformes: Polynemidae) with designation of a neotype for Polynemus paradiseus Linnaeus, 1758. **Ichthyological research,** v. 49, n. 4, p. 307-317, 2002. ISSN 1341-8998.

NEAR, T. J. et al. Phylogeny and tempo of diversification in the superradiation of spiny-rayed fishes. **Proceedings of the national Academy of sciences,** v. 110, n. 31, p. 12738-12743, 2013. ISSN 0027-8424.

NEAR, T. J. et al. Resolution of ray-finned fish phylogeny and timing of diversification. **Proceedings of the National Academy of Sciences,** v. 109, n. 34, p. 13698-13703, 2012. ISSN 0027-8424.

NELSON, J. S. **Fishes of the world**: Wiley & Sons, Hoboken, New Jersey**:** 600 p. 2006.

ROSEN, D. E. **The relationships and taxonomic position of the halfbeaks, killifishes, silversides, and their relatives**. American Museum of Natural History, 1964.

ROSEN, D. E. Interrelationships of higher euteleostean fishes. In: GREENWOOD PH;MILES RS*, et al* (Ed.). **Interrelationships of Fishes**: London: Academic Press, 1973. p.397-513.

SANCIANGCO, M. D.; CARPENTER, K. E.; BETANCUR-R, R. Phylogenetic placement of enigmatic percomorph families (Teleostei: Percomorphaceae). **Molecular phylogenetics and evolution,** v. 94, p. 565-576, 2015. ISSN 1055-7903.

SASAKI, K. Phylogeny of the family Sciaenidae, with notes on its zoogeography (Teleostei, Perciformes). **Memoirs of the Faculty of Fisheries Hokkaido University,** v. 36, n. 1-2, p. 1-137, 1989. ISSN 0018-3466.

SPRINGER, V. G.; JOHNSON, G. D. **Study of the dorsal gill-arch musculature of teleostome fishes, with special reference to the Actinopterygii**. Biological Society of Washington, Smithsonian Institution, 2004.

SPRINGER, V. G.; ORRELL, T. M. **Phylogenetic analysis of the families of acanthomorph fishes based on dorsal gill-arch muscles and skeleton**. Biological Society of Washington, Smithsonian Institution, 2004.

WILEY, E.; JOHNSON, G. D. A teleost classification based on monophyletic groups. **Origin and phylogenetic interrelationships of teleosts,** v. 1, p. 123-182, 2010.

WINTERBOTTOM, R. A descriptive synonymy of the striated muscles of the Teleostei. **Proceedings of the Academy of Natural Sciences of Philadelphia**, p. 225-317, 1974a. ISSN 0097-3157.

WINTERBOTTOM, R. The familial phylogeny of the Tetraodontiformes (Acanthopterygii: Pisces) as evidenced by their comparative myology. **Smithson Contrib Zool,** v. 155, p. 1-201, 1974b.

WINTERBOTTOM, R. Myological evidence for the phylogeny of recent genera of surgeonfishes (Percomorpha, Acanthuridae), with comments on the Acanthuroidei. **Copeia**, p. 21-39, 1993. ISSN 0045-8511.

Chapter 1

Cranial and pectoral musculature of Polynemidae

1. INTRODUCTION

The skeletal musculature is a system that has been traditionally neglected in most systematic studies with fishes, and the ones that address muscle morphologies generally have little focus on the muscle homologies across different lineages (Datovo and Rizzato, 2018). Yet, several studies demonstrate the importance of muscles and associated connective tissues to cladistic studies (Winterbottom, 1974b; 1993; Springer and Johnson, 2004; Datovo and Bockmann, 2010; Datovo and Castro, 2012; Datovo and Vari, 2013; 2014; Springer and Johnson, 2015; Datovo and Rizzato, 2018).

In the past decade several studies addressed some specific traits of the polynemid morphology (Feltes, 1991; 1993; Motomura *et al.*, 2000; Motomura and Iwatsuki, 2001; Motomura, 2002; Motomura *et al.*, 2002; Motomura, 2004; Gusmao-Pompiani *et al.*, 2005; Motomura and Tsukawaki, 2006; Chaklader *et al.*, 2015). However, almost all of them depicted only the external morphology of those fishes and a few osteological structures (*e.g.* number of vertebrae, spines, soft rays, and sparse data on the cranium). Myological data available for polynemids are even scarcer. Until recently, only two papers reported isolated data on the *adductor mandibulae* of *Polydactylus octonemus* (Gosline, 1993) and the suprabranchial musculature of *Polydactylus oligodon* and *Filimanus xanthonema* (Springer and Johnson, 2004). More recently, Kang *et al.* (2017) briefly described 14 characters from osteology and 4 from a few cranial and pectoral muscles of Polynemidae. Nevertheless, these myological descriptions are rather superficial and most skeletal muscles were set aside from their analysis and are completely unknown.

The present study describes in detail the musculature of the mandibular arch, hyopalatine arch, opercular series, branchial arches, and pectoral girdle of polynemids and *Cynoscion*, a representative of Sciaenidae, a family often proposed as closely related to Polynemidae. From these descriptions, several new morphological characters were assembled to test the intrarelationships of Polynemidae (see Chapter 2).

2. MATERIAL AND METHODS

The analyzed specimens are from the following institutions: Academy of Natural Sciences of Drexel University, USA (ANSP); California Academy of Sciences, USA (CAS); and Museu de Zoologia da Universidade de São Paulo, Brazil (MZUSP). In total, 27 specimens belonging to 20 species were analyzed and double stained for musculature analysis: Sciaenidae: *Cynoscion striatus* (2) MZUSP 6891. Polynemidae: *Eleutheronema tetradactylum* (1) MZUSP 123253, (1) ANSP 61928; *Eleutheronema tridactylum* (1) ANSP 89554; *Filimanus similis* (1) MZUSP 124826; *Filimanus xanthonema* (1) MZUSP 123255; *Galeoides decadactylus* (1) MZUSP 123256; *Leptomelanosoma indicum* (1) CAS 50925; *Parapolynemus verekeri* (1) MZUSP 123718; *Pentanemus quinquarius* (2) MZUSP 123254; *Polydactylus approximans* (1) MZUSP 124822; *Polydactylus microstomus* (1) MZUSP 124823; *Polydactylus octonemus* (1) MZUSP 124817; *Polydactylus oligodon* (1) MZUSP 67533; *Polydactylus opercularis* (1) MZUSP 124825; *Polydactylus plebeius* (1) MZUSP 124824; *Polydactylus sexfilis* (1) MZUSP 124812; *Polydactylus sextarius* (1) MZUSP 124811; *Polydactylus virginicus* (3) MZUSP 51249, (1) MZUSP 67546; *Polynemus multifilis* (1) MZUSP 63339; *Polynemus paradiseus* (2) MZUSP 123252. One *Polydactylus virginicus* (MZUSP 51249) was cleared and double stained for osteology analysis.

Eleutheronema tetradactylum (1) MZUSP 123253; *Filimanus similis* (1) *Galeoides decadactylus* (1) MZUSP 123256; *Pentanemus quinquarius* (2) MZUSP 123254; *Polydactylus approximans* (1) MZUSP 124822; *Polydactylus microstomus* (1) MZUSP 124823; *Polydactylus octonemus* (1) MZUSP 124817; *Polydactylus opercularis* (1) MZUSP 124825; *Polydactylus plebeius* (1) MZUSP 124824; *Polydactylus sexfilis* (1) MZUSP 124812; *Polydactylus sextarius* (1) MZUSP 124811; *Polynemus paradiseus* (2) MZUSP 123252 were all donations from the National Museum of Natural History, Smithsonian Institution and *Parapolynemus verekeri* (1) MZUSP 123718 was a donation received from the Museum and Art Gallery of the Northern Territory, Australia.

For the study of the whole musculoskeletal system, specimens were double stained following the protocol of Datovo and Bockmann (2010). Some specimens were cleared and double stained for the study of the osteology following the techniques of Taylor and Van Dyke (1985) and Schnell *et al.* (2016) with minor adaptations. Osteological nomenclature

followed primarily Johnson and Patterson (1993), as commonly used in studies on Percomorphacea, while myological nomenclature followed Datovo and Vari (2013) for the *adductor mandibulae* complex, Datovo and Rizzato (2018) for the hyopalatine musculature, Datovo *et al.* (2014) for the infrabranchial musculature, and Winterbottom (1974a) for the remaining muscles complexes.

The term insertion is herein applied to the attachment of the muscles to a given structure (usually bones) that is more likely to move (or move more intensively) during contraction; the term origin refers to the opposite site of attachment of the muscles that will probably be stationary (or less movable) during movement. Musculous attachment (origin or insertion) is a term used when the attachment to a bone occurs without the mediation of a macroscopically evident tendon; tendinous attachment is when the fibers converge to a macroscopically evident tendon that attaches itself to the bone. The aponeurotic attachment follows the same grounds of the tendinous one, but refers to a broad membranous tendon (aponeurosis).

Photographs were taken from dissected specimens in order to accelerate the illustration process. The images of small structures were obtained through a digital camera Zeiss Axiocam 506 color attached to a stereomicroscope Zeiss SteREO Discovery.V20, while the largest ones were taken via digital camera Nikon D7000. The CT-scan images were obtained from a microtomography Phoenix v|tome|x m microfocus of General Electric Company. The images reconstruction were done by Phoenix datos|x 2 reconstruction; GE Sensing and Inspection Technologies GmbH and edited via VG Studio Max version 2.2.3.69611 64bits, Volume Graphics GmbH.

3. RESULTS

3.1 *Adductor mandibulae* complex

Sciaenidae

The *segmentum facialis* of the *adductor mandibulae* is partitioned into *rictalis*, *malaris*, and *stegalis*, although these sections are not completely independent from each other (Fig. 1). The *rictalis* is the largest component in lateral view, having a nearly conical shape with a broader origin and a narrow insertion (Fig. 2A). Compared with most other acanthomorphs, including the outgroup of the present analysis, the section is posterodorsally expanded. Fibers arise from the vertical arm of the preopercle, lateral surface of the posterior margin of the hyomandibula and posterodorsal region of the quadrate (Fig. 1). The dorsalmost portion of the *rictalis* shares fibers with the *retromalaris* (see below).

The *stegalis*, in turn, has its origin associated with the metapterygoid, where the fibers emerge from the posterodorsal region of the bone. The *stegalis* is a thin layer of muscle fibers and can be distinguishable from the *rictalis* only at its origin. As the *stegalis* has shorter fibers, its origin is more anteriorly displaced than the origin of the *rictalis*, which extends posteriorly and reaches the hyomandibula. Toward insertion, the *rictalis* and *stegalis* merge to each other and the compound *ricto-stegalis* inserts onto the intersegmental aponeurosis, on both the mandibular and meckelian tendons (Fig. 2B).

The *malaris* is divided into a posterodorsal *pars retromalaris* and an anteroventral *pars promalaris* (Fig. 1 and 2A). The *retromalaris* is a ribbon-like shaped muscle with an aponeurotic origin from the hyomandibula and insertion onto the intersegmental aponeurosis, reaching both the lower and upper jaws via transverse tendon embedded on the buccopalatal membrane and paramaxillar ligament, respectively (Fig. 2B). In contrast, the *promalaris* – also a nearly rod-like muscle – is completely separated from and located medial to the *pars retromalaris*. At origin, the *pars promalaris* is further divided into *promalares interna* and *externa* (Fig. 2A and B). The *promalaris externa* originates from the quadrate, metapterygoid and endopterygoid, while the *promalaris interna* originates from

the ectopterygoid and palatine. These muscle subdivisions gradually merge to each other toward their insertions that occur on the medial face of the maxilla. Fibers of the *pars promalaris interna* inserts primarily onto the medial surface of the maxilla, without mediation of any evident tendon or ligament. Most fibers of the *pars promalaris externa*, in turn, converge to the ectomaxillar ligament, which parallels the *promalaris interna* and attach to the anterolateral region of the maxilla (Fig. 2B).

The *segmentum mandibularis* of the *adductor mandibulae* is located at the medial surface of the lower jaw and is differentiated into *partes coronalis* and *mentalis*. The *coronalis* originates from the dorsal region of the mandibular tendon and inserts on the posterodorsal region of the dentary. Origin of the *mentalis* is from the ventral portion of the mandibular tendon and from the faucal ligament. Insertion is on the posteroventral region of the dentary and anterior area of the angulo-articular (Fig. 2B).

The accessory tendon of the intersegmental aponeurosis is medial to the *segmentum mandibularis* and can be easily seen in medial view over the surface of this muscle segment. The preangular tendon, in lateral view, is located posterior to the maxilla and anchors ventrally onto the lateral surface of the angulo-articular. The transverse tendon is not individually distinguishable, being embedded within the interface between the intersegmental aponeurosis and the buccopalatal membrane (Fig. 2B).

The *ramus mandibularis trigeminus* runs between the *retromalaris* and the *rictalis*, passing posteromedial to the former and anterolateral to the latter.

Polynemidae

The *segmentum facialis* of the *adductor mandibulae* is similar to that of the Sciaenidae in terms of the main identifiable muscle partitions, although there are significant differences in the morphology of the *pars promalaris* (Fig. 3). The *rictalis* is the largest section of the *segmentum facialis*, occupying almost the whole lateral surface of the preopercle. The *rictalis* is a conical muscle mass – broader at origin and narrower at insertion (Fig. 4). The fibers originate from the vertical arm of the preopercle and from the lateral surface of the posterior margin of the hyomandibula. The *stegalis* lies medial to all sections of the *segmentum facialis* of the *adductor mandibulae* and is not fully separated from *pars rictalis* at the insertion, where they form a compound *ricto-stegalis* (Fig. 5A, B). These two

sections are superficially differentiable because the *stegalis* forms a thin layer of shorter muscle fibers that arise from the posterodorsal region of the metapterygoid and anterodorsal region of the hyomandibula (Figs. 4, 5). From the identifiable separated origins of the *rictalis* and *stegalis*, the fibers gradually form a single unit that inserts on the intersegmental aponeurosis, on both mandibular and meckelian tendons, and also on the transverse tendon. Uniquely, *Filimanus* and *Pentanemus* have the latter tendon anteriorly located in comparison to the *retromalaris* section (see below).

As in the Sciaenidae, the *malaris* is divided into *pars retromalaris* and *pars promalaris*. The *retromalaris* is completely free from and dorsal to the *rictalis*, with origin on the pterotic, preopercle, and hyomandibula (Fig. 3). In *Pentanemus* and *Parapolynemus* the autosphenotic is additionally involved in the origin of the *retromalaris*. This section associates with both upper and lower jaws through its insertion onto the retrojugal lamina of the buccopalatal membrane and its embedded ligaments. The dorsalmost muscle fibers associate more prominently with the paramaxillar ligament, which anchors to anterolateral region of the maxilla, whereas the ventralmost fibers attach to the transverse tendon that converges to the intersegmental aponeurosis (Figs. 4, 5). A preangular tendon anchoring to the angulo-articular is invariably present at the posteroventral region of the buccopalatal membrane. In all polynemids except *Eleutheronema*, *Polydactylus plebeius*, and *P. sexfilis* (Fig. 6) this ligament does not reach the ventral margin of the angulo-articular and is covered laterally by the posterior margin of the maxilla (Fig. 3).

The *promalaris* is completely lateral to the *retromalaris* and *rictalis*, originating aponeurotically from the preopercle (Fig. 3). Uniquely in *Polynemus paradiseus* this muscle section also arises from the neurocranium, more specifically the pterotic (Fig. 7). In most polynemids, the *promalaris* inserts on the anterior region of the maxilla through the endo- and ectomaxillar ligaments. Near to the insertion, the *promalaris* subtly subdivides into a medial and a lateral section. The former is the *pars promalaris interna*, which converges to the endomaxillar ligament that, in turn, attaches to the anteromedial surface of the maxilla (Figs. 4, 5). The lateral subdivision corresponds to the *pars promalaris externa* that associates with the ectomaxillar ligament (Figs. 4, 5). As in the generalized condition for percomorphaceans, most polynemids have this ligament anchoring to the anterolateral region of the maxilla. However, in *Galeoides* the ectomaxillar ligament is attached to the

medial surface of the maxilla, so that both ecto- and endomaxillar ligaments are visible in medial view (Fig. 8). Surprisingly, the sciaenid condition can be found in *Polydactylus sextarius*, where the *pars promalaris interna* inserts on the maxilla musculously, without the endomaxillar ligament (Fig. 9). The *pars promalaris externa* inserts normally on the maxilla via ectomaxillar ligament. Moreover, the insertion of the *pars promalaris* of *Polydactylus sextarius* is undivided, *i.e.* the musculous insertion of the *pars promalaris interna* is continuous with the insertion of the *pars promalaris externa*. This continuity of insertions is also present in *Polydactylus microstomus* and *P. opercularis*. Nevertheless, despite the continuous insertion, these two species have the *pars promalaris interna* inserting onto the maxilla via endomaxillar ligament. Differences in the distance between ecto- and endomaxillar ligaments were observed across the different polynemid taxa, but this variation could not the coded into unambiguous discrete character states.

In most polynemids, the *segmentum mandibularis* of the *adductor mandibulae* is superficially differentiated into *pars coronalis* and *pars mentalis* and both occupy the medial surface of the lower jaw. The *coronalis* originates from the dorsal area of the mandibular tendon of the intersegmental aponeurosis and from the faucal ligament. Insertion occurs on the posteroventral region of the medial surface of the dentary. The *pars mentalis*, in turn, originates from the ventral region of the mandibular tendon and from the faucal ligament. The fibers insert along the posteroventral region of the medial surface of the dentary and anterior end of the angulo-articular. *Galeoides*, *Leptomelanosoma*, *Parapolynemus*, *Polydactylus microstomus*, *P. sextarius*, *P. plebeius*, *P. sexfilis,* and *Polynemus* have the *segmentum mandibularis* differentiated into *partes coronalis* and *mentalis*, in which they share fibers anteriorly (Figs. 4, 9B). In *Leptomelanosoma*, *Parapolynemus* and *Polynemus*, the origin of the posteroventral fibers of the *segmentum mandibularis* is also associated with a ligament from the buccopalatal membrane and, in such instances, the origin of the *segmentum mandibularis* thus indirectly involves both upper and lower jaws (Fig. 4).

The accessory tendon of the intersegmental aponeurosis is never visible in a superficial medial view because it is invariably covered by the *segmentum mandibularis*. In *Pentanemus* that tendon runs in the middle of the fibers of the *segmentum mandibularis*. All other polynemids have the accessory tendon completely lateral to that muscle segment.

The *ramus mandibularis trigeminus* arrives medially at the *segmentum facialis* and then runs posteromedial to the *retromalaris* and anterolateral to the *rictalis*.

3.2 Hyopalatine and opercular musculature

Sciaenidae

The *levator arcus palatini*, located posterior to the eye, is well developed and originates from the autosphenotic and pterotic. Insertion is on the lateral faces of the preopercle, hyomandibula and metapterygoid. The muscle is narrow at the origin and broader at the insertion. At origin the *levator arcus palatini* is undivided but gradually differentiates ventrally into several distinct sections that are never fully separate from each other. The posterior fibers of the *levator arcus palatini* insert on the preopercle laterally to the *segmentum mandibularis* of the *adductor mandibulae*. This posterior section, which has a bipinnate aspect, corresponds to the *pars temporalis* of the *levator arcus palatini*. The anterior fibers of the muscle form the *pars primordialis* that have a further differentiation into an innermost section, the *primordialis interna*, and an outermost portion, the *pars primordialis externa* (Fig. 10). The former subdivision is smaller than the latter and occupies the posterodorsal region of the autosphenotic at the orbit capsule (Fig. 1). The *pars primordialis externa* is the largest muscle component of the *levator arcus palatini*. The muscle additionally exhibits an extra division termed *pars pharyngealis*. Fibers of this section pass through a slender gap between the hyomandibula and metapterygoid and reach the medial face of the suspensorium, where they insert on the hyomandibula (Fig. 10B).

The *dilatator operculi*, located posterior to the *levator arcus palatini* muscle, originates from the pterotic and inserts on the dilatator process at the anterodorsal region of the opercle (Fig. 1). This muscle has a bipinnate aspect laterally and most of its origin is covered by the dorsal portion of the preopercle (Fig. 10A). Nonetheless, its origin is closely associated with the origin of the *levator arcus palatini*. In medial view, the ventral fibers of the *dilatator operculi* can be seen through a dorsal gap between the hyomandibula and opercle (Fig. 10B).

The *levator operculi* is placed immediately posterior to the *dilatator operculi* and also originates from pterotic and inserts onto the opercle. However, the insertion of the *levator operculi* occurs at the anterodorsal margin of the medial face of the opercle. This is a conical shaped muscle with a narrow origin and a broader insertion (Fig. 10).

The *adductor operculi* originates from the pterotic and its insertion is medial to that of the *levator operculi*, attaching onto the adductor crest at the dorsomedial surface of the opercle (Fig. 10B). The *adductor operculi* and *adductor hyomandibulae pars primordialis* (see below) are fully separated from each other.

The *adductor hyomandibulae* has two major divisions: *pars primordialis* and *pars pterygo-palatina* connected by an extreme thin layer of muscles. The *pars primordialis* lies anterior to the *adductor operculi*, originating from the pterotic and inserting on the opercular process of the hyomandibula. The *pars pterygo-palatina* of the muscle is moderately developed, with more prominent fibers at the posterior and anterior extremities of the orbit capsule. Accordingly, the middle portion of this section is extremely thin, but there is no separation between portions presumably corresponding to the *partes pterygoidea* and *palatina*. The *pars pterygo-palatina* originates from parasphenoid and prootic and inserts on the lateral faces of endopterygoid and palatine and on the medial faces of the hyomandibula and metapterygoid. The origin is as broader as the insertion, rendering an elongated, laminar shaped muscle located posteroventral to the orbit, between the skull and the hyopalatine arch (Fig. 10B).

Polynemidae

The *levator arcus palatini* primarily originates from the autosphenotic and pterotic and inserts on the lateral faces of the hyomandibula and metapterygoid. Except for *Filimanus* and *Pentanemus*, all remaining genera have an anterior prominent expansion of the muscle, with fibers also arising from the frontal and pterosphenoid (Fig. 11A). In all genera it is possible to observe some differentiation of the *levator arcus palatini* into *pars temporalis*, *pars primordialis interna*, and *pars primordialis externa*. Contrary to the condition of sciaenids, there is no trace of the *pars pharyngealis* in all examined polynemids. The whole *levator arcus palatini* of polynemids is situated posteriorly to the eyeball and is

almost completely covered by the *segmentum facialis* of the *adductor mandibulae*, so that only the *pars primordialis interna* is visible in a superficial lateral view (Fig. 7).

The *pars temporalis* of the *levator arcus palatini* is medial to the *segmentum facialis* of the *adductor mandibulae*. The sphenotic spine marks the apparent division between the *temporalis* and *primordialis* sections, which are only slightly differentiated from each other. The musculous origin of the *pars temporalis* is from the autosphenotic and pterotic and its insertion is tendinous on the lateral surface of the hyomandibula. The *pars temporalis* does not exhibit a bipinnate aspect as seen in sciaenids (Fig. 11A).

The *pars primordialis* is further divided into subsections *interna* and *externa*, with varying degrees of separation between them. In *Galeoides*, *Leptomelanosoma*, *Parapolynemus* and *Polydactylus* these subsections are completely separated from each other, whereas in other genera the separation is incomplete. The *pars primordialis externa* is relatively conservative across the examined polynemids, with a narrow musculous origin from the autosphenotic, frontal, and pterosphenoid and a broader and also musculous insertion on the hyomandibula and metapterygoid (Fig 12). In *Filimanus* and *Pentanemus* the origin of this section is restricted to the autosphenotic.

In contrast, the *pars primordialis interna* exhibits a broader variation across the examined polynemid genera, including in its degree of development. Site of insertion is common to all polynemids, occurring at the anterodorsal tip of the hyomandibula (Fig. 11B). This subsection occupies the posterodorsal region of the orbit capsule. In *Filimanus* and *Pentanemus* the origin of the *pars primordialis interna* is restricted to the autosphenotic, whereas in all other genera the fibers arise from the autosphenotic, frontal and pterosphenoid (Fig. 13A). *Galeoides* and *Parapolynemus* have this section with a slightly bipinnate aspect and a tendinous insertion on the anterodorsal process of the hyomandibula (Figs. 11A, 12A).

The *dilatator operculi*, located just posterior to the *pars temporalis* of the *levator arcus palatini*, has a bipinnate aspect and a conical shape (Figs. 11-13). The origin is broad on the pterotic and the insertion is narrower on the dilatator process of the opercle. The ventralmost fibers of the *dilatator operculi* can be seen in medial view through a gap between the hyomandibula and opercle (Fig. 11B). The single exception is *Filimanus* and

Parapolynemus, in which the ventral fibers of the muscle are not visible from a medial view of the suspensorium (Fig. 13B)

In *Parapolynemus*, the *levator operculi* and *adductor operculi* are not separable from each other, thus forming a compound muscle with origin from the pterotic and insertion on the medial face of the opercle (Fig. 12A). In all remaining polynemids, the two muscles are completely separated from each other (Fig. 11A, 12B). The *levator operculi* is placed immediately posterodorsal to the *dilatator operculi* and originates tendinously from the pterotic. Insertion occurs musculously on the anterodorsal margin of the medial face of the opercle. With a flat triangular shape, the muscle is narrow at the origin and wider at the insertion. The *adductor operculi* is located medially to the *levator operculi* and *dilatator operculi* (except in *Parapolynemus*; see above). In most polynemids, the origin of the *adductor operculi* is mixed, with posterolateral fibers arising tendinously and the anteromedial ones originating musculously from the neurocranium (Fig. 11B). The single exception is *Eleutheronema* that presents the condition found in sciaenids in which the *adductor operculi* originates purely musculous from the neurocranium. The insertion is common to all polynemids and occurs on the *adductor* crest at the dorsomedial surface of the opercle (Figs 11B, 13B). The muscle is completely separated from the *pars primordialis* of the *adductor hyomandibulae* (see below).

In most polynemids, the *adductor hyomandibulae* has two major divisions: (i) the *pars primordialis*, situated anteriorly to the *adductor operculi*, with origin from the pterotic and insertion on the opercular process of the hyomandibula; and (ii) the compound *pars pterygo-palatina*, placed anteriorly at the suspensorium and occupying mainly the floor of the orbit capsule (Fig. 11B). Connecting these two sections, there is an extremely thin layer of muscle fibers embedded in connective tissue that extends along the dorsal region of the medial face of the hyomandibula (Fig. 11B). The *pars pterygo-palatina* originates from the parasphenoid and prootic and inserts primarily on the lateral faces of the endopterygoid and palatine and at the medial faces of the hyomandibula and metapterygoid. The sole exception is *Eleutheronema*, in which the fibers do not reach the palatine nor the anterior surface of the lateral face of the endopterygoid, constituting a *pars pterygoidea* restricted mainly to the posterior region of the orbit capsule (Fig. 12B). In general, the anteriormost fibers of the *pars pterygo-palatina* have a smooth surface, with fibers arranged fully parallel to each

other (Fig. 11B). However, the anteriormost fibers of *Filimanus* and *Polydactylus microstomus* present a bipinnate aspect (Fig. 13A) whereas *Leptomelanosoma*, *Parapolynemus*, and *Polynemus* have tendons within the musculature, giving it a multipennate aspect (Fig. 12A).

3.3 Pectoral musculature

Sciaenidae

Lateral portion

The *abductor superficialis* is the lateral most muscle of the pectoral fin and originates musculously from the concave surface of the lateral projection of the cleithrum (Fig. 14A). Insertion occurs tendinously onto the lateral base of all rays but the first one. The ventral fibers are longer than the dorsal ones and the medial surface of the muscle has an aponeurotic portion at its dorsal region. This aponeurotic portion of the muscle is juxtaposed with a similar, aponeurotic portion of the *abductor profundus*, *pars ceterae* (see below). The *abductor superficialis* originates as a single muscle mass that gradually differentiates into small bundles toward insertion on each ray.

The *abductor profundus* is located directly beneath the *abductor superficialis* and is completely divided into two sections (Fig. 14A). The first section, herein termed *pars marginalis*, is a bipinnate muscle that originates from the lateral surface of the cleithrum and coracoid and inserts via elongate tendon on the posteroventral flange of the lateral base of the marginal (first) ray. The second division of the *abductor profundus* serves all pectoral rays except the first one and is accordingly named *pars ceterae* (from Latin *ceterus* meaning others, remainder, rest). This section is shaped as a sole unit at origin and progressively differentiates into bundles that attach tendinously to each individual ray, although some intermingling of fibers between the bundles may occur. The *pars ceterae* of the *abductor profundus* originates from the lateral faces of the cleithrum and coracoid. Insertion on the rays occurs anteromedially to the insertion of the *abductor superficialis*. The dorsalmost portion of the muscle has an aponeurotic coverage at its lateral surface.

The *arrector ventralis* lies dorsal to the *pars marginalis* of the *abductor profundus* and is the dorsalmost muscle associated with the lateral surface of the pectoral fin (Fig. 14A). This muscle also has a bipinnate aspect. It originates musculously from the lateral surface of the cleithrum and coracoid and inserts on the medial base of the first ray through a broad tendon that passes dorsally on the scapula

The *protractor pectoralis* is an extrinsic muscle that serves the pectoral girdle and is posterior to the branchial muscle *levator posterior* (see below). The *protractor pectoralis* is a rather thin, ribbon-like bundle of fibers that originates tendinously from the insertional tendon of the *epaxialis* attached to the pterotic spine. The insertion of the *protractor pectoralis* is embedded into the membrane that connects the last gill arch with the cleithrum and forms the posterior wall of the branchial cavity.

Medial portion

The *adductor superficialis* originates from the medial face of the cleithrum and inserts onto the medial hemitrichia of all rays except the first one (Fig. 14B). This insertion usually occurs a little further away from the rays' bases. The *adductor superficialis* is a well-developed U-shaped muscle with the fibers attaching to the dorsal rays lying progressively more ventromedial to those serving the ventral rays (Fig. 15A). The fibers that attach onto the second and third rays are longer, originating from a more anterior portion of the medial face of the cleithrum. There is no clear superficial division between the fibers attaching to each individual ray.

The *adductor medialis* is placed in between the *adductores superficialis* and *profundus* (Fig. 14B). The *adductor medialis* is composed by a very thin layer of fibers that originate musculously from the anterior margin of the medial face of the cleithrum. Toward insertion, the muscle gradually become aponeurotic and fuses with the insertional tendons of the *adductor superficialis*. However, the tendinous portion of the *adductor medialis* is narrower than the *adductor superficialis* and serves only the central rays of the pectoral fin (Fig. 15A).

The *adductor profundus* locates underneath the *adductores medialis* and *superficialis*, originating from the medial faces of the cleithrum, coracoid, and also from the membrane that covers the fenestra formed between these bones (Fig. 15A). Insertion is on the medial

base of all pectoral rays except the first one. The *adductor profundus* is further differentiated into a superficial layer of fibers herein named *pars ectoprofunda* and a deeper layer termed *pars endoprofunda*. The fibers of the *ectoprofunda* are longer and cover all fibers from the *endoprofunda* counterpart. The *endoprofunda* has shorter fibers that originate from the coracoid bar that forms the posterior margin of the cleithrum-coracoid fenestra (Fig. 15B). Insertion is common to both subsections.

The *arrector dorsalis* attaches tendinously onto the medial process of the medial hemitrichium of the first ray and originates from the medial faces of the cleithrum, coracoid, and scapula. The *arrector dorsalis* is a long slender muscle completely free from the *adductor profundus* and has a bipinnate aspect (Fig. 15A).

Finally, the *adductor radialis* is the smallest muscle of the whole pectoral musculature and does not share any fibers with the *adductor profundus*. The *adductor radialis* originates musculously from the medial faces of the second, third, and fourth pectoral radials and inserts tendinously onto the medial hemitrichia of the five ventralmost rays. From a medial view, the *adductor radialis* is the deepest muscle although some of its ventralmost fibers are exposed posteroventrally to the *adductor profundus* (Fig. 15).

The *Cynoscion* shoulder girdle is innervated by occipito-spinal nerves (OS) which merges with the first spinal nerve (SP1) to form the anterior branch (SP1+OS) that dives into the girdle. This branch is the one that passes through the scapular foramen to innervate the lateral portion of the girdle. The second spinal nerve (SP2) also innervates the girdle and is posterior to the SP1+OS branch. According to Freihofer (1963), *Cynoscion* has a parieto-dorsal branch of the *ramus lateralis accessorius* (RLA-PD) leaving the brain and from this main branch, a subdivision termed pectoral branch (RLA-PP) arrives into the pectoral girdle. However, during my dissections, I could not identify this nerve in the medial portion of the pectoral girdle. This nerve might be small and thin, breaking quite easily during girdle removal. Yet, I could find the RLA nerve arising from the trigeminus-facialis main trunk, which in turn curves dorsoposteriorly and apparently leaves the neurocranium through a small foramen on the pterotic (Fig. X), contrastingly to what Freihofer (1963) reports, in which the RLA-PD actually exits the brain case through the parietal. Once the nerve left the neurocranium, I could not track its path anymore since it merged into *epaxialis* musculature (Fig. 16).

Polynemidae

Lateral portion

The *abductor* and *adductor* muscle masses serving the pectoral fin in all polynemids are divided into two completely independent segments herein named *segmenta radialis* and *filamentaris*. The former is the muscle segment responsible for moving the unmodified fin while the latter serves the pectoral filaments (Fig. 17).

The *segmentum radialis* of the *abductor superficialis* is usually the largest lateral muscle component of the unmodified fin. This muscle is generally a thick unit of fibers occupying most of the lateral surface of the horizontal arm of the cleithrum (Fig. 17). The muscle gradually differentiates into small bundles that serve each individual soft ray, although a degree of fibers sharing can be seen. Nevertheless, these bundles are not fully separated from each other. In most polynemids, the origin of the muscle is mainly musculous from the lateral projection of the cleithrum. The fibers arise from the concave surface of this lateral projection and insert tendinously on the base of the lateral hemitrichia of the pectoral-fin rays, except for the first (marginal) ray. *Parapolynemus* is unique in having the *segmentum radialis* of the *abductor superficialis* originating entirely from the lateral surface of the coracoid (Fig. 18A). Insertion of the muscle is conservative amongst all polynemid genera. The dorsomedial surface of the muscle is aponeurotic and contacts a similarly aponeurotic area of the *adductor profundus radialis* (see below).

As for sciaenids, the *segmentum radialis* of the *abductor profundus* of polynemids is also divided into *partes marginalis* and *ceterae*. This division is complete in all examined members of the family, except *Pentanemus* that has only a superficial differentiation between *partes marginalis* and *ceterae*. Both sections are located immediately beneath the *abductor superficialis* (Fig. 19). The origin of the *pars ceterae* is musculous and usually associated with the lateral surfaces of the cleithrum, coracoid, and third pectoral radial. The scapula is additionally involved in the origin of this muscle in *Eleutheronema*, *Filimanus*, *Pentanemus,* and most *Polydactylus* (except *P. microstomus, P. sexfilis,* and *P. sextarius*). The *pars ceterae* of *Parapolynemus* arises only from the coracoid and third pectoral radial. Insertion of the muscle section in all polynemids occurs tendinously onto the lateral base of

all hemitrichia but the first one, being anteromedial to the insertion of the *adductor superficialis radialis*. The dorsalmost portion of the *pars ceterae* of the *abductor profundus radialis* is more elongate and covered by a lateral aponeurosis (Fig. 19). The *pars marginalis* of the *abductor profundus radialis* is a bipinnate muscle partially covered by the *pars ceterae* and runs parallel to both this section and the *arrector ventralis* (Fig. 19). *Parapolynemus* is the sole exception with a *pars marginalis* not bipinnate and positioned in an oblique angle relative to the adjacent muscles (Fig.18B). Most polynemids have a *pars marginalis* originating primarily from the lateral surfaces of the cleithrum, coracoid, and scapula and inserting onto the ventral process of the lateral base of the marginal (first) ray. In *Galeoides* and *Leptomelanosoma* the muscle additionally arises from the lateral face of the third pectoral radial. In *Parapolynemus* the *pars marginalis* originates only from coracoid and scapula.

The *arrector ventralis* is a long, bipinnate muscle that forms the dorsalmost muscle component serving the lateral portion of the pectoral fin. Most part of the muscle is located medially to the *segmenti radiales* of the *abductores superficialis* and *profundus*. Its origin is musculous from the lateral surface of the cleithrum, coracoid and scapula; insertion is via an elongate tendon onto the medial base of the first ray (Fig. 19).

The *protractor pectoralis* is the only extrinsic muscle of the pectoral girdle. This ribbon-shaped muscle is usually very thin and is placed posterior to the *levator posterior* (see "Branchial musculature", below). In polynemids, the *protractor pectoralis* arises aponeurotically from the insertional tendon of *epaxialis* attached to the posterolateral portion of the neurocranium. This tendon of the *epaxialis* attaches onto the pterotic spine in most polynemids and onto the intercalar in *Eleutheronema*, *Filimanus*, *Pentanemus, Polydactylus opercularis,* and *P. plebeius*. *Eleutheronema* has the *protractor pectoralis* arising directly from the posterior tip of the intercalar. In *Galeoides*, there are some fibers that also arise from the ventral arm of the posttemporal. *Polynemus multifilis* has a *protractor pectoralis* greatly expanded, being larger than the *levator externus IV* (see "Branchial musculature"). Insertion is conservative amongst all examined taxa and occurs onto the membrane that connects the cleithrum with the last gill arch.

The *segmentum filamentaris* of the *abductor superficialis* is generally located at the ventral portion of the girdle. Origin is musculous and primarily from the lateral projection of the cleithrum, where the dorsalmost fibers are overlapped by the ventral portion of the *abductor superficialis radialis* (Fig. 17). *Parapolynemus*, however, have the opposite condition: the *segmentum filamentaris* covers laterally the ventralmost fibers of the *segmentum radialis* (Fig. 18A). Insertion is tendinous onto the dorsal region of the base of the lateral hemitrichia of all filaments. In most polynemids, the *segmentum radialis* is larger than the *segmentum filamentaris*, but in *Parapolynemus*, *Pentanemus*, and *Polynemus* the opposite is true (Fig. 18). The fibers of the *segmentum filamentaris* of the *abductor superficialis* are clustered into bundles that serve each filament individually. A considerable variation in the degree of differentiation of these bundles is observed across the family. *Parapolynemus*, *Pentanemus*, and *Polynemus* have these bundles well-developed and well-separated from each other, while all remaining polynemids have a continuity among bundles, especially at the origin.

The *segmentum filamentaris* of the *abductor profundus* is medial to the same segment of the *abductor superficialis*, originating musculously from the lateral faces of the cleithrum and coracoid (Fig. 18B). In *Galeoides* the fibers additionally arise from the lateral surface of the fourth pectoral radial. Insertion in all polynemids is invariably tendinous onto the lateral base of each filament. The *abductor profundus filamentaris* is also differentiated into bundles corresponding to the number of filaments. The dorsal bundle usually overlaps part of the subsequent ventral ones, except in *Galeoides* and *Parapolynemus*. As seen in the *abductor superficialis filamentaris*, the bundles of the *abductor profundus filamentaris* of *Parapolynemus*, *Pentanemus* and *Polynemus* are well developed and separated from each other in comparison to other genera. The general orientation of the fibers of the *segmenta radiales* of the *abductores superficialis* and *profundus* are usually opposed to each other: the former muscle has a posteroventral orientation towards the insertion, whereas the latter is oriented posterodorsally (Figs. 18B, 19).

Medial portion

The *segmentum radialis* of the *adductor superficialis* is a U-shaped well developed muscle (Fig. 20A) that extends beyond the posterior margin of the cleithrum, being thus

partially visible in lateral view just above the bases of the pectoral-fin rays (Figs. 17-19). The origin of the muscle segment is usually from the medial surface of the cleithrum and scapula. The *adductor superficialis radialis* of *Galeoides* and *Leptomelanosoma* additionally arises from the coracoid. The origin of the muscle in most polynemids is mixed, with the dorsalmost fibers having an aponeurotic origin and ventralmost arising musculously. The only exceptions in this pattern are present in *Galeoides, Polydactylus microstomus*, and *P. sextarius*, which have the *adductor superficialis* originating entirely musculous from the cleithrum and scapula. The insertion of the muscle occurs via tendons in a medioproximal region of the rays that is relatively distally from their bases. All rays except the first one are served by the *adductor superficialis radialis*. The fibers serving the ventral rays have a progressively more dorsal origin (Fig. 20A). The fibers associated with the second and third rays are much more prominent than the remaining fibers and have a well-developed tendinous portion, giving to these muscle portions a nearly bipinnate aspect. Nevertheless, all polynemids lack clear subdivision within the *adductor superficialis radialis*.

In polynemids the *adductor medialis radialis* is undifferentiated from the *adductor profundus radialis*. This muscle is mostly ventral to the *adductor superficialis radialis* and the dorsalmost fibers of the former usually cover the portion of the latter that inserts on the upper rays (usually the second and the third rays). As in sciaenids, the *adductor profundus radialis* of polynemids is differentiated into *partes ectoprofunda* and *endoprofunda* (Fig. 20B). The *pars ectoprofunda* is a robust layer of fibers that originates from the anterior margin of the cleithrum, medial face of the coracoid, and also from the membrane that covers the fenestra between these two bones. The *pars endoprofunda* is a deep, thin layer of shorter fibers originating only from the posterodorsal end of the medial face of the coracoid. Some fibers may also arise from the medial face of the scapula and from the adjoining area between coracoid and scapula. As the fibers proceed to the insertion, the *partes ectoprofunda* and *endoprofunda* gradually merge to each other and the whole *adductor profundus radialis* inserts onto the medial base of all medial hemitrichia.

The *arrector dorsalis* is not fully separated from the *adductor profundus radialis*, with the two muscles sharing some fibers proximate to their attachment on the pectoral girdle (Fig. 20B, 21). Close to the tendinous insertion, fibers of each muscle become more distinguishable from one another. Most of the fibers corresponding to the *arrector dorsalis*

originate musculously from the medial faces of the cleithrum and coracoid. Insertion of the muscle is onto the medial projection of the medial hemitrichium of the first (marginal) ray.

Another muscle that share fibers with the *segmentum radialis* of the *adductor profundus* is the *adductor radialis* (Fig. 20B). This muscle has shorter fibers originating musculously primarily from the medial surface of the first three pectoral radials and from the medial face of the scapula. The muscle insertion is tendinous onto the medial hemitrichium of the ventralmost rays.

The *segmentum filamentaris*, in medial view, is divided into *adductores superficialis, medialis,* and *profundus* (Fig. 20). This division pattern is very conservative across all examined polynemids, with some variations detected on the *adductor medialis* (see below). The *adductor superficialis filamentaris* is the major and most superficial muscle component of the medial face of the pectoral girdle (Fig. 21, 22). Part of this muscle covers the origin of the *adductor superficialis radialis*. This muscle is subdivided into bundles that serve each individual filament. These bundles are well-differentiated from each other since their tendinous origins on the dorsomedial face of the cleithrum until their insertions, via tendon, onto the medial hemitrichia of each pectoral filament. The anteriormost fibers are visible from a lateral view, anteriorly to the cleithrum. Generally the origin of the muscle is ventral to the Baudelot's ligament (Fig. 23B). However, in *Eleutheronema, Polydactylus plebeius,* and *P. sexfilis* the *adductor superficialis filamentaris* does not originates immediately ventral to the Baudelot's, but rather in a more ventral portion of the medial face of the cleithrum (Fig. 20). The thickness of the muscle bundles serving each individual filament varies between genera and, the longer the filament, the thicker the bundle is.

The *segmentum filamentaris* of the *adductor medialis* is located in between the same segments of the *adductores superficialis* and *profundus*. The fibers of the *adductor medialis filamentaris* are more horizontal than those from the two other muscles, which have fibers in a more vertical disposition (Figs. 20-23). None of these muscles share fibers between each other. Furthermore, the *adductor medialis* is differentiated into a lateral, innermost subsection termed *pars endomedialis*, which presents shorter and thinner bundles, and a more superficial, prominent subsection named *pars ectomedialis*, whose fibers form longer and thicker bundles. As the fibers proceed toward insertion, these subsections gradually

intermingle fibers and are no longer separable from each other. Both subsections of the *adductor medialis filamentaris* originate musculously from the medial surface of the coracoid and insert tendinously onto the medial hemitrichia of the filaments. The *adductor medialis filamentaris* of *Parapolynemus* and *Polynemus* additionally originates from the cleithrum (Fig. 22); in *Parapolynemus* the fibers arise from the medial surface of that bone and in *Polynemus* a few dorsal fibers also arise from the lateral surface of the cleithrum, passing through the cleithrum-coracoid fenestra.

Insertion of the *adductor medialis filamentaris* is quite variable among polynemids, with the muscle: *(i)* attaching on all pectoral filaments, a condition present in *Filimanus*, *Polydactylus microstomus, P. octonemus, P. oligodon, P. virginicus*, and *Polynemus*; *(ii)* miss only the ventralmost filament (first filament), which is the case of *Eleutheronema*, *Leptomelanosoma*, *Pentanemus*, *Polydactylus approximans, P. opercularis, P. plebeius,* and *P. sexfilis*; *(iii)* fail to reach the two ventralmost filaments, as in *Parapolynemus*; or *(iv)* attaching only to the three of ten filaments in total as in *Galeoides*.

Most polynemid genera have the *adductor medialis filamentaris* proportionally developed according to the length of their respective pectoral filament. *Galeoides* is an exception, having a poorly developed muscle with no differentiation into *partes endomedialis* and *ectomedialis* exposing its highly perforated coracoid (Fig. 23). *Eleutheronema* and *Polydactylus sexfilis* also present an undivided *adductor medialis filamentaris*. The *adductor medialis filamentaris* is typically subdivided into bundles that usually serve each pectoral filament. These muscle bundles are continuous to each other – the most common condition across polynemids – or fully divided from each other, a disposition present in *Parapolynemus, Pentanemus,* and *Polynemus*. *Parapolynemus* has seven pectoral filaments and only five bundles of the *adductor medialis filamentaris* (Fig. 22). Among these, only four bundles differentiate into *partes endomedialis* and *ectomedialis*; the ventralmost bundle, which attaches onto the third pectoral filament, is a single, undifferentiated muscle mass. The *pars ectomedialis* of *Polynemus* is divided into three large bundles that attach only onto the three dorsalmost pectoral filaments, whereas the *pars endomedialis* serves all filaments. Additionally, the fibers of the *pars endomedialis* of *Polynemus* arise from the medial face of the fourth pectoral radial. In *Pentanemus* all four

bundles have both the *partes endomedialis* and *ectomedialis* serving the four pectoral filaments.

The *segmentum filamentaris* of the *adductor profundus* is the innermost muscle of the medial portion of the pectoral girdle (Fig. 20B). Its origin is musculous mainly from the medial surface of the fourth pectoral radial (which is greatly expanded in polynemids), with fibers also arising from the posteroventral margin of the medial face of the coracoid and from the medial surface of the third radial. Usually, only the posterior fibers of the *adductor profundus filamentaris* (*i.e.* the fibers attaching on the uppermost filament) arise from the third radial. Insertion is tendinous onto the medial hemitrichia of all filaments. The *adductor profundus filamentaris* is normally differentiated into bundles that serve each individual filament and has a fan-like aspect, with a broad origin and a narrower insertion.

The innervation of the pectoral girdle of polynemids is quite distinct from that reported for other percomorphaceans. The orbito-pectoral branch of the *ramus lateralis accessorius* (RLA-OP) is the major highlight in the pectoral girdle (Figs. 20A, 21, 22, 23B). This nerve arises from the *trigeminus-facialis* trunk, curves dorsally and runs posteriorly medial to the autosphenotic and pterotic (Fig. 24). The RLA-OP continues beyond the posterior end of the pterotic and proceeds toward the posttemporal. Medially to the posttemporal, the RLA-OP then runs ventrally passing medial to the supracleithrum and cleithrum. At the level of the dorsal region of the cleithrum, the RLA-OP merges with the second spinal nerve (SP2), which is a massive nerve that runs over the surface of the *adductor superficialis filamentaris* towards the pectoral filaments (Figs. 21, 22, 23B). *Eleutheronema* is unique in having the compound SP2+RLA-OP nerve body running posterior to that muscle (Fig. 20A).

The first spinal nerve (SP1) and the occipito-spinal nerves (OS) also arrive medially to innervate the pectoral girdle. The SP1+OS branch is anterior to and usually thinner than SP2 (Fig. 25). In *Pentanemus* and *Parapolynemus* the main trunk of the SP2 overlaps, in medial view, the main trunk of the SP1+OS at the pectoral girdle level (Figs. 21, 22). In all other polynemids, these two trunks are more easily distinguishable in medial view. SP1+OS passes through the scapular foramen to innervate the lateral portion of the pectoral girdle and runs in between the boundaries of the *segmenta radiales* of the *adductor superficialis* (dorsal) and *adductor profundus* (ventral). This pattern is also present in *Cynoscion*. The RLA-OP varies in thickness across polynemids and *Pentanemus* is the only exception in which the

RLA-OP bifurcates right after exiting the neurocranium. The two resulting branches then merge with SP2 at the cleithrum level as in the other polynemids.

3.4 Branchial musculature

Sciaenidae

Suprabranchial musculature

The *levatores externi* originate from the pterotic and prootic and insert onto the uncinate process of each epibranchial, therefore, there is one *levator externus* for each epibranchial. The origin of all *levatores externi* is tendinous and the insertion varies among muscles. The *levatores externi I* and *II* have a mixed insertion, where the posterior fibers converge to a tendon whereas the anterior ones attach musculously onto the respective epibranchials. On the other hand, the *levatores externi III* and *IV* insert purely musculously. The *levator externus IV* is the most lateral muscle and the first *levator* is the medial one. *Levatores externi III* and *IV* are deep posteroventrally orientated and run parallel to one another. In contrast, *levatores externi I* and *II* are ventrally/slightly posteroventrally orientated and do not run parallel to each other.

The *levatores interni II* and *III* also originates from the neurocranium, with fibers arising from the pterotic and prootic. Insertion occurs onto pharyngobranchials 2 and 3. Both origin and insertion are musculously. The *levator internus II* is medial to and larger than the *levator internus III*. In lateral view, the *levator internus III* is parallel to the *levator externus II* and although they do not share any fibers, the two muscles are very closely associated.

The *levator posterior* is posterior to all *levatores* muscles, originating tendinously from the intercalar and inserting onto the uncinate process of the fourth epibranchial, posterolaterally located in comparison to the *levator externus IV* insertion. The *levator posterior* is considerably thinner than the *levator externus IV* and there is a hiatus between those two muscles (which is where the *adductor operculi* is placed).

The *transversus dorsalis II* (TD II) is a muscle that connects the contralateral elements of the second branchial arch (Fig. 26). Specifically, the TD II attaches only onto the epibranchials (see polynemids below). On the central portion, there is a longitudinal raphe

that runs posteriorly throughout the muscle, separating it into left and right counterparts. From this central raphe towards the edges, the fibers twist before attaching on epibranchial 2. The TD II is completely free from the following *transversus* muscle, the *transversus dorsalis III* (TD III). The TD III is posterior to TD II, showing a gap of connective tissue between muscles. Alternatively to TD II configuration, the *transversus dorsalis III* connects the contralateral epi- and pharyngobranchials from the third branchial arch (Fig. 26). The TD III is visibly less developed than the previous transversus and the posterior fibers are continuous to those from the *sphincter oesophagi* (see below).

The *obliquus dorsalis* is a robust muscle that connects the dorsal face of the third pharyngobranchial with the third and fourth epibranchials (Fig. 26). On epibranchial 3, the fibers of the *obliquus dorsalis* attach on the anterodorsal face of the bone and on the dorsal projection that articulates with epibranchial 4. On the fourth epibranchial, the fibers of the *obliquus dorsalis* attach on the anterodorsal face and onto the projection that articulates with the cartilaginous pharyngobranchial 4. The *obliquus dorsalis* is organized in a way that its origin is dorsal to the *transversus dorsalis III* fibers and its insertion lies ventrally to the *transversus dorsalis II*.

The *obliquus posterior* is immediately posterior to the *obliquus dorsalis*. This muscle connects the posterodorsal end of the fifth ceratobranchial to the posteromedial surface of epibranchial 4 and its uncinate process. The medial portion of the *obliquus posterior* share fibers with the *sphincter oesophagi* and those fibers run ventrally to all suprabranchial musculature described above. The lateral most fibers attach oppositely to the *levator externus IV* insertion, whose insertion lies onto the lateral face of the uncinate process of epibranchial 4.

The *adductores branchiales IV* and *V* together with the *obliquus posterior* form the posterior wall of the branchial arches. The *adductor branchialis IV* is lateral to the *obliquus posterior*, uniting the posterior tip of ceratobranchial 4 to the posteromedial face of epibranchial 4 and its uncinate process. The medial fibers of the *adductor branchialis IV* matches the insertion of the *levator posterior* fibers which, in turn, attaches onto the lateral face of the uncinate process from the fourth epibranchial. The *adductor branchialis V* is a small muscle that is located posteroventrally to the *obliquus posterior* and *adductor branchialis IV*. This muscle connects the posterior tip of ceratobranchial 5 to the

posteromedial face of ceratobranchial 4, where some fibers also attach onto the cartilaginous articulation between cerato- and epibranchials of the fourth branchial arch.

The *retractor dorsalis* is a well developed paired muscle that originates musculously from the second vertebra and inserts onto the pharyngobranchials. The insertion is covered by the *transversus dorsalis III* and immediately posterior to the TD III fibers, some *sphincter oesophagi* fibers are dorsal to the *retractor dorsalis*. The *sphincter oesophagi* is the whole musculature that engulfs the esophagus. This muscle is share fibers anterodorsally with the *transversus dorsalis III*, posterolaterally with the *obliquus posterior*, and anteroventrally with the *transversus ventralis V* (see below).

The *interbranchiales abductores* are small muscles that connect the gill rakers/ceratobranchials to the base of the gill filaments. On the first arch, the fan-shaped muscle originates from the gill raker bases and is visible on the anterior faces of cerato- and epibranchial, covering the articulation site between those bones. However, on the second and third arches the *interbranchiales abductores* lost the fan aspect, in which they are diagonally arranged, originating from the anterior face of the cartilaginous tip of the ceratobranchials. The *interbranchiales abductores* are absent on the fourth branchial arch.

Infrabranchial musculature

The *obliqui ventrales* muscles are present on the first three branchial arches, only. These muscles are practically restricted to the canal formed by the hypobranchials (Fig. 26). Therefore, the *obliqui ventrales I* to *III* originate tendinously from the anteroventral face of each ceratobranchial and insert musculously onto the ventral face of the respective hypobranchials. All three *obliqui ventrales* have a bipinnate aspect and the first one is poorly developed in comparison to the other two.

The *rectus ventralis IV* is a muscle that divides space with the *obliquus ventralis III*, originating tendinously from the anteroventral tip of ceratobranchial 4 and inserting, also tendinously, on the anteroventral projection of hypobranchial 3. The *rectus ventralis IV* origin is located medially to both the *obliquus ventralis III* and *rectus communis* (Fig. 26). The *rectus communis*, in turn, is a muscle that originates aponeurotically from the membrane that attaches itself throughout the ventral margin of ceratobranchial 5. Insertion is

tendinously on the dorsal surface of the urohyal. The two contralateral portion of the *rectus communis* converge medially to insert onto the urohyal.

The *transversi ventrales IV* and *V* form the ventral floor of the branchial arches musculature. These muscles connect the contralateral ceratobranchials from the fourth and fifth branchial arch, respectively (Fig. 26). The *transversus ventralis IV* is very developed, with no raphe on its surface and completely free from the following *transversus* muscle. On the other hand, the *transversus ventralis V* is thinner than its predecessor even though it is longer (on the anteroposterior axis) than the *transversus ventralis IV*. Moreover, the *transversus ventralis V* is differentiated into sections anterior and posterior. The anterior section is continuous throughout the attachment sites (on ceratobranchials 5), with no differentiation within the fibers. This section runs anterodorsally to the *transversus ventralis IV*, therefore, in ventral view, the *transversus ventralis IV* covers the anteriormost fibers of the fifth *transversus ventralis*. The posterior section of the *transversus ventralis V* has a longitudinal raphe cutting the ventral surface of this section and is even thinner than the anterior counterpart. The posterior fibers of the posterior section are common to those from the ventral portion of the *sphincter oesophagi*.

Posterior to the *transversus ventralis IV* there is the *pharyngoclavicularis externus*, which originates from the anterolateral surface of the cleithrum and inserts onto the ventral face of ceratobranchial 5 (Fig. 26). Both origin and insertion are musculously. The anterior margin of the *pharyngoclavicularis externus* is not immediately posterior to the transversus ventralis IV, there is a hiatus between those muscles. The *pharyngoclavicularis externus* is a laminar muscle located medially to the aponeurotic origin of the *rectus communis* and laterally to the fibers of the *pharyngoclavicularis internus* (see below).

The *pharyngoclavicularis internus* is medially placed in comparison to the *pharyngoclavicularis externus* (Fig. 26). The *internus* muscle also originates musculously from the anterior face of the cleithrum (from its concave curvature) and inserts onto the fourth and fifth ceratobranchial. The *pharyngoclavicularis internus* has a further division: it is divided into posterodorsal and anteroventral sections. The posterodorsal section has shortened fibers that insert musculously onto the ventral face of ceratobranchial 5, directly posterior to the *pharyngoclavicularis externus*. However, some fibers also insert medially to the *pharyngoclavicularis externus*. In contrast, the anteroventral section is a rather long

musculature that inserts tendinously on ventral face of the anterior tip of ceratobranchial 4. The anteroventral section dives toward the *transversus ventralis IV* and in ventral view the former covers the anterior region of the anteroventral section of the *pharyngoclavicularis internus*. The insertion site is anterior to and not covered by the *transversus ventralis IV*.

Polynemidae

Suprabranchial musculature

The *levatores externi I* to *IV* are extrinsic branchial muscles that originate from the pterotic and prootic and insert tendinously on the uncinate process of each epibranchial, respectively. The *levatores externi I* and *II* originate musculously whereas the *levatores externi III* and *IV* originate tendinously from the neurocranium. Usually, the tendinous insertion of *levator externus I* is not very developed among polynemids. However, in *Filimanus* and *Pentanemus* it is very expressive: at least half or more of the total length of the *levator externus I* is the tendinous portion that attaches the fibers onto the bone (Fig. 27A). Moreover, the *levator externus I* can have a differentiation within its fibers, separating the muscle into posterolateral and anteromedial portions that share fibers on the origin (Fig. 27B). The posterolateral section is poorly developed while the anteromedial section constitutes the main body of muscles of the *levator externus I*. This condition is present in *Parapolynemus, Polydactylus approximans, P. octonemus, P. virginicus,* and *Polynemus*.

The *levatores externi III* and *IV* run parallel to each other, where their fibers are intensely posteriorly orientated while the *levatores externi I* and *II* are not parallel to each other and are slightly posteriorly orientated (Fig. 27). Nonetheless, *Parapolynemus* is the sole exception for this case. In this genus the fibers of the *levator externus II* and the posterolateral section of the *levator externus I* are disposed in the same direction as the fibers from the *levatores externi III* and *IV*, in which they all are deeply posteriorly orientated while the anteromedial section of the *levator externus I* is the only *levator* that is more vertical orientated. As seen in sciaenids, the *levator externus IV* is lateral to all *levatores* whilst the first one is the medial unity of all *levatores externi*.

The *levatores interni II* and *III* originate musculously from the pterotic and prootic and insert – also musculously – on the dorsal face of pharyngobranchials 2 and 3, respectively. The *levator internus II* is medial to and thicker than the *levator internus III*. Except in

Parapolynemus, the *levator internus III* is immediately medial to the *levator externus II* and both muscles run parallel to one another.

The *levator posterior*, as the name indicates, is posterior to all described *levatores*. It originates musculously from the intercalar and inserts tendinously onto the uncinate process of the fourth epibranchial (Fig. 27). Insertion of the *levator posterior* is posterolateral in comparison to the *levator externus IV*. Moreover, the *levator posterior* usually has the same size or is slightly smaller than the fourth *levator externus* and in between these muscles there is a hiatus which is where the *adductor operculi* is located. The *levator posterior* is frequently arranged as a single bundle of fibers. However, in *Galeoides*, *Leptomelanosoma*, *Polydactylus microstomus*, and *Polynemus* this muscle is differentiated into posterolateral and anteromedial sections that share fibers on the origin site (Fig. 27B). This differentiation is more evident near the insertion and across the main body of the muscle those sections seem to lightly intertwine like a DNA ribbon.

The *transversi dorsales II* and *III* are intrinsic muscles that connect the contralateral dorsal elements of the second and third branchial arches, respectively. The *transversus dorsalis II* has a central longitudinal raphe on its dorsal surface and attaches onto the second epi- and pharyngobranchials (Fig. 28). Therefore, this muscle presents a differentiation within its fibers, in which the anteriormost fibers attach on pharyngobranchials 2 and the posterior ones connects epibranchials 2. In most of the cases, the anterior section of the *transversus dorsalis II* overlaps dorsally – in dorsal view – some fibers from the posterior section. Generally, the anterior section is greatly expanded posteriorly in comparison to the posterior complement, reaching half or more of the longitudinal length of the posterior section (Fig. 28B). Yet, in *Parapolynemus* and *Polynemus*, the anterior section is weakly expanded posteriorly, reaching less than half of the total length of the posterior section (Fig. 28A, 29A). The anterior section of *Parapolynemus* is significantly smaller than the posterior section, in which only a few fibers are dorsally to the former. The shape of the posterior section is very consistent among polynemids, which is differently for the anterior section. Among undistinguished shapes, *Filimanus similis* and *Pentanemus* have a very clear triangular-shaped anterior section. The longitudinal raphe on the dorsal surface of the *transversus dorsalis II*, in most of the cases, fails to reach the anteriormost fibers of the anterior section, thus those anterior fibers connect the second epibranchials continuously

(Fig. 29A). The opposite condition (*i.e.* the longitudinal raphe extends throughout the *transversus dorsalis II* body) is present only in *Eleutheronema, Galeoides,* and *Polydactylus plebeius* (Fig. 28B).

Posterior to the *transversus dorsalis II* is the *transversus dorsalis III*, which connects the contralateral epi- and pharyngobranchials 3. This muscle usually shows continuity to the previous *transversus* muscle and this bond can be seen in *Eleutheronema, Parapolynemus, Polydactylus virginicus, P. microstomus, P. opercularis, P. plebeius, P. sexfilis,* and *Polynemus* (Fig. 28A). Moreover, the boundaries of *transversi dorsales II* and *III* can be intimately associated or in between these muscles can be a gap of connective tissue, visible in dorsal view. This hiatus is present in almost all polynemids and only in *Filimanus, Galeoides, Leptomelanosoma, Polydactylus microstomus,* and *Polynemus paradiseus* there is no band of connective tissue between *transversi* muscles (Fig. 28B). Although the *transversus dorsalis III* connects primarily the elements from the third branchial arch, in almost all polynemids (except *Eleutheronema*) the posteriormost fibers also attach on pharyngobranchial 4 (but not on epibranchial 4). The posterior margin of the *transversus dorsalis III* shares fibers with the *sphincter oesophagi* (see below).

The *obliquus dorsalis* is a sturdy muscle that originates musculously from the anterodorsal face of the uncinate process of epibranchials 3 and 4 and from the projection of epibranchial 4 that articulates with the cartilaginous pharyngobranchial 4 (Figs. 28, 29A). Insertion is also musculous and occurs on the third pharyngobranchial of the same side; therefore – in dorsal view – the anterior region of the *obliquus dorsalis* is ventral to the *transversus dorsalis II* while the posterior region is dorsal to the *transversus dorsalis III*. From this configuration, the insertion of the *obliquus dorsalis* usually is all covered by the fibers of the *transversus dorsalis II*. Nonetheless, in *Parapolynemus, Pentanemus,* and *Polydactylus opercularis* the insertion of the medial fibers is exposed and can be seen in dorsal view (Fig. 28A).

The *obliquus posterior* is located posteriorly to the *obliquus* described above, connecting the posteromedial face of ceratobranchial 5 to the posterior face of the uncinate process of epibranchial 4 and to its projection that articulates with pharyngobranchial 4 (Fig. 30). The medial fibers of the *obliquus posterior* are shared with the *sphincter oesophagi* (see

below) and the lateralmost fibers attach onto epibranchial 4 oppositely to the insertion of the *levator externus IV*.

The *adductores branchiales IV* and *V* with the *obliquus posterior* form the posterior wall of the branchial arches. The *adductor branchialis IV* which is parallel and lateral to the *obliquus posterior* connects ceratobranchial 4 to epibranchial 4 of the same side (Fig. 30). In most of the cases, the *adductor branchialis IV* is undifferentiated (Fig. 31B) but, in *Filimanus, Polydactylus approximans, P. octonemus, P. oligodon, P. virginicus,* and *P. sexfilis* the *adductor branchialis IV* shows a differentiation within its fibers, where it is possible to distinguish an anteromedial and a posterolateral section (Fig. 30). The medialmost fibers of the anteromedial section are covered by the *obliquus posterior* lateral fibers (in a posterior view). These fibers of the anteromedial section are longer, reaching the posterior face of the uncinate process of epibranchial 4 and opposite to the *levator posterior* insertion. The posterolateral section, in turn, has shorter fibers that are not covered by the *obliquus posterior* and reach the posterior portion of the fourth epibranchial, close to the articulation with ceratobranchial 4.

The *adductor branchialis V* is an undersized muscle that is posteroventrally placed in comparison to *adductor branchialis IV* and *obliquus posterior*. The fifth *adductor branchialis* connects the posteriomedial tips of ceratobranchials 4 and 5. The lateralmost fibers also attach on the cartilaginous pads of the articulation between cerato- and epibranchial 4 (Figs. 30, 31B).

The *retractor dorsalis*, which originates from the second vertebra and inserts on the pharyngobranchials, is a very robust muscle located on the posterodorsal end of the branchial arches (Figs. 28-30, 31B). The anterior portion and consequently the insertion of this muscle are covered by the *transversus dorsalis III* fibers. At this point, the *transversus dorsalis III* is continuous to the *sphincter oesophagi* fibers, which in turn, are dorsally positioned to the anterior region of the *retractores dorsales* (Fig. 28). The *sphincter oesophagi* is the entire musculature that surrounds the esophagus, being continuous to several other musculatures (Figs. 28-30). Therefore, the *sphincter oesophagi* shares fibers anterodorsally with the *transversus dorsalis III*, posterolaterally with the *obliquus posterior*, and anteroventrally with the *transversus ventralis V* (see below).

As seen in sciaenids, the *interbranchiales abductores* are tiny muscles that connect the gill rakers/ceratobranchials to the base of the gill filaments. Those muscles are present on the first three branchial arches, only. The *interbranchialis abductor I* (*i.e.* from the first branchial arch) is very conservative among polynemids. This fan-shaped muscle is located on the anterior face of the articulation between cerato- and epibranchial (Fig. 27). Its origin is from the gill rakers bases and insertion occurs on the base of the gill filaments. The *interbranchiales abductores II* and *III* have an oblique arrangement, originating from the anterior faces of the cartilaginous pad of the respective ceratobranchials and inserting on the gill filament bases and on the anterior faces of the respective epibranchials (Fig. 27). Nonetheless, in *Galeoides, Polydactylus microstomus,* and *P. sextarius,* the *interbranchiales abductores II* and *III* apparently lost their insertion onto the gill filaments and attach solely onto the dorsal faces of each respective epibranchials. *P. microstomus* and *P. sextarius* show an intermediate condition from the basic polynemid configuration to what is found in *Galeoides*. In *Galeoides*, the *interbranchiales abductores II* and *III* are greatly expanded onto the dorsal face of the epibranchials (Fig. 28B). In all those three genera, the *interbranchiales abductores II* and *III* have a bipinnate aspect and the third one is more developed than the second.

Infrabranchial musculature

The *obliqui ventrales I* to *III* are bipinnate muscles located on the ventral face of the branchial arches. The main portion of each muscle is restricted to the canal formed on the ventral face of each hypobranchial (Fig. 32). They originate tendinously from the anterior end of the ventral face of each ceratobranchial and insert musculously on the ventral surface of each hypobranchial, respectively. The *obliquus ventralis I* is the smallest of all three *obliquus ventrales* and the *obliquus ventralis III* is normally the largest of all.

The *rectus ventralis IV* is a ventral longitudinal muscle that originates tendinously from the ventral face of the anterior tip of ceratobranchial 4 and inserts onto hypobranchial 3. The insertion is mixed, in which the ventralmost fibers attach tendinously on the anteroventral projection of hypobranchial 3 and musculously on the ventral surface of that same bone. Differently from sciaenids, the origin of the *rectus ventralis IV* of polynemids is always lateral to the *rectus communis* fibers (see below). Therefore the *rectus ventralis IV* is

placed in between the *obliquus ventralis III* (medial to) and *rectus communis* (lateral to) (Fig. 29B, 31A, 32).

The *rectus communis* is a long muscle running towards the anterior region of the branchial arches. This muscle originates from the ventral face of ceratobranchial 5 and this origin is usually aponeurotically (Fig. 32). However, in *Parapolynemus* and *Polynemus* the flat tendinous tissue is thicker, forming a tendon from where the fibers arise (Fig. 29B). The two contralateral portions converge medially to insert tendinously on the dorsal face of the urohyal. The *rectus communis* and *rectus ventralis IV* run parallel to each other and do not share any fibers.

The *transversi ventrales IV* and *V* connects the contralateral ceratobranchials of the fourth and fifth branchial arches, respectively (Fig. 29B, 31A, 32). The *transversus ventralis IV* is a well developed muscle located on the anterior region of ceratobranchial 4 and in most of the cases its ventral surface is smooth, with no raphe or apparent differentiation within the fibers. Still, *Galeoides, Leptomelanosoma,* and *Polydactylus microstomus* show a distinct pattern: their *transversus ventralis IV* has a kind of rough ventral surface due to several tendons within the fibers, giving it a multipennate aspect (Fig. 31A).

The *transversus ventralis V* is considerably thinner than the fourth *transversus ventralis* and occupies a larger portion of ceratobranchial 5 (Fig. 32). The *transversus ventralis V* is differentiated into anterior and posterior section, in which the anterior section runs anteriorly dorsal to the *transversus ventralis IV*, whose fibers, in ventral view, cover the anterior region of the anterior section of the *transversus ventralis V*. This anterior section is continuous between the contralateral ceratobranchials 5, *i.e.* there is not any kind of raphe in between the fibers. On the other hand, the posterior section of the *transversus ventralis V* has a longitudinal central raphe cutting the muscle into two halves. The size of the sections varies among polynemids. In *Filimanus, Leptomelanosoma, Parapolynemus, Pentanemus, Polydactylus octonemus, P. oligodon,* and *Polynemus* the posterior section is smaller than the anterior one (Fig. 29B) and the opposite is present in the rest of polynemids (Fig. 32), except *Polydactylus plebeius* whose *transversus ventralis V* is not differentiated into sections. Usually, the limit between sections is a perpendicular straight line, however in *Eleutheronema tridactylum* and *Polydactylus approximans*, the boundary between sections is oblique. Moreover, independently if the *transversus ventralis V* is or not differentiated into

sections, in almost all polynemids this muscle attaches musculously onto ceratobranchials 5. The only exception is present in *Galeoides* and *Leptomelanosoma*, where the *transversus ventralis V* attaches tendinously on the fifth ceratobranchial (Fig. 31A). The posterior region of the *transversus ventralis V* shares fibers with the anteroventral region of the *sphincter oesophagi*.

Both *pharyngoclavicularis externus* and *internus* are extrinsic branchial muscles that connect the cleithrum to the branchial arches. The *pharyngoclavicularis externus* (Fig. 29B, 30, 31A, 32) is immediately posterior to the *transversus ventralis IV* fibers and this muscle is very conservative among polynemids, originating musculously from the anterolateral surface of the cleithrum and inserting also musculously on the ventral face of ceratobranchial 5. The *pharyngoclavicularis externus* is a ribbon-shaped muscle placed in the middle of the aponeurotic origin of the *rectus communis* and the fibers of the anteroventral section of the *pharyngoclavicularis internus* (see below).

The *pharyngoclavicularis internus* originates aponeurotically from the concave curvature of the anterior face of the cleithrum, right where the pectoral muscle *adductor superficialis* of the *segmentum filamentaris* is visible (in lateral view). Insertion occurs onto the ventral faces of ceratobranchials 4 and 5. The *pharyngoclavicularis internus* is differentiated into section anteroventral and posterodorsal, with a varied degree of separation among genera (Fig. 29B, 30-32). The most common condition within polynemids is the complete separation of sections, yet, *Eleutheronema, Polydactylus plebeius,* and *P. sexfilis* have the anteroventral and the posterodorsal sections sharing fibers on their origin. In between these sections there is a small tendon that attaches fibers from both sections (Fig. 32). The posterodorsal section, which has shorter fibers, inserts on the ventral face of ceratobranchial 5, posteriorly to the *pharyngoclavicularis externus* insertion. Nevertheless, in *Eleutheronema, Filimanus, Galeoides, Polydactylus microstomus, P. plebeius,* and *P. sexfilis* some fibers might also attach medially to the *pharyngoclavicularis externus*. Usually, the posterodorsal section of the *pharyngoclavicularis internus* inserts musculously on ceratobranchial 5, however in *Filimanus*, *Galeoides*, *Parapolynemus*, and *Polynemus* the insertion is tendinous. Additionally, the posterodorsal section of the *pharyngoclavicularis internus* can have a further differentiation into subsections anterior and posterior that share fibers on the origin. This condition is only present in *Filimanus, Parapolynemus,* and

Polynemus. Finally, the anteroventral section of the *pharyngoclavicularis internus* has longer fibers that run anteriorly toward the *transversus ventralis IV*, passing dorsally to the intrinsic branchial muscle and inserting tendinously on the anterior region of the ventral face of ceratobranchial 4. In ventral view, the *transversus ventralis IV* covers the anterior region of the anteroventral section of the *pharyngoclavicularis internus.*

3.5 Pectoral filaments in light of Electron Microscopy

In general, the basic micro-surface of a pectoral filament is constituted by the presence of a smooth region of skin and a rough portion with small papillae and ridges along the surface (Fig. 33). This roughness portion matches the location of the SP2+RLA-OP branch which runs through all the filaments length. The typical taste buds onion-shaped papillae, that are small protuberances with an opening to the environment (Reutter *et al.*, 1974; Kasumyan, 2019), were only visible in *Filimanus xanthonema* (Fig. 34). In *Leptomelanosoma*, it is possible to observe several small openings on the pectoral roughened surface, but with no elevation from the epidermis (Fig. 33B). *Galeoides* present several tiny papillae on the nerve region (Fig. 33A). All the other polynemids have only ridges on the nerve region and it was very difficult to determine any taste-bud like structure (Fig. 33C). Nevertheless, those ridges may represent small grooves, which may lead to even smaller canals to then stimulate the nerve underneath the skin. Furthermore, *Eleutheronema* and *Galeoides* presented in their pectoral filament tip a round-like structure (Fig. 35, 36), implying that the nerve ending is a region of sensory stimulation as well (see discussion).

4. DISCUSSION

The *adductor mandibulae* is the most remarkable cranial muscle of bony fishes, standing out in terms of size, architecture, and involvement in vital functions such as feeding and respiration (Datovo and Vari, 2014). The muscle is primarily responsible for the jaw closing during food intake and gill ventilation. The *adductor mandibulae* is actually a myological complex that may range from a single, mostly undivided muscle mass to an elaborate structure with up to ten subdivisions variously interconnected to each other (Winterbottom, 1974a; Datovo and Vari, 2013). The *malaris* section, located directly posteroventral to the eyeball, is usually the larger component of the *adductor mandibulae* in percomorphaceans. This section can be further subdivided into a posteroventral *retromalaris* and an anterodorsal *promalaris*, but such subdivision is typically partial and observable only at insertion (Datovo and Vari, 2013; 2014). In the most common condition, the *malaris* is undivided at origin and, as the muscle proceeds toward insertion, the fibers originating more dorsomedially gradually separates from the ventrolateral ones to form differentiated *promalaris* and *retromalaris*, respectively. Sciaenidae, Sphyraenidae, and Polynemidae are among the rare taxa with *promalaris* and *retromalaris* completely separated from each other since their origins (present study; Sasaki, 1989; Pastana, 2019; Datovo et al., in prep.). In the former family, the origin of the *promalaris* is medial relative to the origin of the *retromalaris* (Fig. 2; Sasaki, 1989: fig. 29). This medial origin is likely plesiomorphic because it resembles the configuration found in most generalized percomorphaceans with a *promalaris* only partially differentiated (Datovo and Vari, 2013: fig. 7; 2014: fig. 5A, B). Sphyraenids have a highly modified *promalaris* placed anterolateral to all remaining sections of the *segmentum facialis* of the *adductor mandibulae*, with an origin from the lateral ethmoid and infraorbital bones and ligaments (Pastana, 2019; Datovo et al., in prep.; = A1 of Grubich et al., 2008, and Habegger et al., 2011). Polynemids contrastingly have a *promalaris* with a broad aponeurotic origin mainly from the preopercle, lying completely lateral to all remaining facial sections of the *adductor mandibulae* (Figs. 3, 7). Such condition was not found elsewhere among actinopterygians and is herein interpreted to be a unique synapomorphy for the family. This conclusion is partial agreement with that of Kang et al. (2017: character 15). That study considered that the whole subdivision pattern of the *malaris* (their adductor mandibulae

section 1 or A1) was unique to polynemids among perciforms. However, as we discussed above, only the lateral aponeurotic origin of the *promalaris* on the preopercle can be more precisely optimized as a synapomorphy for the family.

The present analysis further reveals that polynemids and sciaenids have a *promalaris* with an additional differentiation into *partes promalares interna* and *externa*, with the *externa* portion attaching onto the maxilla via ectomaxillar ligament and the *interna* portion inserting either via endomaxillar ligament (most polynemids; Figs. 4, 5, 8) or directly on that bone (sciaenids and *Polydactylus sextarius*; Figs. 2B, 9B). This further differentiation of the *promalaris* section is not reported for any other percomorphacean and may be an additional morphological evidence of closer relationship between Sciaenidae and Polynemidae (Johnson, 1993; Kang et al. 2017).

Mugilidae was also previously suggested to be closely related to Polynemidae (Gosline, 1962; Rosen, 1964; Gosline, 1968; 1971). Members of this family, however, present *adductor mandibulae* morphologies markedly distinct from those of polynemids. In mugilids, the *malaris* is undivided and inserts solely on the lower jaw, whereas the *rictalis* attached on the maxilla (Starks, 1916; Eaton, 1935; Van Dobben, 1935; Gosline, 1993; Wu and Shen, 2004). This pattern is relatively rare among acanthomorphs and shared with atherinomorphs (Datovo and Vari, 2013; Datovo et al., in prep.), a group suggested to be closely related to mugilids based on morphological evidence (Stiassny, 1990; Datovo *et al.*, 2014).

The musculature of the hyopalatine arch and the opercular series are other important groups of cephalic muscles that play crucial roles in feeding and gill ventilation (Osse, 1969; Lauder, 1980; 1982; Lauder and Clark, 1984). In polynemids and sciaenids the *pars primordialis* of the *levator arcus palatini* (*sensu* Datovo and Rizzato, 2018) is differentiated – and in some cases even subdivided – into subsections *externa* and *interna*. The *pars primordialis externa* is the largest component of the *levator arcus palatini*, whereas the *pars primordialis interna* is usually a small portion of the whole muscle that is restricted to posterodorsal region of the orbit capsule (Fig. 12B, 13B). In a few polynemid species the inner portion of the *primordialis* section is greatly expanded anteriorly, covering most of the dorsal portion of the orbit capsule (Figs. 11B, 12A). Although some differentiations within

the *levator arcus palatini* has been documented in the literature (Winterbottom, 1974a; 1993; Datovo and Rizzato, 2018), apparently no reference have been made to a similar subdivision pattern into *partes primordiales externa* and *interna*, as well as the massive expansion of the latter in some polynemids. If this subdivision pattern proves to be more widespread across sciaenids, that feature might constitute an additional anatomical evidence of a closer relationship between polynemids and sciaenids.

Another uncommon feature present in the hyopalatine arch of polynemids (except *Filimanus* and *Parapolynemus*) is the visibility – with a varying degree – from a medial view of the posteroventral fibers of the *dilatator operculi* in between the hyomandibula and opercle (Fig. 11B). A slightly similar condition is present in *Aphanopus carbo* and *Trichiurus lepturus* (Trichiuridae). However, the *dilatator operculi* in these trichiurids has two portions, a dorsal one that retains the general morphology of a typical teleostean *dilatator operculi* and an additional ventral portion that extends from the medial face of the hyomandibula to the dilatator process of the opercle (De Schepper *et al.*, 2008: fig. 3). This ventral portion of the *dilatator operculi* is visible in medial view, but it is very distinct from the *dilatator operculi* of polynemids that has only the plesiomorphic dorsal muscle division. To our knowledge this characteristic found in the *dilatator operculi* of polynemids is not documented elsewhere in the literature and interestingly *Cynoscion* also present this *dilatator operculi* condition (Fig. 10B), once again suggesting that these families are closely related.

The gill-arch musculature is an extreme intricate muscular system that exhibits remarkable degrees of variation and high systematic value for different groups of Percomorphacea (Springer and Johnson, 2004; Datovo *et al.*, 2014). *Levator externus I*, usually associated with the first epibranchial, is normally found as a single mass of fibers, with no apparent differentiations or subdivisions (Springer and Johnson, 2004). Nonetheless, as reported herein, in *Parapolynemus, Polydactylus approximans, P. octonemus, P. virginicus,* and *Polynemus* the lateral portion of *levator externus I* is differentiated into a posterolateral thin section and a anteromedial section that represents most of the fibers of the muscle (Fig. 27B). Similar types of differentiations have been reported for other *levatores externi* (*e.g. levator externus II* in *Diaphus mollis*; Winterbottom, 1974a; Springer

and Johnson, 2004). However, we found no report of differentiations in *levator externus I* as herein found in the referred polynemids.

The *interbranchiales abductores* are minute, often overlooked muscles that usually form a thin layer of fibers over the lateral surfaces of the branchial arches, interconnecting parts of its endochondral bones, gill rakers, and gill filaments (Winterbottom, 1974a). The present analysis indicates that polynemids and *Cynoscion* have these small muscles on the first three gill arches only. The first one is very conservative across all analyzed taxa, having a fan aspect and located on the ceratobranchial-epibranchial joint (Fig. 27). This morphology is similar to that reported for *Parahollardia lineata* (Triacanthodidae, Tetraodontiformes) by Springer and Johnson (2004: plate 79). Nevertheless, the *interbranchiales abductores* present in the second and third gill arches of *Galeoides, Polydactylus microstomus,* and *P. sextarius* (clade L – see discussion of Chap. 2) apparently lost their connections with the gill filaments and became greatly expanded dorsally so as to occupy the dorsal face of epibranchials 2 and 3, respectively. *Galeoides* present the most extreme morphology in which the *interbranchiales abductores II* and *III* cover most of the dorsal face of their associated epibranchials (Fig. 28B). Springer and Johnson (2004) commented that this dorsomedial expansion over epibranchials 2 and 3 is also found in other acanthomorphs. However, some uncertainties surround the identity of these modified *interbranchiales abductores* and their distinction from the *adductores branchiales*, which typically interconnect the internal surfaces of the epibranchial and ceratobranchial of each gill arch. The polynemid *interbranchiales abductores II* and *III* are somewhat similar to what had been documented by Springer and Johnson (2004) for *Mastacembelus armatus* (Mastacembelidae, Synbranchiformes) and, although the authors identified such muscles as *adductores branchiales* (= their *adductores* or Ad), they commented that the muscles might correspond to *interbranchiales abductores* (= their "gill filament muscle" or GFM). The polynemid condition is even more similar to that of *Agonostomus monticola* (Mugilidae, Mugiliformes). However, Springer and Johnson (2004) referred to the muscle from the first branchial arch as *interbranchialis abductor* and to those of the subsequent arches as *adductores branchiales II* and *III*. In summary, we agree with Springer and Johnson (2004) conclusions that the distinction between *interbranchiales abductores* and *adductores*

branchiales in the first three gill arches of acanthomorphs is often difficult and possibly subjective. Elucidation of this issue demands broader investigations that are much beyond the scope of the present study and the identifications of these muscles herein provided should be seen as provisional.

The most remarkable morphological characteristic of polynemids is, undoubtedly, their highly modified pectoral fin in which its ventralmost rays are transformed into elongate, tactile filaments. Such a distinctive specialization involves modifications in the skeleton, muscles and nerves of the pectoral fin and girdle. The pectoral filaments are formed by unbranched rays that are thicker and longer than the dorsal ones that compose the unmodified pectoral fin. The enlargement of pectoral radials 3 and 4 are among the most distinctive osteological modifications in the polynemid pectoral girdle (Fig. 23A). The articulation of the third pectoral radial with the adjacent radials (2 and 4) and with the coracoid is quite unusual and can be reinforced by indentations. The fourth radial is more prominently expanded and, in most cases, is the sole element articulating with the elongate pectoral filaments. A similar enlargement in the fourth radial is also known in the tripod fish genus *Bathypterois* (Ipnopidae, Aulopiformes; Sulak, 1977). Curiously, *Bathypterois* also exhibit pectoral-fin rays modified into elongate sensitive structures, but its more elongated rays are the dorsal ones that articulate with radial 1 (Sulak, 1977).

Modifications in the pectoral musculature are even more singular. Apart from the *arrectores* muscles, the whole pectoral musculature is completely subdivided into two independent segments: a *segmentum radialis* serving the unmodified pectoral-fin rays and a *segmentum filamentaris* associated with the pectoral filaments. Kang *et al.* (2017) briefly reported this divided musculature naming these segments as dorsal and ventral subdivisions or sections of the *abductores* and *adductores* muscles. However, the authors missed the deepest portion of the *adductor* muscle of the *segmentum filamentaris*, which is herein identified as the *adductor profundus filamentaris* (Fig. 20B). The muscle division named "ventral section of *adductor profundus* (ADPV)" by Kang *et al.* (2017) actually is not the deepest, but rather an intermediate division of the *adductor* mass associated with the pectoral filaments and thus correspond to our *adductor medialis filamentaris* (Fig. 20-23). Furthermore, the authors did not describe several important aspects in the *adductor*

medialis filamentaris (= "ventral section of the *adductor profundus*" in their terminology), such as its differentiation into *partes endomedialis* and *ectomedialis* and the variation in the insertion on the filaments. Representatives of several scorpaeniform lineages (Apistidae, Eureniidae, Hoplichthyidae, Peristediidae, Synanceiidae, Triglidae) exhibit a few ventralmost pectoral rays free from an interradial membrane that, to varying degrees, are somewhat independent from the main body of the pectoral fin. These modified rays are often termed "free rays" and, despite some obvious differences, they resemble the pectoral filaments of polynemids in some aspects. The musculature associated with the scorpaeniform free rays is variously separated from the muscles serving the remaining pectoral-fin rays (Yabe, 1985; Harris, 2013). However, these separations are reported to be often partial (e.g. common origin and separated insertions) and/or does not involve all the pectoral muscles (Yabe, 1985; Harris, 2013). These conditions contrast with the complete degree of separation into *segmenta radialis* and *filamentaris* seen in polynemids. In any event, the similarities in the subdivision of the musculature of the pectoral musculature of polynemids and the referred scorpaeniforms are most parsimoniously interpreted as convergences given the large phylogenetic distance between these lineages.

The spinal innervation was not thoroughly detailed by Freihofer (1963) across percomorphs, in which the author restricted himself to the specification of the RLA branches amongst families. However, the author described in details six genera (*Roccus saxatilis, Archoplites interruptus, Micrometrus frenatus, Polycentrus schomburgki, Kuhlia rupestris,* and *Macropodus opercularis*) from which he concluded that spinal innervation was very consistent among them. In the most common pattern found the pectoral girdle is innervated mainly by occipito-spinal nerves (OS), which in turn usually share neural fibers with the RLA branch feeding the girdle and by the first spinal nerve (SP1), which arrives in the shoulder girdle via two branches (PR-V and PR-M). Freihofer (1963) further complemented stating that the larger one usually is PR-M, but it is the PR-V *ramus* that normally receives the RLA fibers which, in turn, enter in the ventral rays of the pectoral fin. The OS can also share fibers with SP1. The innervation of the pectoral fin of Polynemidae has also shown outstanding specializations. Polynemids present the SP1 and OS nerves fused in the medial portion of the girdle and contrastingly have the second spinal nerve (SP2) also arriving in the pectoral girdle

(Figs. 20-23). Moreover, the SP2 is extremely thicker in compassion to SP1 and OS nerves (Fig. 25) and it is the SP2 that receives all neural fibers from the RLA branch, going straight to the pectoral filaments (Fig. 20-23), a condition not previously reported by Freihofer (1963).

Kang *et al.* (2017) briefly reported a pair of fused nerves running throughout the filament length and indicated that these filament have "likely tactile or gustatory function". According to Freihofer (1963) the RLA refers to "all nerves whose cell bodies are located in the geniculate ganglion and whose distal fibers extend to the parietal region of the head, (…) trunk, (…), fins (…) and innervate terminal buds, that is, taste buds located on the external surface of the head and body exclusive of the snout." The author still complements by stating that the main branches of the RLA carry only gustatory/taste fibers within. As aforementioned, reaching the pectoral filament, the RLA-OP branch runs throughout its length and its path is marked by different types of roughness on the pectoral filament surface (Fig. 33, 34). From this, the present study has shown enough evidences to support the idea of gustatory sensing of pectoral filaments of polynemids.

In addition, this superficial roughness is slightly similar to the one described on *Prionotus* (Triglidae). Although triglids lacks the RLA branch (Freihofer, 1963), these animals still have a positive reaction towards food substances and Scharrer *et al.* (1947) addressed this sensory capability as a chemical sense, rather than taste. In sea robins the distal tip of each free ray is full of ridges and papillae, ending in a terminal knob (Morrill, 1895), but not bearing taste buds structures (Scharrer *et al.*, 1947; Finger, 1982). Scharrer *et al.* (1947) could not trace the exact path of the nerves into a particular opening or sensory cell and from this, they concluded that the chemical sense of the free rays in *Prionotus* is a "free nerve ending" type, where the nerve endings are scattered everywhere in between the epithelium cells. Moreover, the authors also stated that nerve fibers end in a sort of a knob inside of a clear vesicle, which, in life, has a gelatinous consistency. To elucidate the chemical response and the possible functions of that clear vesicle, the authors conducted and reported an experiment in which the chemically stimulated fish took several seconds to react to the chemical source and remained agitated after the stimuli had ceased. From this, they attributed the delay of reaction to the gelatinous coating, which slows the passage of the stimuli into the epithelium cells and consequently to the free nerve endings.

Additionally, the authors also stated that this delicate coating is easily lost during fixation due to its quite thin thickness.

Besides the pectoral musculature, this free ray nerve morphology might be another adaptive convergence among threadfins and sea robins. In general, in polynemids there is no clear structure on the pectoral filament surface that might be responsible for chemical sensing, except in *Filimanus*, *Galeoides*, and *Leptomelanosoma* which present taste bud-like structures, small papillae, and small openings without an elevation from the epidermis, respectively (Fig. 33, 34). Nevertheless, the ridges reported herein in all genera (Fig. 33C) can form small grooves that lead the chemical stimuli into the epithelium which in turn absorbs the molecules and stimulate the free nerve endings scattered in between the cells. On the other hand, the globose structure on the distal tip of the filament found in *Eleutheronema tetradactylum* (Fig. 35) and in *Galeoides* (Fig. 36) can be a knob ending of the nerve that is the main responsible for sensing the environment and due to its delicacy was not visible in other specimens. In a way or another, the pectoral filaments micro-architecture needs more investigations to determine the morphology of the taste sensing in polynemids.

5. CONCLUSIONS

The present study indicates that polynemids possess several rare or unique specializations in its muscular system, most of which are herein reported for the first time. The *pars promalaris* of the *adductor mandibulae* of polynemids has a configuration unparalleled in any other percomorphacean. The *levator arcus palatini* in the family is differentiated into *partes primordiales externa* and *interna*, a condition that is shared with sciaenids, as well as the *dilatator operculi* posteroventral fibers visibility in medial view. Subgroups within Polynemidae further exhibit notable modifications in the branchial muscles *levator externus I* and *interbranchiales abductores*. The *adductor* and *abductor* muscle masses on the pectoral fin are completely divided into independent segments, which serve the unmodified fin – *segmentum radialis* – and the pectoral filaments – *segmentum filamentaris*. Such a complete degree of separation is more extreme than in any other actinopterygian with some fin rays also independent from the main body of the pectoral fin, such as some scorpaeniform lineages (*e.g.* Triglidae). Finally, I demonstrate for the first time that the pectoral filaments possess not only tactile but also gustative function. This finding is supported by the innervation of the pectoral filaments by massive components of the ramus lateralis accessorius, a nerve uniquely associated with taste reception.

REFERENCES

CHAKLADER, M. R.; SIDDIK, M. A. B.; NAHAR, A. Taxonomic diversity of paradise threadfin Polynemus paradiseus (Linnaeus, 1758) inhabiting southern coastal rivers in Bangladesh. **Sains Malaysiana,** v. 44, n. 9, p. 1241-1248, 2015. ISSN 0126-6039.

DATOVO, A.; BOCKMANN, F. A. Dorsolateral head muscles of the catfish families Nematogenyidae and Trichomycteridae (Siluriformes: Loricarioidei): comparative anatomy and phylogenetic analysis. **Neotropical Ichthyology,** v. 8, n. 2, p. 193-246, 2010. ISSN 1679-6225.

DATOVO, A.; CASTRO, R. M. Anatomy and evolution of the mandibular, hyopalatine, and opercular muscles in characiform fishes (Teleostei: Ostariophysi). **Zoology,** v. 115, n. 2, p. 84-116, 2012. ISSN 0944-2006.

DATOVO, A.; DE PINNA, M. C. C.; JOHNSON, G. D. The infrabranchial musculature and its bearing on the phylogeny of percomorph fishes (Osteichthyes: Teleostei). **PloS one,** v. 9, n. 10, p. e110129, 2014. ISSN 1932-6203.

DATOVO, A.; RIZZATO, P. P. Evolution of the facial musculature in basal ray-finned fishes. **Frontiers in zoology,** v. 15, n. 1, p. 40, 2018. ISSN 1742-9994.

DATOVO, A.; VARI, R. P. The jaw adductor muscle complex in teleostean fishes: evolution, homologies and revised nomenclature (Osteichthyes: Actinopterygii). **PloS one,** v. 8, n. 4, p. e60846, 2013. ISSN 1932-6203.

DATOVO, A.; VARI, R. P. The adductor mandibulae muscle complex in lower teleostean fishes (Osteichthyes: Actinopterygii): comparative anatomy, synonymy, and phylogenetic implications. **Zoological Journal of the Linnean Society,** v. 171, n. 3, p. 554-622, 2014. ISSN 1096-3642.

DE SCHEPPER, N.; VAN WASSENBERGH, S.; ADRIAENS, D. Morphology of the jaw system in trichiurids: trade-offs between mouth closing and biting performance. **Zoological Journal of the Linnean Society,** v. 152, n. 4, p. 717-736, 2008. ISSN 1096-3642.

EATON, T. H. Evolution of the upper jaw mechanism in teleost fishes. **Journal of Morphology,** v. 58, n. 1, p. 157-172, 1935. ISSN 0362-2525.

FELTES, R. M. Revision of the polynemid fish genus Filimanus, with the description of two new species. **Copeia**, p. 302-322, 1991. ISSN 0045-8511.

FELTES, R. M. Parapolynemus, a new genus for the polynemid fish previously known as Polynemus verekeri. **Copeia**, p. 207-215, 1993. ISSN 0045-8511.

FINGER, T. E. Somatotopy in the representation of the pectoral fin and free fin rays in the spinal cord of the sea robin, Prionotus carolinus. The Biological Bulletin, v. 163, n. 1, p. 154-161, 1982. ISSN 0006-3185.

FREIHOFER, W. C. Patterns of ramus lateralis accessorius and their systematic significance in teleostean fishes. **Stanford Ichthyol Bull,** v. 8, p. 80-189, 1963.

GOSLINE, W. A. Systematic position and relationships of the percesocine fishes. **Pacific Science,** v. 16, p. 207-217, 1962.

GOSLINE, W. A. The suborders of perciform fishes. **Proceedings of the United States National Museum,** v. 124, 1968.

GOSLINE, W. A. **Functional morphology and classification of teleostean fishes**. Honolulu: University of Hawaii Press, 1971. 208.

GOSLINE, W. A. A survey of upper jaw musculature in higher teleostean fishes. **Occasional Papers of the Museum of Zoology University of Michigan** v. 724, p. 1-26, 1993.

GRUBICH, J. R.; RICE, A. N.; WESTNEAT, M. W. Functional morphology of bite mechanics in the great barracuda (Sphyraena barracuda). **Zoology (Jena)** v. 111, n. 1, p. 16-29, 2008. ISSN 0944-2006.

GUSMAO-POMPIANI, P.; OLIVEIRA, C.; QUAGIO-GRASSIOTTO, I. Spermatozoa ultrastructure in Sciaenidae and Polynemidae (Teleostei: Perciformes) with some consideration on Percoidei spermatozoa ultrastructure. **Tissue and Cell,** v. 37, n. 3, p. 177-191, 2005. ISSN 0040-8166.

HABEGGER, M. et al. Feeding biomechanics in the Great Barracuda during ontogeny. **Journal of Zoology (London),** v. 283, n. 1, p. 63-72, 2011. ISSN 0952-8369.

HARRIS, J. P. **The Comparative Morphology of the Pectoral Free Rays in Scorpaenoid Fishes (perciformes: Scorpaenoidea)**. 2013. 127 (Master). Loyola University Chicago

JOHNSON, D. G. Percomorph phylogeny: progress and problems. **Bulletin of marine Science,** v. 52, n. 1, p. 3-28, 1993. ISSN 0007-4977.

JOHNSON, D. G.; PATTERSON, C. Percomorph phylogeny: a survey of acanthomorphs and a new proposal. **Bulletin of Marine Science,** v. 52, n. 1, p. 554-626, 1993. ISSN 0007-4977.

KANG, S. **Comparative morphology and phylogenetic relationships of the family Polynemidae (Pisces: Perciformes)**. 2017. Hokkaido University

KANG, S.; IMAMURA, H.; KAWAI, T. Morphological evidence supporting the monophyly of the family Polynemidae (Teleostei: Perciformes) and its sister relationship with Sciaenidae. **Ichthyological Research,** v. 65, n. 1, p. 29-41, 2017. ISSN 1341-8998.

KASUMYAN, A. O. The taste system in fishes and the effects of environmental variables. **Journal of fish biology**, 2019. ISSN 0022-1112.

LAUDER, G. V. Evolution of the feeding mechanism in primitive actionopterygian fishes: a functional anatomical analysis of Polypterus, Lepisosteus, and Amia. **Journal of Morphology,** v. 163, n. 3, p. 283-317, 1980. ISSN 0362-2525.

LAUDER, G. V. Patterns of evolution in the feeding mechanism of actinopterygian fishes. **American Zoologist,** v. 22, n. 2, p. 275-285, 1982. ISSN 0003-1569.

LAUDER, G. V.; CLARK, B. D. Water flow patterns during prey capture by teleost fishes. **Journal of Experimental Biology,** v. 113, n. 1, p. 143-150, 1984. ISSN 0022-0949.

MORRILL, A. D. The pectoral appendages of Prionotus and their innervation. **Journal of Morphology,** v. 11, n. 1, p. 177-192, 1895. ISSN 0362-2525.

MOTOMURA, H. Revision of the Indo-Pacific threadfin genus Polydactylus (Perciformes: Polynemidae) with a key to the species. **Bulletin of the National Science Museum, Tokyo, Series A (Zoology),** v. 28, n. 3, p. 171-194, 2002.

MOTOMURA, H. **Threadfins of the world (Family Polynemidae): An annotated and illustrated catalogue of polynemid species known to date**. Food & Agriculture Org., 2004. ISBN 9251051283.

MOTOMURA, H.; IWATSUKI, Y. Review of Polydactylus species (Perciformes: Polynemidae) characterized by a large black anterior lateral line spot, with descriptions of two new species. **Ichthyological research,** v. 48, n. 4, p. 337-354, 2001. ISSN 1341-8998.

MOTOMURA, H.; TSUKAWAKI, S. New species of the threadfin genus Polynemus (Teleostei: Polynemidae) from the Mekong River basin, Vietnam, with comments on the Mekong species of Polynemus. **The Raffles Bulletin of Zoology,** v. 54, n. 2, p. 459-464, 2006.

MOTOMURA, H. et al. Redescription ofpolydactylus macrochir (günther, 1867), a senior synonym ofP. sheridani (macleay, 1884)(perciformes: Polynemidae). **Ichthyological research,** v. 47, n. 3-4, p. 327-333, 2000. ISSN 1341-8998.

MOTOMURA, H. et al. Review of seven-spined Polynemus species (Perciformes: Polynemidae) with designation of a neotype for Polynemus paradiseus Linnaeus, 1758. **Ichthyological research,** v. 49, n. 4, p. 307-317, 2002. ISSN 1341-8998.

OSSE, J. W. M. Functional morphology of the head of the perch (Perca fluviatilis L.): an electromyographic study. **Netherlands Journal of Zoology,** v. 19, n. 3, p. 289-392, 1969. ISSN 1568-542X.

REUTTER, K.; BREIPOHL, W.; BIJVANK, G. J. Taste bud types in fishes. **Cell and tissue research,** v. 153, n. 2, p. 151-165, 1974. ISSN 0302-766X.

ROSEN, D. E. **The relationships and taxonomic position of the halfbeaks, killifishes, silversides, and their relatives**. American Museum of Natural History, 1964.

SASAKI, K. Phylogeny of the family Sciaenidae, with notes on its zoogeography (Teleostei, Perciformes). **Memoirs of the Faculty of Fisheries Hokkaido University,** v. 36, n. 1-2, p. 1-137, 1989. ISSN 0018-3466.

SCHARRER, E.; SMITH, S.; PALAY, S. Chemical sense and taste in the fishes, Prionotus and Trichogaster. **Journal of Comparative Neurology,** v. 86, n. 2, p. 183-198, 1947. ISSN 0021-9967.

SCHNELL, N. K.; KONSTANTINIDIS, P.; JOHNSON, G. D. High-proof Ethanol Fixation of Larval and Juvenile Fishes for Clearing and Double Staining. **Copeia,** v. 104, n. 3, p. 617-622, 2016. ISSN 0045-8511.

SPRINGER, V. G.; JOHNSON, G. D. **Study of the dorsal gill-arch musculature of teleostome fishes, with special reference to the Actinopterygii**. Biological Society of Washington, Smithsonian Institution, 2004.

SPRINGER, V. G.; JOHNSON, G. D. The Gill-Arch Musculature of Protanguilla, the Morphologically Most Primitive Eel (Teleostei: Anguilliformes), Compared with That of Other Putatively Primitive Extant Eels and Other Elopomorphs. **Copeia,** v. 103, n. 3, p. 595-620, 2015. ISSN 0045-8511.

STARKS, E. C. **The sesamoid articular: a bone in the mandible of fishes**. Stanford: Stanford University Press, 1916.

STIASSNY, M. L. Notes on the anatomy and relationships of the bedotiid fishes of Madagascar: with a taxonomic revision of the genus Rheocles (Atherinomorpha, Bedotiidae). American Museum novitates;; no. 2979. 1990.

SULAK, K. J. The systematics and biology of Bathypterois (Pisces, Chlorophthalmidae). **Gulathea Reports,** v. 14, p. 49-108, 1977.

TAYLOR, W. R.; VAN DYKE, G. Revised procedures for staining and clearing small fishes and other vertebrates for bone and cartilage study. **Cybium,** v. 9, n. 2, p. 107-119, 1985. ISSN 0399-0974.

VAN DOBBEN, W. H. Über den kiefermechanismus der knochenfische. **Archives néerlandaises de Zoologie,** v. 2, n. 1, p. 1-72, 1935. ISSN 0365-5164.

WINTERBOTTOM, R. A descriptive synonymy of the striated muscles of the Teleostei. **Proceedings of the Academy of Natural Sciences of Philadelphia**, p. 225-317, 1974a. ISSN 0097-3157.

WINTERBOTTOM, R. The familial phylogeny of the Tetraodontiformes (Acanthopterygii: Pisces) as evidenced by their comparative myology. **Smithson Contrib Zool,** v. 155, p. 1-201, 1974b.

WINTERBOTTOM, R. Myological evidence for the phylogeny of recent genera of surgeonfishes (Percomorpha, Acanthuridae), with comments on the Acanthuroidei. **Copeia**, p. 21-39, 1993. ISSN 0045-8511.

WU, K.-Y.; SHEN, S.-C. Review of the teleostean adductor mandibulae and its significance to the systematic positions of the Polymixiiformes, Lampridiformes, and Triacanthoidei. **Zoological Studies,** v. 43, n. 4, p. 712-736, 2004. ISSN 1021-5506.

YABE, M. Comparative osteology and myology of the superfamily Cottoidea (Pisces: Scorpaeniformes), and its phylogenetic classification. **Memoirs of the Faculty of Fisheries Hokkaido University,** v. 32, n. 1, p. 1-130, 1985. ISSN 0018-3466.

FIGURES

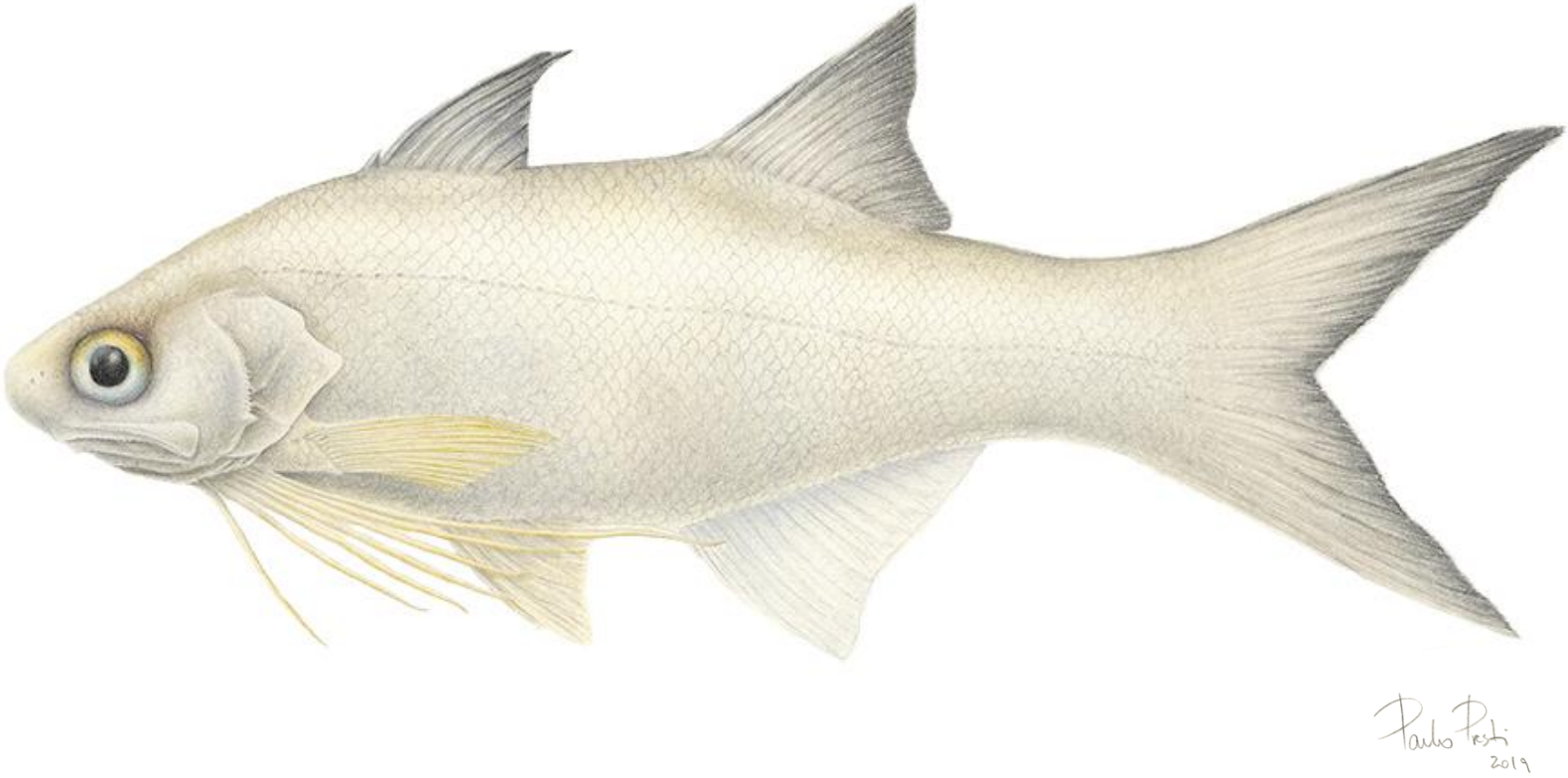

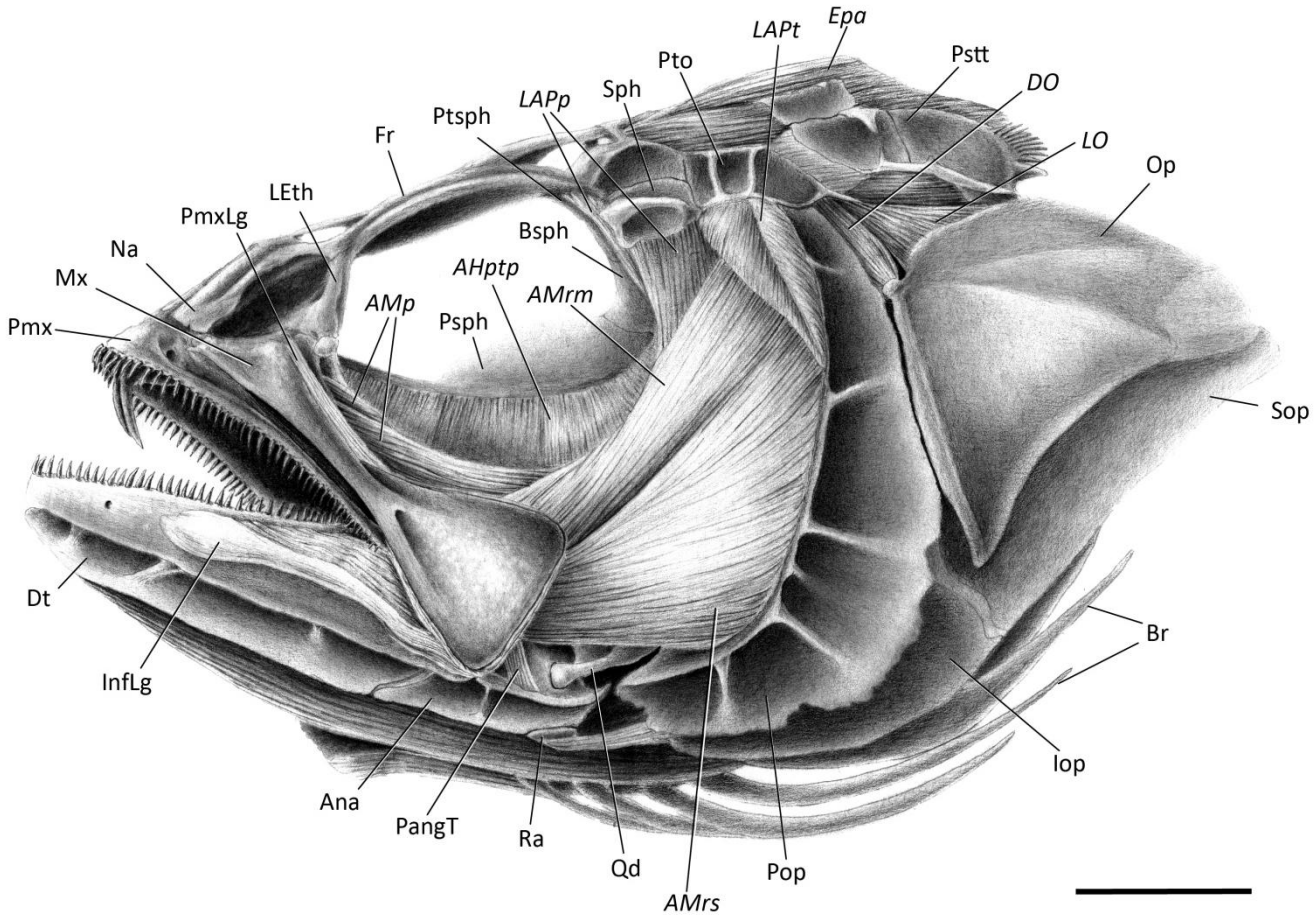

Fig. 1: Lateral view of *Cynoscion striatus* head. AHptp, *adductor hyomandibulae p. pterygo-palatina*; AMp, *adductor mandibulae p. promalaris*; AMrm, *adductor mandibulae p. retromalaris*; AMrs, *adductor mandibulae p. ricto-stegalis*; Ana, angulo-articular; Br, branchiostegal rays; Bsph, basisphenoid; DO, *dilatator operculi*; Dt, dentary, Epa, *epaxialis*; Fr, frontal, InfLg, infralabial ligament; Iop, interopercle; LAPp, *levator arcus palatini p. primordialis*; LAPt, *levator arcus palatini p. temporalis*; LEth, lateral ethmoid, LO, *levator operculi*; Mx, maxilla, Na, nasal, Op, opercle; PangT, preangular tendon; Pop, preopercle; Pmx, premaxilla; PmxLg, paramaxillar ligament; Psph, parasphenoid; Pstt, posttemporal; Pto, pterotic; Ptsph, pterosphenoid; Qd, quadrate; Ra, retroarticular; Sop, subopercle; Sph, sphenotic. Scale bars: 5 mm.

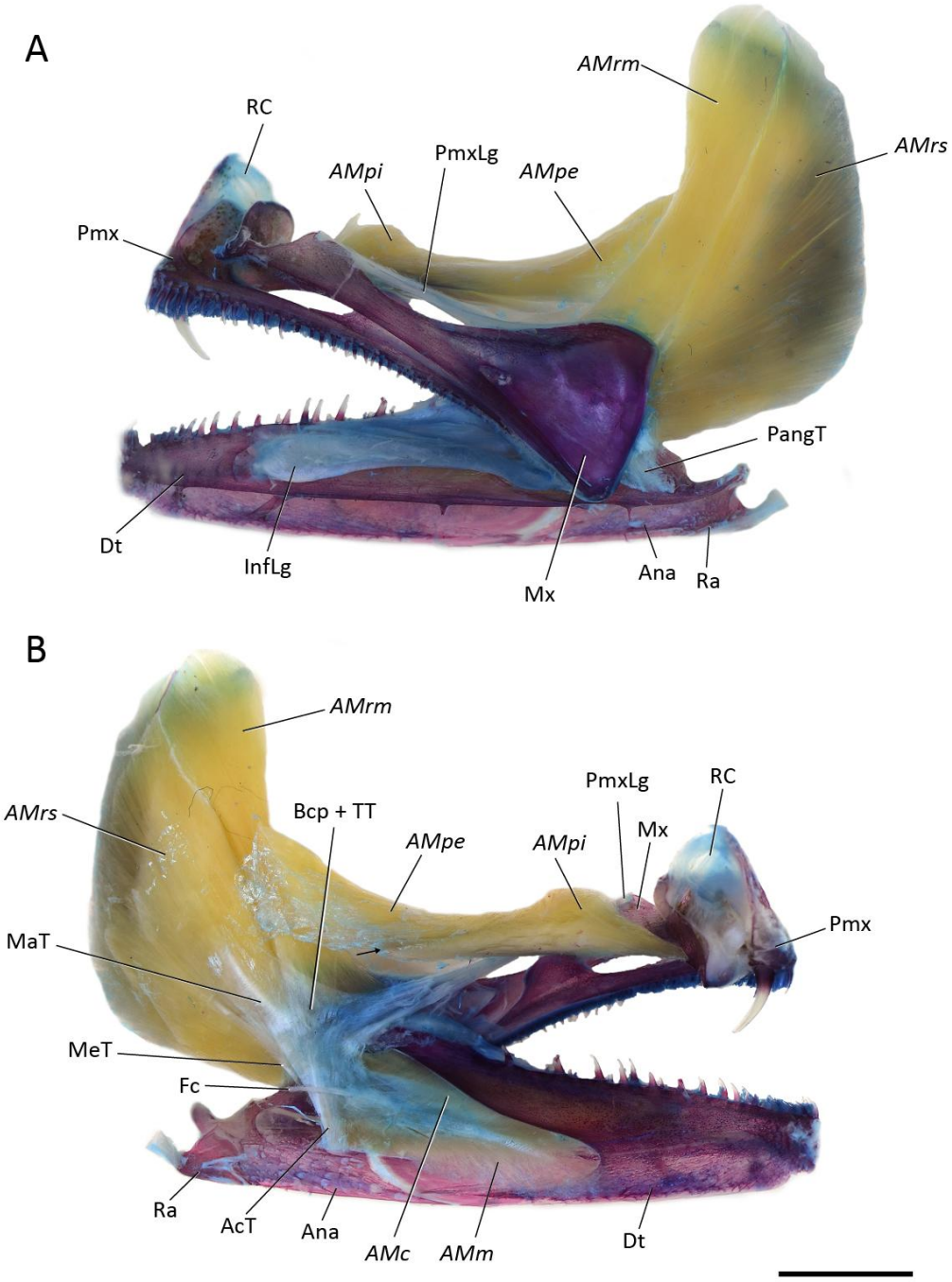

Fig. 2: *Cynoscion striatus* mandibular arch. A: lateral view. B: medial view. AcT, accessory tendon; AMc, *adductor mandibulae p. coronalis;* AMm, *adductor mandibulae p. mentalis*; AMpe, *adductor mandibulae p. promalaris externa*; AMpi, *adductor mandibulae p. promalaris interna;* AMrm, *adductor mandibulae p. retromalaris*; AMrs, *adductor mandibulae p. ricto-stegalis*; Ana, angulo-articular; Bcp+TT, buccopalatal membrane + embedded transverse tendon; Dt, dentary; Fc, faucal ligament; InfLg, infralabial ligament; MaT, mandibular tendon; MeT, meckelian tendon; Mx, maxilla; PangT; preangular tendon; Pmx, premaxilla; PmxLg, paramaxillar ligament; Ra, retroarticular; RC, rostral cartilage. Arrow indicates division of *promalares externa and interna*. Scale bars: 5 mm.

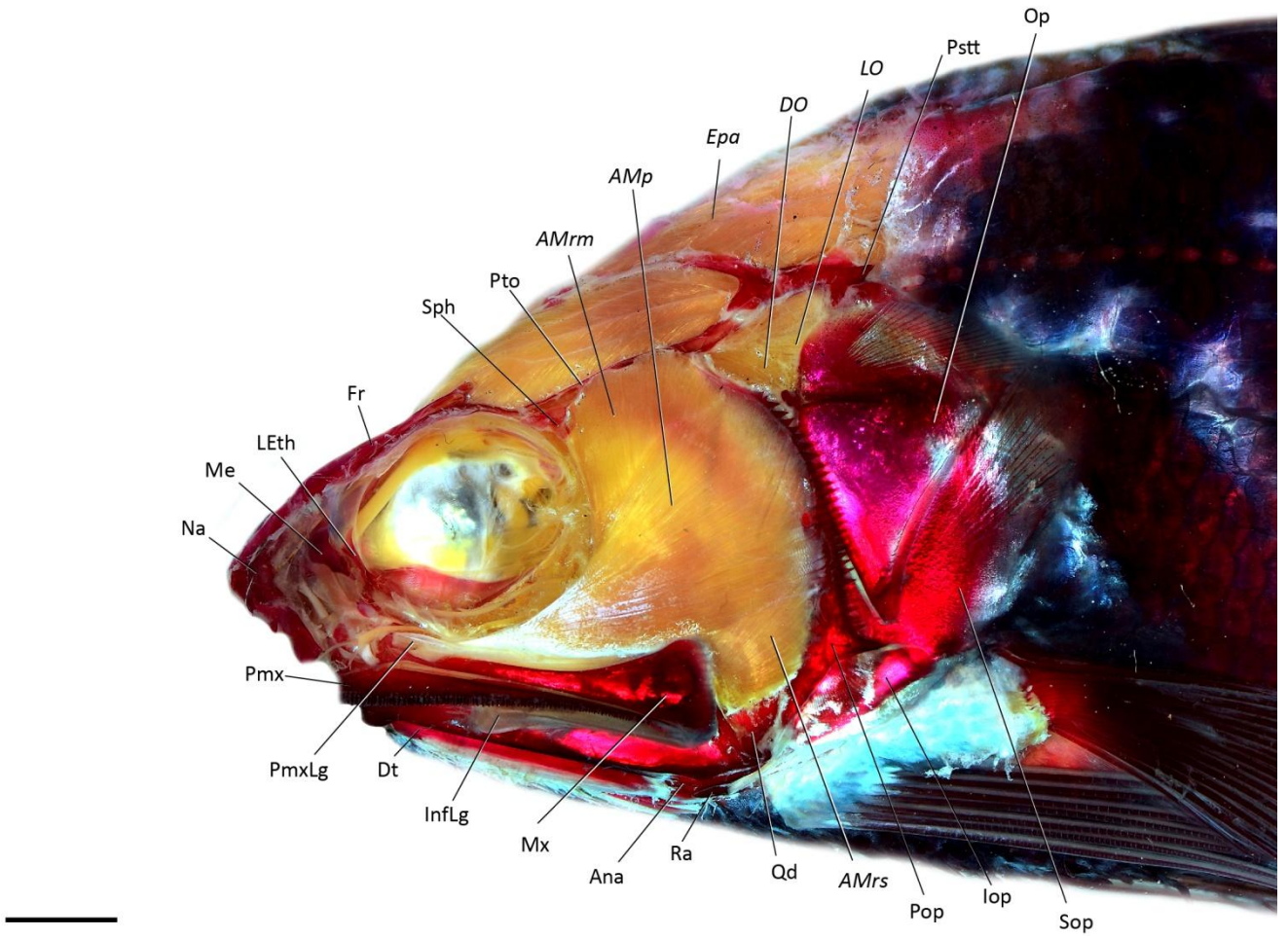

Fig. 3: Lateral view of *Polydactylus virginicus* head. AMp, *adductor mandibulae p. promalaris*; AMrm, *adductor mandibulae p. retromalaris*; AMrs, *adductor mandibulae p. ricto-stegalis*; Ana, angulo-articular; Bsph, basisphenoid; DO, *dilatator operculi*; Dt, dentary; Epa, *epaxialis* Fr, frontal, InfLg, infralabial ligament; Iop, interopercle; LAPp, *levator arcus palatini p. primordialis*; LAPt, *levator arcus palatini p. temporalis*; LEth, lateral ethmoid, LO, *levator operculi*; Mx, maxilla; Na, nasal; Op, opercle; PangT, preangular tendon; Pop, preopercle; Pmx, premaxilla; PmxLg, paramaxillar ligament; Pstt, posttemporal; Pto, pterotic; Ptsph, pterosphenoid; Qd, quadrate; Ra, retroarticular; Sop, subopercle; Sph, sphenotic. Scale bars: 5 mm.

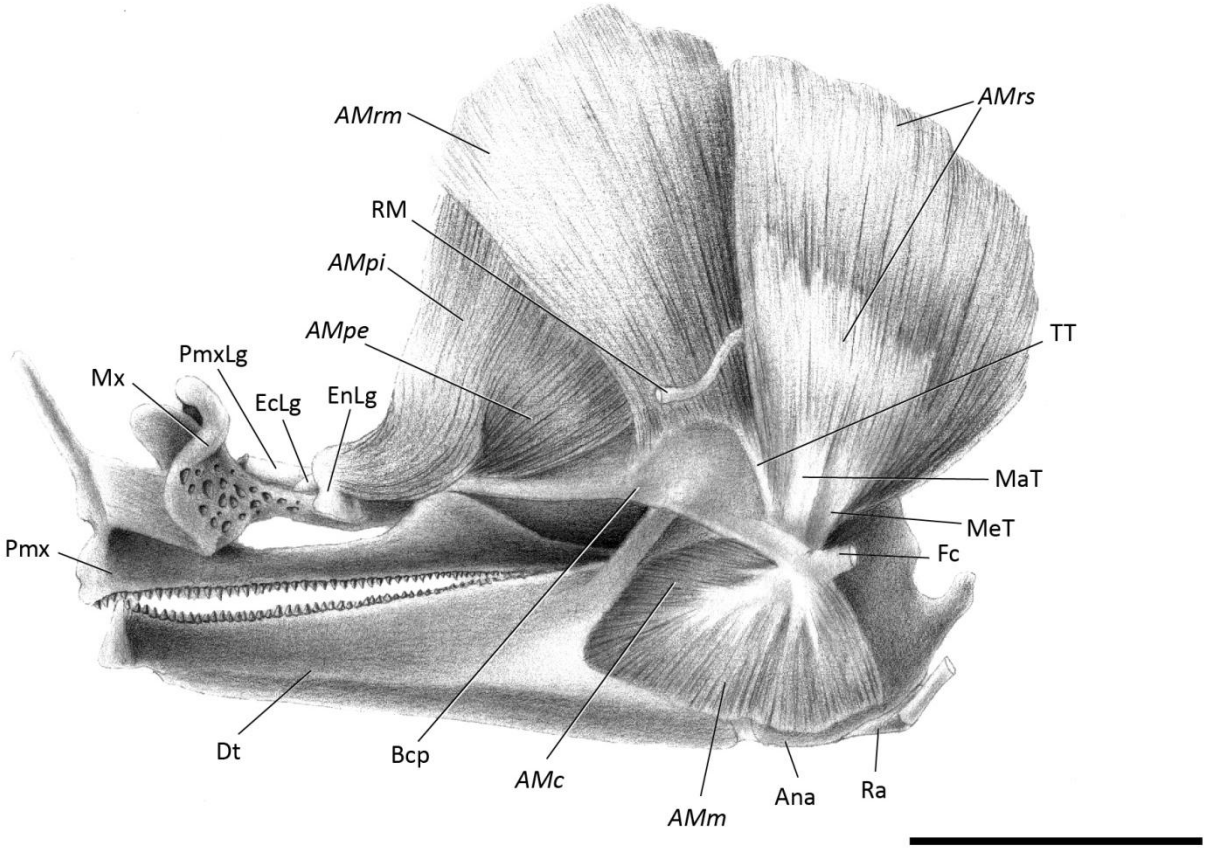

Fig. 4: *Polynemus paradiseus* mandibular arch, medial view. AMc, *adductor mandibulae p. coronalis;* AMm, *adductor mandibulae p. mentalis*; AMpe, *adductor mandibulae p. promalaris externa*; AMpi, *adductor mandibulae p. promalaris interna;* AMrm, *adductor mandibulae p. retromalaris*; AMrs, *adductor mandibulae p. ricto-stegalis*; Ana, angulo-articular; Bcp, buccopalatal membrane; Dt, dentary; EcLg, ectomaxillar ligament; EnLg, endomaxillar ligament; Fc, faucal ligament; MaT, mandibular tendon; MeT, meckelian tendon; Mx, maxilla; Pmx, premaxilla; PmxLg, paramaxillar ligament; Ra, retroarticular; RM, *ramus mandibularis trigeminus*; TT, transverse tendon. Scale bars: 5 mm.

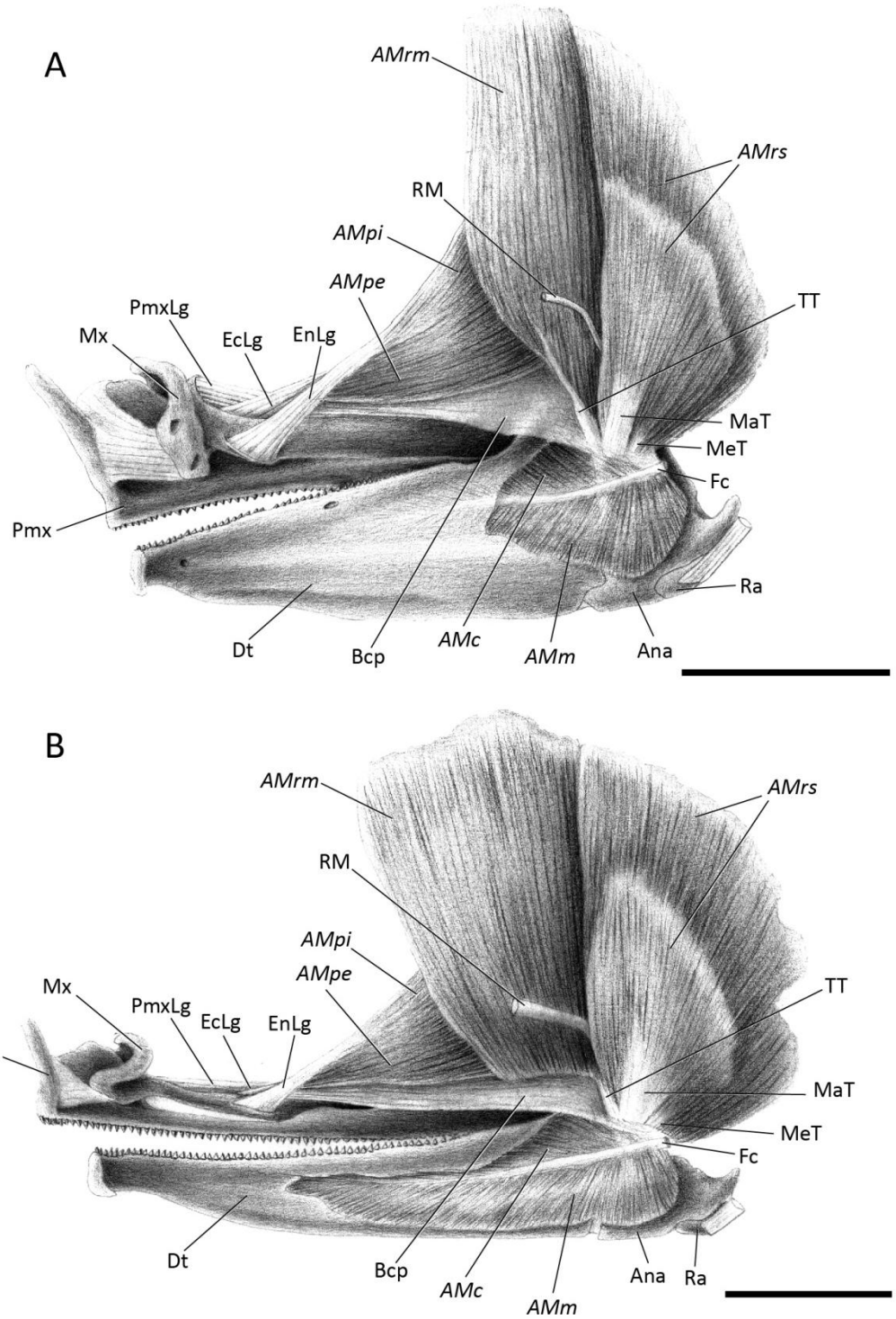

Fig. 5: Mandibular arch, medial view. A: *Filimanus xanthonema*. B: *Eleutheronema tetradactylum*. AMc, *adductor mandibulae p. coronalis;* AMm, *adductor mandibulae p. mentalis*; AMpe, *adductor mandibulae p. promalaris externa*; AMpi, *adductor mandibulae p. promalaris interna;* AMrm, *adductor mandibulae p. retromalaris*; AMrs, *adductor mandibulae p. ricto-stegalis*; Ana, angulo-articular; Bcp, buccopalatal membrane; Dt, dentary; EcLg, ectomaxillar ligament; EnLg, endomaxillar ligament; Fc, faucal ligament; MaT, mandibular tendon; MeT, meckelian tendon; Mx, maxilla; Pmx, premaxilla; PmxLg, paramaxillar ligament; Ra, retroarticular; RM, *ramus mandibularis trigeminus*; TT, transverse tendon. Scale bars: 5 mm.

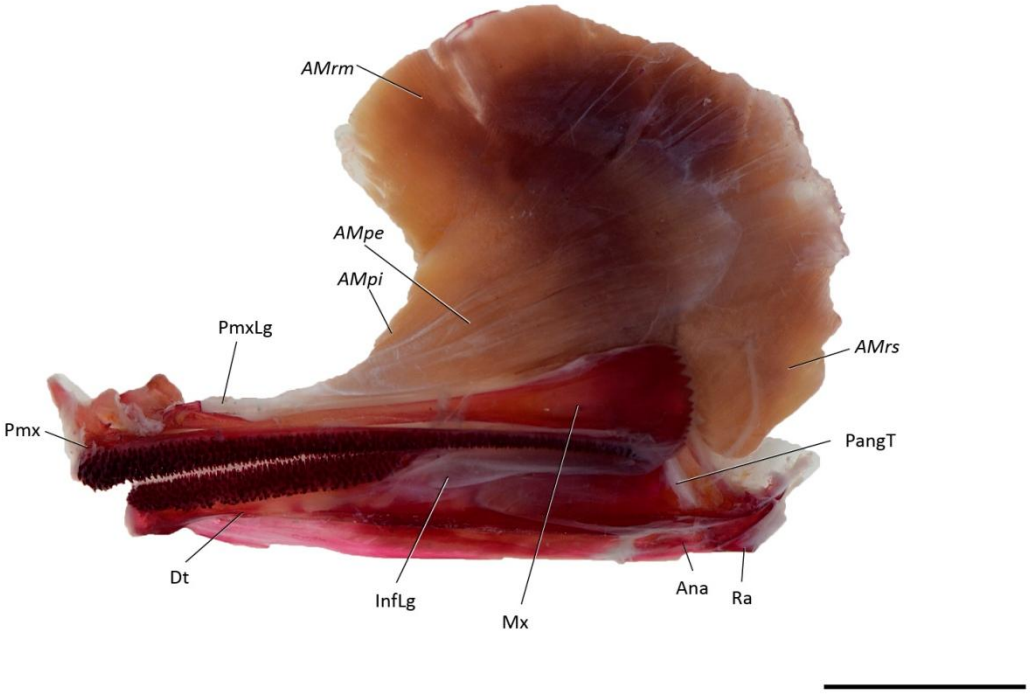

Fig. 6: *Eleutheronema tetradactylum*, mandibular arch, lateral view. AMpe, *adductor mandibulae p. promalaris externa*; AMpi, *adductor mandibulae p. promalaris interna;* AMrm, *adductor mandibulae p. retromalaris*; AMrs, *adductor mandibulae p. ricto-stegalis*; Ana, angulo-articular; Dt, dentary; InfLg, infralabial ligament; Mx, maxilla; PangT, preangular tendon; Pmx, premaxilla; PmxLg, paramaxillar ligament; Ra, retroarticular. Scale bars: 5 mm.

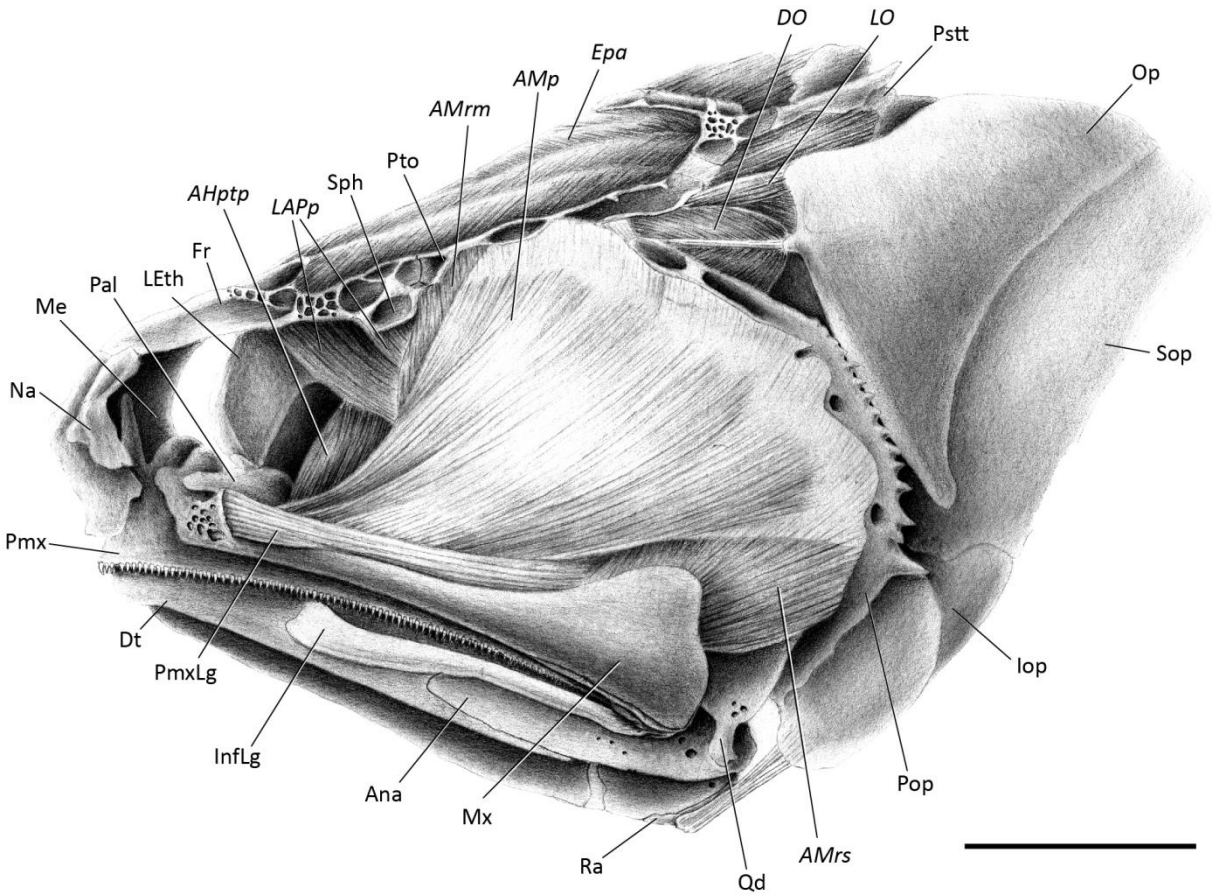

Fig. 7: Lateral view of *Polynemus paradiseus* head. AHptp, *adductor hyomandibulae p. pterygo-palatina*; AMp, *adductor mandibulae p. promalaris*; AMrm, *adductor mandibulae p. retromalaris*; AMrs, *adductor mandibulae p. ricto-stegalis*; Ana, angulo-articular; DO, *dilatator operculi*; Dt, dentary, Epa, *epaxialis*; Fr, frontal, InfLg, infralabial ligament; Iop, interopercle; LAPp, *levator arcus palatini p. primordialis*; LEth, lateral ethmoid, LO, *levator operculi*; Me, mesethmoid; Mx, maxilla, Na, nasal, Op, opercle; Pal, palatine; PangT, preangular tendon; Pop, preopercle; Pmx, premaxilla; PmxLg, paramaxillar ligament; Psph, parasphenoid; Pstt, posttemporal; Pto, pterotic; Ptsph, pterosphenoid; Qd, quadrate; Ra, retroarticular; Sop, subopercle; Sph, sphenotic. Scale bars: 5 mm.

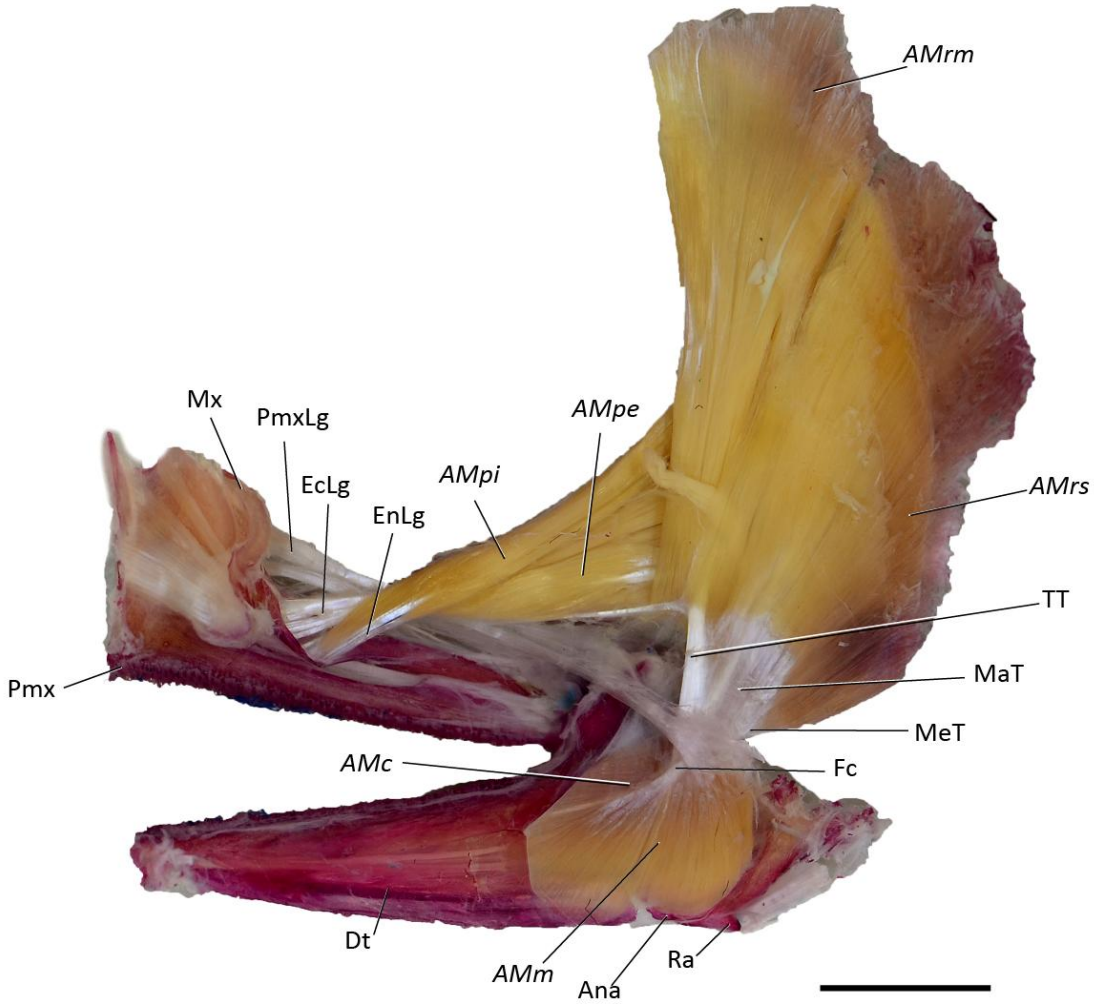

Fig. 8: *Galeoides decadactylus*, mandibular arch, medial view. AMc, *adductor mandibulae p. coronalis;* AMm, *adductor mandibulae p. mentalis*; AMpe, *adductor mandibulae p. promalaris externa*; AMpi, *adductor mandibulae p. promalaris interna;* AMrm, *adductor mandibulae p. retromalaris*; AMrs, *adductor mandibulae p. ricto-stegalis*; Ana, angulo-articular; Dt, dentary; EcLg, ectomaxillar ligament; EnLg, endomaxillar ligament; Fc, faucal ligament; MaT, mandibular tendon; MeT, meckelian tendon; Mx, maxilla; Pmx, premaxilla; PmxLg, paramaxillar ligament; Ra, retroarticular; TT, transverse tendon. Scale bars: 5 mm.

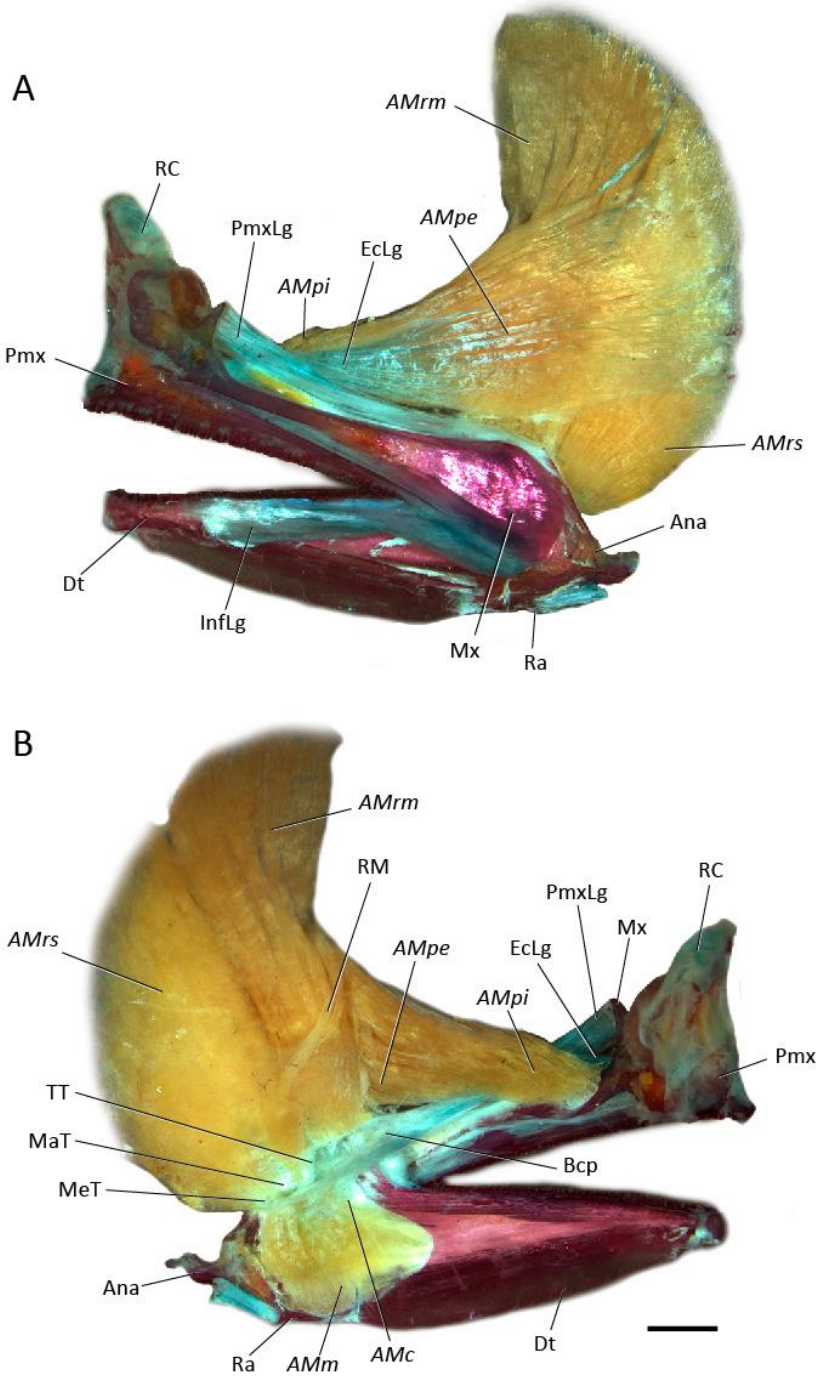

Fig. 9: *Polydactylus sextarius*, mandibular arch. A: lateral view. B: medial view. AMc, *adductor mandibulae p. coronalis;* AMm, *adductor mandibulae p. mentalis*; AMpe, *adductor mandibulae p. promalaris externa*; AMpi, *adductor mandibulae p. promalaris interna;* AMrm, *adductor mandibulae p. retromalaris*; AMrs, *adductor mandibulae p. ricto-stegalis*; Ana, angulo-articular; Bcp, buccopalatal membrane; Dt, dentary; EcLg, ectomaxillar ligament; Fc, faucal ligament; MaT, mandibular tendon; MeT, meckelian tendon; Mx, maxilla; Pmx, premaxilla; PmxLg, paramaxillar ligament; Ra, retroarticular; RC, rostral cartilage; RM, *ramus mandibularis trigeminus*; TT, transverse tendon. Scale bar: 2 mm.

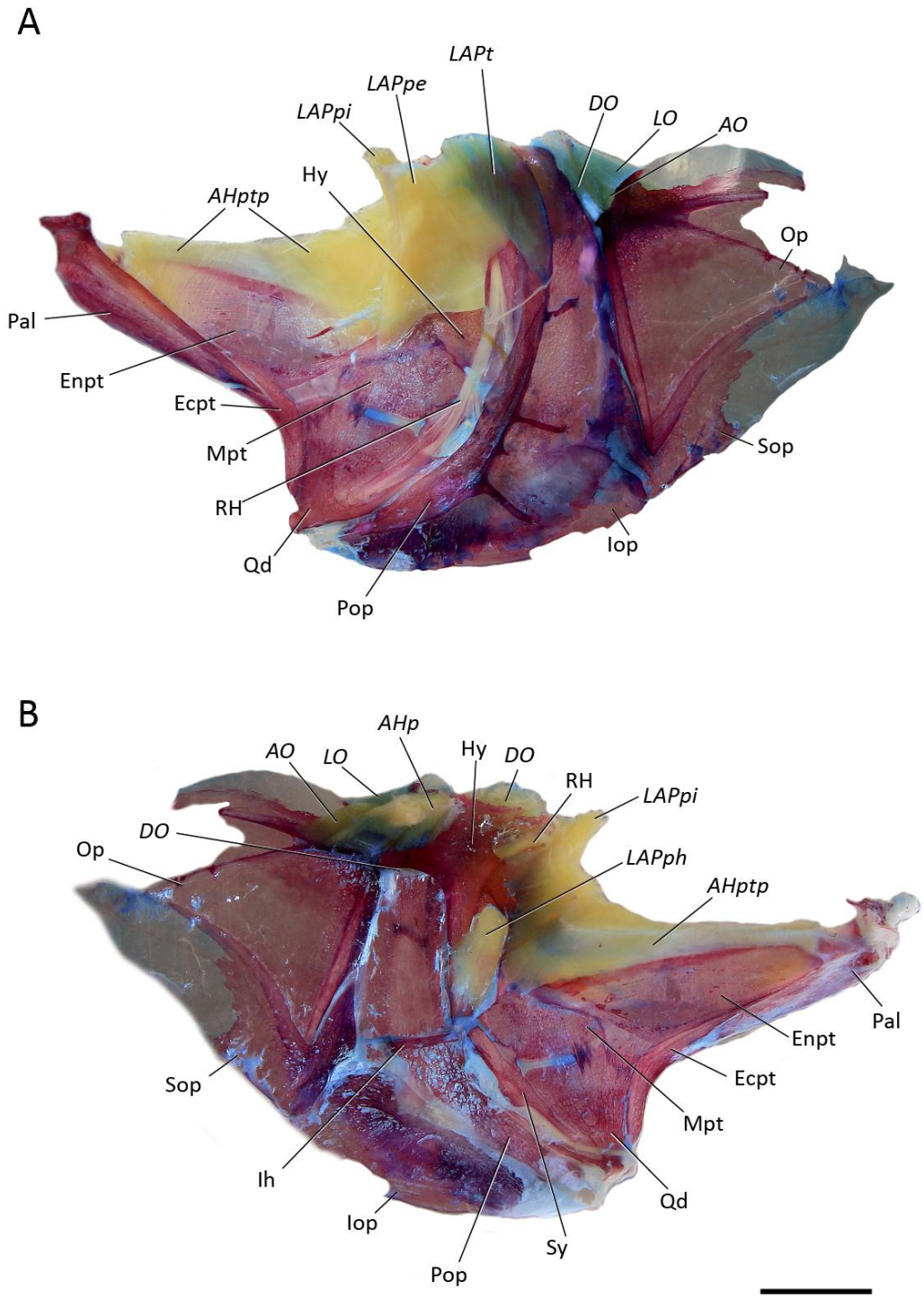

Fig. 10: *Cynoscion striatus*, hyopalatine arch. A: lateral view. B: medial view. AHp, *adductor hyomandibulae p. primordialis;* AHptp, *adductor hyomandibulae p. pterygo-palatina*; AO, *adductor operculi*; DO, *dilatator operculi*; Ecpt, ectopterygoid; Enpt, endopterygoid; Hy, hyomandibular; Ih, interhyal; Iop, interopercle; LAPpe, *levator arcus palatini p. primordialis externa;* LAPph, *levator arcus palatini p. pharyngealis;* LAPpi, *levator arcus palatini p. primordialis interna*; LAPt, *levator arcus palatini p. temporalis;* LO, *levator operculi*; Mpt, metapterygoid; Op, opercle; Pal, palatine; Pop, preopercle; Qd, quadrate; RH, *ramus hyomandibularis facialis*; Sop, subopercle; Sy, symplectic. Scale bar: 5 mm.

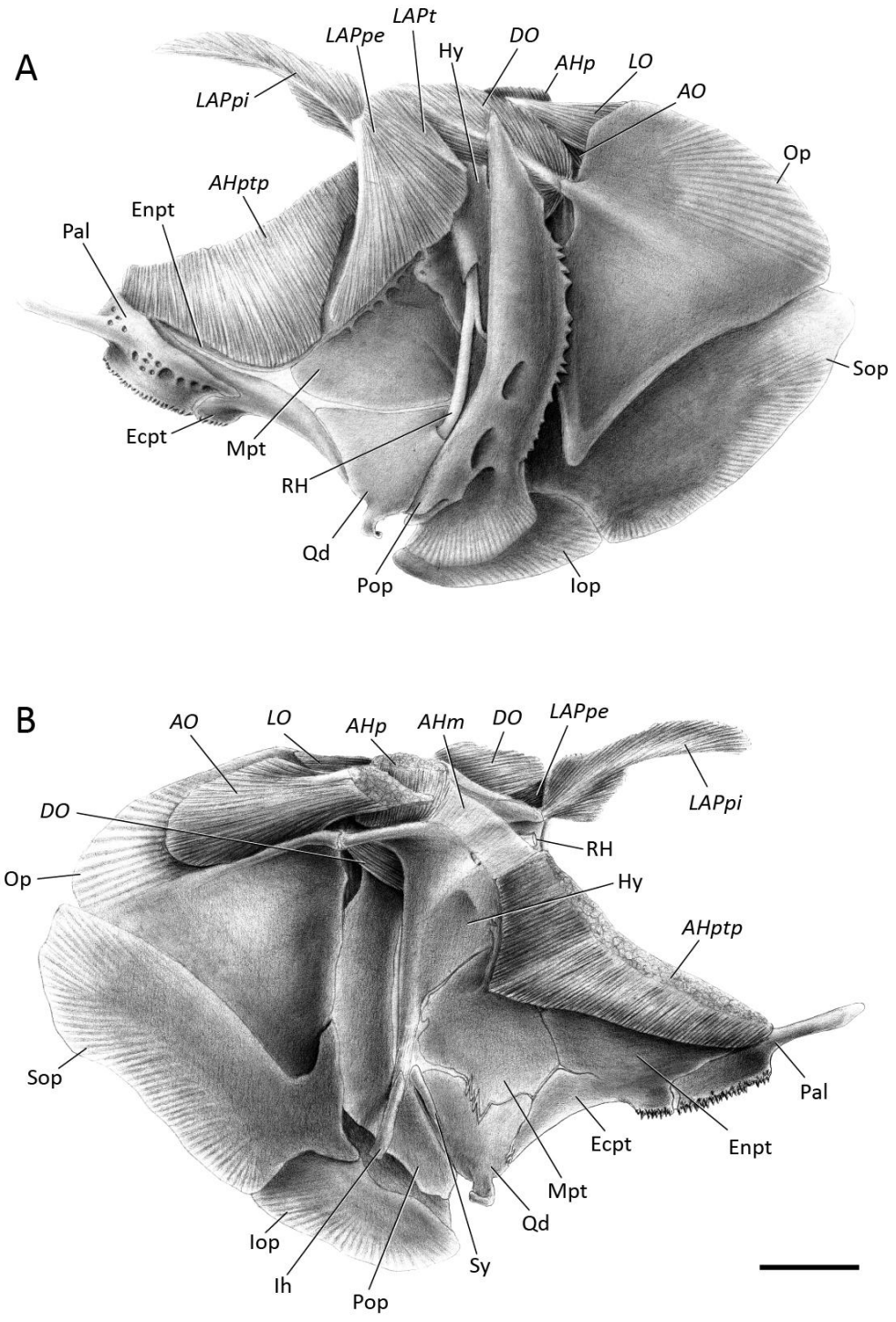

Fig. 11: *Galeoides decadactylus*, hyopalatine arch. A: lateral view. B: medial view. AHm, membrane in between *adductor hyomandibulae* sections; AHp, *adductor hyomandibulae p. primordialis;* AHptp, *adductor hyomandibulae p. pterygo-palatina*; AO, *adductor operculi*; DO, *dilatator operculi*; Ecpt, ectopterygoid; Enpt, endopterygoid; Hy, hyomandibular; Ih, interhyal; Iop, interopercle; LAPpe, *levator arcus palatini p. primordialis externa;* LAPph, *levator arcus palatini p. pharyngealis;* LAPpi, *levator arcus palatini p. primordialis interna*; LAPt, *levator arcus palatini p. temporalis;* LO, *levator operculi*; Mpt, metapterygoid; Op, opercle; Pal, palatine; Pop, preopercle; Qd, quadrate; RH, *ramus hyomandibularis facialis*; Sop, subopercle; Sy, symplectic. Scale bar: 5 mm.

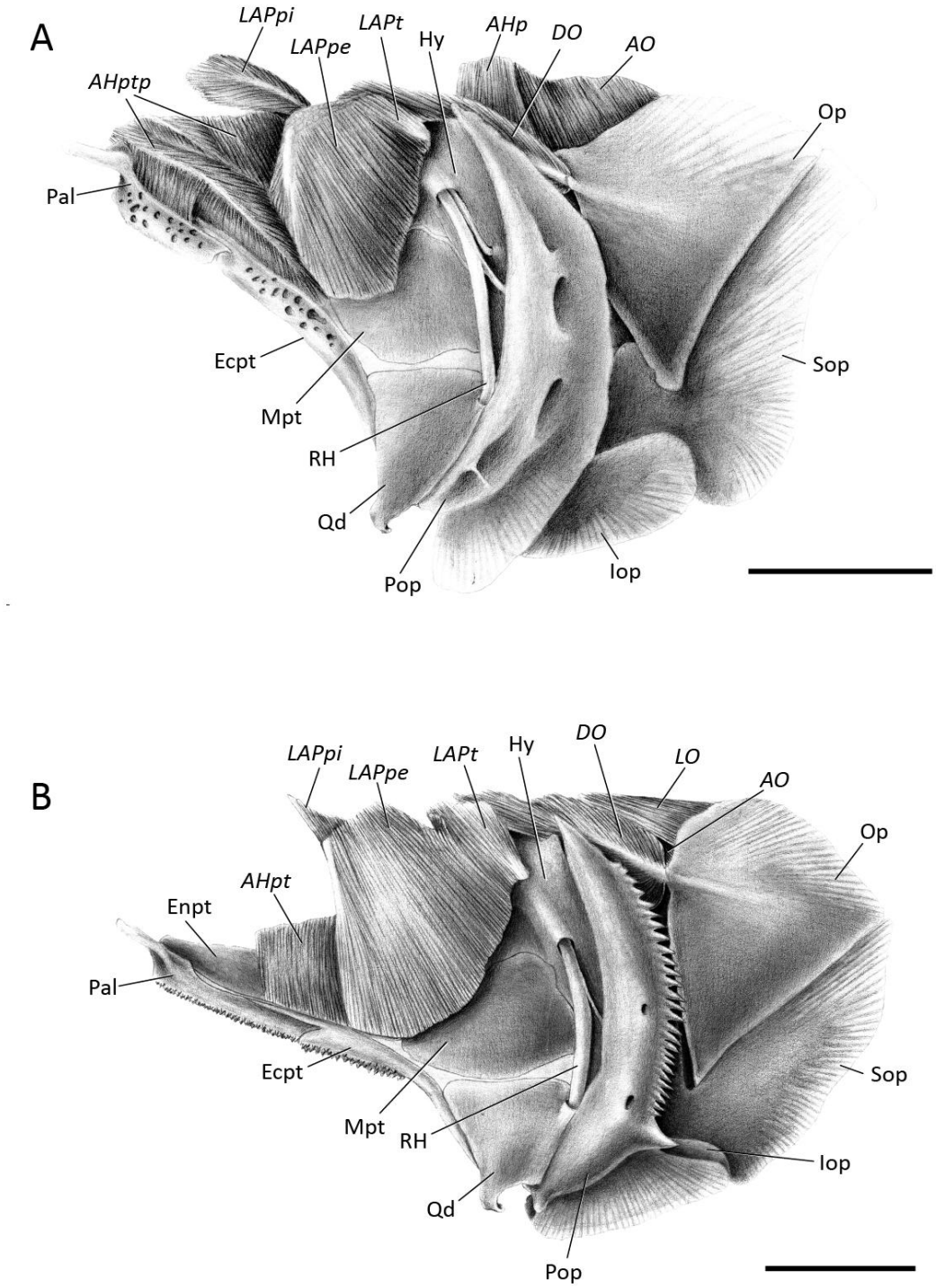

Fig. 12: *H*yopalatine arch, lateral view. A: *Parapolynemus verekeri*. B: *Eleutheronema tetradactylum*. AHp, *adductor hyomandibulae p. primordialis;* AHpt, *adductor hyomandibulae p. pterygoidea;* AHptp, *adductor hyomandibulae p. pterygo-palatina*; AO, *adductor operculi*; DO, *dilatator operculi*; Ecpt, ectopterygoid; Enpt, endopterygoid; Hy, hyomandibular; Ih, interhyal; Iop, interopercle; LAPpe, *levator arcus palatini p. primordialis externa;* LAPph, *levator arcus palatini p. pharyngealis;* LAPpi, *levator arcus palatini p. primordialis interna*; LAPt, *levator arcus palatini p. temporalis;* LO, *levator operculi*; Mpt, metapterygoid; Op, opercle; Pal, palatine; Pop, preopercle; Qd, quadrate; RH, *ramus hyomandibularis facialis*; Sop, subopercle; Sy, symplectic. Scale bar: 5 mm.

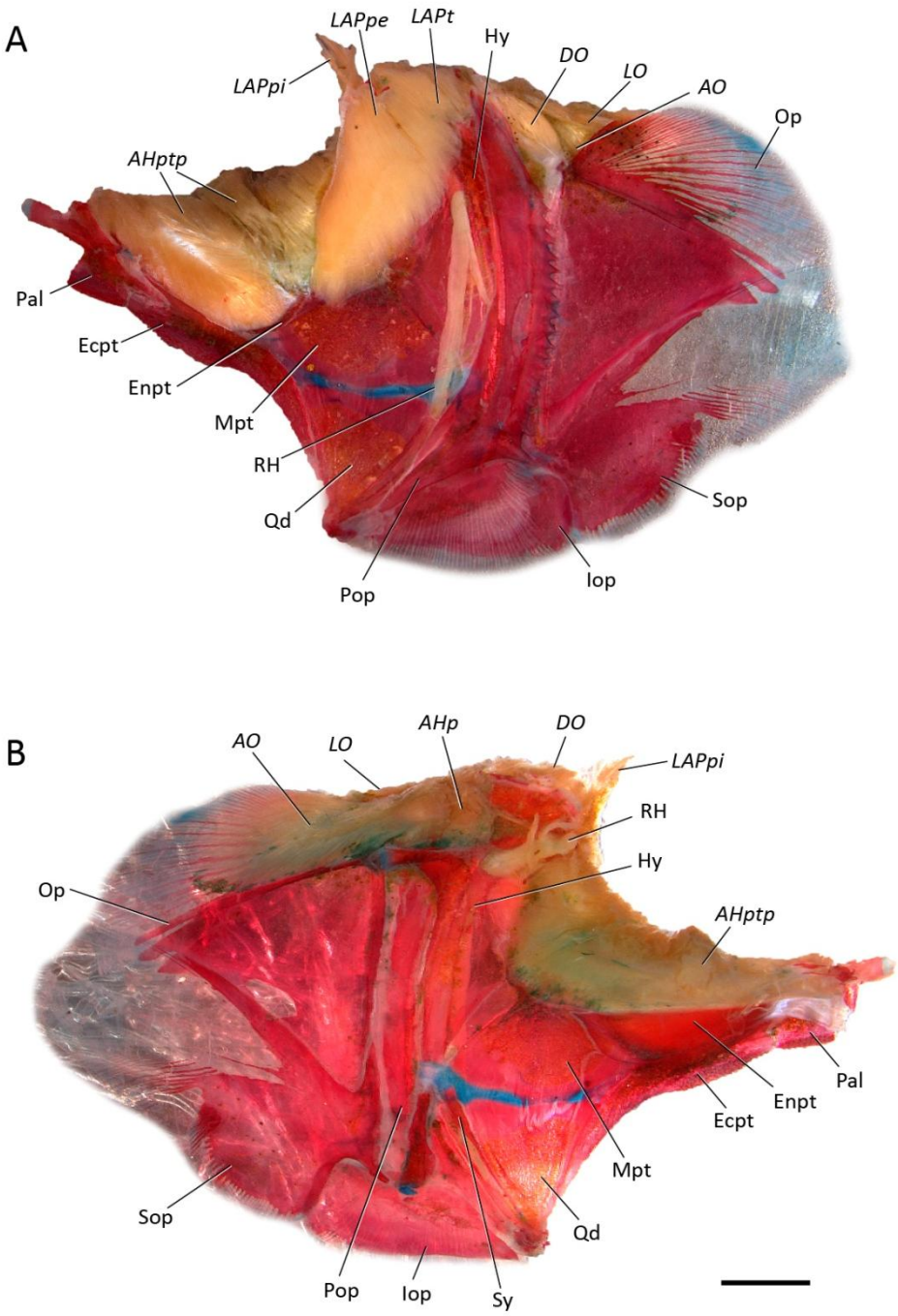

Fig. 13: *Galeoides decadactylus*, hyopalatine arch. A: lateral view. B: medial view. AHp, *adductor hyomandibulae p. primordialis;* AHptp, *adductor hyomandibulae p. pterygo-palatina*; AO, *adductor operculi*; DO, *dilatator operculi*; Ecpt, ectopterygoid; Enpt, endopterygoid; Hy, hyomandibular; Ih, interhyal; Iop, interopercle; LAPpe, *levator arcus palatini p. primordialis externa;* LAPph, *levator arcus palatini p. pharyngealis;* LAPpi, *levator arcus palatini p. primordialis interna*; LAPt, *levator arcus palatini p. temporalis;* LO, *levator operculi*; Mpt, metapterygoid; Op, opercle; Pal, palatine; Pop, preopercle; Qd, quadrate; RH, *ramus hyomandibularis facialis*; Sop, subopercle; Sy, symplectic. Scale bar: 2 mm.

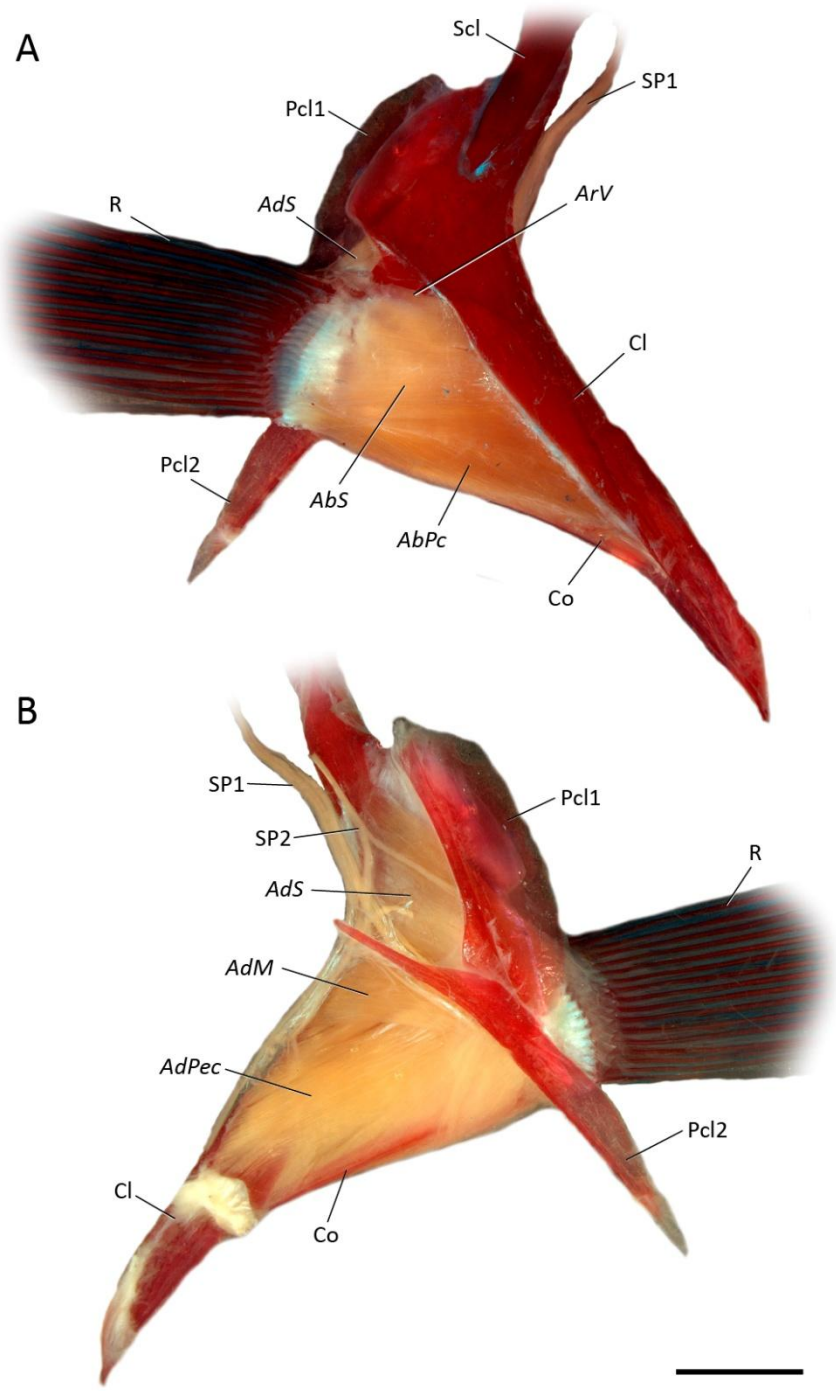

Fig. 14: *Cynoscion striatus*, pectoral girdle. A: lateral view. B: medial view. AbPc, *abductor profundus p. ceterae*; AbS, *abductor superficialis*; AdM, *adductor medialis*; AdPec; *adductor profundus p. ectoprofunda*; AdS, *adductor superficialis*; ArV, arrector ventralis; Cl, cleithrum; Co, coracoid; Pcl1, postcleithrum 1; Pcl2, postcleithrum 2; R, pectoral-fin rays; Scl, supracleithrum; SP, spinal nerve. Scale bar: 3.5 mm.

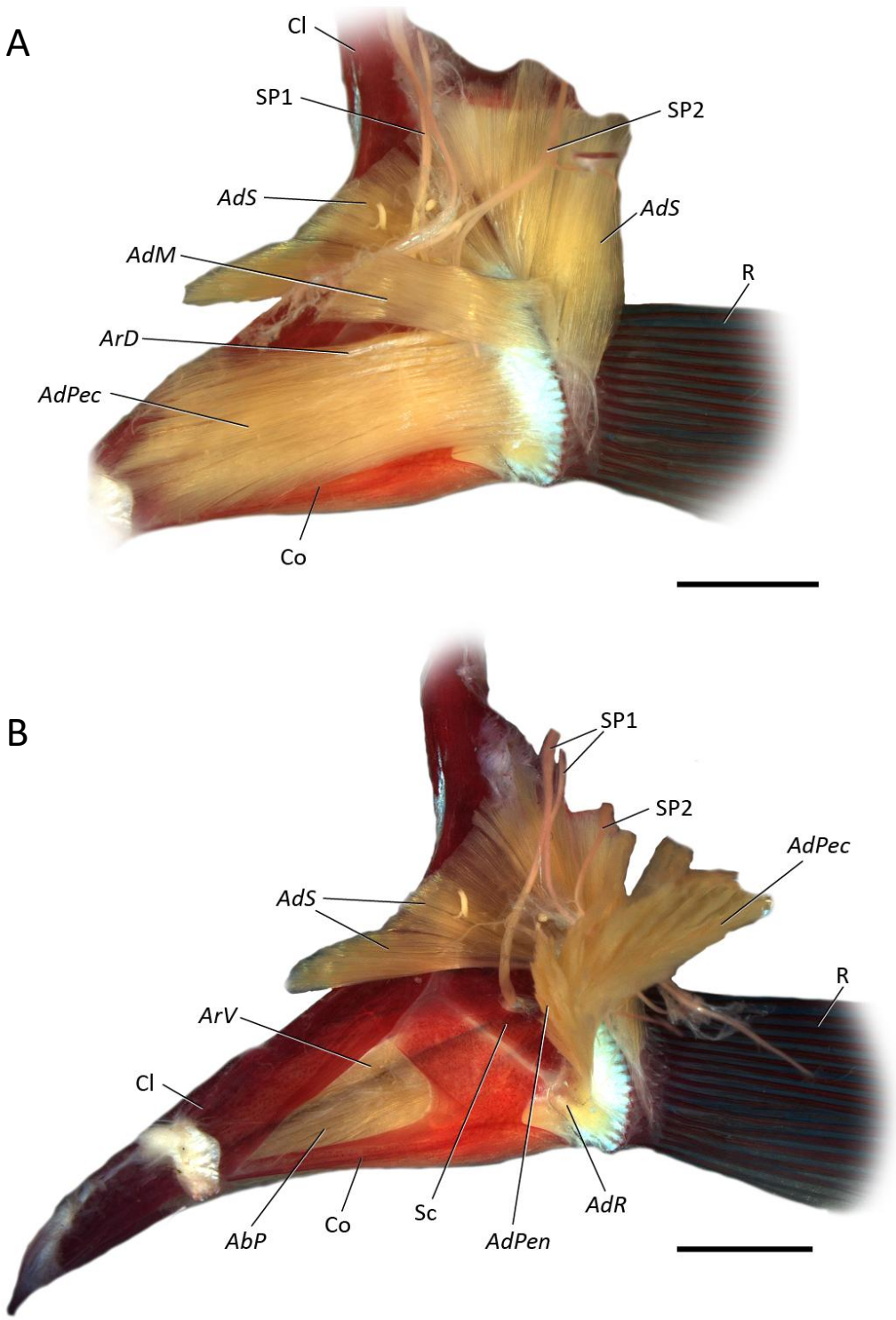

Fig. 15: *Cynoscion striatus*, pectoral girdle. A and B: medial view. AbP, *abductor profundus*; AdM, *adductor medialis*; AdPec; *adductor profundus p. ectoprofunda*; AdPen; *adductor profundus p. endoprofunda;* AdR, *adductor radialis*; AdS, *adductor superficialis*; ArD, *arrector dorsalis*; ArV, arrector ventralis; Cl, cleithrum; Co, coracoid; Pcl1, postcleithrum 1; Pcl2, postcleithrum 2; R, pectoral-fin rays; Sc, scapula; SP, spinal nerve. Scale bar: 3.5 mm.

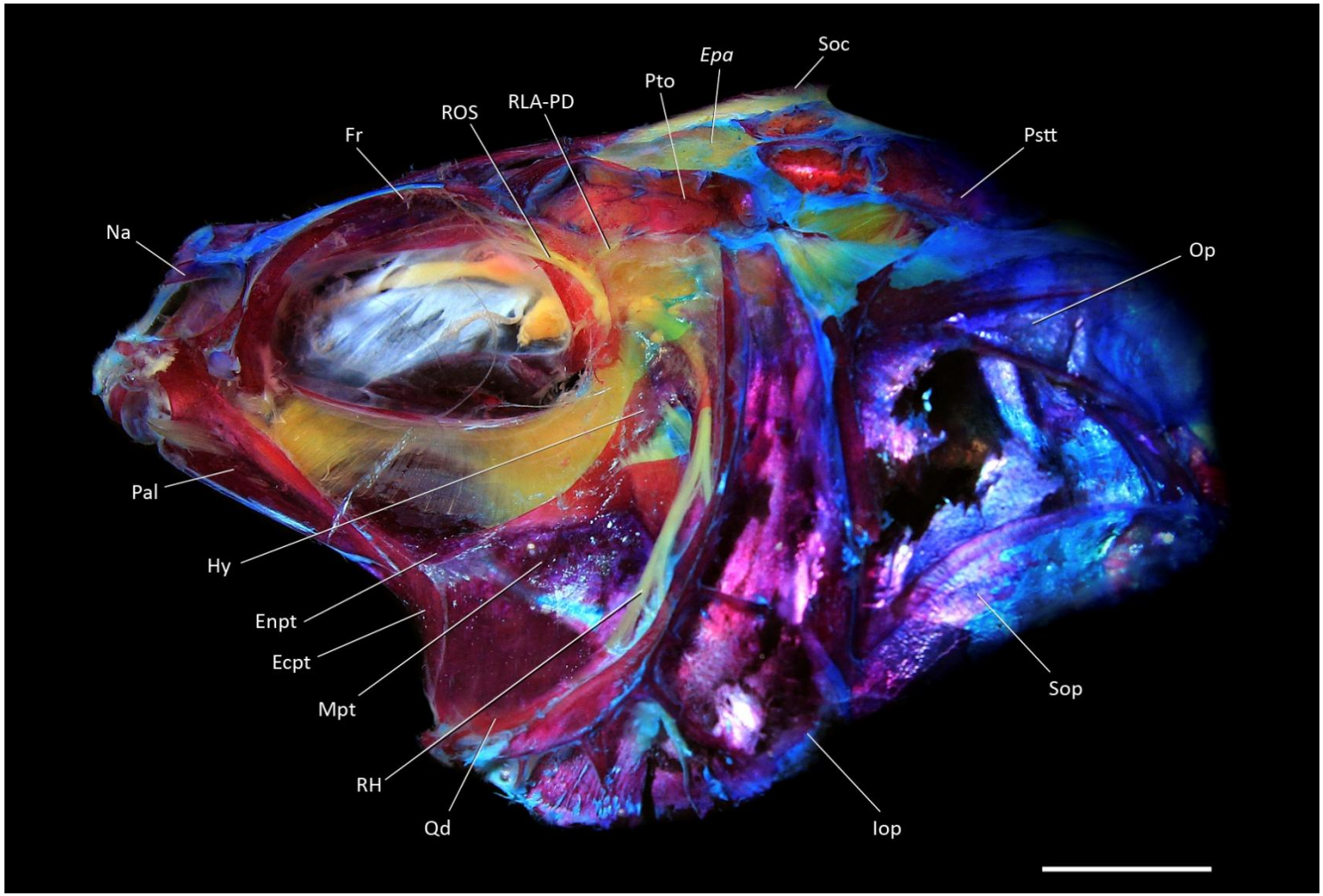

Fig. 16: Lateral view of *Cynoscion striatus* head. Ecpt, ectopterygoid; Enpt, endopterygoid; Epa, *epaxialis*; Fr, frontal; Hy, hyomandibular; Iop, interopercle; Mtp, metapterygoid; Na, nasal; Op, opercle; Pop, preopercle; Pal, palatine; Pstt, posttemporal; Pto, pterotic; Qd, quadrate; RH, *ramus hyomandibularis facialis*; RLA-PD, parieto-dorsal branch of the *ramus lateralis accessorius*; ROS, *ramus ophtalmicus superficialis trigeminus*; Soc, supraoccipital; Sop, subopercle. Scale bars: 5 mm.

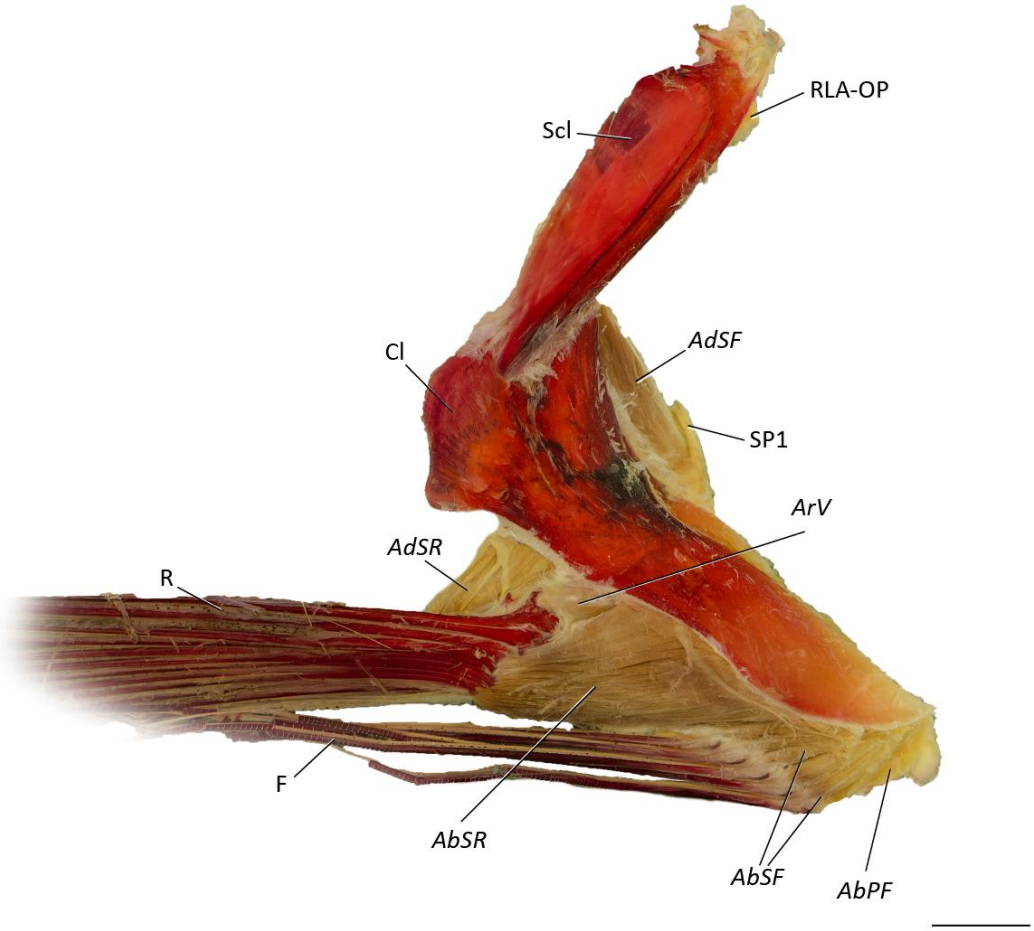

Fig. 17: *Leptomelanosoma indicum*, pectoral girdle, lateral view. AbPF, *abductor profundus filamentaris;* AbSF, *abductor superficialis filamentaris;* AbSR, *abductor superficialis radialis*; AdPec; *adductor profundus p. ectoprofunda*; AdSF, *adductor superficialis filamentaris*; AdSR, *adductor superficialis radialis;* ArV, arrector ventralis; Cl, cleithrum; Co, coracoid; F, pectoral filaments; R, pectoral-fin rays; RLA-OP, orbito-pectoralis branch of the *ramus lateralis accessorius*; Scl, supracleithrum; SP, spinal nerve. Scale bar: 5 mm.

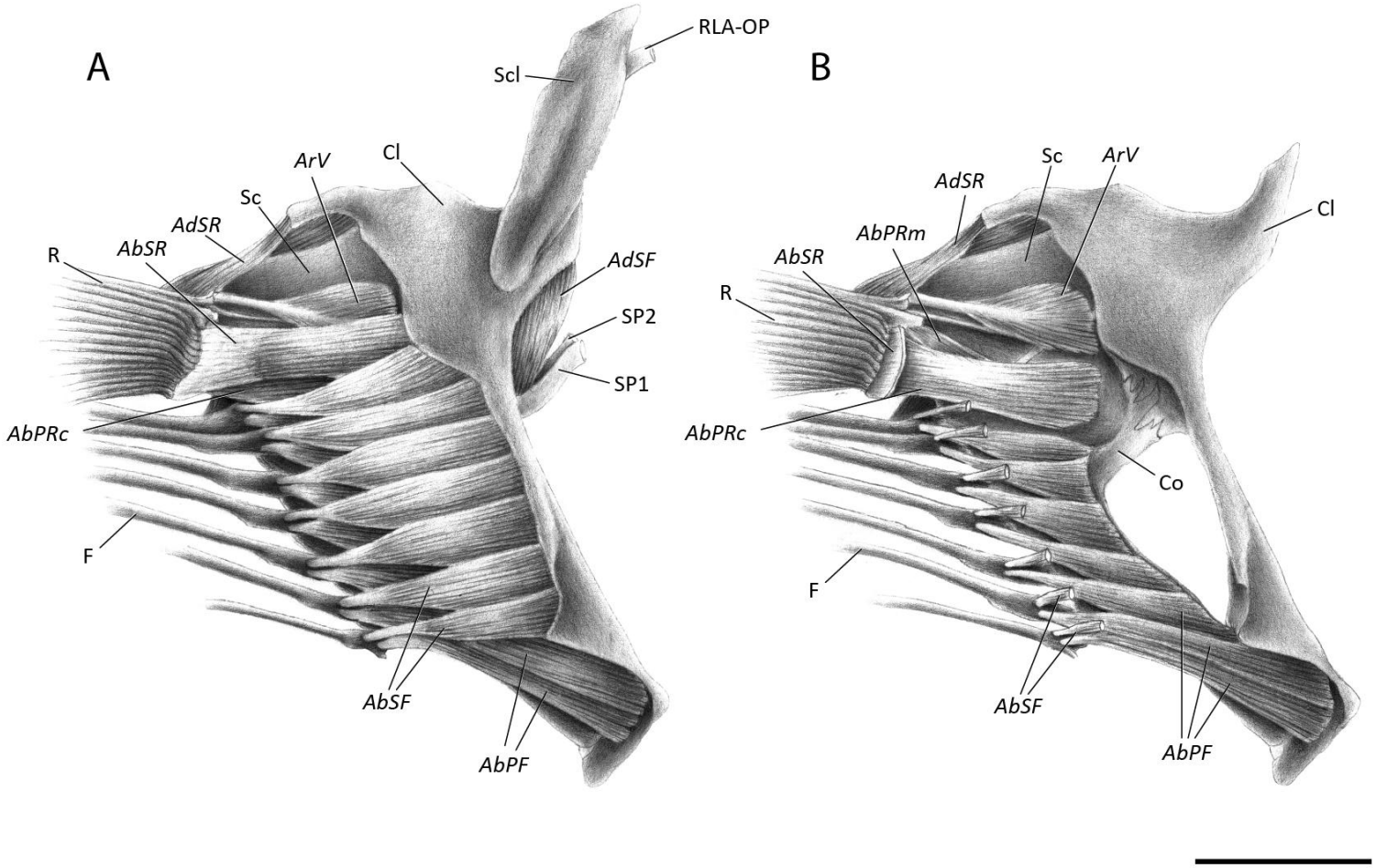

Fig. 18: *Parapolynemus verekeri*, pectoral girdle, lateral view. AbPF, *abductor profundus filamentaris;* AbPRc, *abductor profundus radialis p. ceterae;* AbPRm, *abductor profundus radialis p. marginalis;* AbSF, *abductor superficialis filamentaris;* AbSR, *abductor superficialis radialis*; AdSF, *adductor superficialis filamentaris*; AdSR, *adductor superficialis radialis;* ArV, arrector ventralis; Cl, cleithrum; Co, coracoid; F, pectoral filaments; R, pectoral-fin rays; RLA-OP, orbito-pectoralis branch of the *ramus lateralis accessorius*; Sc, scapula; Scl, supracleithrum; SP, spinal nerve. Scale bar: 2 mm.

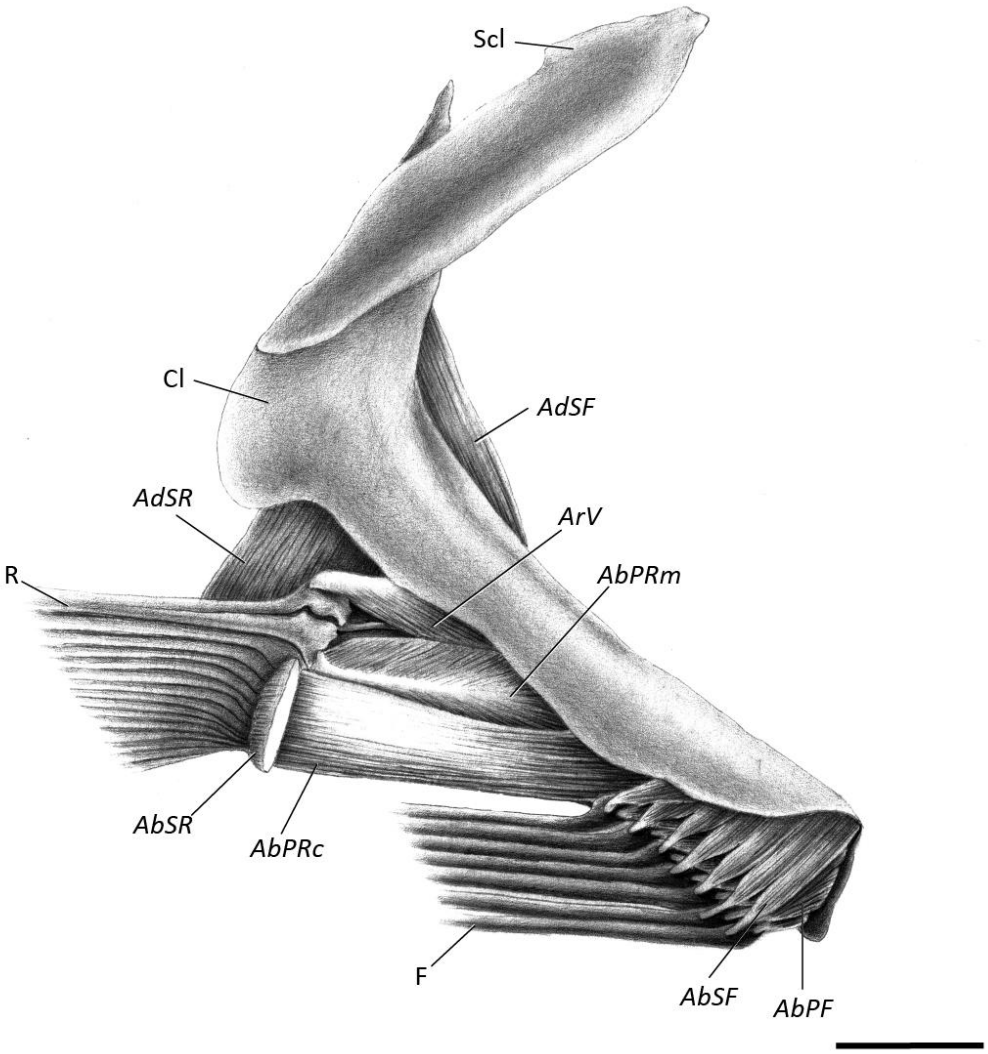

Fig. 19: *Polydactylus oligodon*, pectoral girdle, lateral view. AbPF, *abductor profundus filamentaris;* AbPRc, *abductor profundus radialis p. ceterae;* AbPRm, *abductor profundus radialis p. marginalis;* AbSF, *abductor superficialis filamentaris;* AbSR, *abductor superficialis radialis*; AdSF, *adductor superficialis filamentaris*; AdSR, *adductor superficialis radialis;* ArV, arrector ventralis; Cl, cleithrum; F, pectoral filaments; R, pectoral-fin rays; Scl, supracleithrum. Scale bar: 4 mm.

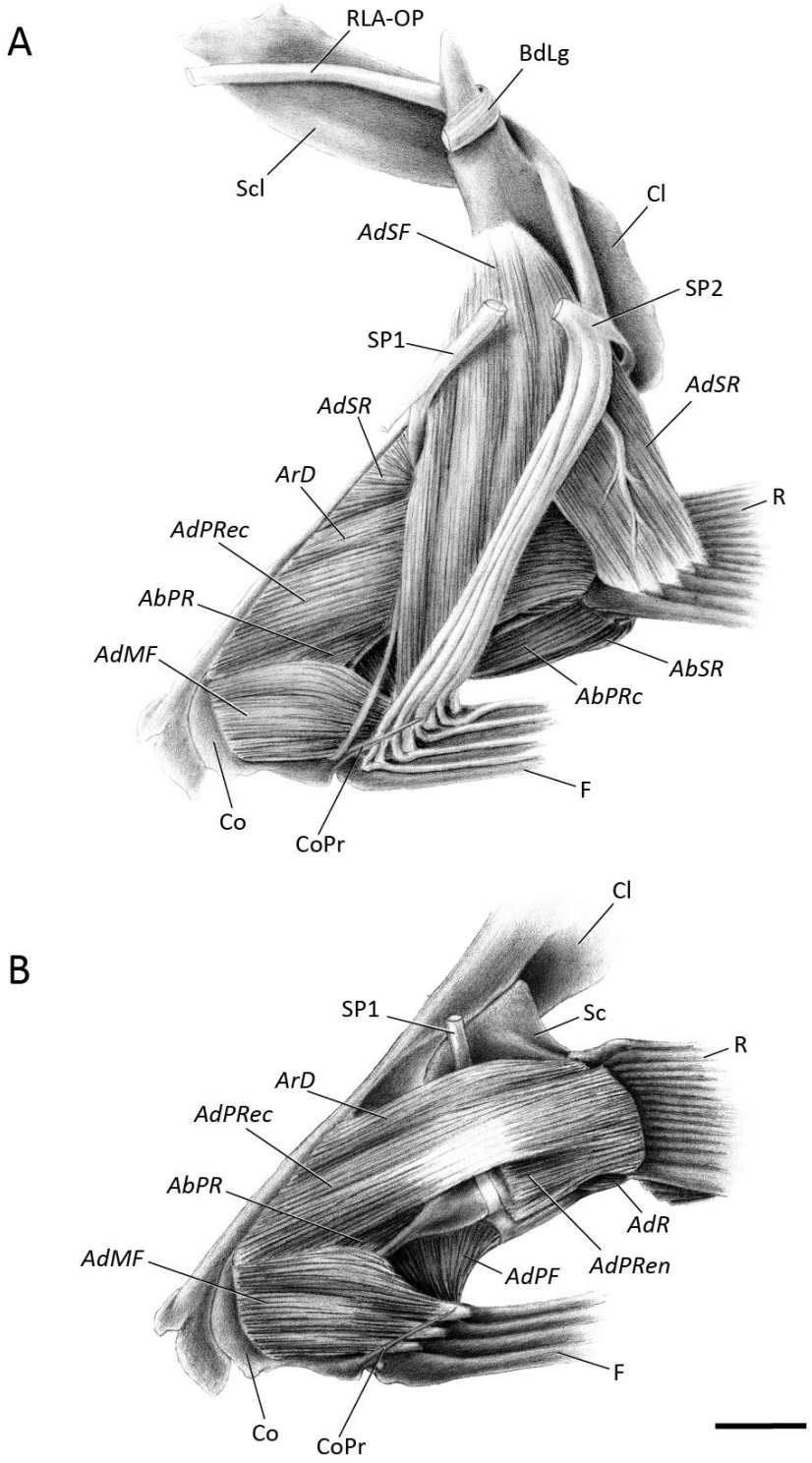

Fig. 20: *Eleutheronema tetradactylum*, pectoral girdle, medial view. AbPRc, *abductor profundus radialis p. ceterae;* AbSR, *abductor superficialis radialis*; AdMF, *adductor medialis filamentaris*; AdPF, *adductor profundus filamentaris*; AdPRec, *adductor profundus radialis p. ectoprofunda*; AdPRen, *adductor profundus radialis p. endoprofunda;* AdR, *adductor radialis*; AdSF, *adductor superficialis filamentaris*; AdSR, *adductor superficialis radialis;* ArD, *arrector dorsalis*; BdLg, Baudelot's ligament; Cl, cleithrum; Co, coracoid; CoPr, coracoid process; F, pectoral filaments; R, pectoral-fin rays; RLA-OP, orbito-pectoralis branch of the *ramus lateralis accessorius*; Sc, scapula; Scl, supracleithrum; SP, spinal nerve. Scale bar: 2 mm.

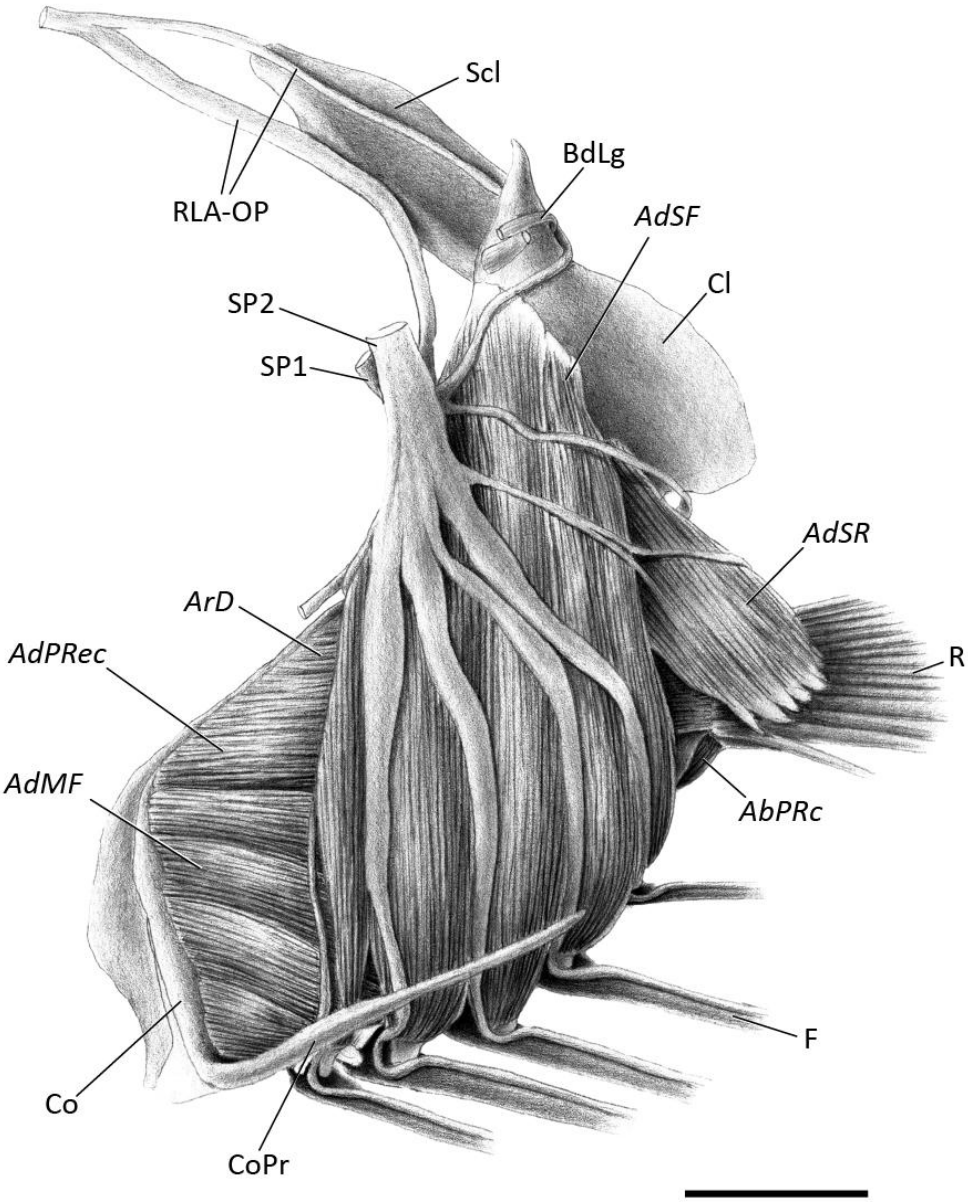

Fig. 21: *Pentanemus quinquarius*, pectoral girdle, medial view. AbPRc, *abductor profundus radialis p. ceterae;* AbSR, *abductor superficialis radialis*; AdMF, *adductor medialis filamentaris*; AdPRec, *adductor profundus radialis p. ectoprofunda*; AdSF, *adductor superficialis filamentaris*; AdSR, *adductor superficialis radialis;* ArD, *arrector dorsalis*; BdLg, Baudelot's ligament; Cl, cleithrum; Co, coracoid; CoPr, coracoid process; F, pectoral filaments; R, pectoral-fin rays; RLA-OP, orbito-pectoralis branch of the *ramus lateralis accessorius*; Scl, supracleithrum; SP, spinal nerve. Scale bar: 4 mm.

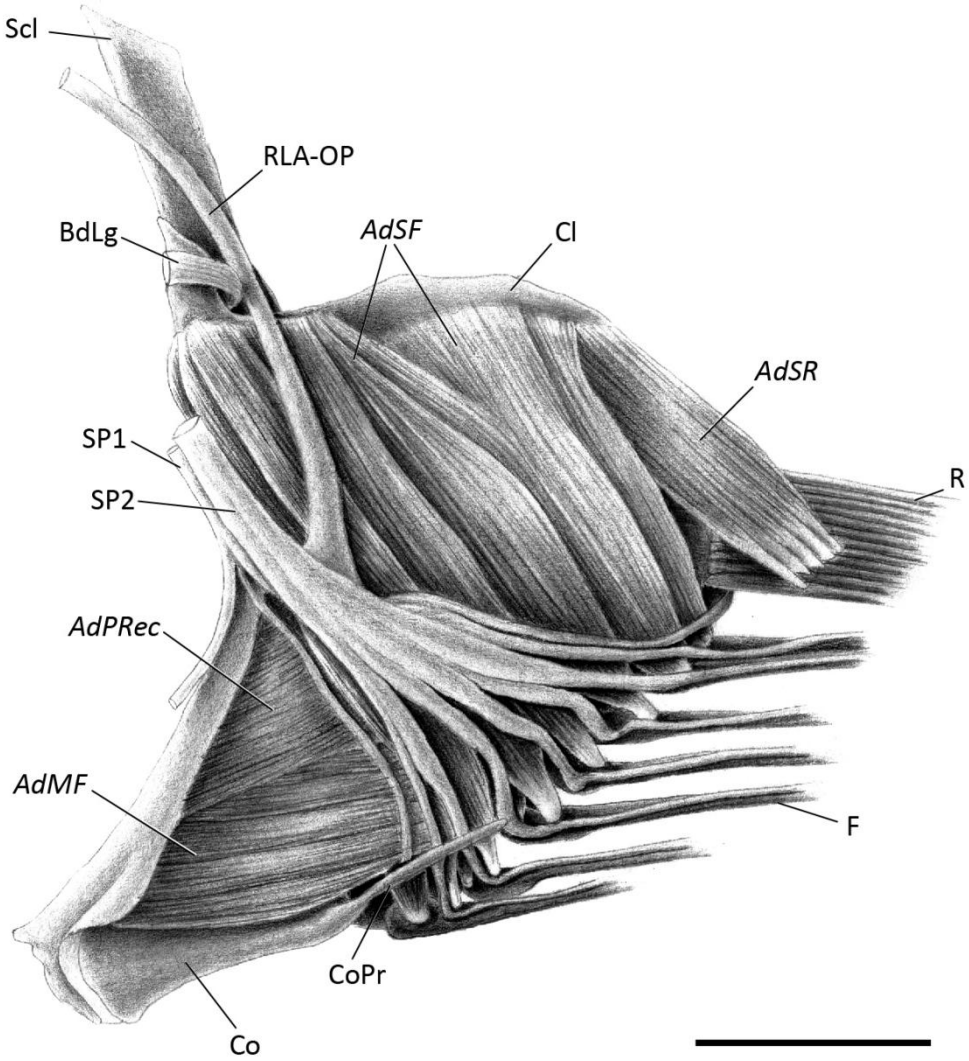

Fig. 22: *Parapolynemus verekeri*, pectoral girdle, medial view. AbPRc, *abductor profundus radialis p. ceterae;* AbSR, *abductor superficialis radialis*; AdMF, *adductor medialis filamentaris*; AdPRec, *adductor profundus radialis p. ectoprofunda*; AdSF, *adductor superficialis filamentaris*; AdSR, *adductor superficialis radialis;* ArD, *arrector dorsalis*; BdLg, Baudelot's ligament; Cl, cleithrum; Co, coracoid; CoPr, coracoid process; F, pectoral filaments; R, pectoral-fin rays; RLA-OP, orbito-pectoralis branch of the *ramus lateralis accessorius*; Scl, supracleithrum; SP, spinal nerve. Scale bar: 4 mm.

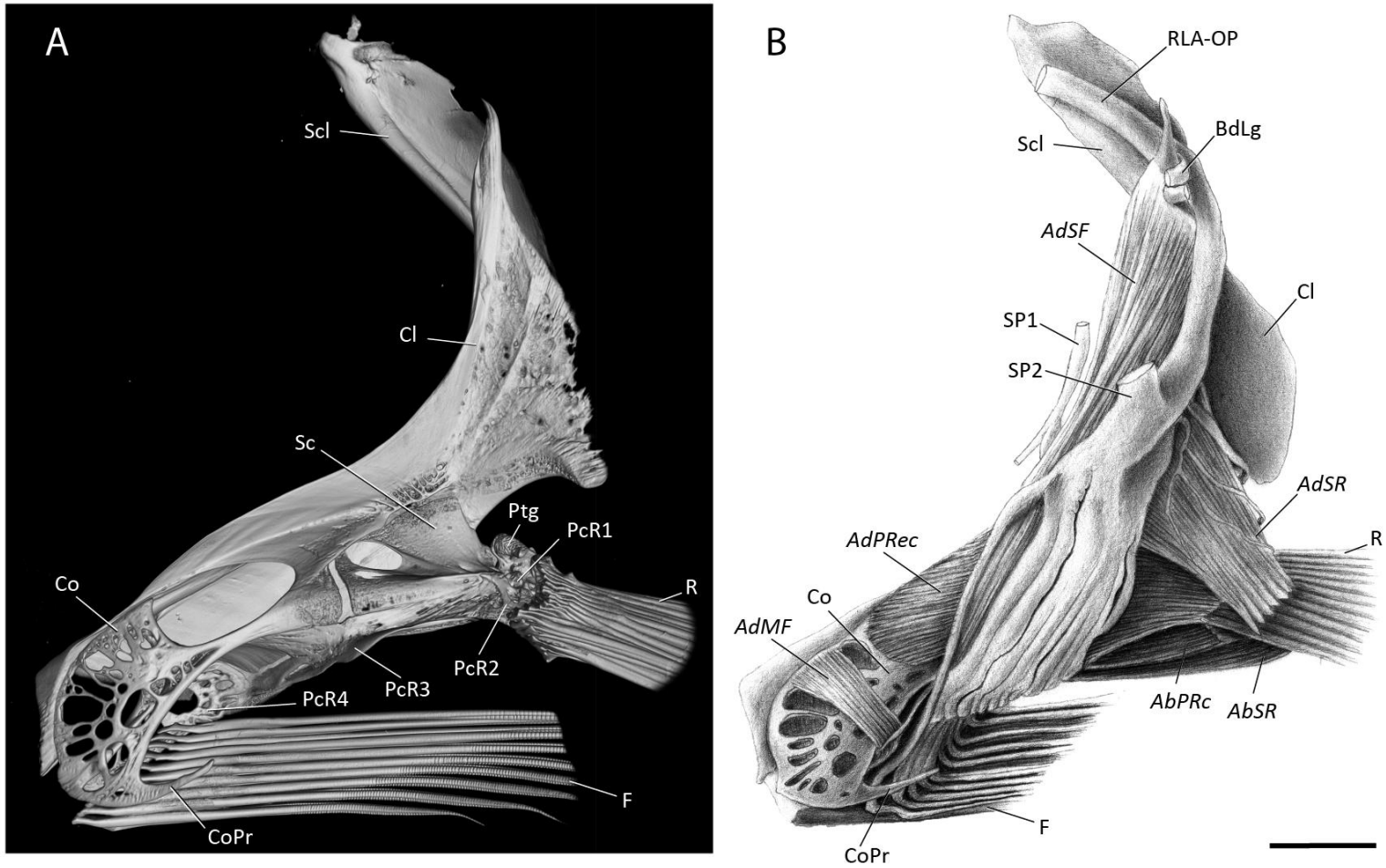

Fig. 23: *Galeoides decadactylus*, pectoral girdle, medial view. AbPRc, *abductor profundus radialis p. ceterae;* AbSR, *abductor superficialis radialis*; AdMF, *adductor medialis filamentaris*; AdPRec, *adductor profundus radialis p. ectoprofunda*; AdSF, *adductor superficialis filamentaris*; AdSR, *adductor superficialis radialis;* BdLg, Baudelot's ligament; Cl, cleithrum; Co, coracoid; CoPr, coracoid process; F, pectoral filaments; PcR, pectoral radial; Ptg, propterygium; R, pectoral-fin rays; RLA-OP, orbito-pectoralis branch of the *ramus lateralis accessorius*; Sc, scapula; Scl, supracleithrum; SP, spinal nerve. Scale bar: 5 mm.

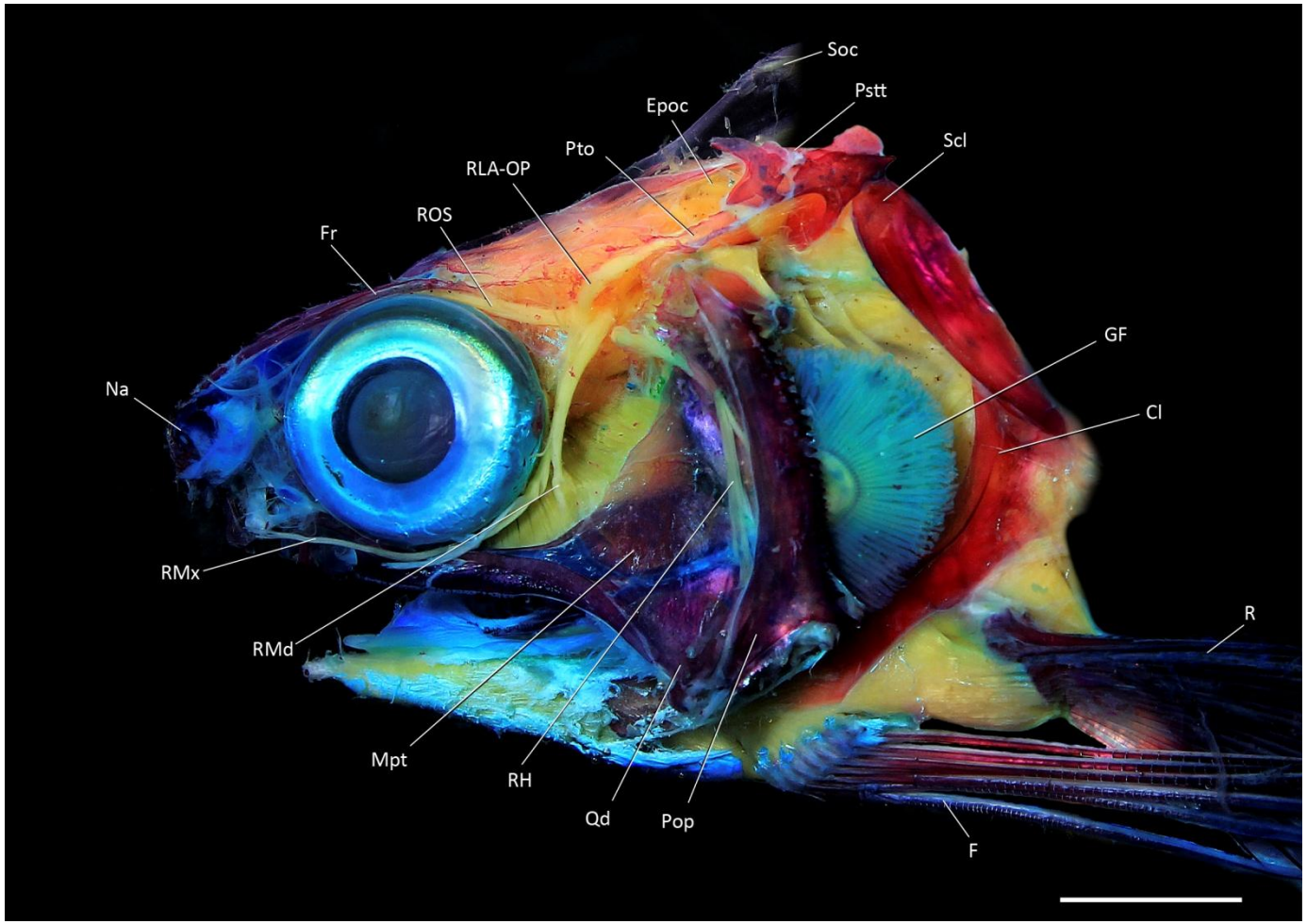

Fig. 24: Lateral view of *Polydactylus virginicus* head. Cl, cleithrum; Epoc, epioccipital; F, pectoral filaments; Fr, frontal; GF, gill filaments; Mtp, metapterygoid; Na, nasal; Pop, preopercle; Pstt, posttemporal; Pto, pterotic; Qd, quadrate; R, pectoral-fin rays; RH, *ramus hyomandibularis facialis*; RLA-OP, orbito-pectoralis branch of the *ramus lateralis accessorius*; RMd, *ramus mandibularis trigeminus*; RMx, *ramus maxillaris trigeminus*; ROS, *ramus ophtalmicus superficialis trigeminus*; Scl, supracleithrum; Soc, supraoccipital; Sop, subopercle. Scale bars: 5 mm.

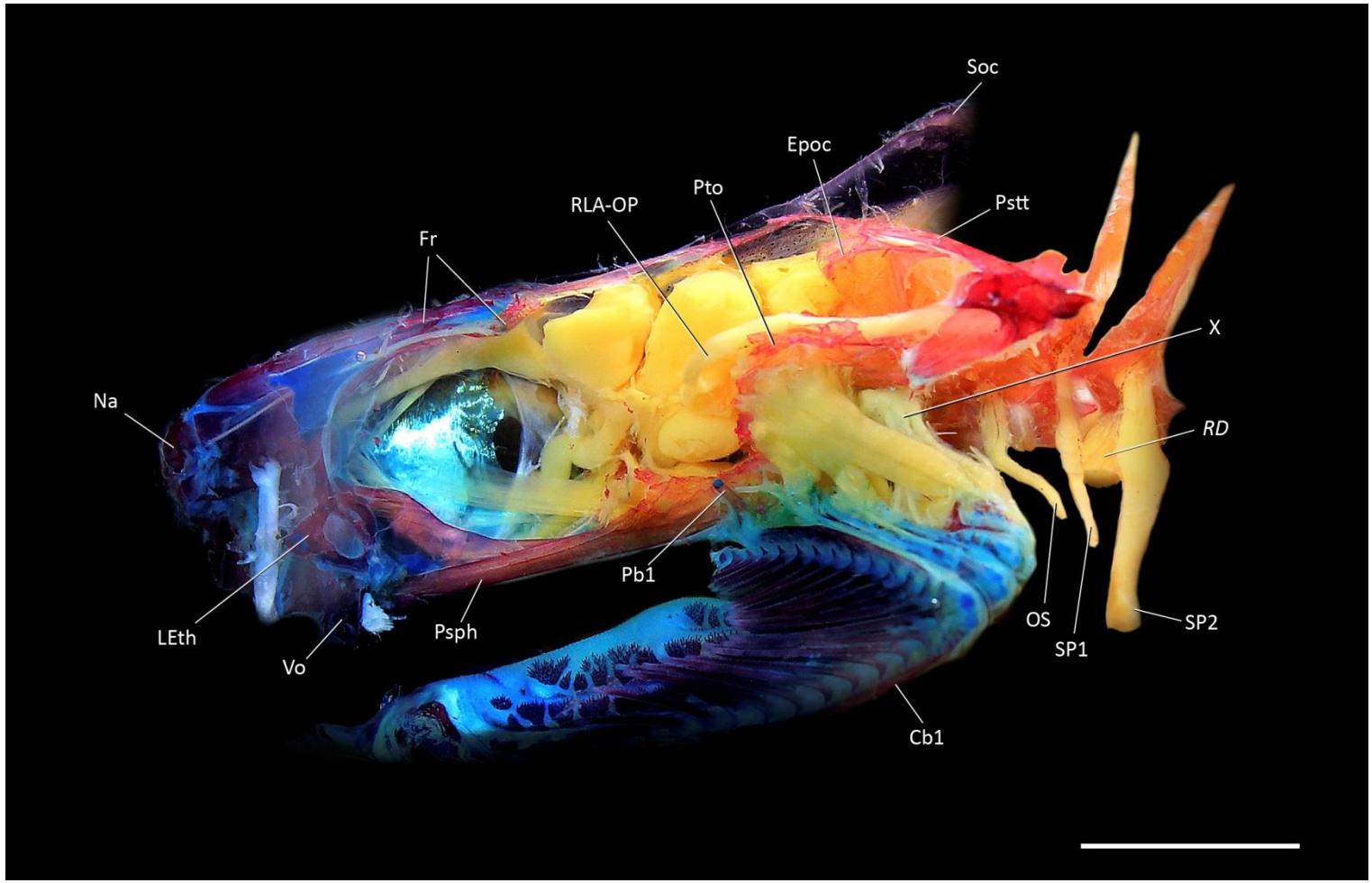

Fig. 25: Lateral view of *Polydactylus virginicus* head. Cb, ceratobranchial; Epoc, epioccipital; Fr, frontal; LEth, lateral ethmoid; Na, nasal; OS, occipito-spinal nerve; Pb, pharyngobranchial; Psph, parasphenoid; Pstt, posttemporal; Pto, pterotic; RD, *retractor dorsalis*; RLA-OP, orbito-pectoralis branch of the *ramus lateralis accessorius*; Soc, supraoccipital; SP spinal nerve; Vo, vomer; X, *vagus*. Scale bars: 5 mm.

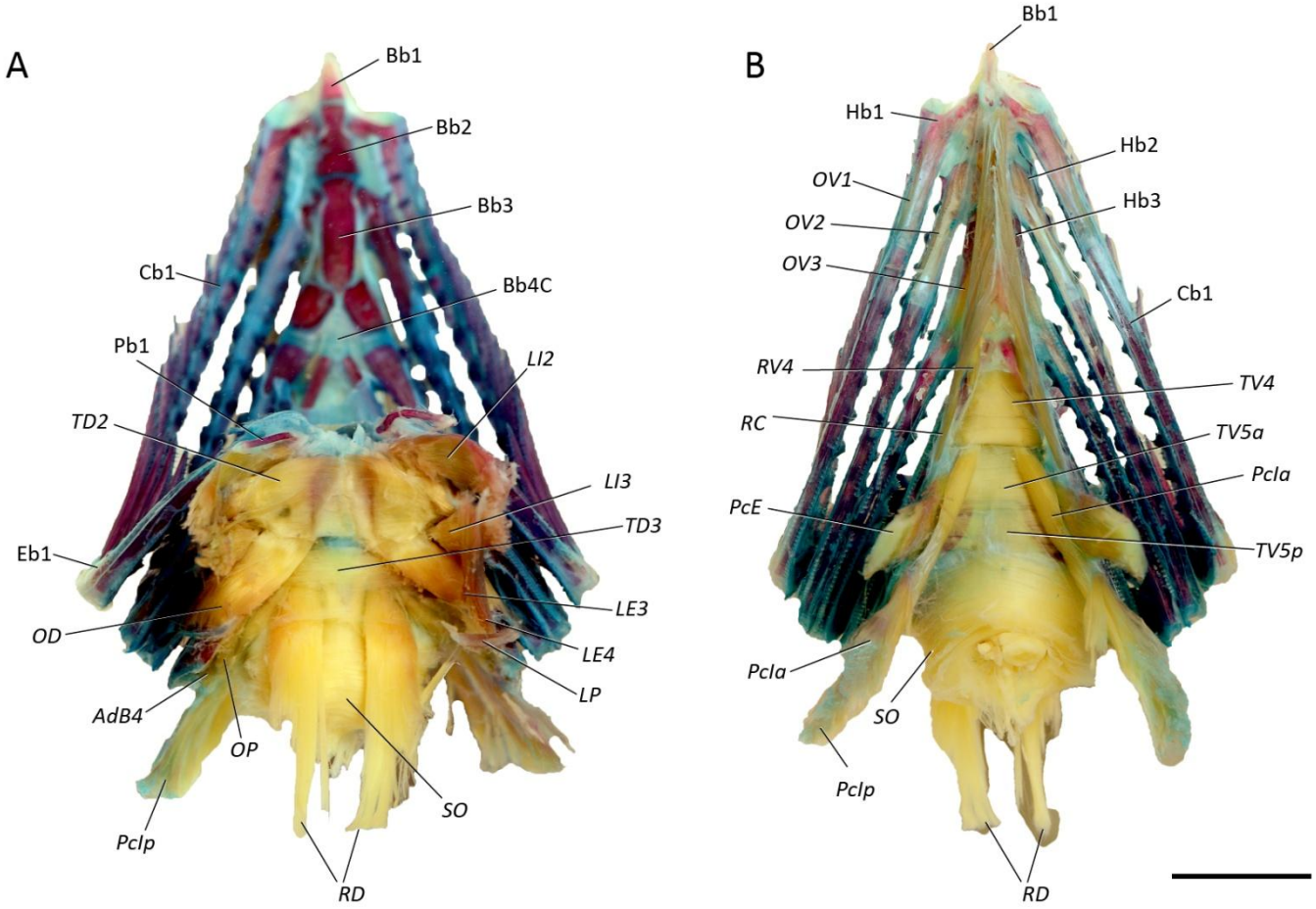

Fig. 26: *Cynoscion striatus,* branchial arches. A: dorsal view. B: ventral view. AdB, *adductor branchialis*; Bb, basibranchial; Bb4C, basibranchial 4 cartilage; Cb, ceratobranchial; Eb, epibranchial; Hb, hypobranchial; LE, *levator externus*; LI, *levator internus*; LP, *levator posterior*; OD, *obliquus dorsalis;* OP, *obliquus posterior*; OV, *obliquus ventralis*; Pb, pharyngobranchial; PcE, *pharyngoclavicularis externus;* PcIa, anteroventral section of *pharyngoclavicularis internus;* PcIp, posterodorsal section of *pharyngoclavicularis internus*; RC, *rectus communis*; RD, *retractor dorsalis*; RV4, *rectus ventralis IV*; SO, *sphincter oesophagi*; TD, *transversus dorsalis*; TV, *transversus ventralis*; TVa, anterior section of *transversus ventralis*; TVp, posterior section of *transversus ventralis*. Scale bars: 5 mm.

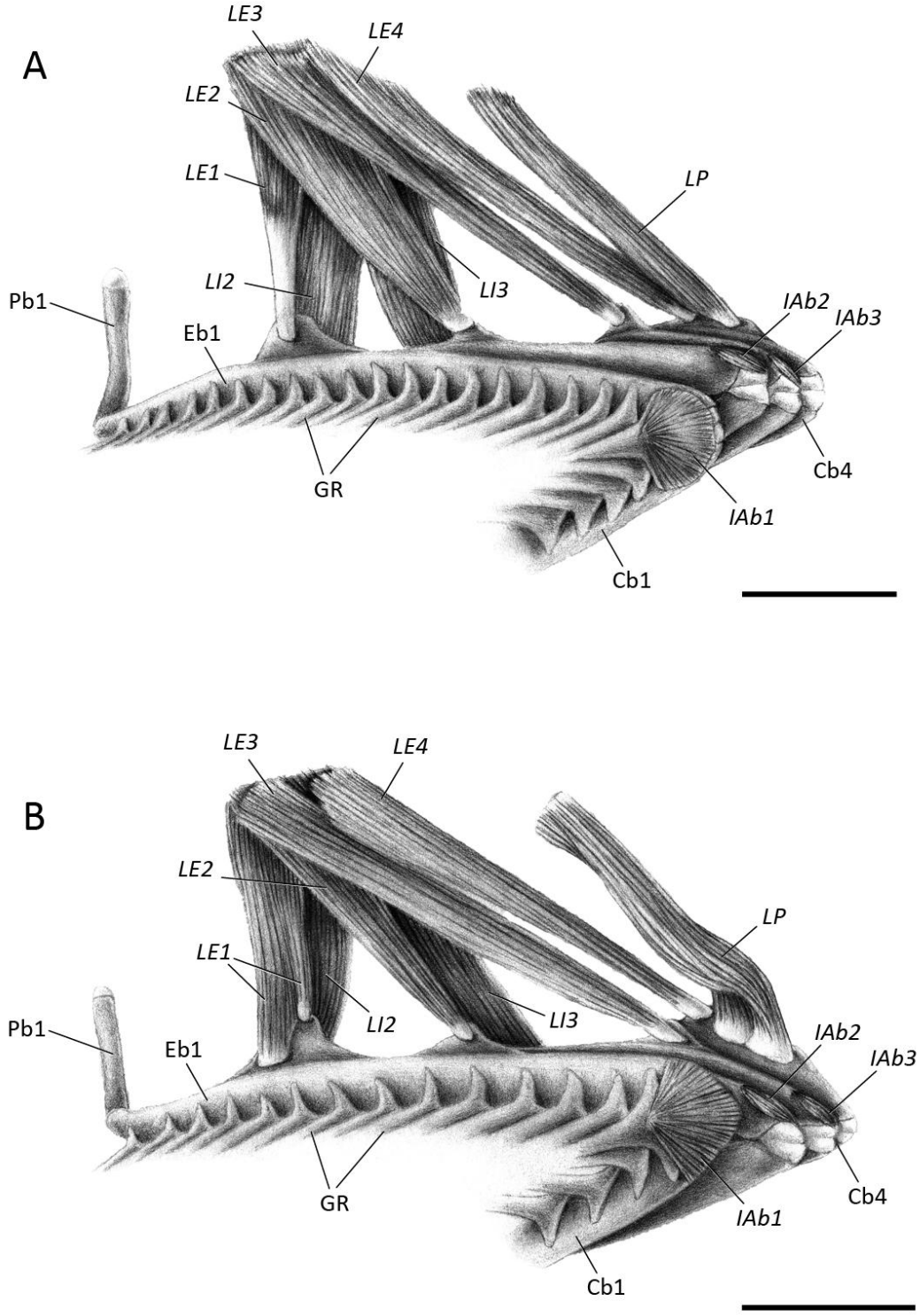

Fig. 27: Branchial arches, lateral view. A: *Pentanemus quinquarius*. B: *Polynemus paradiseus*. Cb, ceratobranchial; Eb, epibranchial; IAb, *interbranchialis abductor*; LE, *levator externus*; LI, *levator internus*; LP, *levator posterior*; Pb, pharyngobranchial. Scale bars: 2 mm.

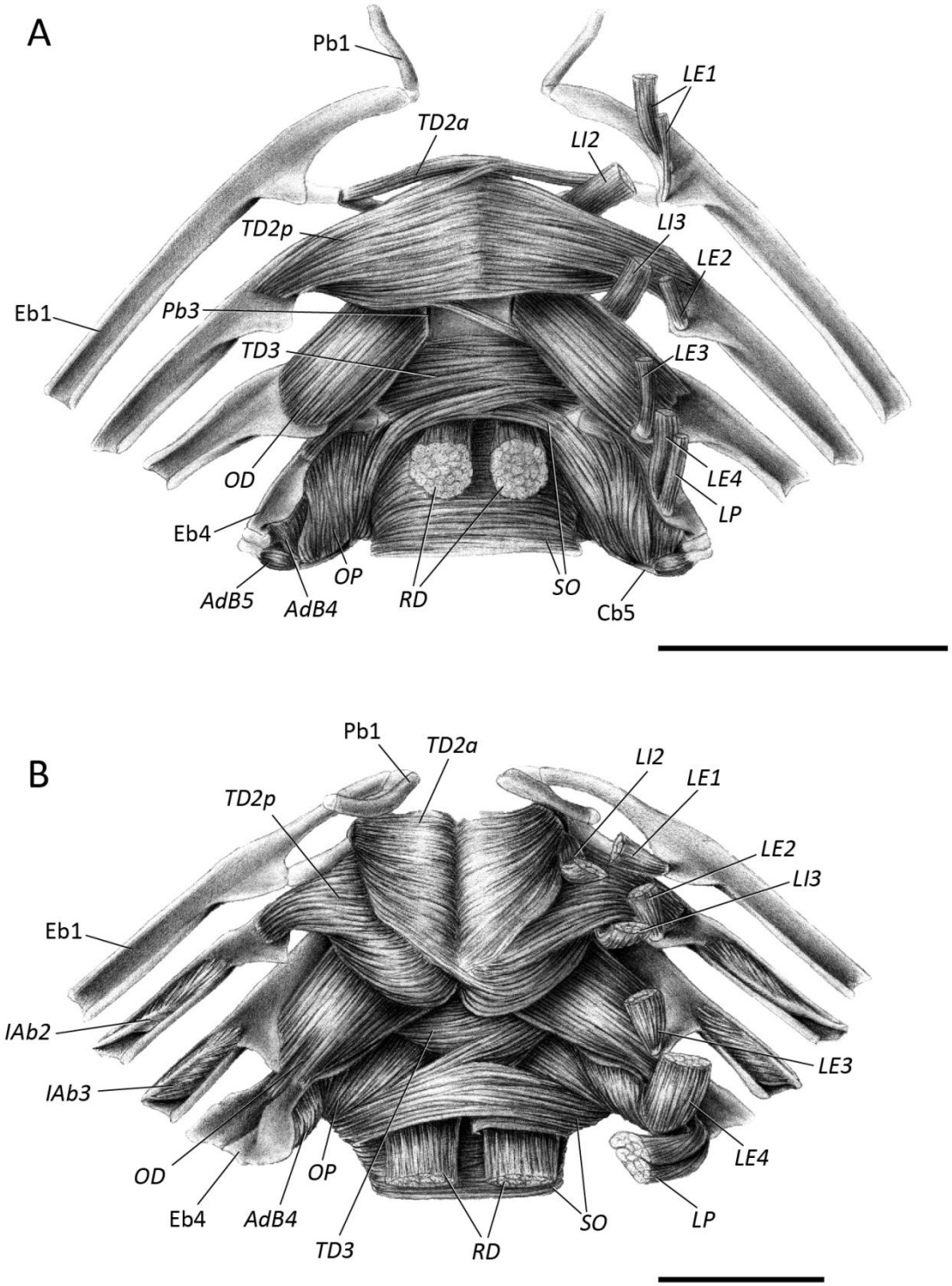

Fig. 28: *B*ranchial arches, dorsal view. A: *Parapolynemus verekeri*. B: *Galeoides decadactylus*. AdB, *adductor branchialis*; Cb, ceratobranchial; Eb, epibranchial; IAb, *interbranchialis abductor*; LE, *levator externus*; LI, *levator internus*; LP, *levator posterior*; OD, *obliquus dorsalis;* OP, *obliquus posterior*; Pb, pharyngobranchial; RD, *retractor dorsalis*; SO, *sphincter oesophagi*; TD, *transversus dorsalis*; TDa, anterior section of *transversus dorsalis*; TDp, posterior section of *transversus dorsalis*. Scale bars: 5 mm.

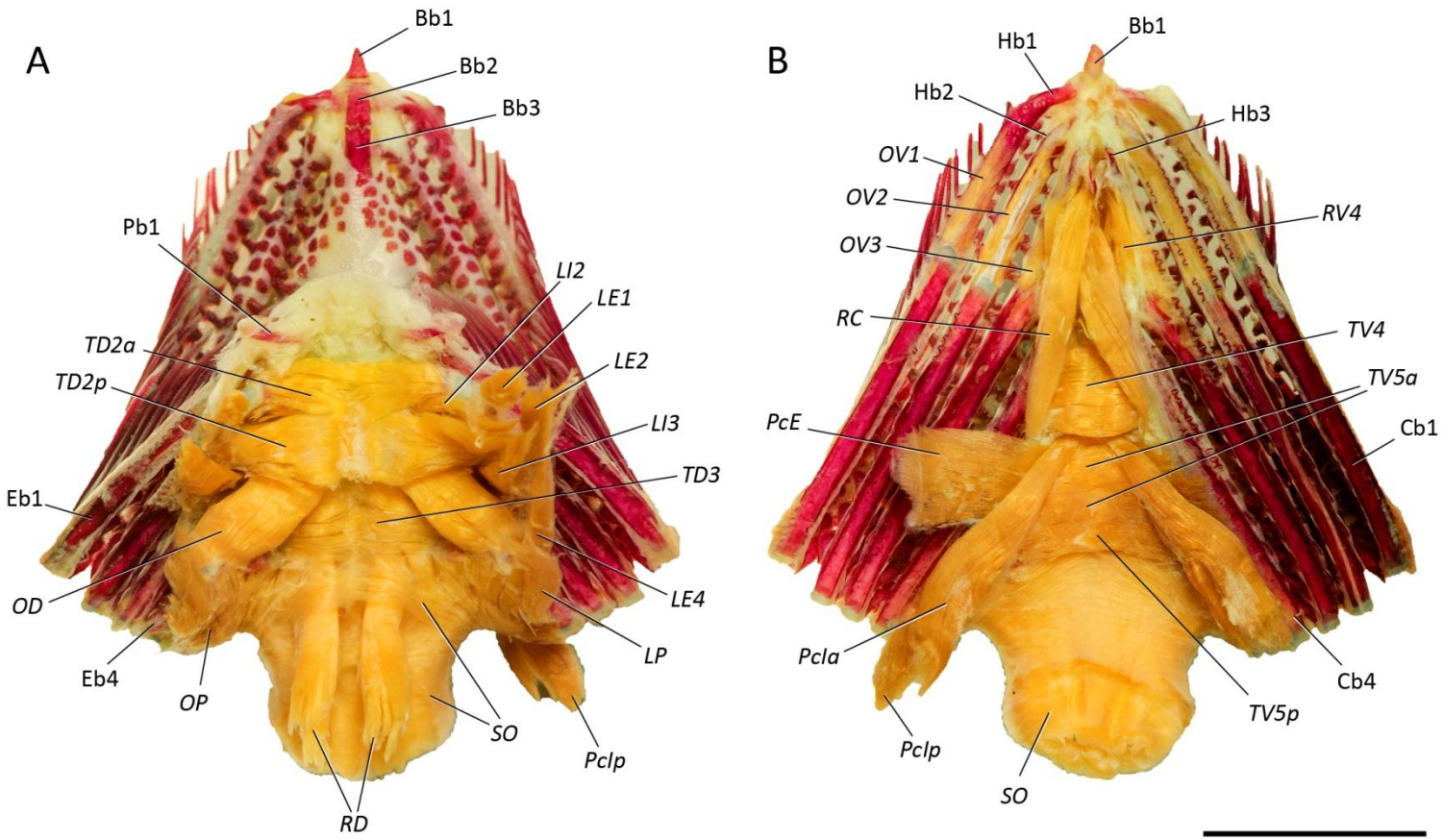

Fig. 29: *Polynemus paradiseus,* branchial arches. A: dorsal view. B: ventral view. AdB, *adductor branchialis*; Bb, basibranchial; Bb4C, basibranchial 4 cartilage; Cb, ceratobranchial; Eb, epibranchial; Hb, hypobranchial; LE, *levator externus*; LI, *levator internus*; LP, *levator posterior*; OD, *obliquus dorsalis;* OP, *obliquus posterior*; OV, *obliquus ventralis*; Pb, pharyngobranchial; PcE, *pharyngoclavicularis externus;* PcIa, anteroventral section of *pharyngoclavicularis internus;* PcIp, posterodorsal section of *pharyngoclavicularis internus*; RC, *rectus communis*; RD, *retractor dorsalis*; RV4, *rectus ventralis IV*; SO, *sphincter oesophagi*; TD, *transversus dorsalis*; TDa, anterior section of *transversus dorsalis*; TDp, posterior section of *transversus dorsalis;* TV, *transversus ventralis*; TVa, anterior section of *transversus ventralis*; TVp, posterior section of *transversus ventralis*. Scale bars: 5 mm.

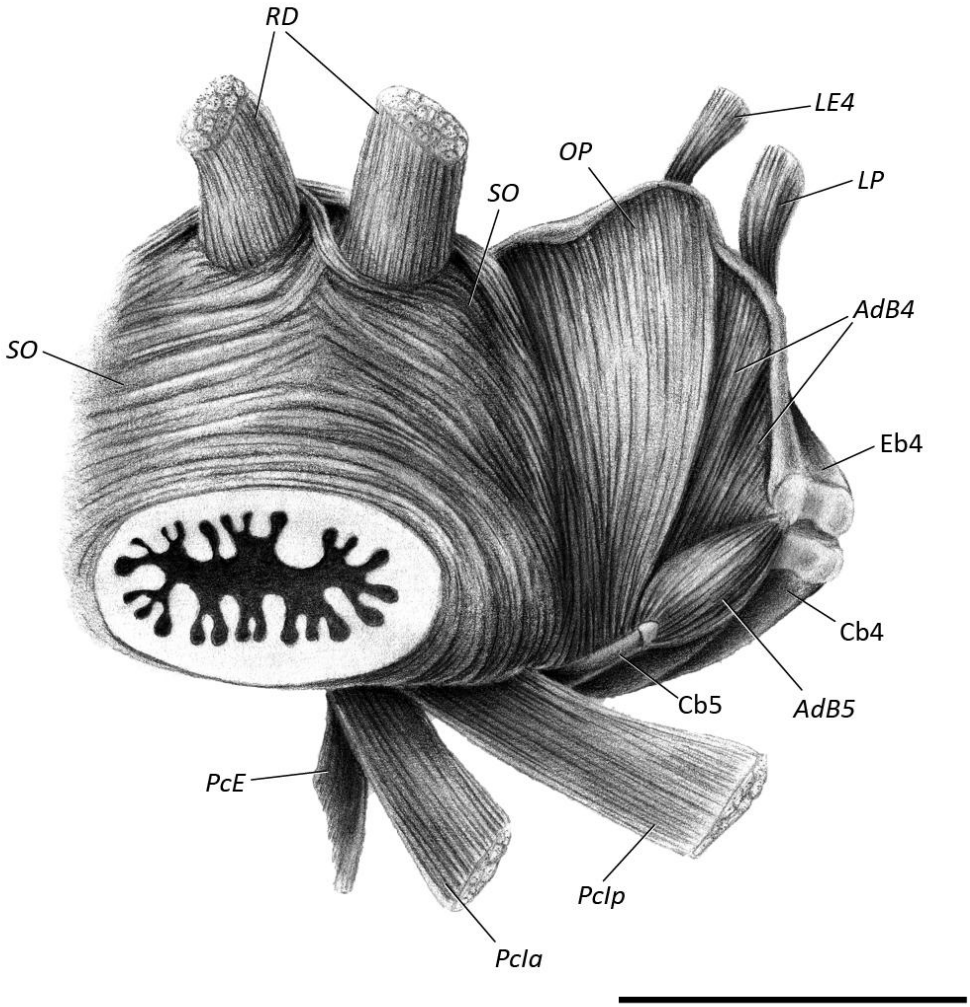

Fig. 30: *Polydactylus approximans*, branchial arches, posterior view. AdB, *adductor branchialis*; Cb, ceratobranchial; Eb, epibranchial; LE, *levator externus*; LP, *levator posterior;* OP, *obliquus posterior*; PcE, *pharyngoclavicularis externus;* PcIa, anteroventral section of *pharyngoclavicularis internus;* PcIp, posterodorsal section of *pharyngoclavicularis internus;* RD, *retractor dorsalis*; SO, *sphincter oesophagi*. Scale bars: 2 mm.

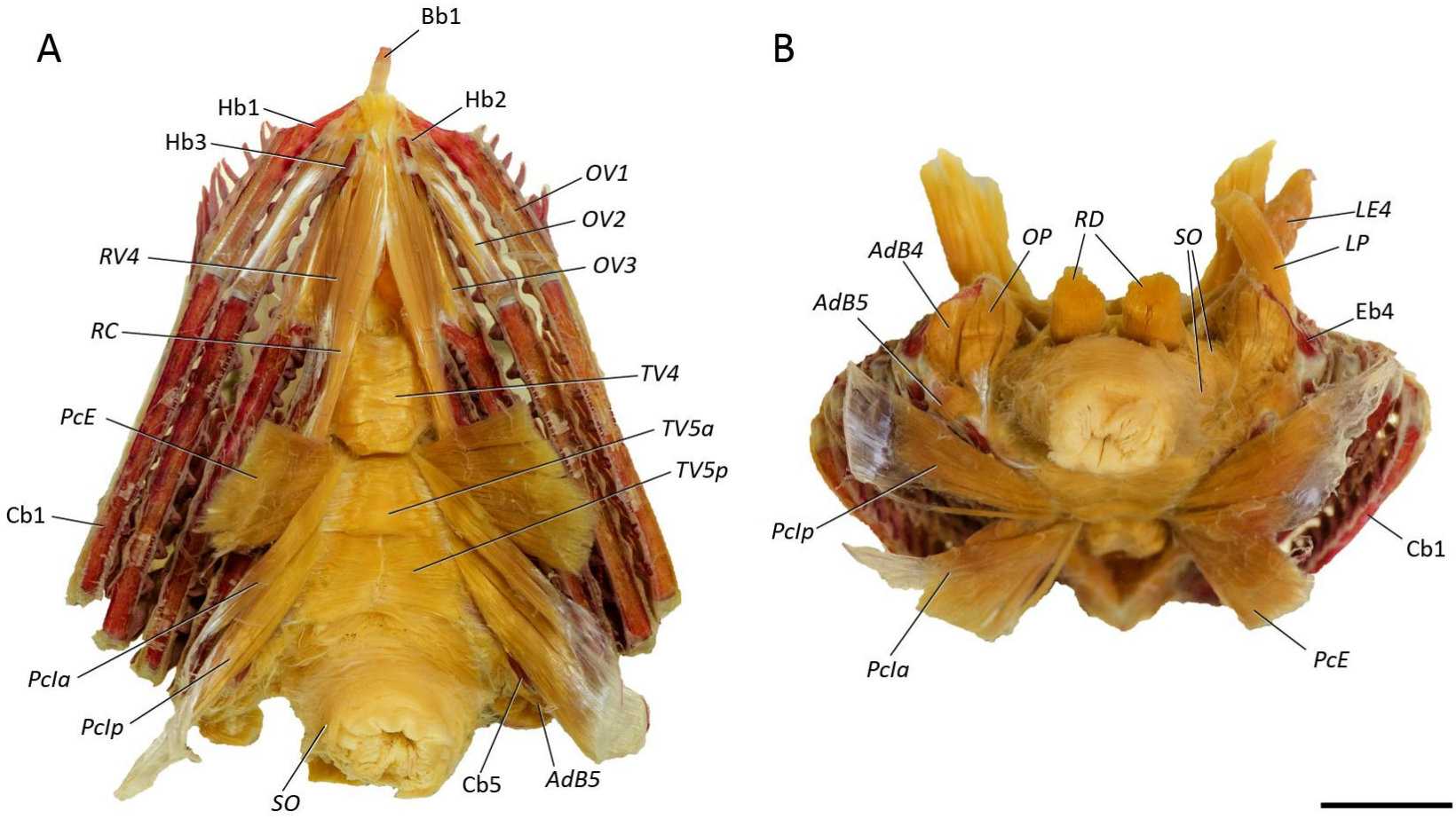

Fig. 31: *Galeoides decadactylus,* branchial arches. A: ventral view. B: posterior view. AdB, *adductor branchialis*; Bb, basibranchial; Cb, ceratobranchial; Eb, epibranchial; Hb, hypobranchial; LE, *levator externus*; LP, *levator posterior;* OP, *obliquus posterior*; OV, *obliquus ventralis*; PcE, *pharyngoclavicularis externus;* PcIa, anteroventral section of *pharyngoclavicularis internus;* PcIp, posterodorsal section of *pharyngoclavicularis internus*; RC, *rectus communis*; RD, *retractor dorsalis*; RV4, *rectus ventralis IV*; SO, *sphincter oesophagi*; TV, *transversus ventralis*; TVa, anterior section of *transversus ventralis*; TVp, posterior section of *transversus ventralis*. Scale bars: 5 mm.

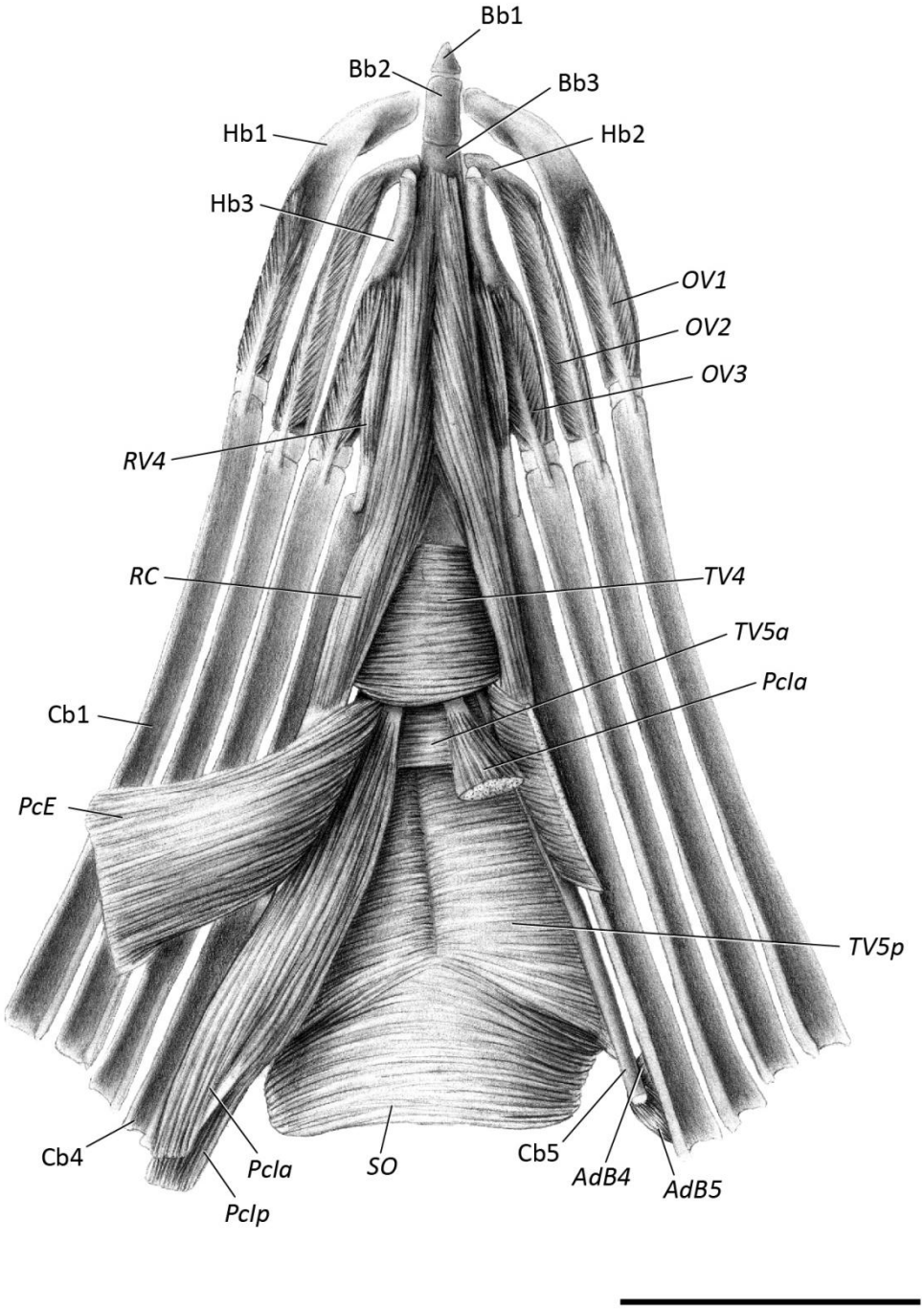

Fig. 32: *Eleutheronema tetradactylum,* branchial arches, ventral view. AdB, *adductor branchialis*; Bb, basibranchial; Cb, ceratobranchial; Hb, hypobranchial; OV, *obliquus ventralis*; PcE, *pharyngoclavicularis externus;* PcIa, anteroventral section of *pharyngoclavicularis internus;* PcIp, posterodorsal section of *pharyngoclavicularis internus*; RC, *rectus communis*; RV4, *rectus ventralis IV*; SO, *sphincter oesophagi*; TV, *transversus ventralis*; TVa, anterior section of *transversus ventralis*; TVp, posterior section of *transversus ventralis*. Scale bars: 5 mm.

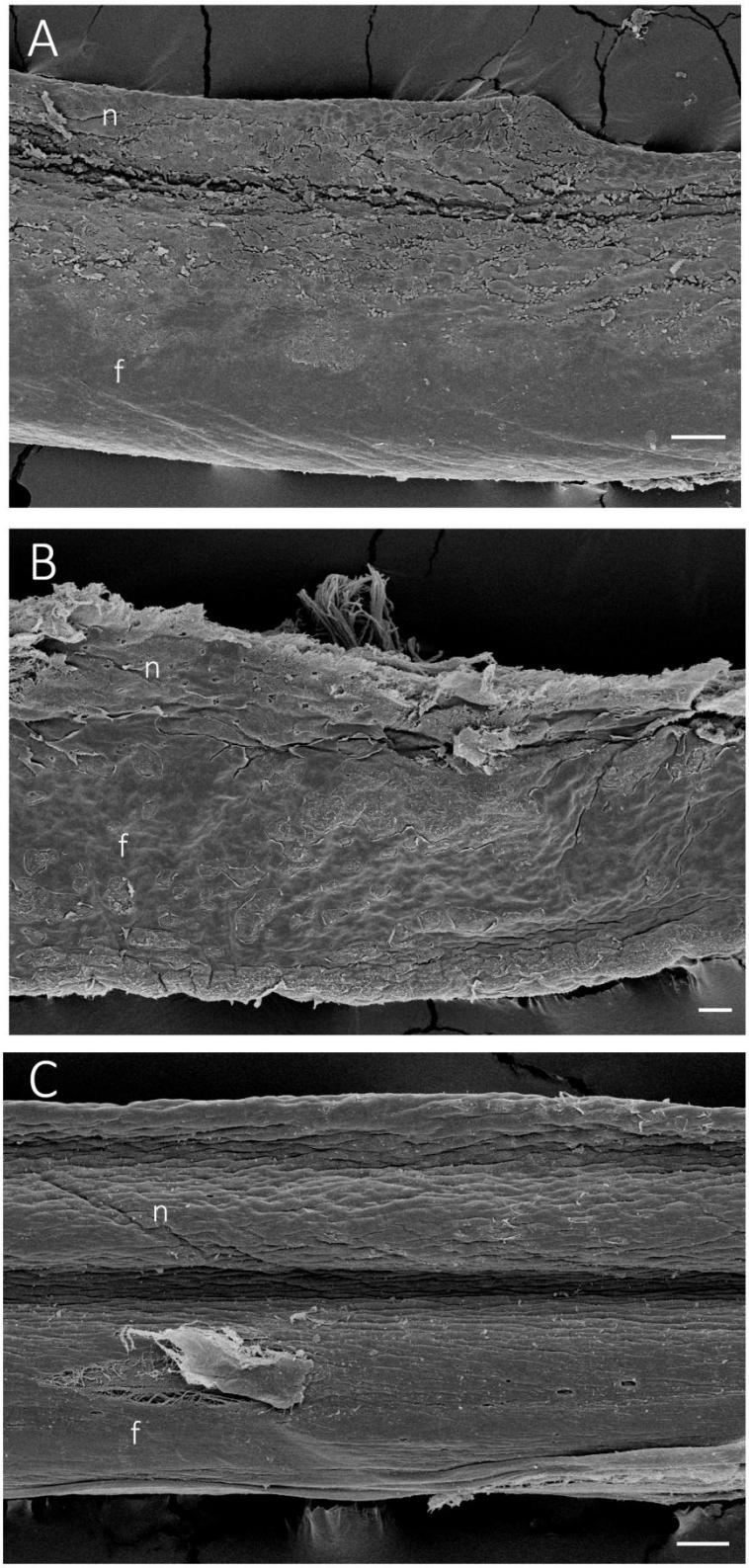

Fig. 33: Electron microscopy, pectoral filaments. A: *Galeoides decadactylus*. B: *Leptomelanosoma indicum*. C: *Polynemus multifilis*. f, region of the pectoral filament composed only by hemitrichia; n, region in which the RLA-OP+SP2 branch run through the pectoral filament. Scale bars: A: 100 µm B: 30 µm. C: 20 µm.

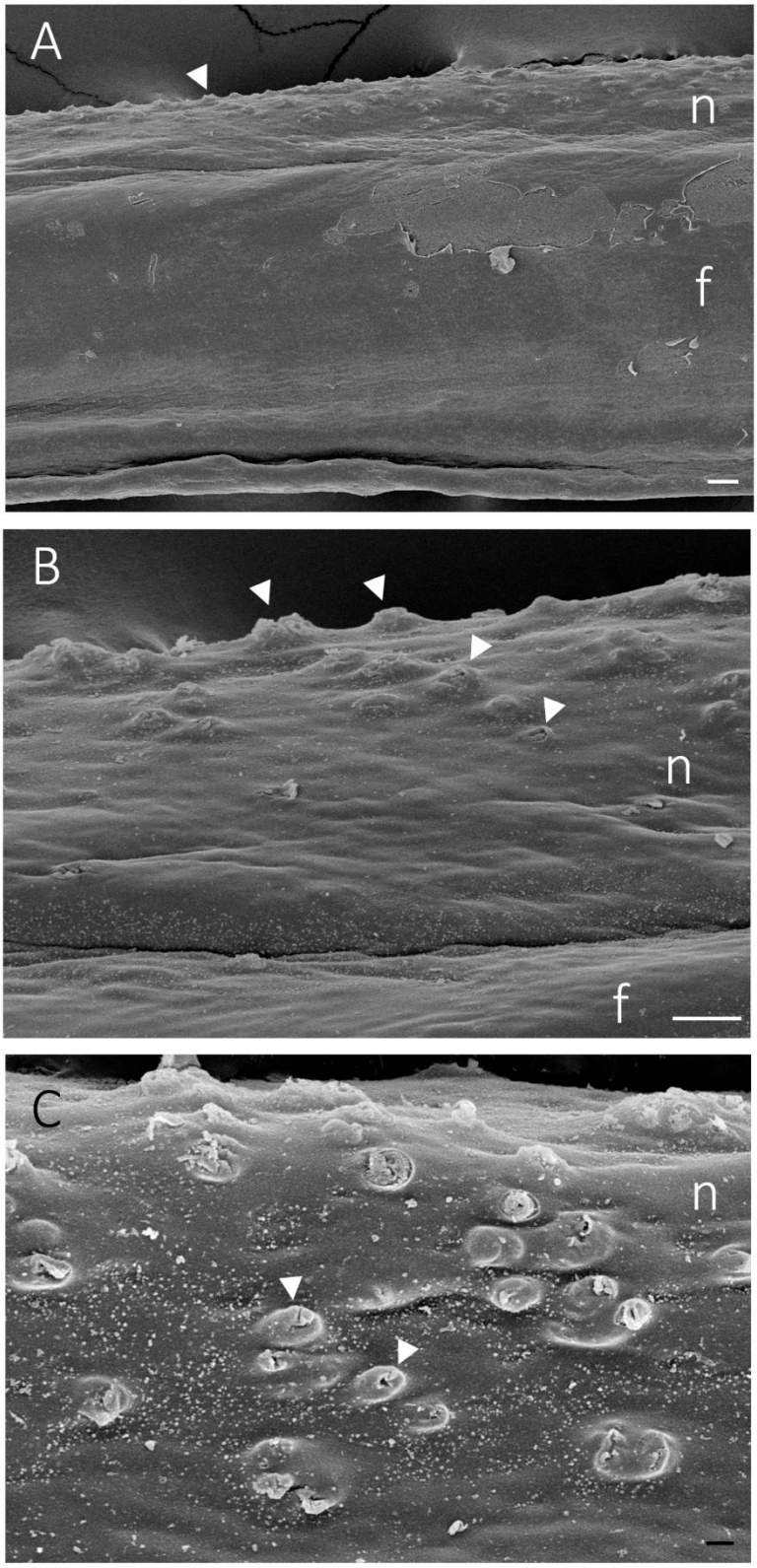

Fig. 34: Electron microscopy, pectoral filaments. *Filimanus xanthonema*. f, region of the pectoral filament composed only by hemitrichia; n, region in which the RLA-OP+SP2 branch run through the pectoral filament. Arrows indicating taste bud-like structures with small openings. Scale bars: A: 20 µm B: 10 µm. C: 3 µm.

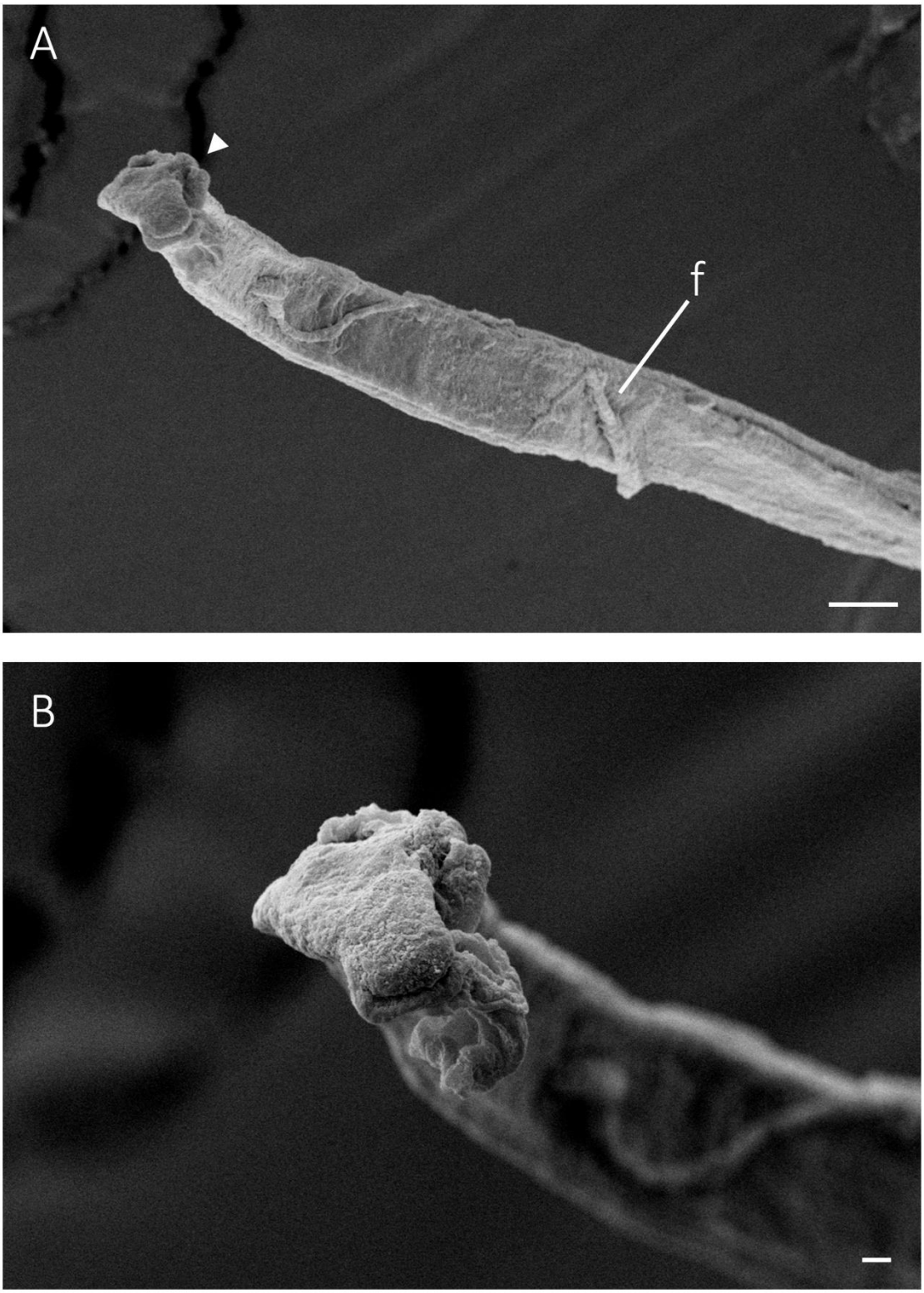

Fig. 35: Electron microscopy, pectoral filaments. *Eleutheronema tetradactylum*. f, pectoral filament. Arrow indicating globose structure on the distal tip of the pectoral filament. Scale bars: A: 10 µm B: 2 µm.

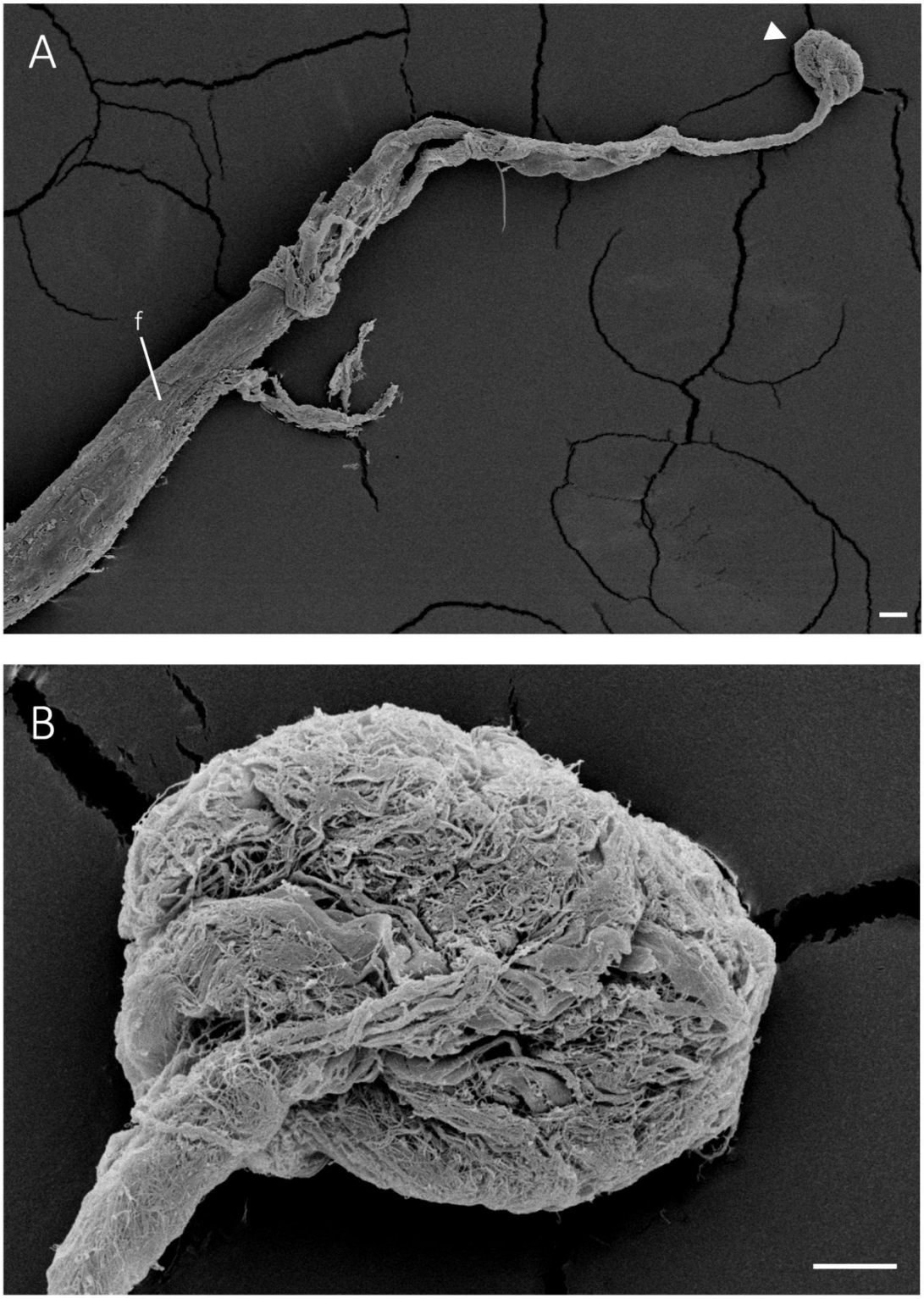

Fig. 36: Electron microscopy, pectoral filaments. *Galeoides decadactylus*. f, pectoral filament. Arrow indicating globose structure on the distal tip of the pectoral filament. Scale bars: A: 30 µm B: 10 µm.

Chapter 2

Phylogenetic relationships within Polynemidae

1. INTRODUCTION

Historically, Polynemidae has been indecisively allocated in incredibly distinct phylogenetic positions within Percomorphacea. Polynemids had been suggested to be closer to Mugilidae and Sphyraenidae (Rosen, 1964); Mugilidae, Sphyraenidae, Atherinidae, and Phallostethoidei (Gosline, 1962; 1968; 1971); and Sciaenidae (De Sylva, 1984; Johnson, 1993; Kang *et al.*, 2017) based on morphological data. Molecular analyses, in turn, alternatively aligned polynemids with Menidae (Betancur-R *et al.*, 2013); Menidae + Lactariidae (Sanciangco *et al.*, 2015); Pleuronectiformes + Carangiformes (Near *et al.*, 2013); and Pleuronectiformes (Harrington *et al.*, 2016; Hughes *et al.*, 2018).

Therefore, Polynemidae clearly lacks a consensual phylogenetic allocation in both morphological and molecular approaches. The intrarelationships of Polynemidae are comparably unclear as the only phylogenetic analyses of the family are two unpublished thesis that propose highly divergent hypotheses (Feltes, 1986; Kang, 2017). Both analyses also have a modest amount of phylogenetic characters. Feltes (1986) did not include all genera currently considered valid (*Leptomelanosoma* is lacking) and was based on 55 characters mostly from skeleton (Fig. 1A). The study of Kang (2017) was based on 64 morphological characters and resulted in several polytomies across the tree (Fig. 1B). Recently Kang *et al.* (2017) have assembled several osteological characters and although the authors did not tested those characters in a cladistic analysis, they claimed to had found new synapomorphies for the family.

The present study proposes a new phylogenetic hypothesis for all genera (Fig. 2) of Polynemidae based on the largest morphological matrix ever assembled including more than one hundred new characters from external morphology, squamation, osteology, myology, and laterosensory system.

2. MATERIAL AND METHODS

A morphological matrix with qualitative and quantitative characters was made using Microsoft Excel 2007 and subsequently concatenated into the text editor Notepad++. The 12 quantitative characters assembled (counts) were rescaled to fit into a distribution ranging from 0 to 1, which represented the lowest and the highest value, respectively. This is necessary in order to equate the transformational series of these quantitative characters with the costs a categorical binary character, thus avoiding over- or underweighting of the qualitative characters (Escapa and Catalano, 2013; Ferrer *et al.*, 2014; Koch *et al.*, 2014). Discrete multistate characters were treated as unordered; ordering of the multistate characters with a clear morphoclinal gradient resulted in no changes in the final topologies. Characters constructions followed Sereno (2007). Character numbering was according to TNT default that starts from zero (therefore the characters are herein numbered from zero to 161). The phylogenetic analysis among terminal taxa was inferred through a maximum parsimony analysis (Farris, 1983) on the TNT software (Goloboff *et al.*, 2008). The search for the most parsimonious tree (MPTs) was achieved via heuristic search with RAS+TBR strategy. The number of replicates adjusted to hit the best score at least 50 times independently, with random seed set to zero. Searches with implied weighting against homoplasies (IW) where performed different values of the constant *k*. Nodal support was expressed as relative Bremer support, which is more appropriate from analyses with quantitative data and implied weighting than the absolute Bremer support (Goloboff and Farris, 2001). Indices were calculated via script *statsall* (designed by Peterson L. Lopes). Suboptimal trees with up to nine extra steps were sampled in order to calculate the relative Bremer supports. Rooting was set on a specimen of Beryciformes (*Holocentrus adscensionis*, MZUSP 60816) an order recurrently treated as possessing plesiomorphic characteristics relative to the Percomorphacea (Johnson and Patterson, 1993; Springer and Johnson, 2004; Wiley and Johnson, 2010) and invariably resolved as basal to percomorphaceans in both molecular and morphology-based hypotheses (Johnson and Patterson, 1993; Betancur-R. *et al.* 2013). All the remaining analyzed specimens are listed in the “Material & Methods” section of chapter 1.

3. RESULTS

3.1 List of characters

3.1.1 Quantitative characters (counts)

Char. #0 (LLS). Lateral line scales; total number: 42 - 107

Description: The lateral line scales of polynemids and *Cynoscion* extend to the posterior margin of the caudal-fin lobes (see Char. #12 below). Therefore the lateral line scales counting was padronized to range from the first scale immediately posterior to the lateral line canal of the posttemporal to the base of the caudal-fin rays.

Char. #1 (AV). Abdominal vertebrae; total number: 10 – 12 (Feltes*,* 1986: ch. #20, modified)

Description: *Holocentrus* and *Cynoscion* posses 12 and 13 abdominal vertebrae, respectively. All polynemids, in turn, have 10 abdominal vertebrae (Fig. 3).

Char. #2 (CV). Caudal vertebrae; total number: 12 – 15 (Feltes*,* 1986: ch. #20, modified).

Description: In almost all polynemid the total number of caudal vertebrae is 14. Nevertheless, Eleutheronema and Polynemus have an extra caudal vertebra. *Holocentrus* also has 15 caudal vertebrae, while *Cynoscion* has only 12. Here, the caudal vertebrae are considered to be from where the hemal spine is formed to the last ural centrum (Fig. 3).

Char. #3 (D2R). Second dorsal fin; number of soft rays: 11 - 17

Inapplicability: This character is inapplicable for taxa lacking the dorsal fin divided into first and second dorsal fins (Char. DF01, state 0 – see below).

Char. #4 (PR). Pectoral fin; number of soft rays: 13 – 17

Char. #5 (FIL). Pectoral fin; number of pectoral filaments: 3 - 14

Inapplicability: This character is inapplicable for taxa lacking the pectoral girdle's soft rays divided into dorsal and ventral portions (Char. PO02, state 0 – see below).

Char. #6 (AS). Anal fin; number of spines: 2 - 4

Char. #7 (AR). Anal fin; number of soft rays: 7 – 29 (Feltes, 1986: ch. #46, modified).

Char. #8 (CF). Caudal fin; total number of branched rays: 14 - 17

Char. #9 (PCD). Dorsal procurrent rays; total number: 6 – 18

Char. #10 (PCV). Ventral procurrent rays; total number: 5 - 16

Char. #11 (GR). Gill rakers of the first branchial arch; total number: 10 – 49 (Feltes, 1986: ch. #34, modified).

3.1.2 Qualitative characters

SCALES

Char. #12 (SC01). Lateral line scales; posterior extent: (0) not reaching the posterior margin of the caudal fin; (1) reaching the posterior margin of the caudal fin.

Description: In polynemids and *Cynoscion* the lateral line extends posteriorly to the posterior margin of the caudal-fin rays, while in Holocentrus the lateral line scales stop before the caudal-fin rays.

Char. #13 (SC02). Lateral line scales; upper caudal-fin lobe; occurrence: (0) absent; (1) present.

Description: The lateral line extended to the posterior margin of the caudal fin can have one or two branches, with a varying degree of orientation. The lateral line scales on the upper caudal-fin lobe are present in *Galeoides, Polydactylus approximans, P. octonemus, P. oligodon,* and *P. virginicus*. The lateral line orientation could not be seen in *Filimanus xanthonema* and *Pentanemus* specimens. For these taxa the character state was obtained from Motomura (2004).

Remarks: *Eleutheronema tetradactylum* is polymorphic for this character. From the two analyzed specimens, one has one branch reaching the lower caudal-fin lobe and the other one has the lateral line scales bifurcated into two branches reaching both caudal-fin lobes. Moreover, when the lateral line scales are bifurcated, the ventral branch has an extra bifurcation on the lower caudal-fin lobe. This condition is also reported by Motomura (2004).

Inapplicability: This character is inapplicable for taxa lacking the lateral line reaching the posterior margin of the caudal fin (Char. SC01, state 0).

Char. #14 (SC03). Lateral line scales; mid-portion of the caudal fin; occurrence: (0) absent; (1) present.

Description: The lateral line scales can also reach the mid-portion of the posterior margin of the caudal fin, i.e. do not reaching any caudal-fin lobe. This condition is present in

Cynoscion, Filimanus, Pentanemus and *Polynemus*. The lateral line orientation could not be seen in *Filimanus xanthonema* and *Pentanemus* specimens. For these taxa the character state was obtained from Motomura (2004).

Inapplicability: This character is inapplicable for taxa lacking the lateral line reaching the posterior margin of the caudal fin (Char. LL01, state 0).

Char. #15 (SC04). Lateral line scales; lower caudal-fin lobe; occurrence: (0) absent; (1) present.

Description: The lateral line scales on the lower caudal-fin lobe are present in *Eleutheronema, Leptomelanosoma, Parapolynemus,* and *Polydactylus*. The lateral line orientation could not be seen in *Filimanus xanthonema* and *Pentanemus* specimens. For these taxa the character state was obtained from Motomura (2004).

Inapplicability: This character is inapplicable for taxa lacking the lateral line reaching the posterior margin of the caudal fin (Char. LL01, state 0).

Char. #16 (SC05). Scales posterodorsally located in comparison to the opercular series; black spot; occurrence: (0) absent; (1) present.

Description: On the anterior region of the lateral line, right posterodorsal to the opercular series, there is a black spot present only in *Polydactylus microstomus* and *P. sextarius* (Fig. 4).

Char. #17 (SC06). Head, dorsal region; scales; occurrence: (0) absent; (1) present.

Description: In all polynemids and in *Cynoscion* the dorsal region of the head, including the occipital, otic, and optic regions, is covered by scales. This condition is not present in *Holocentrus* (Fig. 2D).

Char. #18 (SC07). Maxilla, lateral surface; scales; occurrence: (0) absent; (1) present.

Description: In all polynemids the lateral surface of the maxilla is covered by scales. This condition is not present in *Holocentrus* and in *Cynoscion* (Fig. 2D).

Char. #19 (SC08). Dentary, ventral region; scales; occurrence: (0) absent; (1) present.

FINS & SUPRANEURALS

Char. #20 (DF01). Dorsal fin; degree of division: (0) undivided; (1) divided into first and second dorsal fins.

Description: The dorsal fin is herein considered separated when there is no interradial membrane between elements. In *Cynoscion*, the dorsal fins are very close to one another, but there is no trace of the interradial membrane between the two dorsals. In polynemids the two dorsal fins are widely apart from each other (Fig. 2, 3).

Char. #21 (DF02). First dorsal fin; number of spines: (0) ten; (1) eight.

Inapplicability: This character is inapplicable for taxa lacking the dorsal fin divided into first and second dorsal fins (Char. DF01, state 0).

Char. #22 (DF03). Second dorsal fin; number of spines: (0) three; (1) one.

Inapplicability: This character is inapplicable for taxa lacking the dorsal fin divided into first and second dorsal fins (Char. DF01, state 0).

Char. #23 (PF01). Pelvic fin; number of soft rays: (0) seven; (1) five.

Char. #24 (SN01). Supraneurals; total number: (0) two; (1) three.

Description: The total number of supraneurals is variable across the analyzed taxa. *Holocentrus, Eleutheronema, Galeoides, Leptomelanosoma, Parapolynemus,* and *Polydactylus opercularis* have two supraneurals (Fig. 5B), while all the rest have three supraneurals (Fig. 6B).

OSTEOLOGY

Infraorbitals

Char. #25 (IO01). Infraorbitals; inner borders; disposition: (0) following the eyeball circumference; (1) partially following the eyeball circumference (Feltes, 1986: ch. #5, modified).

Description: In almost all analyzed taxa, the infraorbitals follow the eye circumference (Fig. 7A). However, in Leptomelanosoma, Parapolynemus, and Polynemus the infraorbitals partially follow the eyeball circumference (Fig. 7B).

Char. #26 (IO02). Infraorbital 3, subocular shelf; occurrence: (0) absent; (1) present (Feltes, 1986: ch. #5, modified).

Description: Subocular shelf is a thin bony lamina that extends medially from the third infraorbital. *Parapolynemus* and *Polynemus* are the only taxa that do not present this bony structure.

Char. #27 (IO03). Infraorbitals; posterior margin; shape: (0) truncate/round; (1) pointed.

Description: The posterior margins of the infraorbital bones, especially from the second to the sixth, are usually truncate/round but, in *Eleutheronema, Pentanemus, Polydactylus opercularis, P. plebeius,* and *P. sexfilis,* the posterior margins are pointed (Fig. 7A).

Mandibular arch

Char. #28 (MA01). Dentary; teeth; occurrence: (0) restricted to the dorsal surface of the dentary; (1) extending to the lateral surface of the dentary.

Description: The teeth in most of the cases are restricted to dorsal surface of the dentary (Fig. 8; Fig. 2, 4, 5, 8, 9 – Chap. 1); nevertheless in *Eleutheronema, Leptomelanosoma,* and *Polydactylus opercularis* the teeth are smaller and very abundant, occupying also the lateral surface of the dentary (Fig. 9; Fig. 6 – Chap. 1).

Hyopalatine arch

Char. #29 (HYP01). Quadrate; articulation with the metapterygoid: (0) simple; (1) interdigitated.

Description: In all examined taxa the borders of the quadrate and metapterygoid that contact each other are mostly flat. In addition to this flat articulation, sciaenids and polynemids present a highly indented interdigitation at the medial faces of these bones (Figs. 10B, 11B, 13B – Chap. 1).

Char. #30 (HYP02). Palatine and ectopterygoid; teeth; occurrence: (0) absent; (1) present (Feltes, 1986: ch. #42, modified; Kang *et al.* 2017: ch. #3, modified).

Description: In all examined taxa the palatine and ectopterygoid have teeth on its ventral surface (Figs. 11B, 12, 13 – Chap. 1). *Cynoscion* is the single exception to this condition (Figs. 10B – Chap. 1).

Char. #31 (HYP03). Palatine; length relative to ectopterygoid length in lateral view: (0) palatine equal to/greater than ectopterygoid; (1) palatine smaller than ectopterygoid (Kang *et al.* 2017: ch. #4, modified).

Description: In most of the cases, the palatine is smaller than the ectopterygoid (Figs. 12A, 13A – Chap. 1). However, *Holocentrus, Cynoscion, Eleutheronema, Galeoides, Polydactylus microstomus,* and *P. sexfilis* have the opposite condition (Figs. 10A, 11A, 12B – Chap. 1).

Char. #32 (HYP04). Preopercle; posterior margin; morphology: (0) smooth; (1) serrated (Feltes, 1986: ch. #16, modified).

Description: In almost all analyzed taxa, the preopercle present serration on its posterior margin (Figs. 11A, 12B, 13A – Chap. 1). Nevertheless, Cynoscion, Parapolynemus, and Pentanemus have a smooth preopercle, with no serrations on the posterior margin (Figs. 10A, 12A – Chap. 1).

Char. #33 (HYP05). Preopercle, posterior margin; large and prominent posteroventral spine: (0) absent; (1) present.

Description: The most condition is the presence of a large posteroventral spine on the lateroventral region of the preopercle (Figs. 12B, 13A – Chap. 1). Apart from the ones that bare no serrations at all, Galeoides does not have this large posteroventral spine (Fig. 11A – Chap. 1).

Char. #34 (HYP06). Endopterygoid and ectopterygoid; boundaries in medial view: (0) endopterygoid and ectopterygoid not partially fused; (1) endopterygoid and ectopterygoid partially fused.

Description: In *Filimanus, Galeoides, Leptomelanosoma,* and *Polynemus paradiseus* the endopterygoid and ectopterygoid are partially fused on the anterior region of those bones (Fig. 11B, 13B – Chap. 1). In all other taxa, these bones only articulate to one another, with no degree of fusion (Fig. 10B – Chap. 1).

Neurocranium

Char. #35 (NC01). Neurocranium, autosphenotic; relative position in dorsal view: (0) forming the lateral margin of the neurocranium; (1) not forming the lateral margin of the neurocranium.

Description: In *Holocentrus* and *Cynoscion* the autosphenotic is dorsally visible and, in dorsal view, it forms the lateral margin of the neurocranium, placed in between the pterotic and frontal (Fig. 10A). In polynemids the autosphenotic do not mark the lateral margin of the neurocranium, independently if it is dorsally visible or not (Figs. 10B, C).

Char. #36 (NC02). Neurocranium, autosphenotic; articulation with the parietal in dorsal view: (0) absent; (1) present.

Description: During the polynemid development, the autosphenotic usually is dorsally engulfed by the frontal and pterotic. Therefore, in most adults, the autosphenotic is not visible in dorsal view (Fig. 10B). However, *Leptomelanosoma, Parapolynemus,* and *Polynemus* have the opposite condition, in which the autosphenotic is not completely covered dorsally by the frontal and pterotic, articulating with the parietal (Fig. 10C).

Char. #37 (NC03). Neurocranium, vomer; teeth; occurrence: (0) absent; (1) present (Feltes, 1986: ch. #35, modified).

Description: The most common condition is the presence of teeth on the ventral surface of the vomer. *Cynoscion, Galeoides, Parapolynemus, Polydactylus microstomus,* and *P. sextarius* do not have any teeth on that bone.

Char. #38 (NC04). Neurocranium, basisphenoid; occurrence: (0) absent; (1) present (Feltes, 1986: ch. #8, modified).

Description: In almost all analyzed taxa the basisphenoid is present (Fig. 5, 6, 8, 9). The basisphenoid in *Parapolynemus* and *Polynemus* is absent.

Char. #39 (NC05). Neurocranium, basisphenoid; posterior end: (0) articulating with the prootic; (1) not articulating with the prootic (Feltes, 1986: ch. #8, modified).

Description: Normally, the basisphenoid articulates posteriorly with the prootic (Fig. 11A). *Filimanus* is the single exception, in which the posterior end of the basisphenoid does not articulate with the prootic (Fig. 11B).

Inapplicability: This character is inapplicable for taxa lacking the basisphenoid (Char. NC04, state 0).

Char. #40 (NC06). Neurocranium, intercalar; posterior projection in comparison to the pterotic spine: (0) equally to or smaller than; (1) greater than.

Description: The intercalar, a small bone that articulates with the ventral arm of the posttemporal usually present a small projection that is either smaller than or equal to the

length of the pterotic spine (Fig. 6B). *Eleutheronema* and *Polydactylus opercularis* have the opposite condition, in which the intercalar projection can reach up to three times the pterotic spine length (Fig. 6A).

Char. #41 (NC07). Neurocranium, parasphenoid; central width in comparison to the orbit capsule: (0) less than half of the orbit capsule diameter; (1) half or more of the orbit capsule diameter.

Description: Typically, the parasphenoid is a thin bone marking the ventral portion of the neurocranium (Fig. 5A). In *Leptomelanosoma, Parapolynemus,* and *Polynemus* the parasphenoid is much thicker than the other genera, in which its width matches to half or more the orbit capsule diameter (Fig. 5B).

Pectoral Girdle

Char. #42 (PO01). Pectoral fin, branched soft rays; occurrence: (0) absent; (1) present.

Description: Generally, the pectoral-fin present branched rays. In almost all polynemids, all pectoral-fin rays are unbranched, except in *Polydactylus microstomus* and *P. sextarius*.

Char. #43 (PO02). Ventral pectoral rays; disposition: (0) sharing a complete interradial membrane with the dorsal pectoral rays, forming the ventromedial part of the pectoral fin; (1) dissociated from the dorsal rays and transformed into independent pectoral filaments.

Description: All polynemids have the pectoral fin divided into two portions. A dorsal representing the unmodified fin and a ventral portion with several pectoral filaments, which are the ventralmost pectoral-fin rays that migrate ventrally (see Chapter 3).

Char. #44 (PO04). Pectoral filaments; longest filament position: (0) dorsal; (1) central.

Description: The filaments of the polynemid pectoral girdle are all of different lengths. Usually, the longest one is the dorsalmost filament. However, in *Parapolynemus* and *Pentanemus* the longest filament is a central filament of the girdle (Figs. 2E, F).

Inapplicability: This character is inapplicable for taxa lacking the ventral pectoral soft rays transformed into pectoral filaments (Char. PO02, state 0).

Char. #45 (PO05). Pectoral filaments; longest filament; length in comparison to the body length: (0) smaller than; (1) greater than.

Description: Usually, the longest pectoral filament of the girdle is short to moderate, not reaching the caudal fin, for example. However, in Pentanemus, Parapolynemus, and Polynemus the longest filament is greatly elongated, surpassing the body length (Figs. 2E, F, H).

Inapplicability: This character is inapplicable for taxa lacking the ventral pectoral soft rays transformed into pectoral filaments (Char. PO02, state 0).

Char. #46 (PO06). Coracoid; foramens; occurrence: (0) absent; (1) present (Feltes*,* 1986: ch. #51, modified).

Description: From the analyzed taxa, the most common condition is to have the coracoid with foramens through its surface (Fig. 12; Fig. 23 – Chap. 1). *Holocentrus, Cynoscion, Filimanus, Parapolynemus, Polydactylus sexfilis,* and *Polynemus* are the ones that do not have any kind of foramens on the coracoid (Fig. 13, 14A, B).

Char. #47 (PO07). Pectoral radial 4; foramens; occurrence: (0) absent; (1) present (Feltes, 1986: ch. #30, modified).

Description: Pectoral radial 4, in most of the cases, has foramens on its surface (Fig. 12; Fig. 23A – Chap. 1). However, pectoral radial 4 of *Holocentrus, Cynoscion, Eleutheronema tridactylum, Parapolynemus, Pentanemus,* and *Polynemus* does not have foramens on its surface (Fig. 13, 14A, B).

Char. #48 (PO08). Pectoral radial 3; articulation with both pectoral radial 2 and 4; occurrence: (0) absent; (1) present.

Description: In all polynemids, pectoral radial 3 shifts from its initial position during development (see Chap. 3) and articulates with pectoral radials 2 and 4. In most of the cases, this radial loses its contact with the pectoral-fin rays (except in *Pentanemus*; Fig. 12B, 13B, 14B; Fig. 23 – Chap. 1). In *Holocentrus* and *Cynoscion*, pectoral radial 3 is parallel to all the other radials (Fig. 13A).

Char. #49 (PO09). Pectoral radial 3; articulation with the coracoid; occurrence: (0) absent; (1) present.

Description: Besides the articulation with both pectoral radials 2 and 4, pectoral radial 3 of all polynemids articulates with the coracoid (Fig. 12B, 13B, 14B; Fig. 23 – Chap. 1) which does not happens in *Holocentrus* and *Cynoscion* (Fig. 13A).

Char. #50 (PO10). Pectoral radial 3; medial projection; occurrence: (0) absent; (1) present.

Description: In medial view, the third pectoral radial of *Parapolynemus* and *Polynemus* can have a medial projection which acts as origin site of some fibers of the *adductor profundus* of the *segmentum filamentaris*, giving to this radial a mushroom shape

(Fig. 14C). For all the remaining analyzed species, there is no medial projection from pectoral radial 3 regardless if it is greatly expanded or not (Fig. 12B, 13B; Fig. 23 – Chap. 1).

Char. #51 (PO11). Pectoral radial 3; distal articulation with the dorsalmost pectoral filament; occurrence: (0) absent; (1) present.

Description: The expanded pectoral radial 3 of polynemids usually does not articulates with pectoral filaments. However, in *Parapolynemus* and *Polynemus* the third pectoral radial articulates with the dorsalmost pectoral filament (Fig. 14).

Inapplicability: This character is inapplicable for taxa lacking the ventral pectoral soft rays transformed into pectoral filaments (Char. PO02, state 0).

Char. #52 (PO12). Coracoid; posteroventral process; occurrence: (0) absent; (1) present (Feltes, 1986: ch. #14, modified; Kang *et al.* 2017: ch. #10, modified).

Description: On the posteroventral portion of the coracoid of polynemids, there is a tendon bone that is formed by the ossification of the *hypaxialis* muscles that attach medially on the pectoral girdle (Fig. 12B, 13B, 14B; Fig. 23 – Chap. 1).

Char. #53 (PO13). Postcleithrum 1; articulation with cleithrum relative to the *adductor superficialis filamentaris*: (0) posterior; (1) in the middle of the muscle.

Description: The attachment site of the first postcleithrum is on the posterior region of the medial face of the cleithrum, immediately posterior to the *adductor superficialis filamentaris*. However, *Parapolynemus* holds a distinct arrangement. Although postcleithrum 1 still attaches itself on the same region of the cleithrum described above, it attaches in the middle of the fibers from the *adductor superficialis* that feeds the pectoral filaments (Fig. 22 – Chap. 1).

Inapplicability: This character is inapplicable for taxa lacking the ventral pectoral soft rays transformed into pectoral filaments (Char. PO02, state 0).

Char. #54 (PO14). Pectoral girdle; ligament connecting postcleithrum 2 with the basipterygium; occurrence: (0) absent; (1) present.

Description: In sciaenids and polynemids, on the distal tip of postcleithrum 2, there is a sturdy ligament connecting the pectoral girdle to the bony elements of the pelvic girdle.

Hyoid arch

Char. #55 (HA01). Interdigitation between posterior and anterior ceratohyals; occurrence: (0) absent; (1) present.

Description: In sciaenids and polynemids, the medial faces of the anterior and posterior ceratohyals present an interdigitation between those bones (Fig. 5D – Chap.3).

Char. #56 (HA02). Anterior ceratohyal; path of the hyoid artery: (0) in a canal/groove on the lateral surface of the anterior ceratohyal; (1) lying down dorsally to the dorsal region of the anterior ceratohyal.

Description: In Percomorphaceans, the dorsal region of the anterior ceratohyal usually holds the hyoid artery within a canal or a groove on its lateral surface, which is seen in Holocentridae. Polynemids and sciaenids present an anterior ceratohyal shorter in the anteroposterior axis, in which the hyoid artery lays down on a superficial groove on the dorsal region of the anterior ceratohyal.

Char. #57 (HA03). Posterior ceratohyal; number of associated branchiostegal rays: (0) two; (1) one (Kang *et al.* 2017: ch. #6, modified).

Description: In sciaenids and polynemids, the posterior ceratohyal holds a single branchiostegal ray (Fig. 5D – Chap.3), while in *Holocentrus*, there is two branchiostegal rays articulating with the posterior ceratohyal.

Branchial arches

Char. #58 (BA01). Branchial arches; branchial rudiments on the dorsal surface of basibranchials: (0) absent; (1) present only on basibranchial 3; (2) present in basibranchials 1, 2, and 3

Description: The most common condition within the analyzed taxa is the absence of branchial rudiments on the dorsal surface of basibranchials (Fig. 15A). Polynemus is the single genus that have branchial rudiments only on basibranchial 3 (Fig. 15B), whereas *Eleutheronema, Leptomelanosoma,* and *Polydactylus opercularis* have branchial rudiments on all basibranchials (Fig. 15C).

MYOLOGY

Adductor mandibulae

Char. #59 (AD01). *Adductor mandibulae*, *segmentum facialis*, *pars malaris*; degree of differentiation: (0) undifferentiated; (1) differentiated into a *retromalaris* and *promalaris* subsections.

Description: In lower teleosts, the *malaris* usually reaches only the lower jaw via intersegmental aponeurosis. Several neoteleosts, in turn, have the anterodorsal fibers of the *malaris* more prominent and extending anteriorly over the retrojugal lamina of the buccopalatal membrane and its embedded ligaments leading to the maxilla. In such

instances, the ventral portion of the *malaris* typically retains a connection with the intersegmental aponeurosis. The differentiation between these two portions of the *malaris* allows the recognition of an anterodorsal *promalaris* and a posteroventral *retromalaris* (Figs. 1-9 – Chap. 1).

Char. #60 (AD02). *Adductor mandibulae*, *segmentum facialis*, *promalaris*; origin relative to the *retromalaris*: (0) medial; (1) lateral.

Description: Among the examined taxa, the *promalaris* subsection was found to originate from distinct regions. Sciaenids have the *promalaris* originating medially to the *retromalaris*, with fibers arising from the quadrate, metapterygoid, endopterygoid, ectopterygoid, and palatine (Figs. 1, 2 – Chap. 1). In polynemids, the *promalaris* is completely lateral to the *retromalaris* and originates mainly from the preopercle and, occasionally, also from the pterotic (Figs. 3, 7, 9 – Chap. 1).

Inapplicability: This character is inapplicable for taxa lacking differentiated *retromalaris* and *promalaris* subsections of the *adductor mandibulae* (Char. AD01, state 0).

Char. #61 (AD03). *Adductor mandibulae*, *segmentum facialis*, *promalaris*; origin type: (0) musculous; (1) aponeurotic.

Description: Among the examined taxa, the *promalaris* subsection of sciaenids originates musculously from the hyopalatine arch (Figs. 1, 2 – Chap. 1). In polynemids, the origin of this subsection is aponeurotic (Figs. 3, 7, 9 – Chap. 1).

Inapplicability: This character is inapplicable for taxa lacking differentiated *retromalaris* and *promalaris* subsections of the *adductor mandibulae* (Char. AD01, state 0).

Char. #62 (AD04). *Adductor mandibulae*, *segmentum facialis*; origin of the *promalaris* located lateral to the *retromalaris*: (0) restricted to the suspensorium; (1) on both the suspensorium and pterotic.

Description: In most analyzed polynemids, the *promalaris* subsection originates from the posterodorsal region of the suspensorium, more specifically from the posterodorsal portion (vertical arm) of the preopercle (Figs. 3 – Chap. 1). Only in one taxon, *Polynemus paradiseus*, the *promalaris* exhibits a dorsal expansion, with fibers also originating from the pterotic (Figs. 7 – Chap. 1).

Optimization: State 1 is an autapomorphy for *Polynemus paradiseus*. Its congener, *P. multifilis* exhibit the generalized condition shared with the remaining polynemids.

Inapplicability: This character is inapplicable for taxa lacking the *promalaris* originating lateral to the *retromalaris* (Char. AD03, state 0).

Char. #63 (AD05). *Adductor mandibulae*, *segmentum facialis*, *promalaris*; position of the posterodorsal limit relative to the posterodorsal margin of the *rictalis*: (0) ventral; (1) dorsal.

Description: In all polynemids, the *promalaris* subsection is lateral to all other components of the adductor mandibulae. In most of the cases, the posterodorsal limit of the *promalaris* surpass the posterodorsal margin of the *rictalis* (Figs. 3 – Chap. 1) and in *Eleutheronema, Galeoides, Parapolynemus, Pentanemus, Polydactylus microstomus, P. sextarius, P. plebeius,* and *P. sexfilis* the *promalaris* fibers are completely ventral to the posterodorsal margin of the *rictalis* (Figs. 6, 9 – Chap. 1).

Inapplicability: This character is inapplicable for taxa lacking the *promalaris* originating lateral to the *retromalaris* (Char. AD03, state 0).

Char. #64 (AD06). *Adductor mandibulae*, *segmentum facialis*, *pars malaris*; origins of the *partes promalares interna* and *externa*: (0) separate; (1) continuous.

Description: In the Polynemidae and Sciaenidae the *pars promalaris* of the *adductor mandibulae* is anteriorly differentiated into two subsection named *promalaris interna* and *promalaris externa*. These names are given in allusion to their insertion on the medial or lateral surface of the maxilla, respectively. Sciaenids have the *partes promalares interna* and *externa* with completely separate origins: ectopterygoid and palatine for the former and quadrate, metapterygoid, and endopterygoid for the latter (Figs. 2B – Chap. 1). On the other hand, in polynemids the *partes promalares interna* and *externa* share a common, undivided origin usually on the preopercle (Figs. 3-9 – Chap. 1).

Inapplicability: This character is inapplicable for taxa lacking differentiated *retromalaris* and *promalaris* subsections of the *adductor mandibulae* (Char. AD01, state 0).

Char. #65 (AD07). *Adductor mandibulae*, *segmentum facialis, malaris*; insertion of the *partes promalares interna* and *externa*: (0) common; (1) separate.

Description: In Sciaenidae, the *partes promalares interna* and *externa* have separate origins (Char. AD05, state 0) but, toward insertion, they merge to each other and attach to the maxilla as a single muscle mass (Figs. 2B – Chap. 1). Contrastingly, in almost all polynemids these subsections have a common origin but gradually separate anteriorly, with the *promalaris interna* converging to the endomaxillar ligament and the *promalaris externa* to the ectomaxillar ligament (Figs. 4-8 – Chap. 1). Although having a common origin for the *partes promalares interna* and *externa* (Ch. AD06: 1), *Polydactylus microstomus*, *P. sextarius*, and *P. opercularis* exhibit the same common insertions typical of sciaenids (Figs. 9B – Chap. 1).

Inapplicability: This character is inapplicable for taxa lacking differentiated *retromalaris* and *promalaris* subsections of the *adductor mandibulae* (Char. AD01, state 0).

Char. #66 (AD08). *Adductor mandibulae*, *segmentum facialis*, *pars promalaris interna*; type of insertion: (0) musculous; (1) mediated by the endomaxillar ligament.

Description: Sciaenids have the fibers of the *pars promalaris interna* directly attaching onto the medial surface of the maxilla, without the mediation of any distinguishable tendon or ligament. The same condition is also present in *Polydactylus sextarius* (Figs. 2B, 9B – Chap. 1). On the other hand, in all other polynemids, the fibers of the *promalaris interna* converge to an evident endomaxillar ligament that mediates the connection of this muscle component with the anteromedial aspects of the maxilla (Figs. 4, 5, 8 – Chap. 1). In all polynemids and the examined sciaenid, a cylindrical ectomaxillar ligament is additionally present, but this component only collects the fibers of the *pars promalaris externa* and lacks any direct connection with the *promalaris interna*.

Inapplicability: This character is inapplicable for taxa lacking differentiated *retromalaris* and *promalaris* subsections of the *adductor mandibulae* (Char. AD01, state 0).

Char. #67 (AD09). *Adductor mandibulae*, *segmentum facialis*, *retromalaris*; sites of origin: (0) restricted to the suspensorium; (1) both suspensorium and neurocranium.

Description: The subsection *retromalaris* of the *pars malaris* of the *adductor mandibulae* usually originates from the lateral face of the hyomandibula and from the posterodorsal portion (vertical arm) of the preopercle in most acanthomorphs (Figs. 1 – Chap. 1). In contrast, in Polynemidae, the origin site of the *retromalaris* is expanded dorsally and reaches the neurocranium (Figs. 3 – Chap. 1).

Inapplicability: This character is inapplicable for taxa lacking differentiated *retromalaris* and *promalaris* subsections of the *adductor mandibulae* (Char. AD01, state 0).

Char. #68 (AD10). *Adductor mandibulae*, *segmentum facialis*, *retromalaris*; sites of origin from the neurocranium: (0) pterotic only; (1) pterotic and autosphenotic.

Description: In Polynemidae, the origin of the retromalaris on the neurocranium may involve only the pterotic, condition found only in *Parapolynemus* and *Pentanemus* or both this bone and the autosphenotic, condition found in all other genera.

Inapplicability: This character is inapplicable for taxa lacking a *retromalaris* with fibers originating from the neurocranium (Char. AD10, state 0).

Char. #69 (AD11). *Adductor mandibulae*, *segmentum facialis*, *retromalaris* and *ricto-stegalis* compound; connection between sections: (0) sharing fibers; (1) completely separated.

Description: In all analyzed taxa herein the *rictalis* and *stegalis* are differentiable from each other only at their origin sites, with the *rictalis* usually originating from the preopercle and dorsoposterior region of the hyomandibula and the *stegalis* from the metapterygoid and anterodorsal region of the hyomandibula. Toward insertion, the two sections become to share fibers and gradually merge to each other, forming a compound *ricto-stegalis*. In the examined sciaenid, this compound section share fibers dorsally and is thus partially continuous with the *retromalaris* (Figs. 1, 2 – Chap. 1). In Polynemidae, *retromalaris* and *ricto-stegalis* are completely separated from each other (Figs. 3-9 – Chap. 1).

Inapplicability: This character is inapplicable for taxa lacking differentiated *retromalaris* and *promalaris* subsections of the *adductor mandibulae* (Char. AD01, state 0).

Char. #70 (AD12). *Adductor mandibulae*, *segmentum facialis*, *rictalis*; posterodorsal expanse: (0) restricted to the middle portion of the preopercle; (1) reaching the level of the *dilatator operculi*.

Description: The dorsal limit of the *rictalis* in *Holocentrus* is at mid-level of the preopercle, with the dorsal profile of the muscle not reaching the *dilatator operculi*. Sciaenids and polynemids have the dorsalmost fibers of the *rictalis* more expanded dorsally

along the preopercle, so as to contact the ventral profile of the *dilatator operculi* (Figs. 1, 3 – Chap. 1).

Char. #71 (AD13). *Adductor mandibulae*, *segmentum mandibularis*, *pars coronalis*; posterior expanse: (0) trespassing the posterior margin of the lower jaw, being visible in lateral view; (1) restricted to the limits of the lower jaw, being not visible in lateral view.

Description: In the most common condition among percomorphaceans, the *segmentum mandibularis* of the *adductor mandibulae* is restricted to the medial portion of the lower jaw and is not visible in lateral view. However, in *Holocentrus adscensionis*, the *coronalis* portion of the *segmentum mandibularis* is expanded posterodorsally and can be observed in lateral view. In this taxon, the limit between the *pars coronalis* and the *segmentum facialis* is marked laterally by a mandibular myoseptum.

Char. #72 (AD14). *Adductor mandibulae*, *segmentum mandibularis*; degree of separation between *partes coronalis* and *mentalis*: (0) partially separated; (1) completely separated.

Description: The *segmentum mandibularis* of the *adductor mandibulae* can be differentiated into two subunits, the *pars coronalis* and the *pars mentalis*, usually separated by a central tendinous axis. Therefore, in such a configuration, the *segmentum mandibularis* generally have a bipinnate aspect. In the Holocentridae the *partes coronalis* and *mentalis* are not differentiated from each other anteriorly in the *segmentum mandibularis*. This condition is also found in *Galeoides*, *Leptomelanosoma*, *Parapolynemus*, *Polydactylus microstomus*, *P. sextarius*, *P. plebeius*, *P. sexfilis*, and *Polynemus* (Figs. 4, 8, 9B – Chap. 1). All other polynemids and *Cynoscion*, have the *segmentum mandibularis* with fibers of the *partes coronalis* and *mentalis* completely separated from each other (Figs. 2B, 5 – Chap. 1).

Char. #73 (AD15). *Adductor mandibulae*, *segmentum mandibularis*, posteroventral fibers; origin: (0) from the intersegmental aponeurosis; (1) from the intersegmental aponeurosis and buccopalatal membrane.

Description: All analyzed taxa present the posteroventral fibers of the *segmentum mandibularis* of the *adductor mandibulae* originating from the faucal ligament and the mandibular tendon of the intersegmental aponeurosis (Figs. 2B, 5, 8 – Chap. 1). Some of these fibers additionally arise from a vertical ligament embedded into the buccopalatal membrane in *Leptomelanosoma*, *Parapolynemus*, *Polydactylus octonemus*, *P. microstomus, P. sextarius,* and *Polynemus* (Figs. 4, 9B – Chap. 1).

Char. #74 (AD16). *Adductor mandibulae*, *segmentum mandibularis*; anterior expanse: (0) at the level of the buccopalatal ligaments that attach on the maxilla; (1) posterior to the buccopalatal ligaments that attach on the maxilla.

Description: The *segmentum mandibularis* of the *adductor mandibulae* can be greatly expanded anteriorly, reaching the level of the buccopalatal ligaments that attach on the maxilla. *Holocentrus* and *Cynoscion* have the anterior margin of the *segmentum mandibularis* aligned with the ecto- and paramaxillar ligaments; in *Eleutheronema* and *Polydactylus opercularis,* this muscle segment is also aligned with the endo- and ectomaxillar ligaments (Figs. 2B, 5B – Chap. 1). The *segmentum mandibularis* of all remaining genera is comparatively much shorter and located fully posterior to the body of the buccopalatal ligaments attaching onto the maxilla (Figs. 4, 5A, 8, 9B – Chap. 1). In this case, the anterior margin of the *segmentum mandibularis* is aligned with the anterior margin of the *pars retromalaris*.

Char. #75 (AD17). Buccopalatal membrane; preangular ligament; attachment onto the lateral face of the lower jaw: (0) reaching the ventral margin of the angulo-articular; (1) not reaching the ventral margin of the angulo-articular.

Description: The preangular ligament is always present in all analyzed taxa, but it shows variations regarding its attachment on the lower jaw. In *Holocentrus*, *Cynoscion*, *Eleutheronema*, *Polydactylus plebeius,* and *P. sexfilis* the ligament trespasses the limits of the maxilla and reaches the ventral margin of the angulo-articular (Figs. 1, 2A, 6 – Chap. 1). In the remaining taxa, the whole ligament lies underneath the posterior end of the maxilla, falling short of the ventral border of the angulo-articular.

Char. #76 (AD18). *Adductor mandibulae*; intersegmental aponeurosis; accessory tendon; insertion on the angulo-articular: (0) medial to the *segmentum mandibularis*; (1) lateral to the *segmentum mandibularis*.

Description: In addition to the mandibular and meckelian tendons, the intersegmental aponeurosis can develop a third branch called accessory tendon, which usually extends ventrally to the meckelian cartilage and anchors to the angulo-articular. All examined species the accessory tendon attaches to the ventral portion of the medial surface of the angulo-articular, but the relationship between that tendon and the *segmentum mandibularis* varied between the families. In Polynemidae the accessory tendon is always lateral to the *segmentum mandibularis*, while in *Holocentrus* and *Cynoscion* the tendon lies medial to that muscle segment (Figs. 2B – Chap. 1).

Char. #77 (AD19). *Adductor mandibulae*; intersegmental aponeurosis; morphology of the dorsal portion: (0) undivided; (1) bifurcated.

Description: In the examined outgroups, the dorsal portion of the intersegmental aponeurosis lacks any evident subdivision, with a continuum of tendinous fibers between the anterior and posterior limits of the aponeurosis (Figs. 2B – Chap. 1). Polynemids have the dorsal portion of the intersegmental aponeurosis bifurcated, with a series of muscles fibers lying between an anterior and a posterior tendinous arm (Figs. 4, 5, 8, 9B – Chap. 1). The anterior arm is topologically correspondent to the transverse tendon of Datovo & Vari (2013).

Char. #78 (AD20). *Adductor mandibulae*; intersegmental aponeurosis; transverse tendon (= anterior arm); position relative to the ventral limits of the *retromalaris*: (0) posterior; (1) anterior.

Description: Polynemids may have the dorsal end of the transverse tendon (= anterior arm of the dorsal portion of the intersegmental aponeurosis; see Ch. AD20, state 1) located either anteriorly (*Filimanus* and *Pentanemus*; Fig. 5A – Chap. 1) or posteriorly (remaining genera; Figs. 4, 5B, 8, 9B – Chap. 1) to the *retromalaris*.

Inapplicability: This character is inapplicable for taxa lacking an identifiable transverse tendon (Char. AD20, state 0).

Char. #79 (AD21). *Adductor mandibulae*; buccopalatal membrane; infralabial ligament; anterior end: (0) not surpassing the level of the posterior margin of the orbit capsule; (1) surpassing the level of the posterior margin of the orbit capsule.

Description: The infralabial ligament is a stout element visible laterally, connecting the dentary to the ventral distal portion of the maxilla. In all examined taxa, the infralabial ligament length was very conservative except in *Eleutheronema tridactylum* and *Polydactylus opercularis*, which presented comparatively shorter ligaments. In these two species, the infralabial ligament does not surpass the level of the posterior margin of the orbit capsule, whereas all other taxa have this ligament expanded anteriorly and aligned with the center or anterior margin of the orbit capsule (Figs. 1, 3, 7 – Chap. 1).

Hyopalatine musculature

Char. #80 (AHY01). *Adductor hyomandibulae*, fibers reaching the anterolateral region of the endopterygoid: (0) absent; (1) present.

Description: The *adductor hyomandibulae* (= *adductor arcus palatini*; Datovo & Rizzato, 2018) is a muscle typically located at the base of the orbital capsule, extending between the skull and the hyopalatine arch. In Holocentridae, the anterior end of the *adductor hyomandibulae* is on the posterior part of the endopterygoid, not reaching the anterolateral region of that bone (and consequently the palatine). The same condition can be found in the polynemid genus *Eleutheronema* (Figs. 12B – Chap. 1). Contrastingly, the examined sciaenid and all other polynemids have the *adductor hyomandibulae* extending more anteriorly on the suspensorium and reaching the palatine (Figs. 10, 11, 12A, 13 – Chap. 1).

Char. #81 (AHY02). *Adductor hyomandibulae*; anterior portion; arrangement of fibers: (0) parallel; (1) bipinnate; (2) multipinnate.

Description: Most analyzed species have the anterior fibers of the *adductor hyomandibulae* – i.e., those primarily associated with the anterior region of the endopterygoid and palatine – arranged in a parallel disposition (Figs. 10, 11 – Chap. 1). In *Filimanus* and *Polydactylus microstomus* these fibers are disposed in a bipinnate aspect (Fig. 13A – Chap. 1), whereas a multipinnate arrangement is present in *Leptomelanosoma*, *Parapolynemus* and *Polynemus* (Fig. 12A – Chap. 1).

Inapplicability: This character is inapplicable for taxa lacking the *adductor hyomandibulae* extending to the anterior region of the endopterygoid and palatine (Char. AHY01, state 0).

Char. #82 (AHY03). *Adductor hyomandibulae*; insertion on the ectopterygoid: (0) absent; (1) present.

Description: Most examined species have the *adductor hyomandibulae* originating from the parasphenoid and prootic and inserting on the hyomandibula, metapterygoid, endopterygoid, and palatine (Figs. 11A – Chap. 1). However, the muscle can be more

expanded anteroventrally and additionally inserts onto the lateral surface of the ectopterygoid. This condition is present in *Filimanus, Leptomelanosoma, Parapolynemus, Polydactylus microstomus, P. sextarius,* and *Polynemus* (Figs. 12A, 13A – Chap. 1).

Char. #83 (LAP01). *Levator arcus palatini*, *pars temporalis*; location in comparison to the *segmentum facialis* of the *adductor mandibulae*: (0) lateral; (1) medial.

Description: The *levator arcus palatini* is usually located at the rear portion of the orbit, right between the skull and the palatal arch. Usually, the *temporalis* section of the muscle is covered by the *segmentum facialis* of the *adductor mandibulae*. In Sciaenidae and Holocentridae, the *pars temporalis* of the *levator arcus palatini* is lateral to the *segmentum facialis* of the *adductor mandibulae* covering only the *primordialis* section of the muscle (Fig. 1 – Chap. 1). On the other hand, in all polynemids, the *segmentum facialis* of the *adductor mandibulae* covers both the *partes temporalis* and *primordialis* of the *levator arcus palatini* (Figs. 3, 7 – Chap. 1).

Char. #84 (LAP02). *Levator arcus palatini*, *pars primordialis;* origin: (0) restricted to autosphenotic and pterotic; (1) besides autosphenotic and pterotic, fibers also arise from pterosphenoid and frontal bones.

Description: The origin of the *pars primordialis* of the *levator arcus palatini* is mainly from autosphenotic and pterotic bones, although sometimes the frontal and pterosphenoid also serve as origin site for the fibers. The insertion is primarily at hyomandibula and metapterygoid, with little variation. For instance, the posterior fibers in Sciaenidae inserts on the preopercle. In Sciaenidae, Holocentridae and Polynemidae (*Filimanus* and *Pentanemus* genera) the *levator arcus palatini* fibers arise from only autosphenotic and pterotic bones, whereas in the rest of the genera of Polynemidae, the anterodorsal fibers of the *levator arcus palatini* are more expanded, originating also from frontal and pterosphenoid bones.

Char. #85 (LAP03). *Levator arcus palatini, pars primordialis*; differentiation into *partes primordialis externa* and *interna*: (0) undifferentiated; (1) differentiated.

Description: The *levator arcus palatini* can be a single muscle mass, as seen in Holocentridae, or it can be differentiated into a posterolateral subsection termed *pars primordialis externa* and an anteromedial portion named *pars primordialis interna*. This differentiation is present in Sciaenidae and Polynemidae, varying the degree of separation between subsections and the anterior expansion of the *pars primordialis interna* of the *levator arcus palatini* (Figs. 10-13 – Chap. 1). The *pars primordialis externa* fibers generally remain associated to autosphenotic and pterotic, while the *pars primordialis interna* fibers originate from the anterior portion of the autosphenotic and also from the frontal and pterosphenoid. In Sciaenidae, the *pars primordialis interna* fibers originate from autosphenotic only.

Char. #86 (LAP04). *Levator arcus palatini, pars primordialis*; degree of separation between the *partes primordialis externa* and *interna*: (0) sharing fibers; (1) completely separated.

Description: The *pars primordialis interna* of the *levator arcus palatini* can be shorter and share fibers with the *pars primordialis externa* subsection, which can be seen in sciaenids and in *Eleutheronema, Filimanus, Pentanemus, Polydactylus sexfilis,* and *Polynemus*. On the other hand, the *pars primordialis interna* can be completely independent from the *pars primordialis externa*, condition present in *Galeoides, Leptomelanosoma, Parapolynemus,* and the other *Polydactylus* species.

Inapplicability: This character is inapplicable for taxa lacking the *levator arcus palatini* differentiated into *partes primordialis externa* and *interna* (Char. LAP03, state 0).

Opercular musculature

Char. #87 (OP01). *Dilatator operculi*; origin sites: (0) autosphenotic and pterotic; (1) pterotic only.

Description: Among the examined taxa, the origin of the *dilatator operculi* may involve either solely the pterotic, which is the polynemid and sciaenid condition or both the pterotic and the autosphenotic, condition found in *Holocentrus*.

Char. #88 (OP02). *Adductor operculi*; origin type: (0) musculous only; (1) mixed (musculous and tendinous).

Description: The origin of the *adductor operculi* is solely musculous from the neurocranium of *Holocentrus*, *Cynoscion*, and *Eleutheronema* (Figs. 10B – Chap. 1). In all remaining polynemids, the posterolateral fibers of the *adductor operculi* arise tendinously whereas the anteromedial fibers originate musculously from the neurocranium (Fig. 11B – Chap. 1).

Char. #89 (OP03). *Dilatator operculi*; insertion site; visibility in superficial lateral view: (0) insertion covered by the preopercle; (1) insertion site visible and posterior to the preopercle.

Description: The insertion of the *dilatator operculi* in Holocentridae is medial to the posterodorsal region of the preopercle, being thus not visible from a superficial lateral view of musculoskeletal system. On the other hand, in Polynemidae and Sciaenidae that insertion is easily observable laterally, as it is located completely caudal to the posterodorsal border of the preopercle (Figs. 10A, 11A, 12, 13A – Chap. 1).

Char. #90 (OP04). *Dilatator operculi*; visibility between hyomandibula and opercle in medial view: (0) not visible; (1) visible.

Description: In a medial view of the suspensorium, the *dilatator operculi* can be seen between the hyomandibula and opercle of the examined sciaenid and most polynemids (Figs. 10B, 11B – Chap. 1). In *Holocentrus*, *Filimanus*, and *Parapolynemus* the *dilatator operculi* is not visible in that region from a medial view (Figs. 13B – Chap. 1).

Char. #91 (OP05). *Levator operculi* and *adductor operculi*; degree of separation from each other in adults: (0) separated; (1) not separated.

Description: The *levator operculi* and *adductor operculi* are ontogenetically derived from the posterior portion of a single primordial muscle mass, the *constrictor hyoideus dorsalis*. Late in development, these two muscles separate and become completely independent from each other in most analyzed taxa. Only *Parapolynemus* retains the two muscles undifferentiated from each other in the adult specimen, configuring a single muscle mass behind the *dilatator operculi* (Figs. 12A – Chap. 1).

Char. #92 (OP06). *Levator operculi*; insertion sites: (0) at the dorsomedial face of the opercle; (1) solely on the dorsal margin of the opercle.

Description: The insertion of the *levator operculi* of teleosts is usually at the medial face of the opercle, in a region far ventral to the dorsal margin of that bone, as seen in Holocentridae and several other Perciformes. In Sciaenidae and Polynemidae the insertion of the *levator operculi* is restricted to the dorsal margin of the opercle (Figs. 10-13 – Chap. 1).

Inapplicability: This character is inapplicable for taxa lacking a *levator operculi* differentiated from the *adductor operculi* (Char. OP05, state 0).

Pectoral musculature

Lateral pectoral musculature

Char. #93 (PG01). Pectoral musculature, *abductor* and *adductor* muscle components; subdivision into dorsal and ventral segments: (0) undivided; (1) divided (Kang *et al.* 2017; ch. #16, modified).

Description: Almost all teleosteans have the *abductor* and *adductor* components of the pectoral musculature as single masses of muscles, without the segmentation into a dorsal and a ventral segment (Figs. 14, 15 – Chap. 1). Polynemids have the ventralmost pectoral-fin rays transformed into pectoral filaments that are isolated from the rest of the fin. Two completely divided muscle segments associate with each of these subdivisions, a dorsal *segmentum radialis*, serving the unmodified pectoral-fin rays, and a ventral *segmentum filamentaris*, attaching to the pectoral filaments (Figs. 17-23B – Chap. 1).

Char. #94 (PG02). Pectoral musculature, *abductor* muscle components*, segmentum radialis;* origin from the cleithrum: (0) present; (1) absent.

Description: Among the analyzed taxa, the cleithrum is usually associated with the origin of the *segmentum radii* of all lateral pectoral muscles (abductor components). *Parapolynemus* is the solely exception to this pattern, with the cleithrum not serving as origin site for these muscles, which arise only from the coracoid (Fig. 18 – Chap. 1).

Char. #95 (PG03). *Abductor superficialis*, *segmentum radialis;* origin relative to the *segmentum filamentaris*: (0) lateral; (1) medial.

Description: The fibers of the *abductor superficialis radialis* are usually the lateralmost elements of the pectoral musculature (Fig. 17 – Chap. 1). Nevertheless, in *Parapolynemus* the ventralmost portion of that muscle is overlaid laterally the dorsalmost bundle of fibers of the *abductor superficialis filamentaris* (Fig. 18 – Chap. 1).

Inapplicability: This character is inapplicable for taxa lacking the *segmentum filamentaris* (Char. PG01, state 0).

Char. #96 (PG04). *Abductor profundus*, *segmentum radialis;* visibility through the cleithrum-coracoid fenestra in medial view: (0) not visible; (1) visible.

Description: The *abductor profundus radialis* is a lateral component of the musculature that, in some cases, is visible in medial view through the cleithrum-coracoid fenestra, ventrally to the fibers of the *adductor profundus radialis*. This condition is observed only in *Eleutheronema, Filimanus,* and all *Polydactylus* except *P. opercularis* (Fig. 20 – Chap. 1).

Char. #97 (PG05). *Abductor profundus*, *segmentum radialis;* origin from pectoral radial 3: (0) absent; (1) present.

Description: Among the analyzed taxa, the origin of the *abductor profundus radialis* is usually from the cleithrum and coracoid bones only. In polynemids, that origin additionally involves pectoral radial 3, which is a greatly elongated ossification.

Char. #98 (PG06). *Abductor profundus*, *segmentum radialis;* origin from the scapula: (0) absent; (1) present.

Description: As aforementioned, the origin of the *abductor profundus radialis* is usually restricted to the cleithrum and coracoid. Besides the additional origin from the third pectoral radial (all polynemids; Ch. #97), *Eleutheronema*, *Filimanus*, *Pentanemus,* and *Polydactylus* (except *P. microstomus, P. sexfilis,* and *P. sextarius*) have fibers also arising from the scapula.

Char. #99 (PG07). *Abductor profundus*, *segmentum radialis*; subdivision into *partes marginalis* and *ceterae*: (0) undivided; (1) divided.

Description: In most analyzed specimens, the *abductor profundus radialis* is completely divided into (i) *pars ceterae*, which is the main section of the muscle that attaches onto all pectoral-fin rays, except the first one; and (ii) *pars marginalis*, which is the section inserting only on the marginal (first) ray (Figs. 18, 19 – Chap. 1). Uniquely in

Pentanemus these sections of the *abductor profundus radialis* are only superficially differentiated, but not truly separated from each other.

Char. #100 (PG08). *Abductor profundus, segmentum radialis, pars marginalis;* fibers disposition relative to the *arrector ventralis*: (0) parallel; (1) oblique.

Description: The *abductor profundus radialis* is usually divided into *partes marginalis* and *ceterae* (Ch. #99). Typically, the fibers of both muscles run parallel to those of the *arrector ventralis* (Figs. 19 – Chap. 1). However, *Parapolynemus* has the fibers of the *pars marginalis* arranged in an oblique angle relative to the *arrector ventralis* (Figs. 18B – Chap. 1).

Inapplicability: This character is inapplicable for taxa lacking the *abductor profundus radialis* divided into *partes marginalis* and *ceterae* (Char. PG07, state 0).

Char. #101 (PG09). *Arrector ventralis;* origin from the scapula: (0) absent; (1) present.

Description: The *arrector ventralis* usually originates from cleithrum and coracoid. Most polynemids have this muscle originating also from the scapula.

Char. #102 (PG10). *Abductor profundus, segmentum radialis, pars marginalis;* origin from the third pectoral radial: (0) absent; (1) present.

Description: The *abductor profundus radialis, pars marginalis* usually originates from cleithrum and coracoid. *Galeoides* and *Leptomelanosoma* have fibers of this muscle also originating from the lateral surface of pectoral radial 3.

Inapplicability: This character is inapplicable for taxa lacking the *abductor profundus* divided into *partes marginalis* and *ceterae* (Char. PG07, state 0).

Char. #103 (PG11). Pectoral musculature, *abductor* and *adductor* muscle components, *segmentum filamentaris;* degree of posterodorsal expansion: (0) restricted to the anteroventral portion of the cleithrum; (1) fibers well expanded dorsally reaching approximately half of the horizontal arm of the cleithrum.

Description: In polynemids, the *segmenta filamentares* of the *abductor* and *adductor* muscle components are usually restricted to the anteroventral portion of the cleithrum, rendering the *segmentum radialis* the most massive muscle component of the lateral portion of the pectoral girdle (Figs. 17, 19, 20, 23B – Chap. 1). *Parapolynemus*, *Pentanemus* and *Polynemus* have the opposite condition: the *segmentum filamentaris* is much expanded posterodorsally and occupies most part of the lateral face of the pectoral girdle (Figs. 18, 21, 22 – Chap. 1). In those instances, the *segmentum filamentaris* reaches the dorsal half of the horizontal arm of the cleithrum.

Inapplicability: This character is inapplicable for taxa lacking the *segmentum filamentaris* (Char. PG01, state 0).

Char. #104 (PG12). *Abductores superficialis* and *profundus*, *segmentum filamentaris;* degree of subdivision between bundles of fibers serving the filaments: (0) bundles closely associated and united by fascia; (1) bundles of fibers well developed and isolated from one another.

Description: The fibers of the *segmentum filamentaris* of the *abductores superficialis* and *profundus* are usually organized into individual bundles that inserts on each pectoral filament. In the more usual condition among polynemids, these bundles of fibers are in intimate contact and united to each other by fascia. *Parapolynemus*, *Pentanemus* and *Polynemus* have the bundles completely separated from one another (Figs. 18 – Chap. 1). In this condition, it is possible to visualize fibers of the bundles of the *abductor profundus* in between the superficial bundles of the *abductor superficialis*.

Inapplicability: This character is inapplicable for taxa lacking the *segmentum filamentaris* (Char. PG01, state 0).

Char. #105 (PG13). *Abductor profundus, segmentum filamentaris;* origin from pectoral radial 4: (0) absent; (1) present.

Description: The *abductor profundus filamentaris* originates mainly from the lateral surfaces of the cleithrum and coracoid. *Galeoides* is the only exception in this pattern with fibers arising also from the fourth pectoral radial.

Inapplicability: This character is inapplicable for taxa lacking the *segmentum filamentaris* (Char. PG01, state 0).

Char. #106 (PG14). *Protractor pectoralis;* origin: (0) from the *epaxialis* tendon that attaches on the intercalar; (1) from the *epaxialis* tendon that attaches on the pterotic spine.

Description: The *protractor pectoralis* originates from the *epaxialis* tendon that attaches onto the neurocranium. Nevertheless, the attachment site differs among genera. In Holocentridae, *Eleutheronema*, *Filimanus*, *Pentanemus, Polydactylus opercularis,* and *P. plebeius* the *protractor pectoralis* arise from the tendon that attaches the *epaxialis* fibers on the intercalar while in all other polynemids and in *Cynoscion*, the *protractor pectoralis* originates from the *epaxialis* tendon arriving on the pterotic spine.

Medial pectoral musculature

Char. #107 (PG15). *Adductor superficialis*, *segmentum radialis;* origin type: (0) musculous only; (1) mixed – musculous and tendinous.

Description: The *segmentum radialis* of the *adductor superficialis* of the analyzed outgroup taxa has a musculous origin from the medial surface of the pectoral girdle. In most

polynemids the same muscle presents a mixed origin in which the dorsalmost fibers (that insert onto the lower rays) have an aponeurotic origin while the ventralmost fibers (that insert onto the upper rays) have a musculous origin. The only exception for this condition within Polynemidae is present in *Galeoides, Polydactylus microstomus* and *P. sextarius*, which have the same condition as the outgroups.

Char. #108 (PG16). *Adductor superficialis*, *segmentum radialis;* origin: (0) from the cleithrum only; (1) from the cleithrum and scapula; (2) from the cleithrum, scapula, and coracoid.

Description: The *adductor superficialis* of the *segmentum radii* usually originates from the dorsal region of the medial face of the cleithrum. For most polynemids, the *adductor superficialis* has fibers arising from both the cleithrum and scapula. Moreover, the *adductor superficialis* of *Galeoides* and *Leptomelanosoma* originates from the cleithrum, scapula, and coracoid.

Char. #109 (PG17). *Adductor medialis, segmentum radialis;* degree of division from the *adductor profundus*: (0) divided; (1) undivided.

Description: In *Cynoscion* and *Holocentrus*, the *adductor medialis radialis* is a thin layer of fibers completely separated from the *adductor profundus radialis* and inserting onto the central pectoral-fin rays (*i.e.* failing to reach the outer- and innermost rays; Figs. 14B, 15A – Chap. 1). However, the *adductor medialis radialis* of polynemids is not differentiated from the main body of the *adductor profundus radialis* (Figs. 20-23B – Chap. 1).

Char. #110 (PG18). *Adductor profundus, segmentum radialis;* degree of differentiation into *partes endoprofunda* and *ectoprofunda*: (0) undifferentiated; (1) differentiated.

Description: In *Holocentrus*, the *segmentum radialis* of the *adductor profundus* is a single muscle mass, with no apparent subdivisions. Polynemids and *Cynoscion* have the *adductor profundus* differentiated into a lateral thin component, with origin from the posterior bar of the coracoid (*pars endoprofunda*), and a medial thick muscle mass with origin from both the coracoid and the cleithrum (*pars ectoprofunda*) and that usually covers part or the entire cleithrum-coracoid fenestra (Figs. 15B, 20B – Chap. 1).

Char. #111 (PG19). *Adductor profundus*, *segmentum radialis*; fibers originating from the lateral portion of the pectoral girdle: (0) absent; (1) present.

Description: In the analyzed taxa, the *adductor profundus radialis* usually originates entirely from the medial portion of the pectoral girdle. Nevertheless, *Polynemus* additionally has a few fibers originating from the lateral portion of the girdle, passing through the cleithrum-coracoid fenestra and inserting onto the medial hemitrichia.

Char. #112 (PG20). *Arrector dorsalis;* degree of separation from the *adductor profundus*: (0) completely separated; (1) sharing fibers.

Description: The *arrector dorsalis* is a muscle that typically attaches only onto the first (marginal) ray of the pectoral fin. The fibers of the muscle are usually completely separated from those belonging to adjacent muscles of the medial portion of the pectoral girdle, as seen in *Cynoscion* and *Holocentrus* (Fig. 15 – Chap. 1). Contrastingly, the *arrector dorsalis* of polynemids shares fibers with the *adductor profundus radialis* (Fig. 20-23B – Chap. 1).

Char. #113 (PG21). *Adductor radialis;* degree of separation from the *adductor profundus*: (0) completely separated; (1) sharing fibers.

Description: The *adductor radialis* is the smallest among the pectoral muscles. It generally originates from the medial faces of the pectoral radials and inserts onto the

ventralmost pectoral-fin rays. The *adductor radialis* is completely separated from the adjacent muscles in the examined outgroups (Fig. 15B – Chap. 1). However, in polynemids that muscle share fibers with the *segmentum radialis* of the *adductor profundus* (Fig. 20B – Chap. 1).

Char. #114 (PG22). *Adductor superficialis*, *segmentum filamentaris;* origin relative to the Baudelot's ligament: (0) distant, separated from the ligament by a gap that is much greater than the Baudelot's ligament width; (1) immediately ventral to the ligament or with a small gap that is lesser than the Baudelot's ligament width.

Description: The *adductor superficialis filamentaris* is the major component of the musculature serving the medial portion of the pectoral fin of polynemids and its origin is from the medial surface of the cleithrum. In *Eleutheronema, Polydactylus plebeius,* and *P. sexfilis* there is a gap between the origin of dorsalmost fibers of that muscle and the Baudelot's ligament (Fig. 20A – Chap. 1). In these taxa, the gap is much greater than the Baudelot's ligament width. In all other polynemids, the *adductor superficialis filamentaris* originates immediately ventral to the Baudelot's ligament or present a rather small gap of bone which is lesser than the Baudelot's ligament width (Figs. 21-23B – Chap. 1).

Inapplicability: This character is inapplicable for taxa lacking the *segmentum filamentaris* (Char. PG01, state 0).

Char. #115 (PG23). *Adductor medialis, segmentum filamentaris;* degree of separation between bundles serving the filaments: (0) bundles of fibers closely united by fascia; (1) bundles of fibers free from each other.

Description: The *segmentum filamentaris* of the *adductor medialis* is a muscle mass that differentiates into bundles that serve each pectoral filament, although these bundles are usually not fully separated from each other, with some sharing of fibers. In *Pentanemus*,

Parapolynemus, and *Polynemus* these differentiated bundles are completely separated from each other.

Inapplicability: This character is inapplicable for taxa lacking the *segmentum filamentaris* (Char. PG01, state 0).

Char. #116 (PG24). *Adductor medialis, segmentum filamentaris;* insertion sites: (0) on all pectoral filaments; (1) on all pectoral filaments but the ventralmost one; (2) two or more pectoral filaments do not receive fibers.

Description: The *adductor medialis* of the *segmentum filamentaris* attaches onto the medial base of the pectoral filaments. In *Filimanus*, *Polydactylus microstomus, P. octonemus, P. oligodon, P. virginicus*, and *Polynemus*, the *medialis* muscle inserts on all filaments, whereas in *Eleutheronema*, *Leptomelanosoma*, *Pentanemus*, *Polydactylus approximans, P. opercularis, P. plebeius,* and *P. sexfilis* the muscle do not reach the ventralmost filament (Fig. 20 – Chap. 1). *Parapolynemus* and *Galeoides* have the *adductor medialis* failing to reach more than one filament, varying between them. The *adductor medialis* of *Parapolynemus* does not reach the two ventralmost filaments (Fig. 21 – Chap. 1) whereas the *adductor medialis* of *Galeoides* reaches only the three filaments of ten in total (Fig. 23B – Chap. 1).

Inapplicability: This character is inapplicable for taxa lacking the *segmentum filamentaris* (Char. PG01, state 0).

Char. #117 (PG25). *Adductor medialis, segmentum filamentaris;* origin sites: (0) coracoid only; (1) cleithrum and coracoid.

Description: The *segmentum filamentaris* of the *adductor medialis* of the usually originates solely from the medial face of the coracoid. *Parapolynemus* and *Polynemus* have fibers arising from the medial faces of both the coracoid and cleithrum (Fig. 22 – Chap. 1). Remarkably, the origin of some fibers of the dorsalmost bundle of the *adductor medialis filamentaris* of *Polynemus* is associated with the lateral face of the cleithrum.

Inapplicability: This character is inapplicable for taxa lacking the *segmentum filamentaris* (Char. PG01, state 0).

Char. #118 (PG26). *Adductor medialis, segmentum filamentaris;* degree of differentiation into *partes endomedialis* and *ectomedialis*: (0) undifferentiated; (1) differentiated.

Description: In most polynemids, the *adductor medialis filamentaris* is differentiated into two sections: *endomedialis* and *ectomedialis*. The *pars ectomedialis* is larger, has longer fibers, and is visible superficially in medial view. The *pars endomedialis*, in turn, lies underneath the former section and has shorter fibers. These two sections are differentiable from each other at origin but invariably share fibers near the insertion. *Eleutheronema*, *Galeoides,* and *Polydactylus sexfilis* are the only polynemids that lack any kind of differentiation of the *adductor medialis* into *ecto*- and *endomedialis*.

Inapplicability: This character is inapplicable for taxa lacking the *segmentum filamentaris* (Char. PG01, state 0).

Char. #119 (PG27). SP2 + RLA-OP branch; position relative to the *segmentum filamentaris* of the *adductor superficialis* : (0) running on the surface of the muscle; (1) running posterior to the muscle.

Description: The SP2 + RLA-OP branch runs along the medial surface of the *adductor superficialis filamentaris* in most examined taxa (Figs. 21-23B – Chap. 1). However, in *Eleutheronema*, this nerve passes posterior to that muscle (Fig. 20A – Chap. 1).

Inapplicability: This character is inapplicable for taxa lacking the *segmentum filamentaris* (Char. PG01, state 0).

Char. #120 (PG28). Second spinal nerve; position relative to the first spinal nerve: (0) not covering the fisrt spinal nerve; (1) covering the fisrt spinal nerve.

Description: The main trunk of the second spinal nerve is usually posterior that of the first spinal nerve along their entire extend, with varying degree of distance between them (Figs. 20, 23B – Chap. 1). However, in *Parapolynemus* and *Pentanemus* the second spinal nerve overlaps laterally the first one at the level of the pectoral fin (Figs. 21, 22 – Chap. 1).

Char. #121 (PG29). *Ramus lateralis accessorius,* orbito-pectoral branch*;* fusion with the second spinal nerve; occurrence: (0) absent; (1) present.

Description: In polynemids, the orbito-pectoral branch of the *ramus lateralis accessorius* (RLA-OP) is a massive nerve that arises from the trigeminus-facialis trunk and runs posteriorly towards the back portion of the neurocranium. Medially to the posttemporal, the RLA-OP runs ventrally passing also medially to the supracleithrum and cleithrum. When the RLA-OP arrives at the cleithrum, it merges with the second spinal nerve (Figs. 20-23B – Chap. 1). In *Cynoscion* RLA branch that arrives in the pectoral girdle is not the orbito-pectoralis and in *Holocentrus*, the RLA nerve is absent.

Char. #122 (PG30). *Ramus lateralis accessorius,* orbito-pectoral branch; pattern of bifurcation before reaching the pectoral girdle: (0) unbranched; (1) branched.

Description: Most examined taxa have the main trunk of the RLA-OP usually undivided along most of its length. In *Pentanemus*, right after exiting the neurocranium, the RLA-OP bifurcates and then merges with the second spinal nerve (Fig. 21 – Chap. 1).

Inapplicability: This character is inapplicable for taxa lacking the orbito-pectoralis branch of the *ramus lateralis accessorius* running into the pectoral girdle (Char. PG29, state 0).

Branchial arches musculature

Suprabranchial musculature

Char. #123 (BM01). *Levator externus I*; degree of differentiation into posterolateral and anteromedial portions: (0) undifferentiated; (1) differentiated.

Description: The *levatores externi* originates from the neurocranium and inserts onto the epibranchials. Usually, each *levator* is a single bundle of fibers (Fig. 27A – Chap. 1) however, the *levator externus I* can present a differentiation near the insertion, where it is possible to distinguish a small posterolateral portion inserting on the dorsal process of the first epibranchial while the main body (anteromedial portion) of fibers attaches medially to this site (Fig. 27B – Chap. 1). This condition is found in *Parapolynemus, Polydactylus approximans, P. octonemus, P. virginicus,* and *Polynemus*.

Char. #124 (BM02). *Levator externus I*; insertion type: (0) musculously; (1) mixed; (2) tendinously.

Description: The *levator externus I* inserts onto the uncinate process of epibranchial 1 and can have the following arrangement: (0) insert musculously – Holocentridae; (1) have a mixed insertion in which the posterior fibers converge to a tendon while the anterior ones attach musculously on the uncinate process; (2) insert tendinously, which is the case of all polynemids (Fig. 27 – Chap. 1).

Char. #125 (BM03). *Levator externus I*; length of the tendinous insertion: (0) not very developed, shorter than half of the fiber's length; (1) very developed, longer than half or more of the fiber's length.

Description: The *levator externus I* inserts tendinously onto the uncinate process of epibranchial 1 and in almost every polynemid this tendinous insertion is not very developed (Fig. 27B – Chap. 1). However, *Filimanus* and *Pentanemus* have a long tendinous portion,

which is equivalent of at least half of the fibers length (Fig. 27A – Chap. 1). In *Pentanemus* the tendinous portion is even longer than the fibers.

Inapplicability: This character is inapplicable for taxa lacking the *levator externus I* inserting tendinously onto the first epibranchial (Char. BM02, states 0, 1).

Char. #126 (BM04). *Levator externus II*; arrangement in comparison to the *levatores externi III* and *IV*: (0) not parallel; (1) parallel.

Description: The *levatores externi III* and *IV* generally runs parallel to each other while the *levatores externi I* and *II* are arranged in a different position. However, in *Parapolynemus* the *levator externus II* is placed parallel to the *levatores externi III* and *IV*.

Char. #127 (BM05). *Levatores externi I* and *II*; origin type: (0) tendinous; (1) musculous.

Description: The *levatores externi I* and *II* originates musculously from the neurocranium in all polynemids. *Cynoscion* and *Holocentrus* present the *levatores externi I* and *II* originating tendinously.

Char. #128 (BM06). *Levatores externi III* and *IV*; origin type: (0) aponeurotic; (1) musculous.

Description: The *levatores externi III* and *IV* originates aponeurotically from the neurocranium in all polynemids and in *Cynoscion*. *Holocentrus* present the *levatores externi I* and *II* originating musculously.

Char. #129 (BM07). *Levator posterior*; origin type: (0) tendinous; (1) musculous.

Description: The *levator posterior* is the most posterior muscle in lateral view. It originates from the intercalar and attaches onto the uncinate process of the fourth

epibranchial, posterolateral to the *levator externus IV* insertion. In Holocentridae and Sciaenidae, the origin is tendinous and visible from the intercalar. On the other hand, in polynemids this origin is musculous and is medial to the intercalar posterior projection.

Char. #130 (BM08). *Levator posterior*; degree of differentiation into portions anterior and posterior: (0) undifferentiated; (1) differentiated.

Description: The *levator posterior* can be arranged as a single muscle mass, condition present in almost all analyzed taxa (Fig. 27A – Chap. 1) or it can be differentiated into a posterolateral and an anteromedial portions (Fig. 27B – Chap. 1). This differentiation is evident in *Galeoides*, *Leptomelanosoma*, *Polydactylus microstomus,* and *Polynemus.*

Char. #131 (BM09). *Transversus dorsalis II*; degree of differentiation into anterior and posterior portions: (0) undifferentiated; (1) differentiated.

Description: The *transversus dorsalis II* (TD II) is the anteriormost muscle that originates and inserts onto contralateral elements from the branchial arches. This muscle specifically connects the dorsal contralateral elements of the second branchial arch. The TD II can only attach to epibranchials 2 (Fig. 26A – Chap. 1) or have two sections: one in between epibranchials 2 and another in between pharyngobranchials 2 (Fig. 28 – Chap. 1). The first condition is present in Sciaenidae and the TD II differentiated into sections anterior and posterior is present in Holocentridae and Polynemidae.

Char. #132 (BM10). *Transversus dorsalis II*, anterior section; degree of posterior expansion in comparison to the posterior section: (0) extended at least half or more than half of the posterior section length; (1) extended less than half of the posterior section length.

Description: The anterior section of the *transversus dorsalis II* can have distinct patterns of posterior expansion. It can either be greatly expanded, occupying approximately

half or more of the fibers from the posterior section of the TD II (Fig. 28B – Chap. 1) or overlap only the anteriormost fibers of the posterior section, occupying less than half of its fibers (Fig. 28A – Chap. 1). The fist condition is present in Holocentridae and in almost all polynemids, whereas the second one is present only in *Parapolynemus* and *Polynemus*. In *Parapolynemus* this configuration is very evident, where the fibers of the anterior section are much reduced in comparison to other genera.

Inapplicability: This character is inapplicable for taxa lacking the *transversus dorsalis II* differentiated into sections anterior and posterior (Char. BM09, states 0).

Char. #133 (BM11). *Transversus dorsalis II*, longitudinal raphe of the anterior section; anterior extension: (0) extending to the anteriormost fibers; (1) not extending to the anteriormost fibers.

Description: The *transversus dorsalis II* has a longitudinal central raphe that runs on the dorsal surface of the muscle. However, this longitudinal raphe may be or not complete throughout the muscle. In almost all polynemid the longitudinal raphe fails to reach the anteriormost fibers of the anterior section (Fig. 28A, 29A – Chap. 1). The raphe is complete in *Holocentrus, Eleutheronema, Galeoides,* and *Polydactylus plebeius* (Fig. 28B – Chap. 1).

Inapplicability: This character is inapplicable for taxa lacking the *transversus dorsalis II* differentiated into sections anterior and posterior (Char. BM09, states 0).

Char. #134 (BM12). *Transversus dorsalis II*; continuity with the *transversus dorsalis III*: (0) absent; (1) present.

Description: The posterior fibers from the *transversus dorsalis II* can be continuous to the anterior fibers of the *transversus dorsalis III* and this condition is present in *Eleutheronema, Parapolynemus, Polydactylus virginicus, P. microstomus, P. opercularis, P. plebeius, P. sexfilis,* and *Polynemus* (Fig. 28A – Chap. 1). However, TD II and III can also be

independent and not share fibers between each other, which is the case of the rest of Polynemidae, Holocentridae, and Sciaenidae (Fig. 26A, 28B – Chap. 1).

Char. #135 (BM13). *Transversi dorsales II* and *III*; gap of connective tissue between both musculatures: (0) absent; (1) present.

Description: Some taxa present in between TD II and III a small gap between musculatures, showing a small portion of connective tissue (Fig. 28A – Chap. 1). This conformation is the most common arrangement. Nevertheless, *Holocentrus, Filimanus, Galeoides, Leptomelanosoma, Polydactylus microstomus,* and *Polynemus paradiseus* have the *transversus dorsalis III* immediately posterior to the *transversus dorsalis II*, with no hiatus of connective tissue between them (Fig. 28B, 29A – Chap. 1).

Char. #136 (BM14). *Transversus dorsalis III*; posterior fibers attaching onto the fourth pharyngobranchial: (0) absent; (1) present.

Description: The posterior fibers from the *transversus dorsalis III* usually attaches only onto epibranchial and pharyngobranchial of the third branchial arch (Holocentridae and Sciaenidae condition). However, almost in all polynemids, the posterior fibers of TD III also attach on pharyngobranchial 4 with exception of *Eleutheronema*.

Char. #137 (BM15). *Transversus dorsalis IV*; occurrence: (0) present; (1) absent.

Description: The *transversus dorsalis IV* that attaches onto the epibranchial 4 and pharyngobranchial 4 is visible only in Holocentridae. Several polynemids have a few fibers of the TD III arriving on the pharyngobranchial 4, but none on the epibranchial 4, not constituting a “true” *transversus dorsalis IV*

Char. #138 (BM16). *Obliquus dorsalis*; visibility of the insertion of the posteromedial fibers beneath *transversus dorsalis II*: (0) not visible; (1) visible.

Description: Normally, for all analyzed taxa, the *obliquus dorsalis* insertion is placed beneath the *transversus dorsalis II* and is not visible in dorsal view. Nonetheless, in *Parapolynemus*, *Pentanemus*, and *Polydactylus opercularis* the insertion of the posteromedial fibers is visible in dorsal view.

Char. #139 (BM17). *Obliquus dorsalis*; degree of differentiation on the origin: (0) undifferentiated; (1) differentiated.

Description: In practically every analyzed taxon, the *obliquus dorsalis* is a single unit of fibers, with no differentiations whatsoever. Nevertheless, the *obliquus dorsalis* of *Polydactylus opercularis* have a differentiation near the attachment onto the epibranchials. The dorsal fibers arises from the primarily origin site of the *obliquus dorsalis* while the ventral ones originates on the dorsal face of the third epibranchial.

Char. #140 (BM18). *Obliquus dorsalis*; raphe separating it from the *obliquus posterior*: (0) present; (1) absent.

Description: The medial fibers of both the *obliqui dorsalis* and *posterior* can have a raphe separating them, which is found in *Holocentrus*. In sciaenids and polynemids the medial fibers of both muscles attach directly onto epibranchial 4.

Char. #141 (BM19). *Adductor branchialis IV*; degree of differentiation into anterior and posterior sections: (0) undifferentiated; (1) differentiated.

Description: The *adductor branchialis IV* is positioned at the posteriormost region of the branchial arches, connecting ceratobranchial 4 and epibranchial 4. In most of the

analyzed cases, this muscle is a single mass of fibers (Fig. 31B – Chap. 1) and in *Holocentrus, Filimanus, Polydactylus approximans, P. octonemus, P. oligodon, P. virginicus,* and *P. sexfilis*, the *adductor branchialis IV* is differentiated into anterior and posterior sections (Fig. 30 – Chap. 1).

Char. #142 (BM20). *Adductor branchialis V*; esophageal raphe separating it from the *obliquus posterioris*: (0) present; (1) absent.

Description: The *adductor branchialis V* is the ventralmost muscle acting on the branchial arches. This muscle generally is placed posteroventrally to *obliquus posterior* and *adductor branchialis IV*. In Holocentridae the *adductor branchialis V* is completely ventral to the *obliquus posterior* and in the boundary between muscles there is a raphe separating the fibers. In Sciaenidae and Polynemidae, this raphe is absent as the *adductor branchialis V* is located lateroventrally to the *obliquus posterior* (Fig. 30 – Chap. 1).

Char. #143 (BM21). *Interbranchiales abductores II* and *III*; disposition of the fibers: (0) radiated, fan-shaped; (1) oblique.

Description: On the articulation point between ceratobranchials and epibranchials from the second and third gill arches there are smalls muscle placed on the anterior faces of these bones. These muscles can have a fan aspect, which is the condition of *Holocentrus* or it can be obliquely arranged, connecting ceratobranchials to gill filaments/epibranchials. This condition is present in *Cynoscion* and polynemids (except *Polynemus multifilis*; Fig. 27 – Chap. 1).

Char. #144 (BM22). *Interbranchiales abductores II* and *III*; degree of dorsal expansion: (0) restricted to the anterior faces of the epibranchials; (1) dorsally positioned on the epibranchials.

Description: Frequently, the *interbranchiales abductores II* and *III* are very small muscles on the anterior face of cerato- and epibranchials. However, in *Polydactylus microstomus, P. sextarius,* and especially in *Galeoides*, these muscles are much more developed and also occupy the dorsal surface of the respective epibranchials (Fig. 28B – Chap. 1).

Infrabranchial musculature

Char. #145 (BM23). *Rectus ventralis IV*; degree of separation from the *rectus communis* fibers: (0) sharing fibers; (1) completely separated.

Description: The *rectus ventralis IV* is a muscle that is derived from the main body of the *rectus communis*. In Holocentridae both muscles share fibers and it is difficult to establish boundaries close to their insertion. However, in sciaenids and polynemids the *rectus ventralis IV* and *rectus communis* are completely separated and do not share fibers (Figs. 26B, 29B, 31A, 32 – Chap. 1).

Char. #146 (BM24). *Rectus ventralis IV*; position of the origin in comparison to the *rectus communis* fibers: (0) medial; (1) lateral.

Description: The *rectus ventralis IV* is a muscle that is derived from the main body of the *rectus communis*. The origin of the *rectus ventralis IV* of *Cynoscion* is medial to the fibers from the *rectus communis* (Fig. 26B – Chap. 1) while the origin of the *rectus ventralis IV* of *Holocentrus* and all polynemids is lateral to the fibers of the *rectus communis* (Figs. 29B, 31A, 32 – Chap. 1).

Char. #147 (BM25). *Rectus communis*; origin type: (0) aponeurotic; (1) tendinous.

Description: The origin of the *rectus communis* is from the ventral face of ceratobranchial 5. This origin, for almost all analyzed species, is aponeurotic (Fig. 32 – Chap. 1). However, the origin of the *rectus communis* in *Parapolynemus* and *Polynemus* is thicker and forms a tendinous structure from the fifth ceratobranchial (Fig. 29B – Chap. 1).

Char. #148 (BM26). *Pharyngoclavicularis internus*; origin type: (0) tendinous; (1) musculous; (2) aponeurotic.

Description: The *pharyngoclavicularis internus* (PCI) origin varies among families. The PCI of Holocentridae, which is a single muscle mass, originates tendinously from the anterior face of the cleithrum. The PCI of Sciaenidae, which is differentiated into anteroventral and posterodorsal portions, originates musculously. The PCI of Polynemidae, which is also differentiated into two sections, originates aponeurotically from the cleithrum (Fig. 31B – Chap. 1).

Char. #149 (BM27). *Pharyngoclavicularis internus*; degree of differentiation into anteroventral and posterodorsal section: (0) undifferentiated; (1) differentiated.

Description: As mentioned on the previous character, the *pharyngoclavicularis internus* can be undifferentiated (Holocentridae) and inserts only at the anterior tip of the fifth ceratobranchial or it can be differentiated into anteroventral and posterodorsal sections. In this case, which is the condition of sciaenids and polynemids, the anteroventral section inserts onto the anterior tip of the fourth ceratobranchial, anterior to the *transversus ventralis IV* whereas the posterodorsal section inserts onto ceratobranchial 5, posterior to the *pharyngoclavicularis externus* (with variations – see below).

Char. #150 (BM28). *Pharyngoclavicularis internus*; degree of division between anteroventral and posterodorsal portions: (0) sharing fibers; (1) completely separated.

Description: The *pharyngoclavicularis internus* can be simply differentiated into sections anteroventral and posterodorsal or present a fully division within the sections (the most common condition within polynemids and *Cynoscion*). The sections of PCI of *Eleutheronema, Polydactylus plebeius,* and *P. sexfilis* share fibers between one another (Fig. 32 – Chap. 1).

Inapplicability: This character is inapplicable for taxa lacking the *pharyngoclavicularis internus* differentiated into two sections (Char. BM27, state 0).

Char. #151 (BM29). *Pharyngoclavicularis internus*, posterodorsal section; insertion onto ceratobranchial 5 in comparison to the *pharyngoclavicularis externus* (PCE): (0) some fibers insert medially to PCE; (1) all fibers are posterior to PCE.

Description: The posterodorsal section of the *pharyngoclavicularis internus* usually attaches onto the fifth ceratobranchial, posterior to the *pharyngoclavicularis externus* insertion. However, in some species, the PCI insertion is not restricted posteriorly to PCE and some fibers insert medially to the former. This is the case of sciaenids, *Eleutheronema, Filimanus, Galeoides, Polydactylus microstomus, P. plebeius,* and *P. sexfilis*.

Inapplicability: This character is inapplicable for taxa lacking the *pharyngoclavicularis internus* differentiated into two sections (Char. BM27, state 0).

Char. #152 (BM30). *Pharyngoclavicularis internus*, posterodorsal section; insertion type: (0) musculous; (1) tendinous.

Description: The insertion of the posterodorsal section of the *pharyngoclavicularis internus* can be musculous, which is the condition of Sciaenidae and several polynemids or it can be tendinous, condition present only in *Filimanus*, *Galeoides*, *Parapolynemus*, and *Polynemus*.

Inapplicability: This character is inapplicable for taxa lacking the *pharyngoclavicularis internus* differentiated into two sections (Char. BM27, state 0).

Char. #153 (BM31). *Pharyngoclavicularis internus*, posterodorsal section; degree of differentiation into subsections anterior and posterior: (0) undifferentiated; (1) differentiated.

Description: The posterodorsal section of the *pharyngoclavicularis internus* can be either undifferentiated - as most of the analyzed cases - or it can be differentiated into two further subsections: anterior and posterior. Those subsections can be only distinguished from one another on the insertion, where the fibers converge to distinct tendons to attach onto the fifth ceratobranchial. This is the case of *Filimanus*, *Parapolynemus*, and *Polynemus*.

Inapplicability: This character is inapplicable for taxa lacking the *pharyngoclavicularis internus* differentiated into two sections (Char. BM27, state 0).

Char. #154 (BM32). *Transversus ventralis IV*; aspect of the surface of the muscle: (0) smooth with no differentiation within the musculature; (1) multipennate.

Description: Generally, the superficial texture of the *transversus ventralis IV* is smooth; the muscle does not present any tendon within the fibers (Fig. 32 – Chap. 1). However, the *transversus ventralis IV* of *Galeoides*, *Leptomelanosoma*, and *Polydactylus microstomus* have multiples tendons within the fibers, giving it a multipennate texture in their ventral surface (Fig. 31A – Chap. 1).

Char. #155 (BM33). *Transversus ventralis V*; attachment onto ceratobranchials 5: (0) musculous; (1) tendinous.

Description: The *transversus ventralis V* is a muscle that connects the contralateral ceratobranchials 5. Most of times, this attachment is musculous and only in *Galeoides* and *Leptomelanosoma* the attachment is tendinous (Fig. 31A – Chap. 1).

Char. #156 (BM34). *Transversus ventralis V*; degree of differentiation indo portions anterior and posterior: (0) undifferentiated; (1) differentiated.

Description: Usually, the *transversus ventralis V* is superficially differentiated into anterior and posterior sections (Fig. 26B, 29B, 31A, 32 – Chap. 1). This condition is present in sciaenids and almost all polynemids. Only *Polydactylus plebeius* and *Holocentrus* have the *transversus ventralis V* undifferentiated.

Char. #157 (BM35). *Transversus ventralis V*; length of the posterior section in comparison to the anterior counterpart: (0) larger than; (1) smaller than.

Description: The sections of the *transversus ventralis V* differs among taxa considering the length of each section. In *Eleutheronema tetradactylum*, *Galeoides*, and *Polydactylus* (except *P. octonemus* and *P. oligodon*) the posterior section is larger than the anterior one (Fig. 31A, 32 – Chap. 1). In *Cynoscion* and the rest of polynemids the posterior section is smaller than the anterior (Fig. 26B, 29B – Chap. 1).

Inapplicability: This character is inapplicable for taxa lacking the *transversus ventralis V* differentiated into two sections (Char. BM34, state 0).

Char. #158 (BM36). *Transversus ventralis V*; limit between anterior and posterior sections; shape: (0) perpendicular straight line; (1) oblique line.

Description: The limit between sections of the *transversus ventralis V* is usually a perpendicular straight line. Yet, in *Eleutheronema tridactylum* and *Polydactylus approximans* this limit is arranged as an oblique line.

Inapplicability: This character is inapplicable for taxa lacking the *transversus ventralis V* differentiated into two sections (Char. BM34, state 0).

Axial musculature

Char. #159 (AM01). *Epaxialis*; degree of extension on the dorsal portion of the neurocranium: (0) restricted to the rear portion of the neurocranium; (1) reaches the frontal.

Char. #160 (AM02). *Epaxialis*; fibers attaching on the lateroventral portion of the neurocranium; occurrence: (0) absent; (1) present.

Char. #161 (AM03). *Epaxialis*; degree of extension on the lateroventral portion of the neurocranium: (0) fibers restricted to the basioccipital; (1) fibers reach the basioccipital and prootic.

Inapplicability: This character is inapplicable for taxa lacking the *epaxialis* reaching the lateroventral portion of the neurocranium (Char. AM02, state 0).

3.2 Phylogenetic analysis

The 162 morphological characters are herein categorized into 12 quantitatives (counts), 12 from external anatomy, 35 osteological, and 103 myological, which are divided into: 21 from the *adductor mandibulae* complex, seven from the hyopalatine musculature,

six from the opercular muscles, 30 from the pectoral girdle musculature, 36 from the branchial arches muscles, and three from axial myology.

The analysis based on all morphological characters in 21 terminal taxa, including 19 polynemid species always recovered a single MPT according to the parameters set (EW or IW with different values of *k*). The traditional search on TNT without homoplasies weighting parameters (EW) resulted into a topology (Fig. 16) that was consistent to the topology obtained with IW (*k* = 7 to ∞). From *k* = 3 – 6 a different topology was recovered and adopted here as the phylogenetic relationship of Polynemidae (Fig. 17). Moreover, using strong weighting against homoplasies (*k* = 1 and 2) resulted into two new different MPTs.

The MPT obtained with IW (*k* = 3 – 6) was chosen to be the representative topology for the relations within Polynemidae due to its interval, excluding therefore the extreme weightings (too strong: *k* = 1 and 2; and too soft: EW). Nevertheless, the only difference between the topology from k = 7 to EW and the one from k = 3 – 6 is *Galeoides* and *Polydactylus sextarius* placement. In the first configuration, *P. sextarius* is sister group to *Galeoides* and *Polydactylus microstomus* whereas the second one present *Galeoides* as sister group to *P. sextarius* and *P. microstomus* (see discussion).

The resulting topology (Fig. 17) has tree length = 300.39, total fit = 88.20376, consistency index = 0.559, retention index = 0.626, and rescaled consistency index = 0.350. The consistency indices, retention indices, rescaled consistency indices, and fitness of each character are depicted in Tab. 1, 2, 3, and 4 – Appendix A, respectively.

4. DISCUSSION

The only two previous phylogenetic hypotheses for the family are from unpublished theses based on approximately 50 characters, most of which were from osteology. The topology proposed by Feltes (1986) encompassed only seven of the eight genera currently considered valid (*Leptomelanosoma* has not been erected and *Marginiserrula* is currently synonymized in *Polydactylus;* Feltes, 2001). Many of the 55 characters from that author present problems, such as ambiguous delimitations of multistates and mixing of variables into a same character. Because of these sorts of problems, none of the characters of Feltes (1986) were directly incorporated in the present study. In Feltes (1986) topology (Fig. 1A), Polynemidae is basally divided in two major lineages: one including *Parapolynemus* and *Polynemus*, which are grouped based on 11 synapomorphies, and another including all remaining polynemids. Only a single synapomorphy supports the monophyly of the latter clade – the presence of foramina in the fourth pectoral radial. This clade has *Eleutheronema* as sister group to the remaining genera that are clustered into two major clades: one including *Filimanus* and *Pentanemus* and another with *Marginiserrula* (currently synonymized in *Polydactylus*) and *Polydactylus* as successive sister taxa of *Galeoides*.

The recent study of Kang (2017) proposed a different hypothesis (Fig. 1B) based on 64 morphological characters which resulted in a considerable amount of polytomies part of the tree. Only an expanded abstract of this study was available, so that the characters used in the analysis were unavailable for comparisons. The topology of Kang (2017) also basally divides Polynemidae into two major lineages: one with *Pentanemus* (*Parapolynemus*, *Polynemus*) supported by four synapomorphies and a second one with the remaining polynemid genera. In the second lineage, *Filimanus* appears as sister group to a clade with a large basal pentatomy in which several species of a polyphyletic *Polydactylus* are intercalated with a monophyletic *Eleutheronema* and the monotypic genera *Galeoides* and *Leptomelanosoma*.

The present study is the most comprehensive cladistic analysis of Polynemidae in terms of size and range of morphological characters, with 162 characters from the external anatomy, squamation, osteology, myology, and laterosensory system. The analysis also

included all polynemid genera currently recognized as valid plus two outgroup taxa. In agreement with previous hypotheses, *Polydactylus* was the only polytypic genus not recovered as monophyletic. In the resulting topology (Fig. 17), *Pentanemus* (East Atlantic) and *Filimanus* (Indo-West Pacific) are successive sister groups of a large lineage clustering all remaining polynemids. This lineage is subdivided into four subsequent clades: the first include three species of *Polydactylus* plus *Eleutheronema* (all from the Pacific); the second groups four *Polydactylus* (one from the Pacific and three from the Atlantic), including the type-species of the genus (*P. virginicus*); the third clusters two *Polydactylus* from Pacific with *Galeoides* (East Atlantic); and the fourth includes *Leptomelanosoma*, *Parapolynemus*, and *Polynemus* (all from Indo-West Pacific). Synapomorphies for each obtained clades as well as comments as to previous hypotheses are detailed in the following sections.

Intrarelationships of Polynemidae

Clade A (TNT clade 29) = Polynemidae: *Eleutheronema tetradactylum, Eleutheronema tridactylum, Filimanus similis, Filimanus xanthonema, Galeoides decadactylus*, *Leptomelanosoma indicum*, *Parapolynemus verekeri*, *Pentanemus quinquarius*, *Polydactylus approximans*, *Polydactylus microstomus*, *Polydactylus octonemus*, *Polydactylus oligodon*, *Polydactylus opercularis*, *Polydactylus plebeius*, *Polydactylus sexfilis, Polydactylus sextarius*, *Polydactylus virginicus*, *Polynemus multifilis*, *Polynemus paradiseus.*

Synapomorphies: Char. #1: (12>10); Char. #4: (17>15); Char. #7: (9>11); Char. #9: (9>13-14); Char. #10: (8>12); Char. #11: (22>31-42); Char. #18: (0>1); Char. #31: (0>1); Char. #35: (0>1); Char. #42: (1>0); Char. #43: (0>1); Char. #48: (0>1); Char. #49: (0>1); Char. #52: (0>1); Char. #74: (0>1); Char. #75: (0>1); Char. #76: (0>1); Char. #77: (0>1); Char. #83: (0>1); Char. #88: (0>1); Char. #93: (0>1); Char. #97: (0>1); Char. #98: (0>1); Char. #101: (0>1); Char. #107: (0>1); Char. #108: (0>1); Char. #109: (0>1) Char. #112: (0>1); Char. #113: (0>1); Char. #121: (0>1); Char. #127: (0>1); Char. #129: (0>1); Char. #136: (0>1); Char. #160: (0>1).

Support: relative Bremer = 91%

Polynemidae is an undoubting monophyletic group that shares 33 synapomorphies, six of which involve quantitative characters and 28 are qualitative. The family is also strongly supported by a rather high relative Bremer support. Among the synapomorphic qualitative characters are: presence of scales on the lateral surface of the maxilla (ch. #18); palatine length lesser than the ectopterygoid in lateral view (ch. #31; Fig. X); autosphenotic not forming the lateral margin of the neurocranium in dorsal view (ch. #35; Fig. X); pectoral-fin rays unbranched (ch. #42); ventral pectoral-fin soft rays transformed into tactile and gustatory filaments (ch. #43; Fig. X); pectoral radial 3 articulating with pectoral radials 2 and 4 (ch. #48; Fig. X); pectoral radial 3 articulating with the coracoid (ch. #49; Fig. X); coracoid with posteroventral process (ch. #52; Fig. X); *segmentum mandibularis* of the *adductor mandibulae* restricted to the posterior portion of the lower jaw, *i.e.* located posteriorly to the attachment of the buccopalatal ligaments onto the maxilla (ch. #74; Fig. X); preangular tendon not reaching the ventral margin of the angulo-articular (ch. #75; Fig. X); accessory tendon located laterally to the *segmentum mandibularis* of the *adductor mandibulae* (ch. #76); intersegmental aponeurosis bifurcated on its dorsal portion, in which the anterior region of the branched portion corresponds to the transverse tendon whereas the posterior region includes the mandibular and meckelian tendons (ch. #77; Fig. X); *pars temporalis* of the *levator arcus palatini* medial to the *segmentum facialis* of the *adductor mandibulae* (ch. #83; Fig. X); *adductor operculi* with a mixed origin from the neurocranium (ch. #88; Fig. X); *adductor* and *abductor* pectoral muscles entirely divided into two independent segments: a *segmentum radialis* attaching onto the pectoral-fin rays and a *segmentum filamentaris* onto the pectoral filaments (ch. #93; Fig. X); *abductor profundus radialis* originating from the third pectoral radial (ch. #97); *abductor profundus* and *arrector ventralis* originating from the scapula (ch. #98 and #101, respectively); *adductor superficialis radialis* with a mixed origin (ch. #107); *adductor superficialis radialis* arising from the cleithrum and scapula (ch. #108); *adductor medialis radialis* undifferentiated from the *adductor profundus radialis* (ch. #109); *arrector dorsalis* and *adductor radialis* sharing fibers with the *adductor profundus* of the *segmentum radialis* (ch. #112 and #113, respectively); RLA-OP merging with the second spinal nerve and innervating the pectoral filaments (ch. #121; Fig. X); *levatores externi I* and *II* and *levator posterior* originating musculously from the neurocranium (ch. #127 and #129, respectively); posterior fibers of the *transversus dorsalis III* reaching pharyngobranchial 4

(ch. #136); and the lateroventral portion of the *epaxialis* with anterior expanse reaching the neurocranium (ch. #160).

Kang *et al.* (2017) listed several putative synapomorphies for Polynemidae, but without providing an explicit phylogenetic analysis for the group. Moreover, the authors contradict themselves in several passages of the text as to the diagnostic nature of the discussed characters. They mentioned in several passages the existence of 19 synapomorphies for the family (pp. 29, 35, and 36), but indicated that six of them are shared with sciaenids (their characters 3, 5, 8, 10, 16, and 19; p. 36) and stated, in the last sentence of the paper, that the monophyly of Polynemidae is "directly supported by 13 additional synapomorphies" (p. 39). Despite these confusing statements, I can only understand that Kang et al. (2017) are actually proposing six synapomorphies supporting the sister-group relationship between Sciaenidae and Polynemidae and only 13 synapomorphies for the latter family. Among the 13 supposedly synapomorphic characters for polynemids, the authors highlight four that would be unique to the family: (i) the presence of an ossification of the cephalic laterosensory canal extending from the extrascapular (= supratemporal in their study), (ii) pectoral radial 3 (= third actinost in their study) not supporting any pectoral-fin ray, (iii) the *pars malaris* of the *adductor mandibulae* (= A1 in their study) divided into a medial *retromalaris* (= A1α in their study) and a lateral *promalaris* (= A1β in their study), (iv) *obliquus inferioris* of the *hypaxialis* in between the second postcleithrum and the coracoid posteroventral process.

The first character is, in fact, present in all polynemid species analyzed herein. Nevertheless the original character description is a bit imprecise as the referred bone correspond to an autogenous ossification of the anterodorsal portion of the supratemporal canal of the cephalic laterosensory system itself, rather than a bone bearing a sensory canal as stated by the authors (M. Pastana*, pers comm.*; Figs. 5, 11). The presence of the ossification might indicate a synapomorphic character for polynemids, but it requires further investigations about the homology of the cephalic sensory canals. The second character is refused as *Pentanemus* have the dorsal region of the pectoral radial 3 articulating with the ventralmost pectoral-fin rays (Fig. 13B). In our analysis, two states involving the third pectoral radial characteristic that are recovered as synapomorphic for Polynemidae: its

articulation with the adjacent radials (2 and 4; ch. #48; Figs. 12, 13B, 14) and with the coracoid (ch. #49; Figs. 12, 13B, 14). The character number three was also not recovered as a synapomorphic for Polynemidae in our analysis, as the whole subdivision of the *promalaris* into *promalaris* and *retromalaris* is shared with sciaenids. Based on the difference in the origin of the *malaris* in polynemids and sciaenids, Kang et al. (2017) rejected a priori the hypothesis of homology of the subdivision of the *malaris*. Such a conclusion is unjustified because the differences in the origin of the *promalaris* in polynemids and sciaenids do not cancel their shared similarity in the complete subdivision of the *malaris*. What is indeed unique to polynemids and synapomorphic for the family is the lateral aponeurotic origin of the *promalaris* on the preopercle (vs. *promalaris* with musculous origin lying medial relative to the origin of the *retromalaris* in sciaenids; ch. #60 and #61; Figs. 3-9 – Chap. 1). Finally, the fourth character is corroborated but, again, the synapomorphic characteristic recovered herein is different. Kang et al. (2017) stated that the fibers from the *hypaxialis* muscle in between postcleithrum 2 and the posteroventral process of the coracoid are the morphological trait shared by all polynemids. However, the pectoral girdle is normally engulfed by axial musculature that attaches onto several bony elements of the girdle, such as cleithrum and coracoid, which normally occurs in taxa outside Polynemidae (Winterbottom, 1974a). What happens in Polynemidae is that the tendon of the *hypaxialis* that attaches onto the medial face of the ventral portion of the coracoid ossifies and thus forms the posteroventral process, which is, in turn, a synapomorphy for the family in our analysis (ch. #52; Figs. 12B, 13B, 14).

From the remaining 15 characters of Kang *et al.* (2017), only three were herein corroborated as synapomorphic for polynemids: the palatine smaller than the ectopterygoid in lateral view (ch. #31; Figs. 12A, 13A – Chap. 1) , coracoid with a posteroventral process (ch. #52; Figs. 12B, 13B, 14), and the pectoral musculature divided into *segmenta radialis* and *filamentaris* (ch. #93; Figs. 17-23B – Chap. 1). Kang (2017) further pointed as a new synapomorphy for the family the *levator arcus palatini* divided into subsections anterior and posterior. This vague description does not provide the information necessary to identify such divisions. The *levator arcus palatini* of the analyzed polynemids, *Cynoscion* and *Holocentrus* is actually differentiated (not divided) into *partes temporalis* and *primordialis*, which are

placed respectively posterior and anterior and might represent the supposed subdivision documented by the authors. Yet, this differentiation is clearly not a synapomorphy for Polynemidae, as it is shared with the two outgroups. Moreover, the *pars primordialis* of the *levator arcus palatini* of threadfins has a further differentiation into subsections *interna* and *externa* and this condition is shared with *Cynoscion* (Figs. 10-13 – Chap. 1).

Clade B (TNT clade 28) = new, unnamed: *Eleutheronema tetradactylum, Eleutheronema tridactylum, Filimanus similis, Filimanus xanthonema, Galeoides decadactylus*, *Leptomelanosoma indicum*, *Parapolynemus verekeri*, *Polydactylus approximans*, *Polydactylus microstomus*, *Polydactylus octonemus*, *Polydactylus oligodon*, *Polydactylus opercularis*, *Polydactylus plebeius*, *Polydactylus sexfilis, Polydactylus sextarius*, *Polydactylus virginicus*, *Polynemus multifilis*, *Polynemus paradiseus.*

Synapomorphies: Char. #3: (15>12-13); Char. #47: (0>1).

Support: relative Bremer = 34%

Clade B includes all polynemids except *Pentanemus* and is supported by two synapomorphies: reduction to 12-13 soft rays on the second dorsal fin (ch. #3) and presence of foramina on the surface of pectoral radial 4 (ch. #47; Fig. 12; Fig. 23A – Chap. 1). Existence of Clade B is a new hypothesis for polynemids since it was not recovered by any previous analysis. *Pentanemus* is contrastingly grouped with *Polynemus* and *Parapolynemus* in the hypothesis of Kang (2017) and with *Filimanus* in the topology of Feltes (1986).

Clade C (TNT clade 27) = new, unnamed: *Eleutheronema tetradactylum, Eleutheronema tridactylum, Galeoides decadactylus*, *Leptomelanosoma indicum*, *Parapolynemus verekeri*, *Polydactylus approximans*, *Polydactylus microstomus*, *Polydactylus octonemus*, *Polydactylus oligodon*, *Polydactylus opercularis*, *Polydactylus plebeius*, *Polydactylus sexfilis, Polydactylus sextarius*, *Polydactylus virginicus*, *Polynemus multifilis*, *Polynemus paradiseus.*

Synapomorphies: Char. #14: (1>0); Char. #15: (0>1); Char. #46: (0>1); Char. #78: (1>0); Char. #84: (0>1); Char. #86: (0>1); Char. #125: (1>0); Char. #161: (1>0).

Support: relative Bremer = 21%

Clade C clusters all polynemid genera except *Pentanemus* and *Filimanus*. The clade is supported by eight synapomorphies: absence of lateral line on the midportion of the caudal fin (ch. #14); the presence of a ramus of the lateral line on the dorsal region of the lower lobe of the caudal fin (ch. #15); presence of foramina on the coracoid (ch. #46; Fig. 12); transverse tendon (anterior arm of the intersegmental aponeurosis) posteriorly located relative to the *retromalaris* fibers (ch. #78; Fig. 4, 5B – Chap. 1); *pars primordialis* of the *levator arcus palatini* originating from pterosphenoid and frontal (in addition to the usual origin from the hyomandibula and autosphenotic) (ch. #84); *partes primordialis interna* and *externa* of the *levator arcus palatini* not sharing fibers (ch. #86); tendinous insertion of *levator externus I* not very developed, being shorter than half of the fibers length (ch. #125; Fig. 27B – Chap. 1); fibers of the ventrolateral expanse of the *epaxialis* on the neurocranium restricted to the basioccipital, rather than reaching the prootic as seen in other polynemids (ch. #161).

Filimanus is the sister group to clade C, which is not recovered by the past phylogenies. In previous hypotheses, *Filimanus* is either included in a large lineage with *Eleutheronema*, *Galeoides*, *Leptomelanosoma*, and *Polydactylus* (Kang, 2017) or grouped with *Pentanemus* (Feltes, 1986). Moreover, *Filimanus* and *Pentanemus* have a straight lateral-line pattern on the caudal fin whereas other polynemids have a distinct pattern (except *Polynemus*). Kang *et al.* (2017) reported the same four lateral-line patterns herein identified (ch. #13, #14, and #15) but pointed out that the plesiomorphic state for Polynemidae would still be unknown until a phylogenetic analysis of the family. In our analysis, the plesiomorphic condition is exactly the straight line pattern seen in *Filimanus* and *Pentanemus*.

Clade D (TNT clade 26) = new, unnamed: *Eleutheronema tetradactylum, Eleutheronema tridactylum*, *Polydactylus opercularis*, *Polydactylus plebeius*, *Polydactylus sexfilis*.

Synapomorphies: Char. #27: (0>1); Char. #134: (0>1); Char. #157: (1>0).

Support: relative Bremer = 35%

Clade D groups three species of *Polydactylus* – *P. opercularis, P. plebeius,* and *P. sexfilis* – and *Eleutheronema*. These taxa share three synapomorphies that include infraorbitals with a pointed posterior margin (ch. #27; paralleled in *Pentanemus;* Fig. 7A), *transversi dorsales II* and *III* sharing fibers (ch. #134; paralleled in clade O; Fig. 28A – Chap. 1), and the posterior section of the *transversus ventralis V* larger than the anterior counterpart (ch. #157; paralleled in clade J and L; Fig. 32 – Chap. 1).

Clade D is not recovered in any previous analysis, although a similar group is present in the analysis of Kang (2017: clade G1). In light of the present hypothesis, *Eleutheronema* could be expanded for clade D, embracing these three species of *Polydactylus*.

Clade E (TNT clade 25) = new, unnamed: *Eleutheronema tetradactylum, Eleutheronema tridactylum*, *Polydactylus plebeius*, *Polydactylus sexfilis*.

Synapomorphies: Char. #11: (31-35>25-29); Char. #63: (1>0); Char. #75: (1>0); Char. #114: (1>0); Char. #150: (1>0).

Support: relative Bremer = 14%

Clade E includes *Polydactylus plebeius*, *P. sexfilis*, and *Eleutheronema*. Two synapomorphies are optimized for the group: the reduction of gill rakers (ch. #11); *promalaris* fibers completely ventral to the posterodorsal margin of the *rictalis* (ch. #63; paralleled in Clade L and in *ParapolynemusI;* Figs. 6, 9 – Chap. 1); preangular ligament attaching onto the ventral margin of the angulo-articular (ch. #75; reversion from Clade A; Fig. 6 – Chap. 1); *adductor superficialis filamentaris* originating far from the Baudelot ligament (ch. #114; Fig. 20A – Chap. 1); and posterodorsal and anteroventral sections of the *pharyngoclavicularis internus* sharing fibers (ch. #150; Fig. 32 – Chap. 1). Again, Clade E was not recovered in the past phylogenetic analyses.

Clade F (TNT clade 24) = new, unnamed: *Eleutheronema tetradactylum, Eleutheronema tridactylum*, *Polydactylus sexfilis*.

Synapomorphies: Char. #10: (12>13); Char. #31: (1>0); Char. #86: (1>0); Char. #118: (1>0).

Support: relative Bremer = 14%

Clade F shows *Polydactylus sexfilis* as sister group to a monophyletic *Eleutheronema*. The clade is diagnosed by four synapomorphies: an increase of ventral procurrent rays (ch. #10); palatine equal to/greater than the ectopterygoid length in lateral view (ch. #31; reversion of clade A; Fig. 12B – Chap. 1); *partes primordialis externa* and *interna* of the *levator arcus palatini* sharing fibers (ch. #86; reversion of clade C and paralleled in *Polynemus*); and *adductor medialis filamentaris* undifferentiated into *partes endomedialis* and *ectomedialis* (ch. #118; paralleled in *Galeoides*). Clade F was not recovered in the past phylogenies.

Clade G (TNT clade 33) = new, unnamed: *Galeoides decadactylus*, *Leptomelanosoma indicum*, *Parapolynemus verekeri*, *Polydactylus approximans*, *Polydactylus microstomus*, *Polydactylus octonemus*, *Polydactylus oligodon*, *Polydactylus sextarius*, *Polydactylus virginicus*, *Polynemus multifilis*, *Polynemus paradiseus.*

Synapomorphies: Char. #106: (0>1).

Support: relative Bremer = 83%

Clade G is sister group to Clade D (*Eleutheronema*, *Polydactylus opercularis*, *P. plebeius*, and *P. sexfilis*). Clade G shares one synapomorphy: *protractor pectoralis* originating from the *epaxialis* tendon, which in turn attaches on the pterotic spine. Clade G is a completely new proposal since it is not present in neither of the past studies of Polynemidae.

Clade H (TNT clade 38) = *Polydactylus sensu stricto*: *Polydactylus approximans*, *Polydactylus octonemus*, *Polydactylus oligodon*, *Polydactylus virginicus*.

Synapomorphies: Char. #4: (15>16); Char. #5: (6>7); Char. #7: (11>13); Char. #13: (0>1); Char. #141: (0>1).

Support: relative Bremer = 73%

This clade includes four species of *Polydactylus*, including its type species *P. virginicus*. Clade H is herein supported by five synapomorphies: increase in the number of pectoral-fin soft rays, pectoral filaments, and anal-fin soft rays (ch. #4, #5, and #7); presence of lateral line on the ventral region of the upper lobe of the caudal fin (ch. #13; paralleled in *Galeoides*); and *adductor branchialis IV* differentiated into anterior and posterior sections (ch. #141; paralleled in *Filimanus*; Fig. 30 – Chap. 1).

This monophyletic group, herein provisionally termed *Polydactylus sensu stricto*, was also recovered in the analysis of (Kang, 2017: clade F2), although with an internal resolution distinct from that obtained in the present study.

Clade I (TNT clade 37) = new, unnamed: *Polydactylus approximans*, *Polydactylus octonemus*, *Polydactylus virginicus*.

Synapomorphies: Char. #123: (0>1).

Support: relative Bremer = 46%

Clade I clusters all *Polydactylus sensu stricto* except *P. oligodon*. This group is supported by a single synapomorphy, the *levator externus I* differentiated into anterior and posterior sections (Fig. 27B – Chap. 1). This character state is paralleled in clade O.

Clade J (TNT clade 36) = new, unnamed: *Polydactylus approximans, Polydactylus virginicus*.

Synapomorphies: Char. #157: (1>0).

Support: relative Bremer = 46%

Clade J is composed by *Polydactylus approximans* and *P. virginicus*, which share one synapomorphy regarding the relative lengths of each section of the *transversus ventralis V*. In these species, the posterior section of the *transversus ventralis V* is larger than its anterior counterpart (Fig. 32 – Chap. 1. This character is paralleled in clades D and L.

Clade K (TNT clade 32) = new, unnamed: *Galeoides decadactylus*, *Leptomelanosoma indicum*, *Parapolynemus verekeri*, *Polydactylus microstomus*, *Polydactylus sextarius*, *Polynemus multifilis*, *Polynemus paradiseus.*

Synapomorphies: Char. #4: (15>14); Char. #72: (1>0); Char. #98: (1>0); Char. #130: (0>1).

Support: relative Bremer = 31%

This clade is the sister group to the *Polydactylus sensu stricto*. Species within Clade K share four synapomorphies: reduction of pectoral-fin soft rays (ch. #4); *partes coronalis* and *mentalis* of the *segmentum mandibularis* of the *adductor mandibulae* sharing fibers anteriorly (ch. #72; Fig. 9B – Chap. 1); origin of the *abductor profundus* of the *segmentum radialis* restricted to the cleithrum, coracoid, and pectoral radial 3 (not arising from the scapula) (ch. #98; reversion of clade A); *levator posterior* differentiated into a posterolateral and an anteromedial portion (ch. #130; Fig. 27B – Chap. 1). Clade K was not recovered in any previous topologies and therefore is a new proposal within Polynemidae.

The only difference between the adopted phylogenetic tree (Fig. 17) and the one resulting based on prior weight only (Fig. 16) is the shifted position of *Galeoides* and *Polydactylus sextarius*. Due to this change, ch. #4 (15>14) and #130 (0>1) are no longer optimized as synapomorphies of Clade K in the EW tree. On the other hand, two new synapomorphies for clade K are recovered: posteroventral fibers of the *segmentum mandibularis* of the *adductor mandibulae* associated with the buccopalatal membrane (ch.

#73: 0>1) and *adductor hyomandibulae* inserting on the anterolateral surface of the ectopterygoid (ch. #82: 0>1).

Clade L (TNT clade 31) = new, unnamed: *Galeoides decadactylus*, *Polydactylus microstomus*, *Polydactylus sextarius***.**

Synapomorphies: Char. #0: (61-62>42-44); Char. #37: (1>0); Char. #63: (1>0); Char. #107: (1>0); Char. #144: (0>1); Char. #157: (1>0).

Support: relative Bremer = 24%

Clade L is a monophyletic group composed by *Galeoides*, *Polydactylus microstomus, and P. sextarius*. The group is supported by six synapomorphies: considerable reduction of lateral line scales (ch. #0); vomer without teeth (ch. #37; paralleled in *Parapolynemus*); *promalaris* fibers completely ventral to the posterodorsal margin of the *rictalis* (ch. #63; paralleled in Clade E and in *Parapolynemus*), *adductor superficialis radialis* originating purely musculously from the medial surface of the pectoral girdle (ch. #107; reversion of clade A); *interbranchiales abductores II* and *III* with a dorsal expansion onto epibranchials 2 and 3, respectively (ch. #144; Fig. 28B – Chap. 1); and posterior section of the *transversus ventralis V* larger than the anterior counterpart (ch. #157; paralleled in Clades D and J). From these synapomorphic characters, the most distinctive one is the dorsal expanse of the *interbranchiales abductores II* and *III*. This configuration was not seen in any of the analyzed taxa and is considered herein a rather rare condition for clade L.

Monophyly of Clade L was also recovered by Kang (2017). In their analysis, these species are grouped based on two unknown synapomorphies (their clade D3). In Feltes (1986) *Galeoides* is nested within *Polydactylus*, but as his tree includes only genera as terminal taxa, it is unclear which species of *Polydactylus* were chosen as representative of the genus in the analysis.

Clade M (TNT clade 39) = new, unnamed: *Polydactylus microstomus, Polydactylus sextarius*.

Synapomorphies: Char. #7: (11>12); Char. #11: (31>29); Char. #16: (0>1); Char. #42: (0>1); Char. #65: (1>0).

Support: relative Bremer = 21%

Clade M represents the sister-group relationship between *Polydactylus microstomus* and *P. sextarius*. The clade is well supported by five synapomorphies: increase of anal-fin soft rays (ch. #7); reduction of gill rakers (ch. #11); black spot posterodorsal to the opercle (ch. #16); presence of branched pectoral-fin rays (ch. #42; reversion of clade A; Fig. 4); *partes promalaris interna* and *externa* with a common insertion on the maxilla (*i.e.* there is no hiatus between insertions as most of polynemids have; ch. #65; Fig. 9B – Chap. 1).

Although Kang (2017) also obtained a group corresponding to our Clade L, its internal relationships differs from ours, with *Galeoides* allocated closer to *P. sextarius* than to *P. microstomus*. Our analysis with EW (Fig. 16) alternatively grouped *Galeoides* with *P. microstomus* based on the following synapomorphies: reduction of lateral line scales (ch. #0: 44>42); reduction of pectoral-fin rays (ch. #4: 14-15>13); palatine equal to/greater than ectopterygoid (ch. #31: 1>0; a reversal of the synapomorphy for Polynemidae that is also paralleled in Clade F); *transversus dorsales II* and *III* in contact, with no gap of connective tissue between muscles (ch. #135: 1>0; paralleled in *Filimanus*); *pharyngoclavicularis internus* with some fibers inserting medially to *pharyngoclavicularis externus* (ch. #151: 1>0); *transversus ventralis IV* with a multipennate surface (ch. #154: 0>1). *Polydactylus malagasyensis, P. mullani,* and *P. persicus*, which were not included in the present study due to their rarity in collections, possess some of the synapomorphies herein proposed for *P. microstomus* and *P. sextarius*: the black spot posterodorsal to the opercle and the branched pectoral-fin rays (Motomura and Iwatsuki, 2001; Motomura, 2004). They also have the vomer without teeth, which is also a synapomorphic character for clade L (Motomura and Iwatsuki, 2001; Motomura, 2004). These evidences indicate that *Polydactylus malagasyensis, P. mullani,* and *P. persicus* possibly belong to Clade M.

Clade N (TNT clade 34) = new, unnamed: *Leptomelanosoma indicum*, *Parapolynemus verekeri*, *Polynemus multifilis*, *Polynemus paradiseus.*

Synapomorphies: Char. #25: (0>1); Char. #36: (0>1); Char. #41: (0>1); Char. #81: (0>2).

Support: relative Bremer = 24%

Clade N is the sister group of Clade L and includes *Leptomelanosoma*, *Parapolynemus*, and *Polynemus*. These genera share four synapomorphies, including the infraorbitals partially following the eyeball circumference (ch. #25; Fig. 7B); autosphenotic articulating with the parietal in dorsal view (ch. #36; Fig. 10C); thick parasphenoid, where its width is more than half of the eye capsule height (ch. #41; Fig. 5B); anterior fibers of the *pars pterygo-palatina* of the *adductor hyomandibulae* with a multipinnate aspect (ch. #81; Fig. 12A – Chap. 1). In the EW topology (Fig. 16), an extra synapomorphy for clade N is the *abductor profundus* visible in medial view through the cleithrum-coracoid fenestra (ch. #96: 1>0).

Clade N is a new proposal within Polynemidae since it was not recovered by previous analyses. *Leptomelanosoma* is missing from the analysis of Feltes (1986). Kang (2017), in turn, placed *Leptomelanosoma* as sister group to their clade *Polydactylus opercularis* + *Eleutheronema*, whereas *Parapolynemus* and *Polynemus* are grouped with *Pentanemus*. In our analysis *Pentanemus* is far removed from the clade *Parapolynemus* + *Polynemus*.

Clade O (TNT clade 35) = new, unnamed: *Parapolynemus verekeri*, *Polynemus multifilis*, *Polynemus paradiseus.*

Synapomorphies: Char. #26: (1>0); Char. #38: (1>0); Char. #45: (0>1); Char. #46: (1>0); Char. #47: (1>0); Char. #50: (0>1); Char. #51: (0>1); Char. #103: (0>1); Char. #104: (0>1); Char. #115: (0>1); Char. #117: (0>1); Char. #123: (0>1); Char. #132: (0>1); Char. #134: (0>1); Char. #147: (0>1); Char. #152: (0>1); Char. #153: (0>1).

Support: relative Bremer = 60%

Clade O is a highly stable clade of our analysis, regardless the search parameters used (EW or IW with different values of *k*). There are 17 synapomorphies supporting the grouping of *Parapolynemus* and *Polynemus*: absence of subocular shelf on the third infraorbital (ch. #26); absence of basisphenoid (ch. #38); longest pectoral filament longer than body length (ch. #45); coracoid with no foramina on its surface (ch. #46; reversion of clade C; Fig. 14A, B); absence of any kind of foramina on pectoral radial 4 surface (ch. #47; reversion of clade B; Fig. 14A, B); pectoral radial 3 with a medial projection (mushroom-shaped) from where the last bundle of fibers of the *adductor profundus filamentaris* arise (ch. #50; Fig. 14C); pectoral radial 3 articulating with the dorsalmost pectoral filament (ch. #51; Fig. 14); *segmentum filamentaris* well developed posterodorsally occupying most of the area of the lateral region of the pectoral girdle, reaching almost half or more of the horizontal arm of the cleithrum (ch. #103; Fig.18, 22 – Chap. 1); bundles of fibers of *abductores superficialis* and *profundus filamentaris* and *adductor medialis filamentaris* well developed and isolated from each other (ch. #104 and #115, respectively; Fig.18, 22 – Chap. 1); *adductor medialis filamentaris* originating from the coracoid and cleithrum (ch. #117); *levator externus I* differentiated into anterior and posterior sections (ch. #123; paralleled in clade I; Fig. 27B – Chap. 1); anterior portion of the *transversus dorsalis II* restricted to the anterior portion of its posterior counterpart (ch. #132; Fig. 28A, 29A – Chap. 1); *transversus dorsales II* and *III* sharing fibers (ch. #134; paralleled in clade D; Fig. 28A – Chap. 1); *rectus communis* with a tendinous origin (ch. #147); posterodorsal section of the *pharyngoclavicularis internus* originating tendinously (ch. #152; paralleled in *Filimanus* and in *Galeoides*); posterodorsal section of the *pharyngoclavicularis internus* differentiated into subsections anterior and posterior (ch. #153; paralleled in *Filimanus*).

Monophyly of clade O is very consistent and has been recovered by the past phylogenetic hypotheses. Feltes (1986) presented 11 synapomorphies for the clade *Parapolynemus* + *Polynemus*, which are few serrations on the posterior margin of the preopercle; the shape of the pterosphenoid; the shape of the hypurals; absence of basisphenoid; the size of the supraoccipital and parietal crests; the oblique orientation of the lateral ethmoid; six reduced infraorbitals; indistinct borders between the metapterygoid and hyomandibular; the shape of postcleithrum 1; the relative position of the scapula in

comparison to the cleithrum; length of the supracleithrum in comparison to the coracoid length. Among these, only the absence of basisphenoid is corroborated by the present study. Serrations on the posterior margin of the preopercle are absent in *Parapolynemus*; the limits between the metapterygoid and hyomandibula are clear enough to be distinguished (Fig. 12A – Chap. 1). The remaining characters of Feltes (1986) involve delimitations of character states that proved to be ambiguous and were, therefore, excluded from our analysis. Kang (2017) also recovered the sister-group relationship between *Parapolynemus* and *Polynemus*, but the synapomorphies supporting this clade are inaccessible.

***Eleutheronema* (TNT clade 23):** *Eleutheronema tetradactylum & Eleutheronema tridactylum*.

Synapomorphies: Char. #0: (62>76); Char. #2: (14>15); Char. #4: (15-16>17); Char. #5: (5-6>4); Char. #7: (11>15); Char. #9: (14>15); Char. #10: (13>14); Char. #11: (25-29>13); Char. #24: (1>0); Char. #28: (0>1); Char. #40: (0>1); Char. #58: (0>2); Char. #74: (1>0); Char. #80: (1>0); Char. #88: (1>0); Char. #119: (0>1); Char. #136: (1>0).

Support: relative Bremer = 46%

Eleutheronema has been recovered as a monophyletic group by both previous analyses. This genus is phylogenetically diagnosed by 17 synapomorphies and several of them are unique among polynemids. Although the most parsimonious tree of the analysis of Feltes (1986) allocated *Eleutheronema* as the sister group of all polynemids except *Polynemus* and *Parapolynemus*, the author is uncertain of the polarizations of some pertinent characters and discussed the possibility of alternative allocations of that genus, including as the basalmost lineage of the family. None of these alternative hypotheses are corroborated by our analysis.

***Filimanus* (TNT clade 30):** *Filimanus similis & Filimanus xanthonema*.

Synapomorphies: Char. #0: (54-62>49); Char. #34: (0>1); Char. #39: (0>1); Char. #81: (0>1); Char. #82: (0>1); Char. #90: (1>0); Char. #135: (1>0); Char. #141: (0>1); Char. #152: (0>1); Char. #153: (0>1).

Support: relative Bremer = 92%

Filimanus has invariably been recovered as a monophyletic group. Herein, *Filimanus* is supported by ten synapomorphies whereas in the study of Kang (2017) this genus is supported by four unknown synapomorphies.

***Galeoides*:** monotypic – *Galeoides decadactylus*

Autapomorphies: Char. #5: (6>10); Char. #7: (11>7); Char. #13: (0>1); Char. #15: (1>0); Char. #33: (1>0); Char. #34: (0>1); Char. #102: (0>1); Char. #105: (0>1); Char. #108: (1>2); Char. #116: (0>2); Char. #118: (1>0); Char. #133: (1>0); Char. #152: (0>1); Char. #155: (0>1).

Galeoides is a monotypic genus that presents 14 autapomorphies. In the EW topology, the genus exhibits four additional autapomorphies: two supraneurals (ch. #24: 1>0); posteroventral fibers of the *segmentum mandibularis* of the *adductor mandibulae* restricted to the intersegmental aponeurosis (ch. #73: 1>0; a reversal of the synapomorphy for Clade K under EW), *adductor hyomandibulae* not inserting on the anterolateral surface of the ectopterygoid (ch. #82: 1>0; a reversal of the synapomorphy for Clade K under EW), *abductor profundus* visible in medial view through the cleithrum-coracoid fenestra (ch. #96: 1>0; paralleled in clade N under EW).

***Leptomelanosoma*:** monotypic – *Leptomelanosoma indicum*

Autapomorphies: Char. #5: (6>5); Char. #9: (13-14>12); Char. #11: (31>18); Char. #28: (0>1); Char. #34: (0>1); Char. #58: (0>2); Char. #102: (0>1); Char. #108: (1>2); Char. #116: (0>1); Char. #155: (0>1).

Leptomelanosoma is a monotypic genus that has ten autapomorphies.

***Parapolynemus*:** monotypic – *Parapolynemus verekeri*

Autapomorphies: Char. #0: (61-70>57); Char. #3: (13>12); Char. #4: (14>13); Char. #11: (31-33>39); Char. #32: (1>0); Char. #33: (1>0); Char. #37: (1>0); Char. #44: (0>1); Char. #53: (0>1); Char. #63: (1>0); Char. #68: (1>0); Char. #90: (1>0); Char. #91: (1>0); Char. #94: (0>1); Char. #95: (0>1); Char. #100: (0>1); Char. #116: (0>2); Char. #120: (0>1); Char. #126: (0>1); Char. #130: (1>0); Char. #138: (0>1).

Parapolynemus is a rather derived monotypic genus that is phylogenetically diagnosed by 21 autapomorphies

***Pentanemus*:** monotypic – *Pentanemus quinquarius*

Autapomorphies: Char. #0: (54-62>70); Char. #7: (11>29); Char. #9: (13-14>17); Char. #10: (12>14); Char. #11: (31-42>49); Char. #27: (0>1); Char. #99: (1>0); Char. #120: (0>1); Char. #138: (0>1).

Pentanemus is a monotypic genus that has nine autapomorphies

***Polynemus* (TNT clade 40):** *Polynemus multifilis & Polynemus paradiseus*.

Synapomorphies: Char. #0: (61-70>75); Char. #2: (14>15); Char. #3: (13>15); Char. #4: (14>16); Char. #5: (6>7); Char. #6: (3>2); Char. #7: (11>12); Char. #9: (14>17); Char. #10: (13>14); Char. #14: (0>1); Char. #15: (1>0); Char. #58: (0>1); Char. #86: (1>0); Char. #111: (0>1).

Support: relative Bremer = 93%

Polynemus monophyly was always recovered in the past analysis and it was not different in this present study. This genus is well supported by the relative Bremer index of 93% and 14 synapomorphies.

5. CONCLUSIONS

The phylogenetic hypothesis presented herein (Fig. 17) is the most robust cladistic analysis ever done in order to test the intrarelationships of Polynemidae, assembling and describing over one hundred new musculoskeletal characters. The resulting phylogenetic tree of polynemids is fully resolved and includes all polynemid genera currently recognized as valid. From the eight established genera, only *Polydactylus*, which holds almost half of the family diversity, was recovered as non-monophyletic thus corroborating past analyses (Feltes, 1986; Kang, 2017). The remaining three non-monotypic genera (*Eleutheronema, Filimanus,* and *Polynemus*) were recovered as well-supported monophyletic groups, a result that also agrees with previous hypotheses.

The present study indicates the possibility of important taxonomic changes in the family, such as the expansion in the definition some genera and the proposition of a few new supraspecific taxa. However, we reckon that such changes demand a broader sampling of species and should be ideally performed along with a taxonomic revision of the family.

REFERENCES

BETANCUR-R, R. et al. The tree of life and a new classification of bony fishes. **PLOS Currents Tree of Life**, 2013. ISSN 2157-3999.

DATOVO, A.; VARI, R. P. The jaw adductor muscle complex in teleostean fishes: evolution, homologies and revised nomenclature (Osteichthyes: Actinopterygii). **PloS one,** v. 8, n. 4, p. e60846, 2013. ISSN 1932-6203.

DE SYLVA, D. Polynemoidei: development and relationships. In: MOSER, H. G.;RICHARDS, W. J.*, et al* (Ed.). **Ontogeny and systematics of fishes**. Lawrence, Kansas: American Society of Ichthyologists and Herpetologists, v.Special Publication 1, 1984. p.540-541.

ESCAPA, I. H.; CATALANO, S. A. Phylogenetic analysis of Araucariaceae: integrating molecules, morphology, and fossils. **International Journal of Plant Sciences,** v. 174, n. 8, p. 1153-1170, 2013. ISSN 1058-5893.

FARRIS, J. The logical basis of phylogenetic analysis. In: PLATNICK N e VA., F. (Ed.). **Advances in Cladistics, 2. Proceedings of the second meeting of the Willi Hennig Society**. New York: Columbia University Press, 1983. p.7-36.

FELTES, R. M. **A systematic revision of the Polynemidae (pisces)**. 1986. The Ohio State University

FELTES, R. M. Revision of the polynemid fish genus Filimanus, with the description of two new species. **Copeia**, p. 302-322, 1991. ISSN 0045-8511.

FELTES, R. Polynemidae, Threadfins. In: CARPENTER, K. e NIEM, V. (Ed.). **FAO species identification guide for fishery purposes: the living marine resources of the western central Pacific**. Rome, v.5, 2001. p.3090-3116.

FERRER, J.; WINGERT, J. M.; MALABARBA, L. R. Description of a new species and phylogenetic analysis of the subtribe Cynopoecilina, including continuous characters without discretization (Cyprinodontiformes: Rivulidae). **Zoological Journal of the Linnean Society,** v. 172, n. 4, p. 846-866, 2014. ISSN 0024-4082.

GOLOBOFF, P. A.; FARRIS, J. S. Methods for quick consensus estimation. **Cladistics,** v. 17, n. 1, p. S26-S34, 2001. ISSN 0748-3007.

GOLOBOFF, P. A.; FARRIS, J. S.; NIXON, K. C. TNT, a free program for phylogenetic analysis. **Cladistics,** v. 24, n. 5, p. 774-786, 2008. ISSN 1096-0031.

GOSLINE, W. A. Systematic position and relationships of the percesocine fishes. **Pacific Science,** v. 16, p. 207-217, 1962.

GOSLINE, W. A. The suborders of perciform fishes. **Proceedings of the United States National Museum,** v. 124, 1968.

GOSLINE, W. A. **Functional morphology and classification of teleostean fishes**. Honolulu: University of Hawaii Press, 1971. 208.

HARRINGTON, R. C. et al. Phylogenomic analysis of carangimorph fishes reveals flatfish asymmetry arose in a blink of the evolutionary eye. **BMC evolutionary biology,** v. 16, n. 1, p. 224, 2016. ISSN 1471-2148.

HUGHES, L. C. et al. Comprehensive phylogeny of ray-finned fishes (Actinopterygii) based on transcriptomic and genomic data. **Proceedings of the National Academy of Sciences,** v. 115, n. 24, p. 6249-6254, 2018. ISSN 0027-8424.

JOHNSON, D. G. Percomorph phylogeny: progress and problems. **Bulletin of marine Science,** v. 52, n. 1, p. 3-28, 1993. ISSN 0007-4977.

JOHNSON, D. G.; PATTERSON, C. Percomorph phylogeny: a survey of acanthomorphs and a new proposal. **Bulletin of Marine Science,** v. 52, n. 1, p. 554-626, 1993. ISSN 0007-4977.

KANG, S. **Comparative morphology and phylogenetic relationships of the family Polynemidae (Pisces: Perciformes)**. 2017. Hokkaido University

KANG, S.; IMAMURA, H.; KAWAI, T. Morphological evidence supporting the monophyly of the family Polynemidae (Teleostei: Perciformes) and its sister relationship with Sciaenidae. **Ichthyological Research,** v. 65, n. 1, p. 29-41, 2017. ISSN 1341-8998.

KOCH, N. M.; SOTO, I. M.; RAMÍREZ, M. J. First phylogenetic analysis of the family Neriidae (Diptera), with a study on the issue of scaling continuous characters. **Cladistics,** v. 31, n. 2, p. 142-165, 2014. ISSN 0748-3007.

MOTOMURA, H. **Threadfins of the world (Family Polynemidae): An annotated and illustrated catalogue of polynemid species known to date**. Food & Agriculture Org., 2004. ISBN 9251051283.

MOTOMURA, H.; IWATSUKI, Y. Review of Polydactylus species (Perciformes: Polynemidae) characterized by a large black anterior lateral line spot, with descriptions of two new species. **Ichthyological research,** v. 48, n. 4, p. 337-354, 2001. ISSN 1341-8998.

MOTOMURA, H. et al. Revision of the Indo-West Pacific polynemid fish genus Eleutheronema (Teleostei: Perciformes). **Ichthyological Research,** v. 49, n. 1, p. 47-61, 2001. ISSN 1341-8998.

NEAR, T. J. et al. Phylogeny and tempo of diversification in the superradiation of spiny-rayed fishes. **Proceedings of the national Academy of sciences,** v. 110, n. 31, p. 12738-12743, 2013. ISSN 0027-8424.

ROSEN, D. E. **The relationships and taxonomic position of the halfbeaks, killifishes, silversides, and their relatives**. American Museum of Natural History, 1964.

SANCIANGCO, M. D.; CARPENTER, K. E.; BETANCUR-R, R. Phylogenetic placement of enigmatic percomorph families (Teleostei: Percomorphaceae). **Molecular phylogenetics and evolution,** v. 94, p. 565-576, 2015. ISSN 1055-7903.

SERENO, P. C. Logical basis for morphological characters in phylogenetics. **Cladistics,** v. 23, n. 6, p. 565-587, 2007. ISSN 0748-3007.

SPRINGER, V. G.; JOHNSON, G. D. **Study of the dorsal gill-arch musculature of teleostome fishes, with special reference to the Actinopterygii**. Biological Society of Washington, Smithsonian Institution, 2004.

WILEY, E.; JOHNSON, G. D. A teleost classification based on monophyletic groups. **Origin and phylogenetic interrelationships of teleosts,** v. 1, p. 123-182, 2010.

WINTERBOTTOM, R. A descriptive synonymy of the striated muscles of the Teleostei. **Proceedings of the Academy of Natural Sciences of Philadelphia**, p. 225-317, 1974a. ISSN 0097-3157.

FIGURES

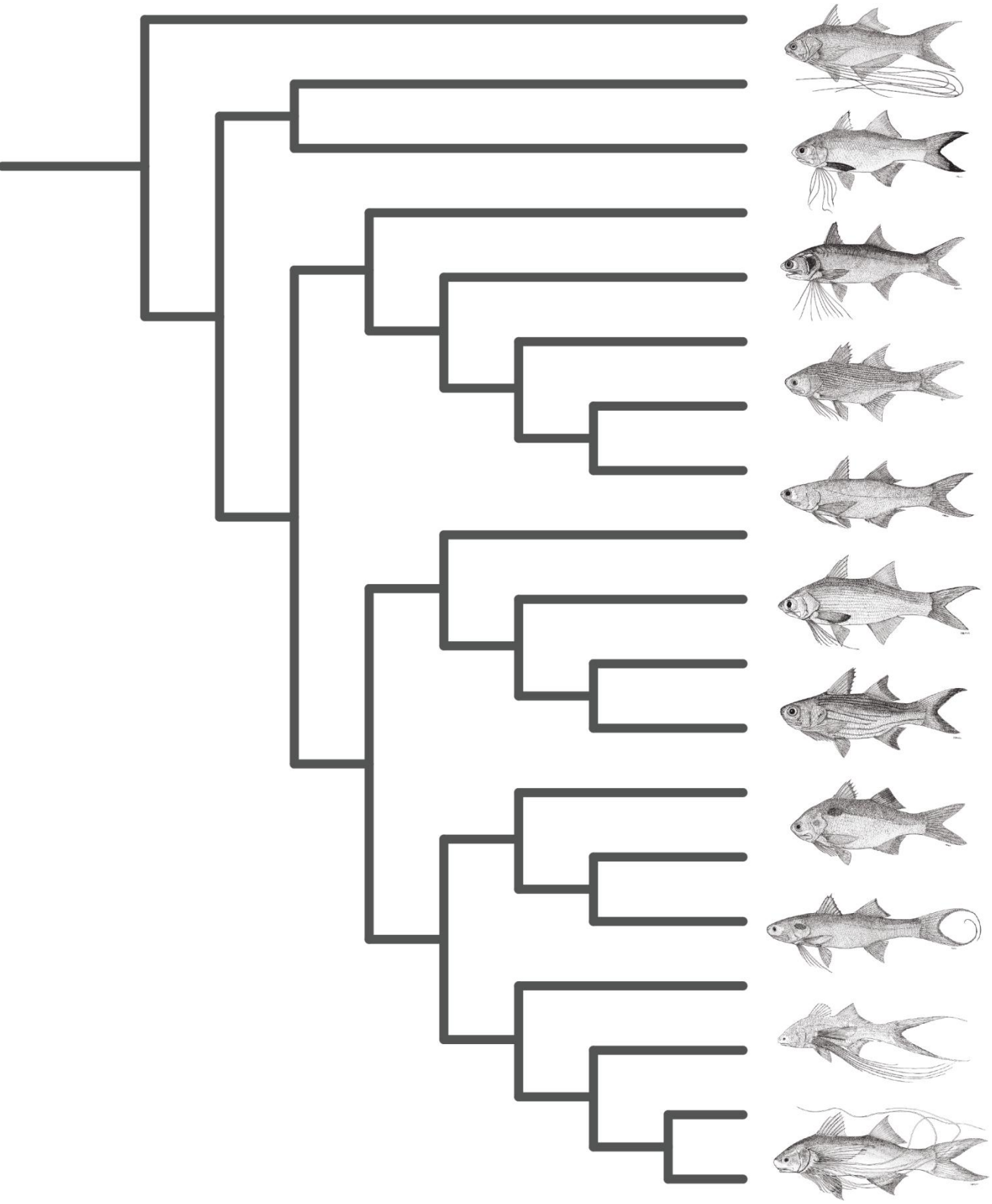

A

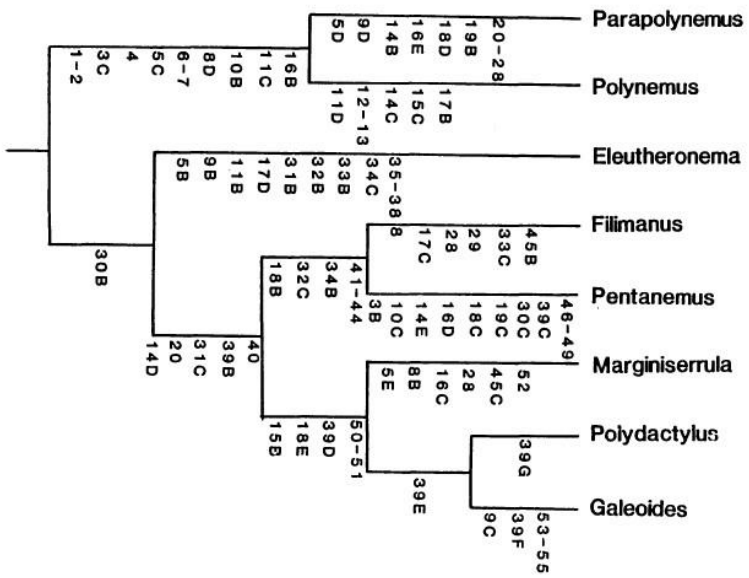

B

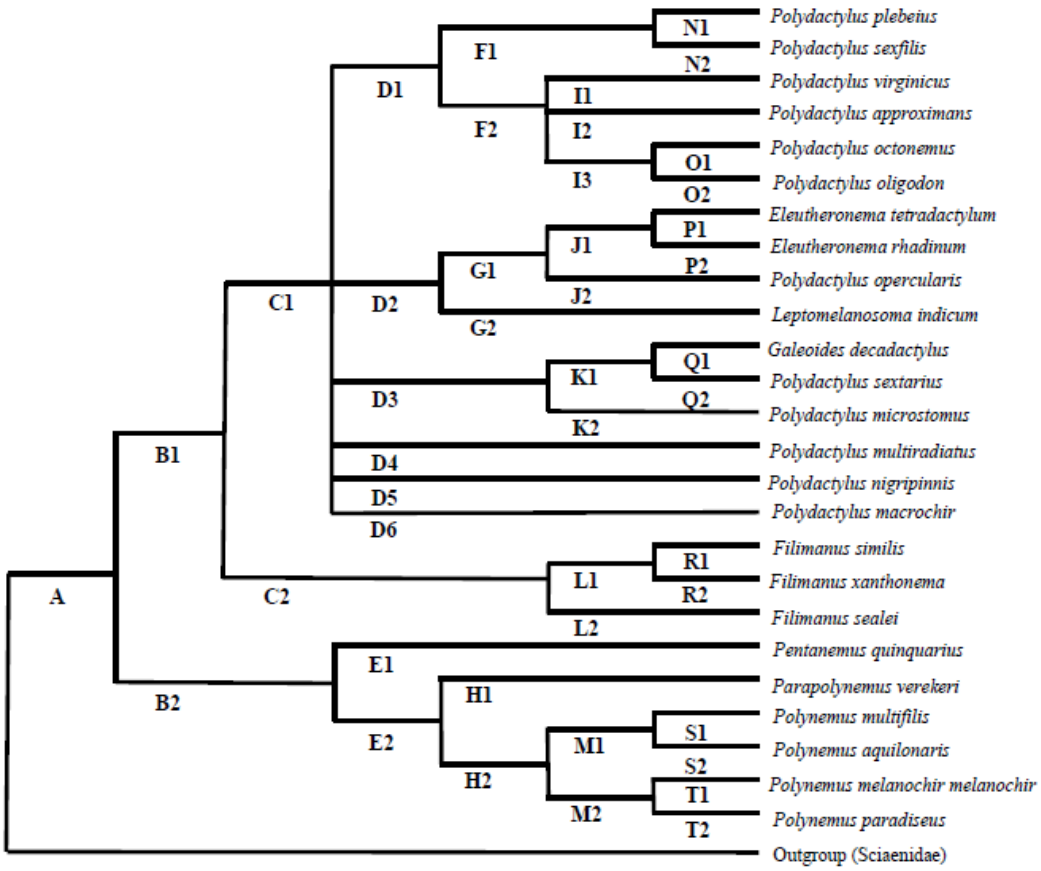

Fig. 1: Hypotheses of the relationships of Polynemidae from morphological characters according to: A) Feltes (1986) – Leptomelanosoma was not sampled – and B) Kang (2017).

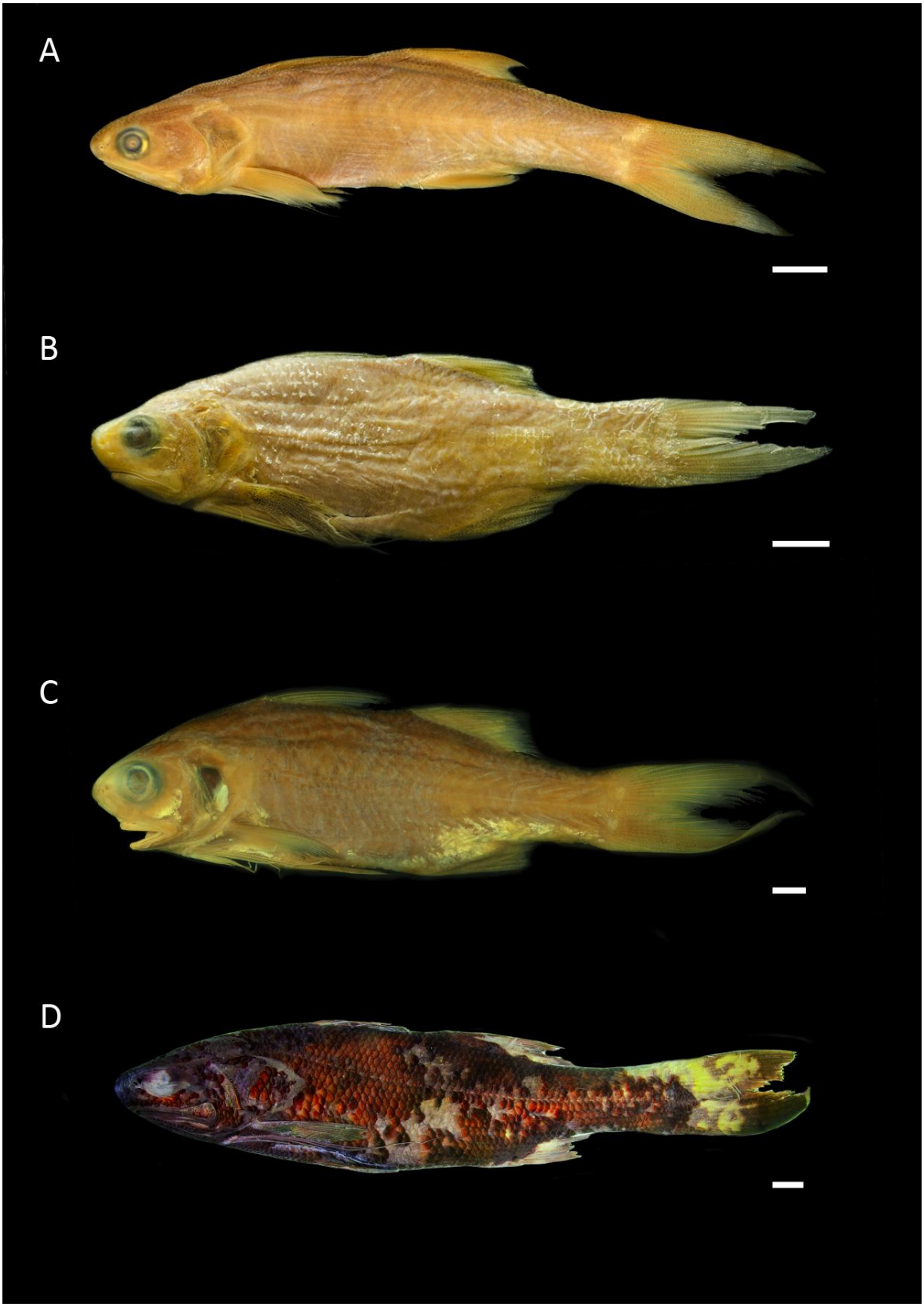

Fig. 2: Lateral view of representative of each Polynemidae genera. A: *Eleutheronema tetradactylum*. B: *Filimanus xanthonema*. C: *Galeoides decadactylus*. D: *Leptomelanosoma indicum*. E: *Parapolynemus verekeri*. F: *Pentanemus quinquarius*. G: *Polydactylus virginicus*. H: *Polynemus paradiseus*. Scale bar: 10 mm.

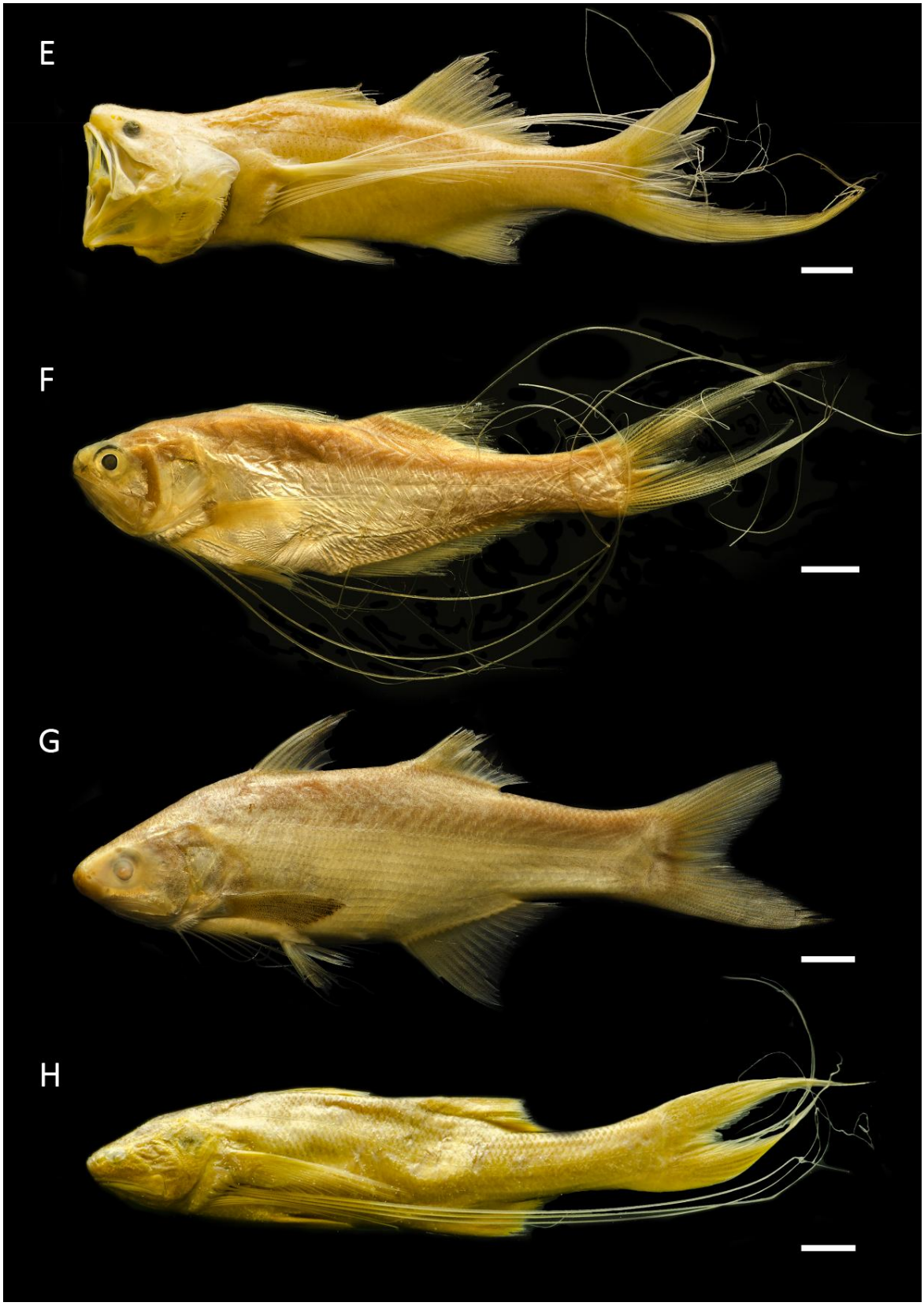

Fig. 2: Continued.

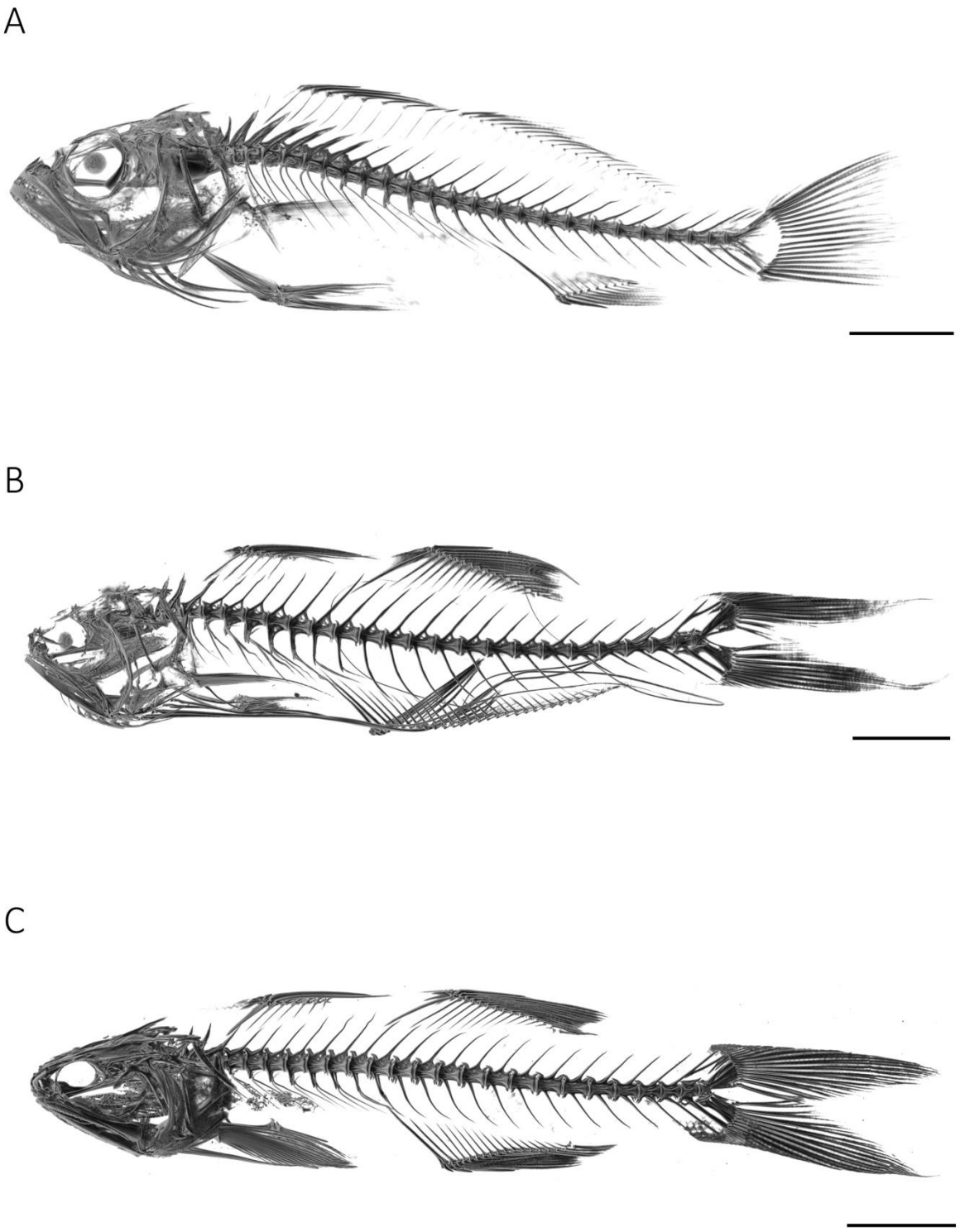

Fig. 3: Lateral view of full body. A: *Cynoscion striatus*. B: *Pentanemus quinquarius*. C: *Eleutheronema tetradactylum*. Scale bar: 15 mm.

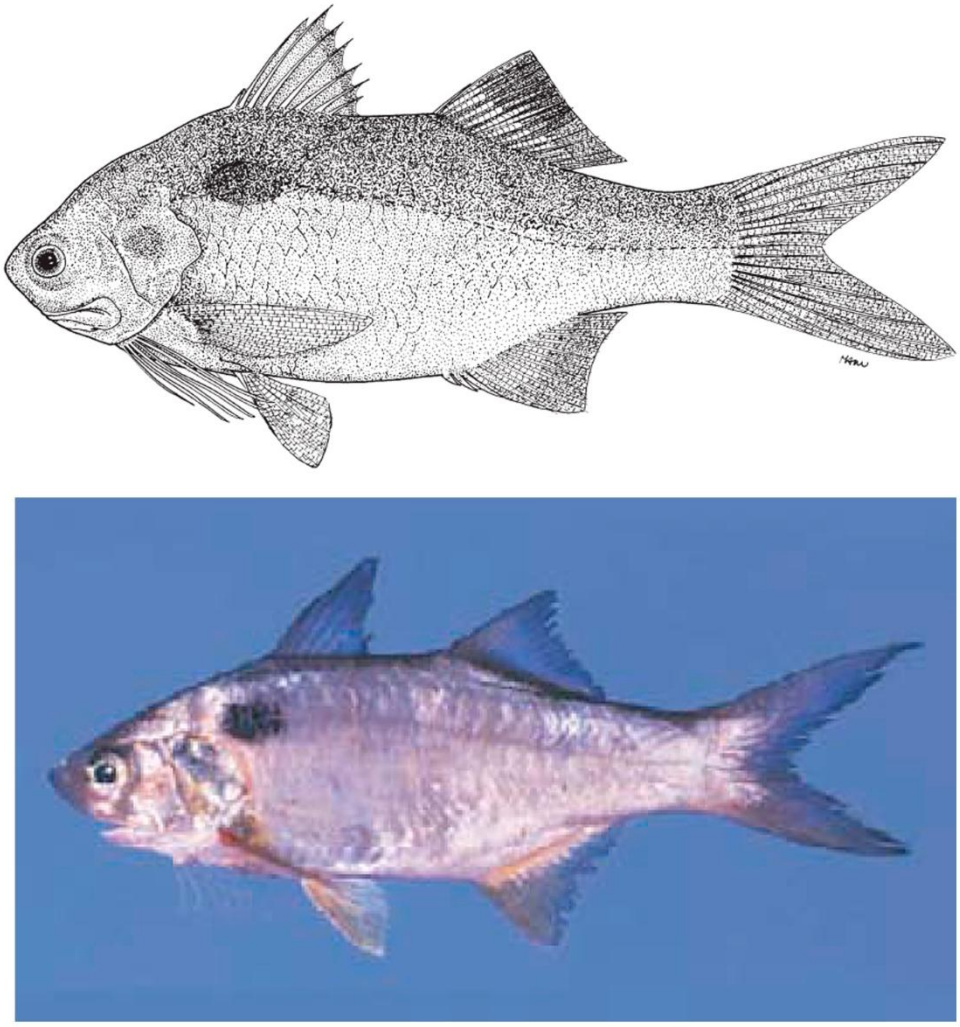

Fig. 4: Lateral view of full body. *Polydactylus sextarius*. 164 mm SL, Miyazaki, Japan (H. Motomura). Adapted from Motomura (2004).

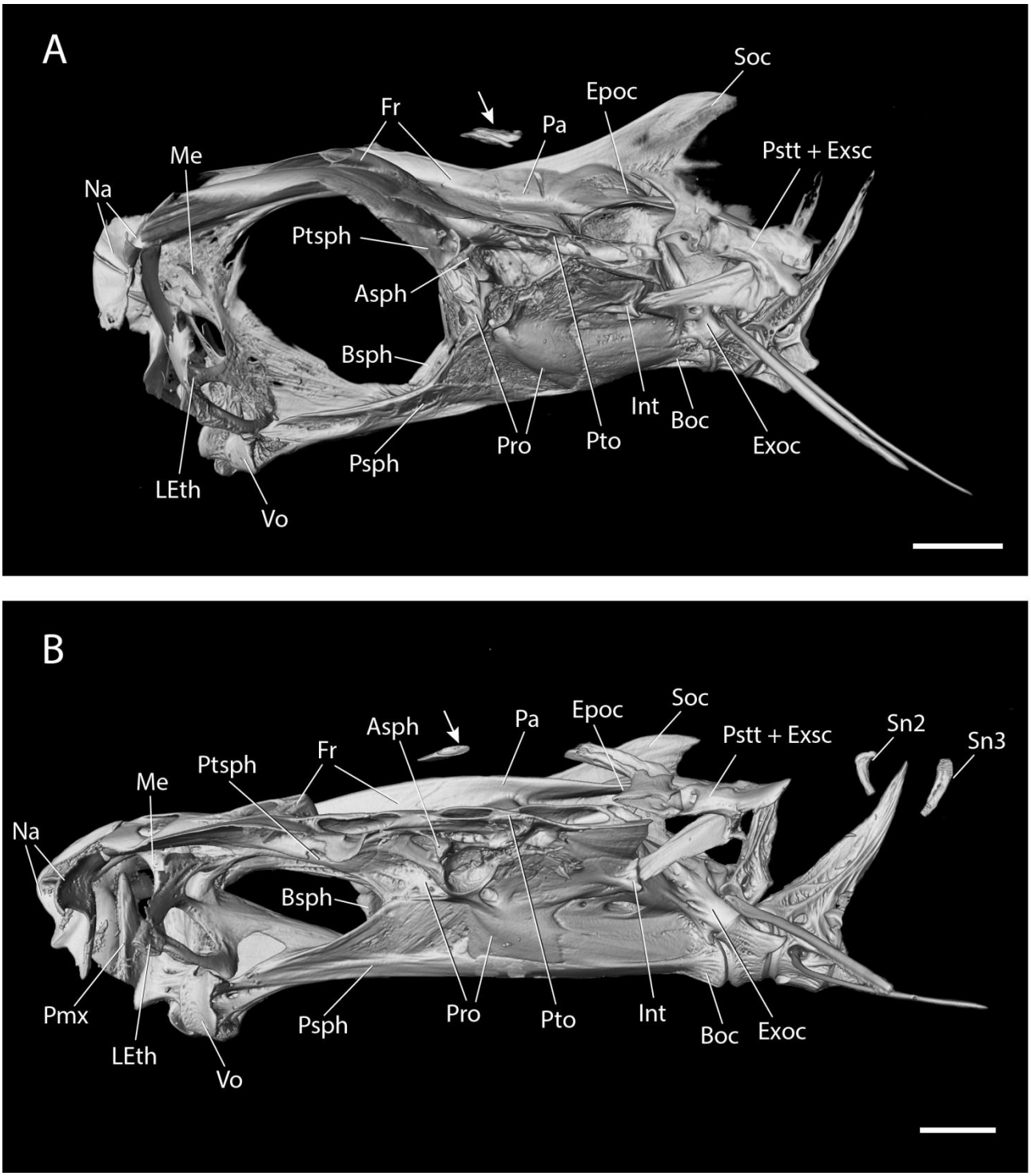

Fig. 5: Neurocranium, lateral view. A: *Galeoides decadactylus*. B: *Leptomelanosoma indicum.* Asph, autosphenotic; Boc, basioccipital; Bsph, basisphenoid; Epoc, epioccipital; Exoc, exoccipital; Exsc, extrascapula; Fr, frontal; Int, intercalar; LEth, lateral ethmoid; Me, mesethmoid; Na, nasal; Pa, parietal; Pmx, premaxilla; Pro, prootic; Psph, parasphenoid; Pstt, posttemporal; Pto, pterotic; Ptsph, pterosphenoid; Sn, supraneurals; Soc, supraoccipital; Vo, vomer. Scale bars: 5 mm. Arrow indicates the anterodorsal ossification of the supratemporal canal.

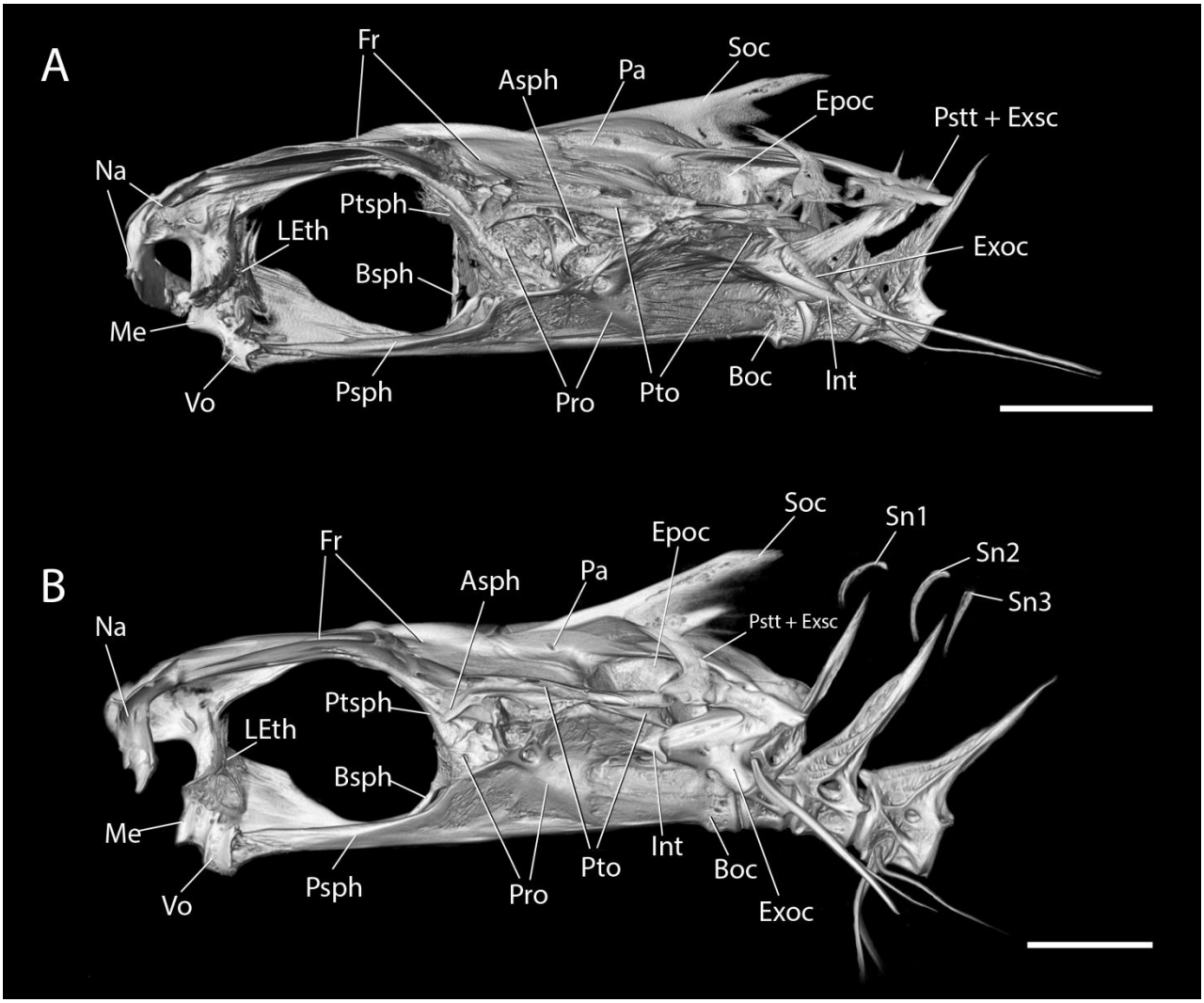

Fig. 6: Neurocranium, lateral view. A: *Eleutheronema tridactylum*. B: *Polydactylus virginicus*. Asph, autosphenotic; Boc, basioccipital; Bsph, basisphenoid; Epoc, epioccipital; Exoc, exoccipital; Exsc, extrascapula; Fr, frontal; Int, intercalar; LEth, lateral ethmoid; Me, mesethmoid; Na, nasal; Pa, parietal; Pro, prootic; Psph, parasphenoid; Pstt, posttemporal; Pto, pterotic; Ptsph, pterosphenoid; Sn, supraneural; Soc, supraoccipital; Vo, vomer. Scale bars: 5 mm.

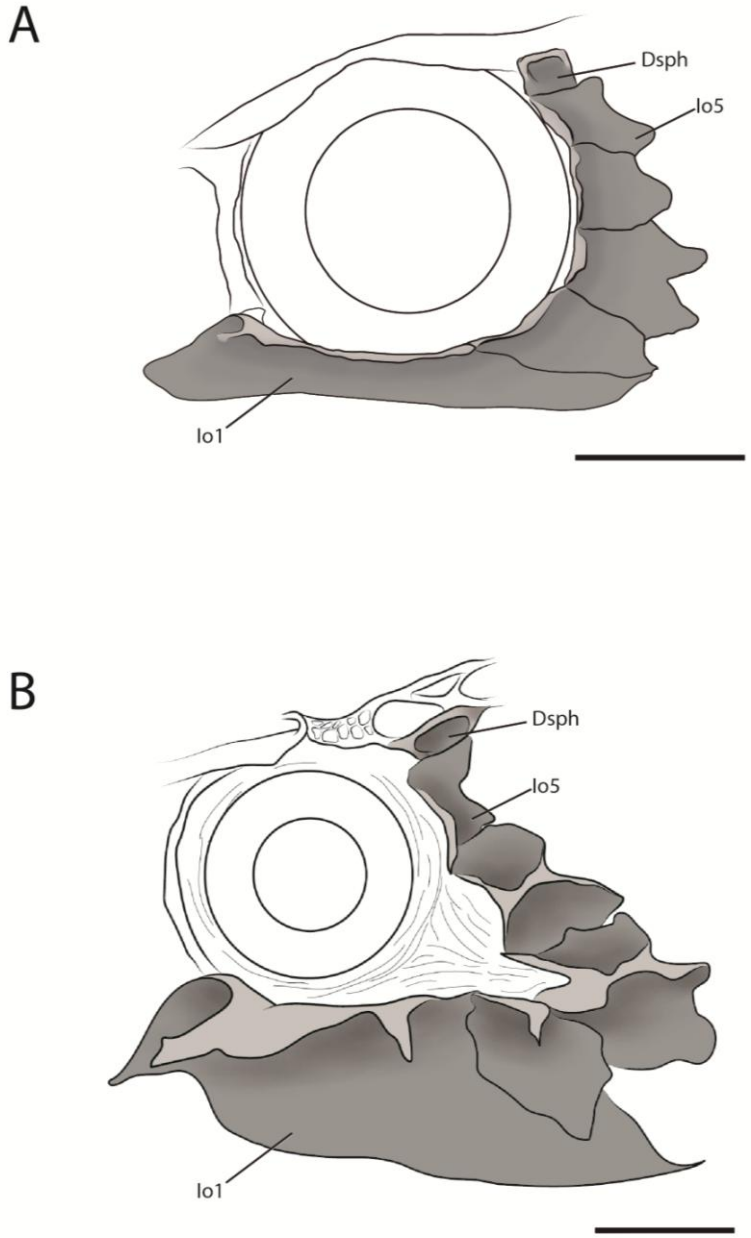

Fig. 7: Infraorbitals, lateral view. A: *Eleutheronema tetradactylum*. B: *Polynemus paradiseus*. Io, infraorbital; Dsph, dermosphenotic. Scale bars: 2 mm.

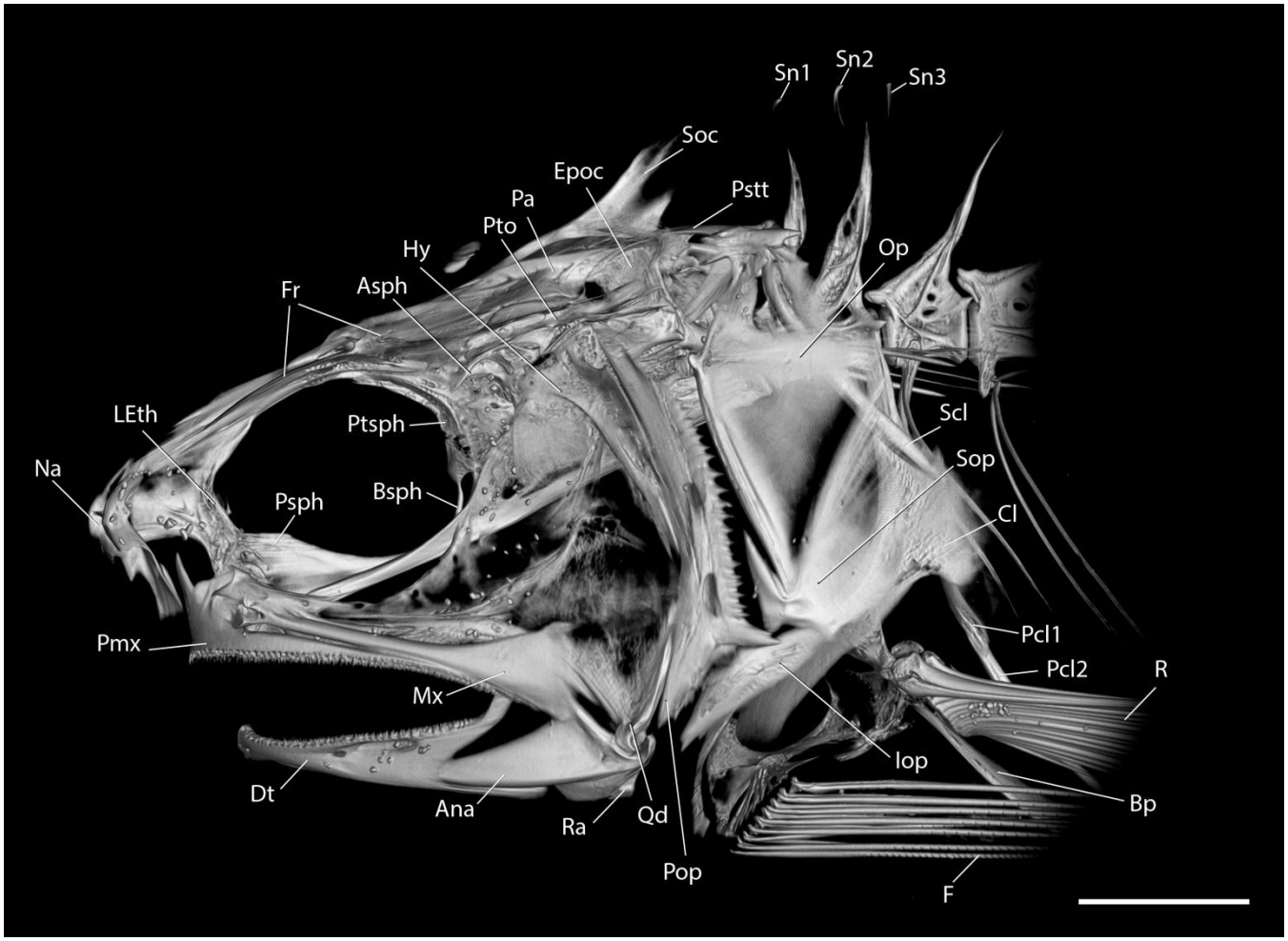

Fig. 8: Head, lateral view. *Polydactylus octonemus*. Ana, angulo-articular; Asph, autosphenotic; Bp, basipterygium; Bsph, basisphenoid; Cl, cleithrum; Dt, dentary; Epoc, epioccipital; F, pectoral filament; Fr, frontal; Hy, hyomandibular; Iop, interopercle; LEth, lateral ethmoid; Mx, maxilla; Na, nasal; Op, opercle; Pa, parietal; Pcl, postcleithrum; Pop, preopercle; Pmx, premaxilla; Pstt, posttemporal; Pto, pterotic; Ptsph, pterosphenoid; Qd, quadrate; R, pectoral-fin rays; Ra, retroarticular; Scl, supracleithrum; Sn, supraneural; Socc, supraoccipital; Sop, subopercle. Scale bars: 4.5 mm.

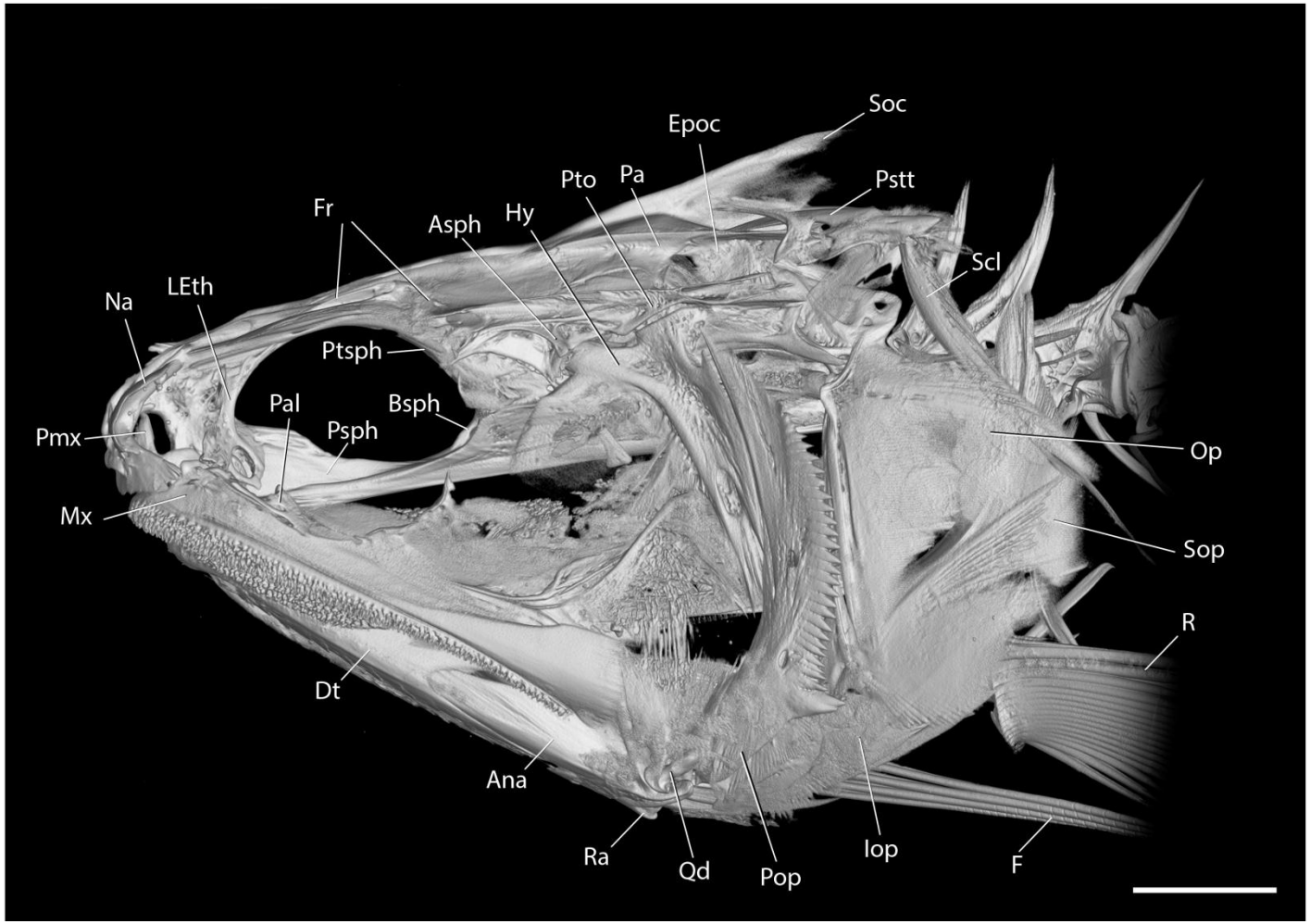

Fig. 9: Head, lateral view. *Eleutheronema tetradactylum*. Ana, angulo-articular; Asph, autosphenotic; Bsph, basisphenoid; Dt, dentary; Epoc, epioccipital; F, pectoral filament; Fr, frontal; Hy, hyomandibular; Iop, interopercle; LEth, lateral ethmoid; Mx, maxilla; Na, nasal; Op, opercle; Pa, parietal; Pal, palatine; Pop, preopercle; Pmx, premaxilla; Pstt, posttemporal; Pto, pterotic; Ptsph, pterosphenoid; Qd, quadrate; R, pectoral-fin rays; Ra, retroarticular; Scl, supracleithrum; Socc, supraoccipital; Sop, subopercle. Scale bars: 4 mm.

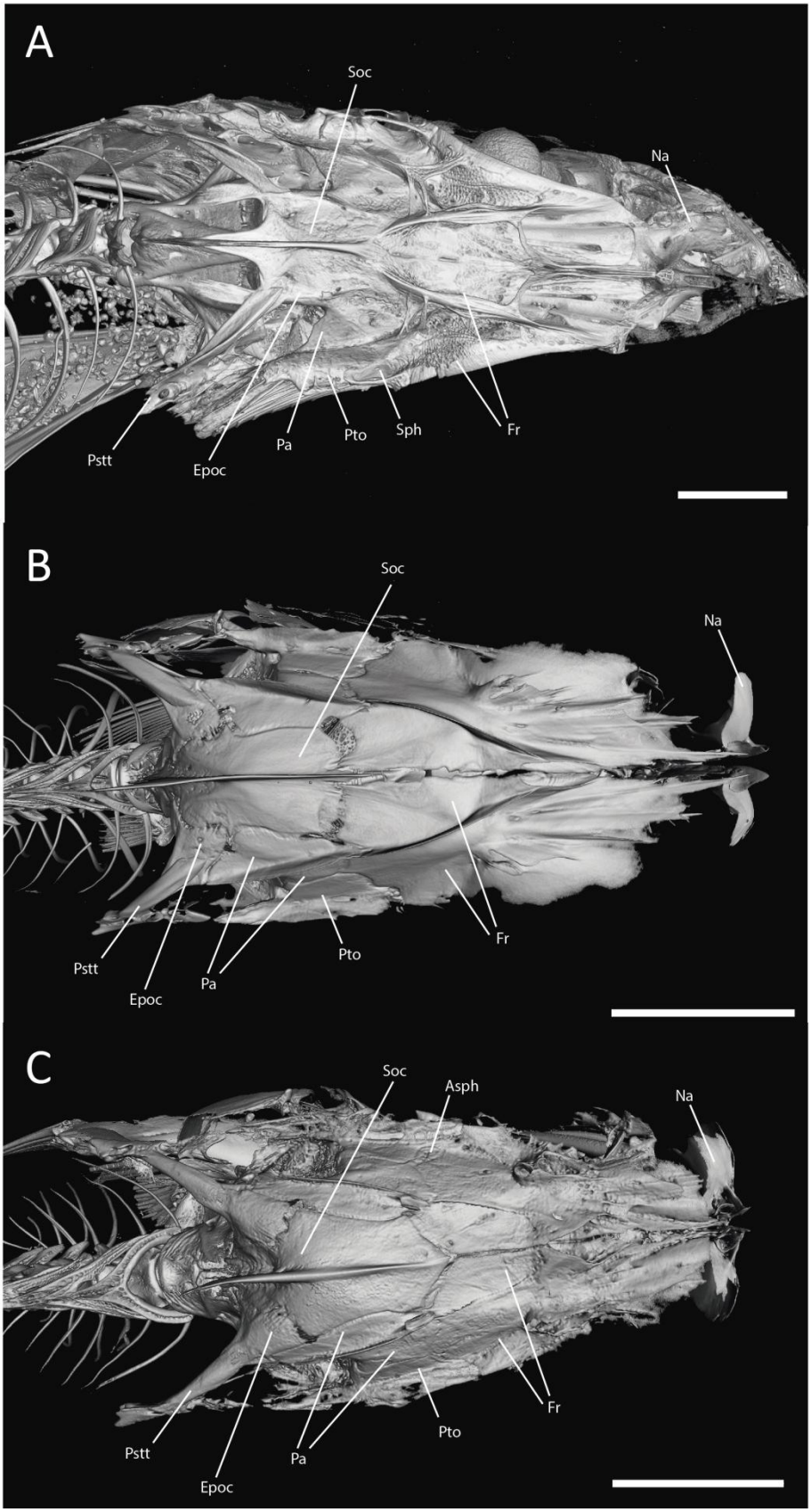

Fig. 10: Neurocranium, dorsal view. A: *Cynoscion striatus*. B: *Polydactylus sexfilis.* C: *Polynemus multifilis.* Asph, autosphenotic; Epoc, epioccipital; Fr, frontal; Na, nasal; Pa, parietal; Pstt, posttemporal; Pto, pterotic; Socc, supraoccipital. Scale bars: 5 mm.

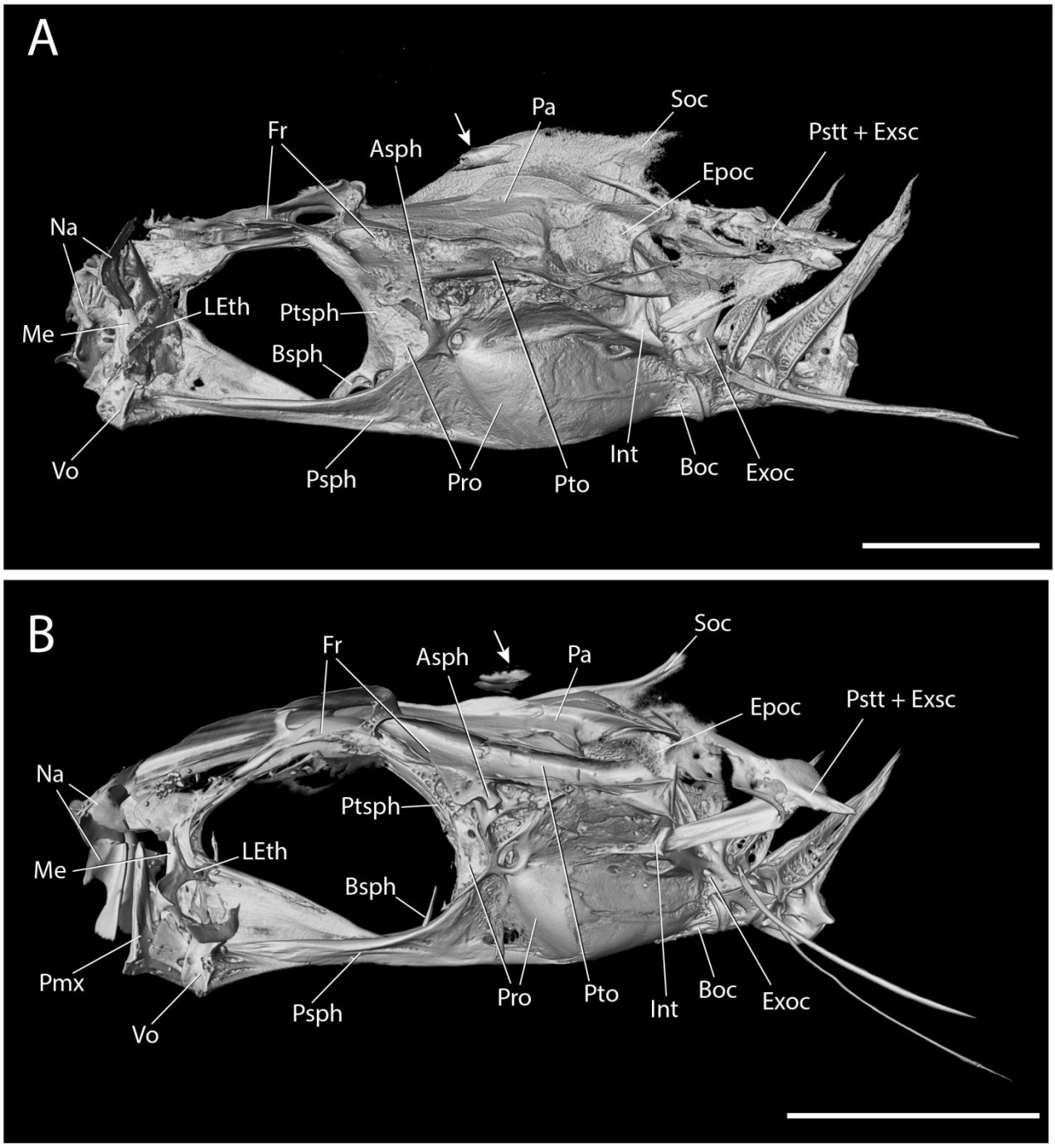

Fig. 11: Neurocranium, lateral view. A: *Pentanemus quinquarius.* B: *Filimanus similis*. Asph, autosphenotic; Boc, basioccipital; Bsph, basisphenoid; Epoc, epioccipital; Exoc, exoccipital; Exsc, extrascapula; Fr, frontal; Int, intercalar; LEth, lateral ethmoid; Me, mesethmoid; Na, nasal; Pa, parietal; Pmx, premaxilla; Pro, prootic; Psph, parasphenoid; Pstt, posttemporal; Pto, pterotic; Ptsph, pterosphenoid; Socc, supraoccipital; Vo, vomer. Scale bars: 5 mm. Arrow indicates the anterodorsal ossification of the supratemporal canal.

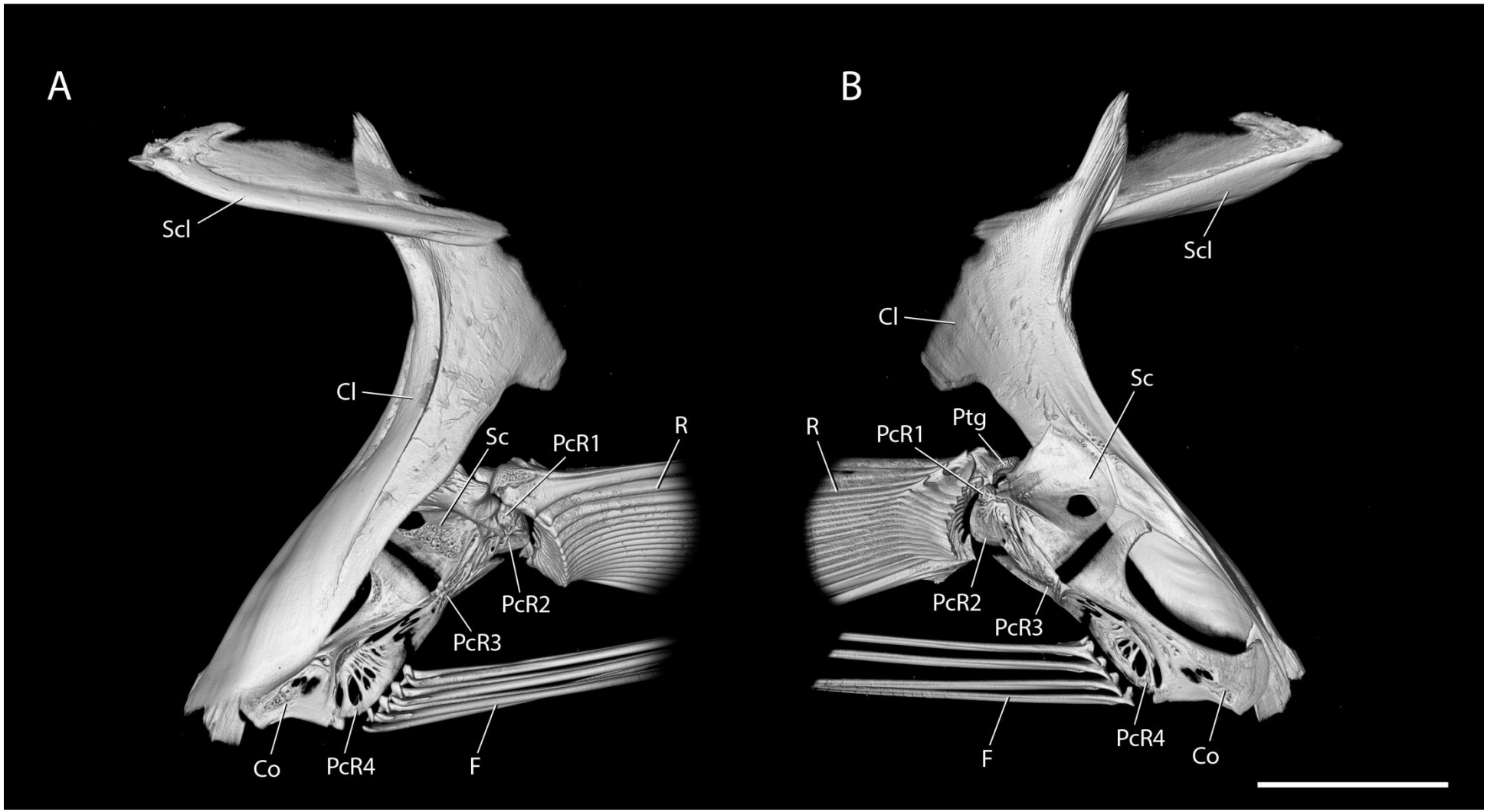

Fig. 12: Pectoral girdle. *Eleutheronema tetradactylum*. A: lateral view. B: medial view. Cl, cleithrum; Co, coracoid; F, pectoral filament; Pcl, postcleithrum; PcR, pectoral radial; Ptg, propterygium; R, pectoral-fin rays; Ra, retroarticular; Sc, scapula; Scl, supracleithrum. Scale bars: 5 mm.

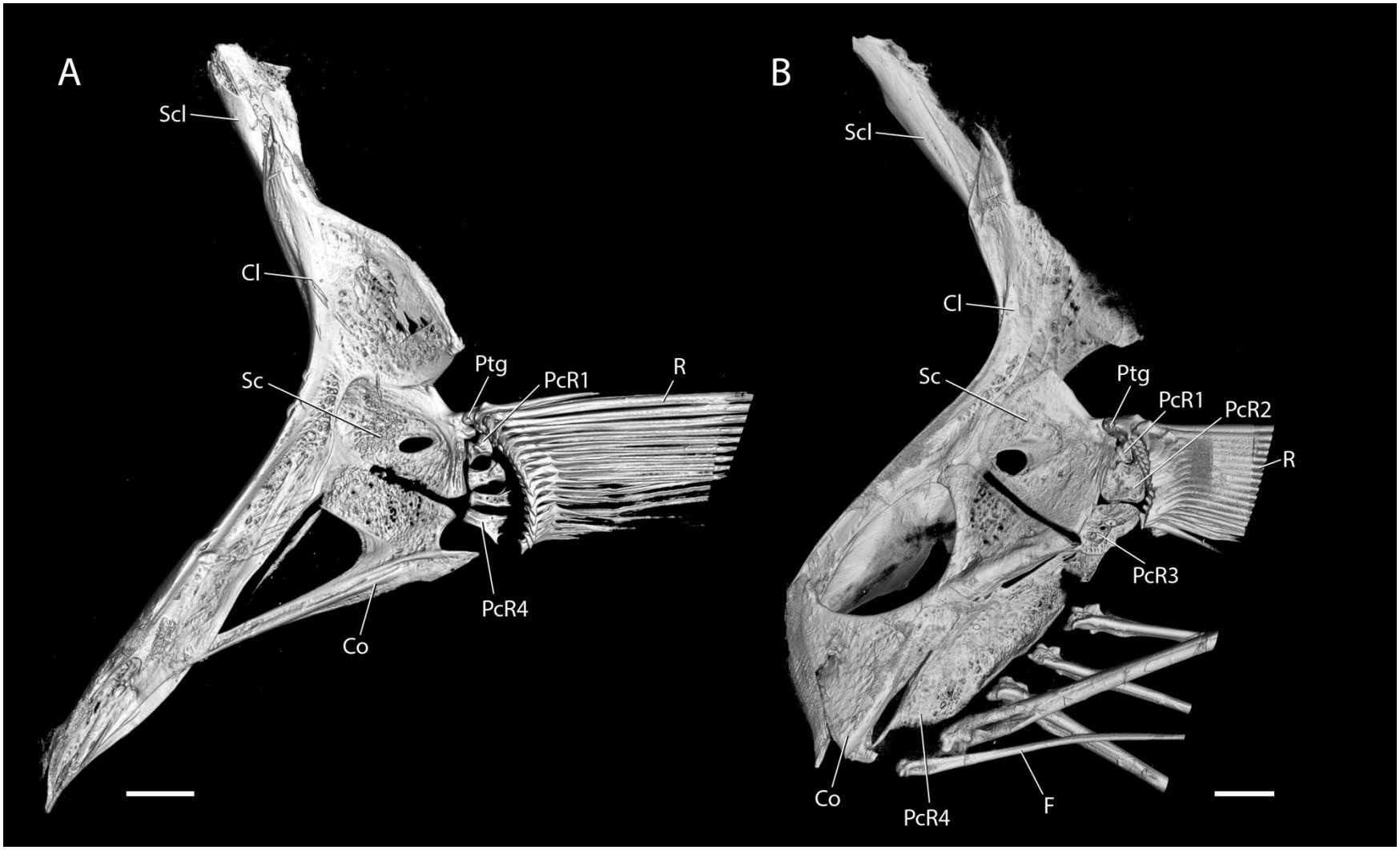

Fig. 13: Pectoral girdle, medial view. A: *Cynoscion striatus*. B: *Pentanemus quinquarius*. Cl, cleithrum; Co, coracoid; F, pectoral filament; Pcl, postcleithrum; PcR, pectoral radial; Ptg, propterygium; R, pectoral-fin rays; Ra, retroarticular; Sc, scapula; Scl, supracleithrum. Scale bars: 2 mm.

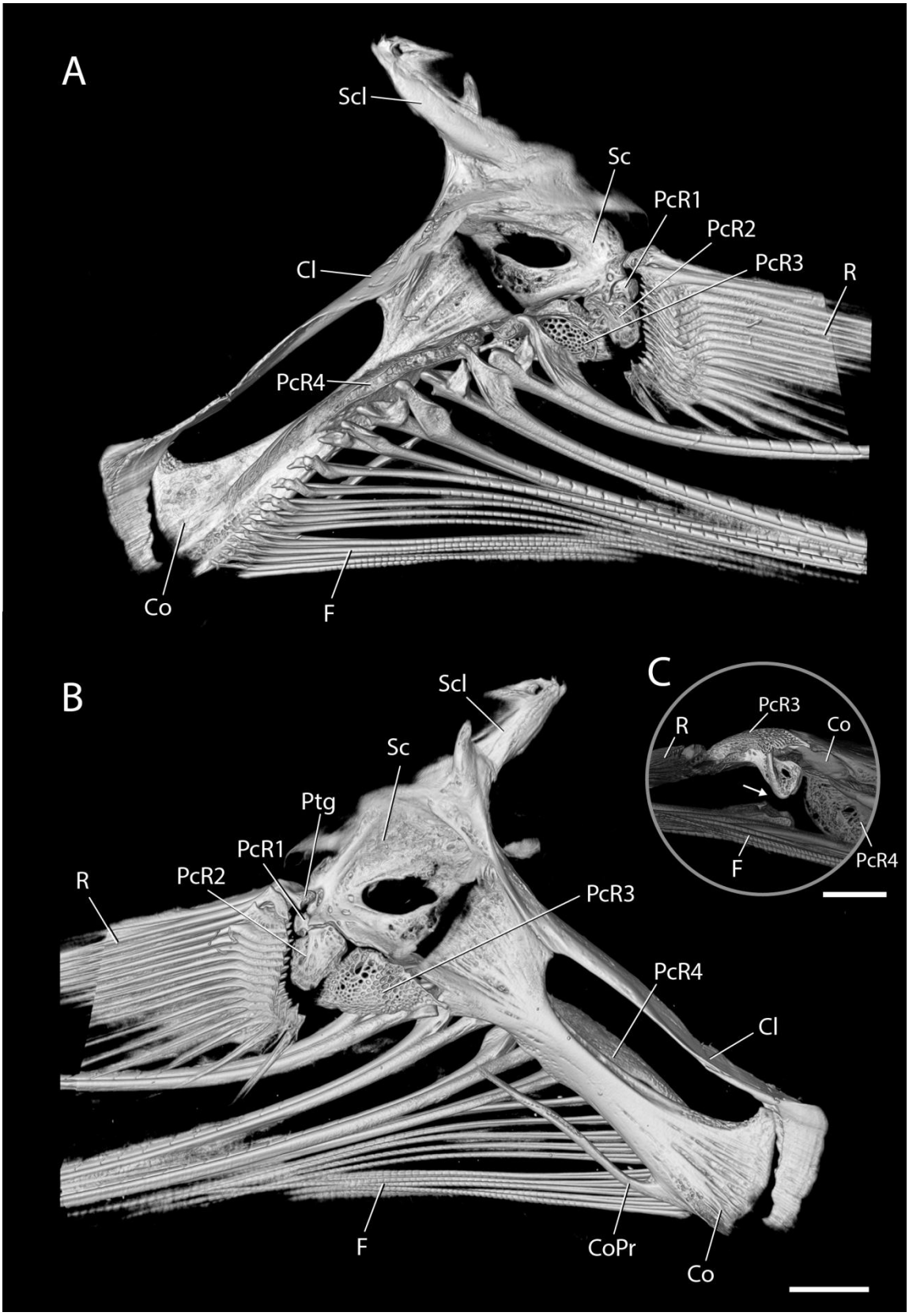

Fig. 14: Pectoral girdle. *Polynemus multifilis*. A: lateral view. B: medial view. C: ventral view. Cl, cleithrum; Co, coracoid; CoPr; coracoid process; F, pectoral filament; Pcl, postcleithrum; PcR, pectoral radial; Ptg, propterygium; R, pectoral-fin rays; Ra, retroarticular; Sc, scapula; Scl, supracleithrum. Scale bars: 2 mm. Arrow indicates site of articulation between pectoral radial 3 and the dorsalmost pectoral filament.

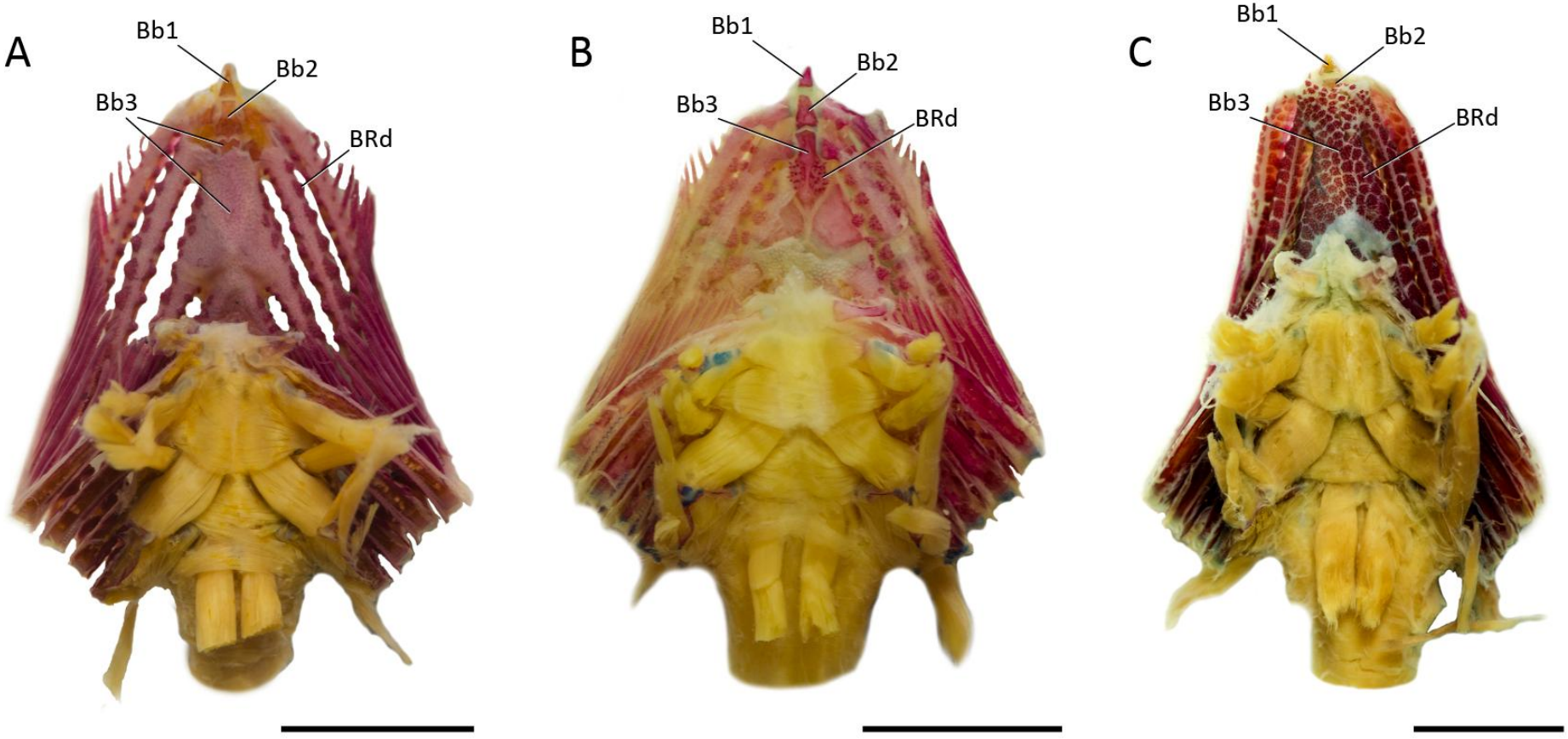

Fig. 15: Branchial arches, dorsal view. A: *Polydactylus sexfilis*. B: *Polynemus multifilis*. C: *Eleutheronema tetradactylum*. Bb, basibranchial; BRd, branchial rudiments. Scale bars: 5 mm.

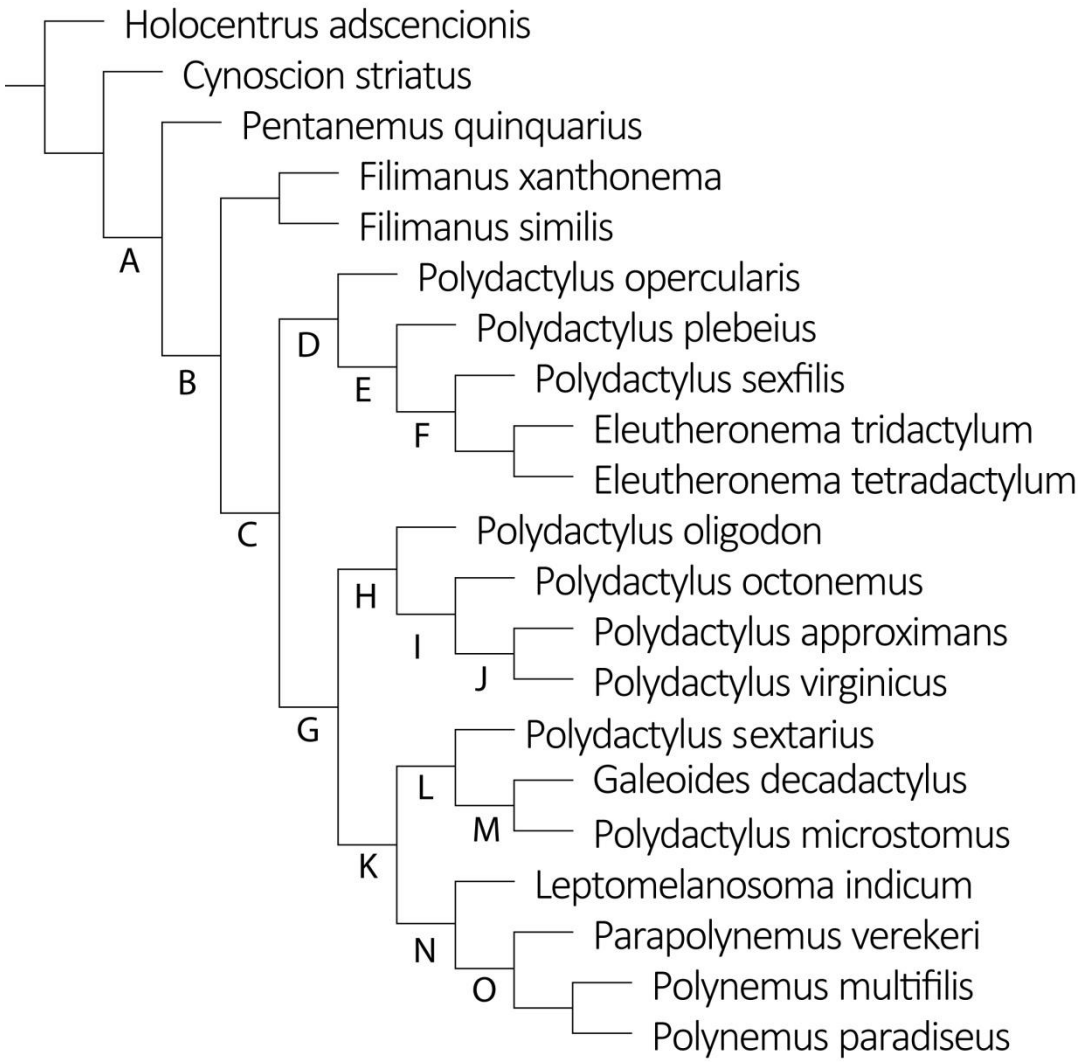

Fig. 16: Hypothesis of the relationships of Polynemidae from 162 morphological characters using equal weighing against homoplasies.

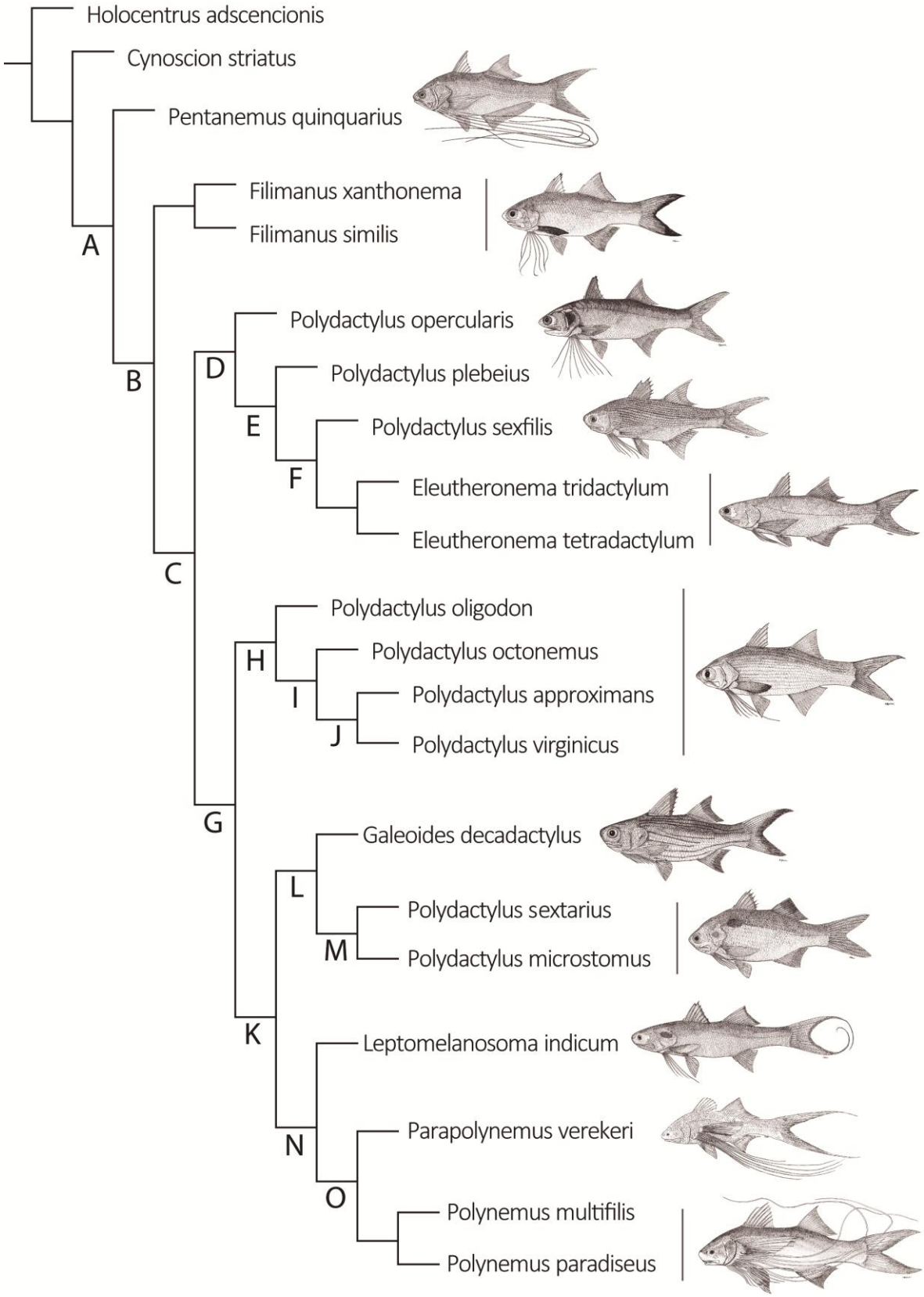

Fig. 17: Adopted hypothesis of the relationships of Polynemidae from 162 morphological characters using implied weighting against homoplasies with k varying from 3 to 6. Illustrations adapted from Motomura (2004).

APPENDIX A

Tab. 1: Consistency index of all 162 characters

Consistency Index of characters-tree 0

0	1	2	3	4	5	6	7	8	9
0.420	1.000	0.602	0.355	0.286	0.422	0.667	0.559	0.752	0.495
10	11	12	13	14	15	16	17	18	19
0.552	0.312	1.000	0.500	0.500	0.333	1.000	1.000	1.000	1.000
20	21	22	23	24	25	26	27	28	29
1.000	1.000	1.000	1.000	0.167	1.000	1.000	0.500	0.333	1.000
30	31	32	33	34	35	36	37	38	39
1.000	0.250	0.333	0.250	0.250	1.000	1.000	0.333	1.000	1.000
40	41	42	43	44	45	46	47	48	49
0.500	1.000	0.500	1.000	0.500	0.500	0.333	0.333	1.000	1.000
50	51	52	53	54	55	56	57	58	59
1.000	1.000	1.000	1.000	1.000	1.000	1.000	1.000	0.500	1.000
60	61	62	63	64	65	66	67	68	69
1.000	1.000	1.000	0.250	1.000	0.333	0.500	1.000	0.500	1.000
70	71	72	73	74	75	76	77	78	79
1.000	1.000	0.250	0.333	0.333	0.500	1.000	1.000	1.000	0.500
80	81	82	83	84	85	86	87	88	89
0.500	0.667	0.333	1.000	1.000	1.000	0.333	1.000	0.500	1.000
90	91	92	93	94	95	96	97	98	99
0.333	1.000	1.000	1.000	1.000	1.000	0.250	1.000	0.333	1.000
100	101	102	103	104	105	106	107	108	109
1.000	1.000	0.500	0.500	0.500	1.000	0.333	0.500	0.667	1.000
110	111	112	113	114	115	116	117	118	119
1.000	1.000	1.000	1.000	1.000	0.500	0.333	1.000	0.500	1.000
120	121	122	123	124	125	126	127	128	129
0.500	1.000	1.000	0.500	1.000	1.000	1.000	1.000	1.000	1.000
130	131	132	133	134	135	136	137	138	139
0.333	1.000	1.000	0.250	0.250	0.167	0.500	1.000	0.333	1.000
140	141	142	143	144	145	146	147	148	149
1.000	0.250	1.000	0.500	1.000	1.000	1.000	1.000	1.000	1.000
150	151	152	153	154	155	156	157	158	159
1.000	0.200	0.333	0.500	0.333	0.500	0.500	0.250	0.500	1.000
160	161								
1.000	0.200								

Tab. 2: Retention index of all 162 characters

Retention Index of characters-tree 0

0	1	2	3	4	5	6	7	8	9
0.481	1.000	0.500	0.420	0.412	0.208	0.500	0.383	0.000	0.452
10	11	12	13	14	15	16	17	18	19
0.503	0.305	1.000	0.750	0.800	0.667	1.000	1.000	1.000	1.000
20	21	22	23	24	25	26	27	28	29
1.000	1.000	1.000	1.000	0.167	1.000	1.000	0.800	0.333	1.000
30	31	32	33	34	35	36	37	38	39
1.000	0.500	0.000	0.000	0.250	1.000	1.000	0.500	1.000	1.000
40	41	42	43	44	45	46	47	48	49
0.500	1.000	0.667	1.000	0.000	0.667	0.750	0.667	1.000	1.000
50	51	52	53	54	55	56	57	58	59
1.000	1.000	1.000	1.000	1.000	1.000	1.000	1.000	0.500	1.000
60	61	62	63	64	65	66	67	68	69
1.000	1.000	1.000	0.625	1.000	0.333	0.000	1.000	0.000	1.000
70	71	72	73	74	75	76	77	78	79
1.000	1.000	0.667	0.667	0.500	0.800	1.000	1.000	1.000	0.000
80	81	82	83	84	85	86	87	88	89
0.500	0.800	0.714	1.000	1.000	1.000	0.750	1.000	0.667	1.000
90	91	92	93	94	95	96	97	98	99
0.333	1.000	1.000	1.000	1.000	1.000	0.625	1.000	0.778	1.000
100	101	102	103	104	105	106	107	108	109
1.000	1.000	0.000	0.667	0.667	1.000	0.714	0.750	0.500	1.000
110	111	112	113	114	115	116	117	118	119
1.000	1.000	1.000	1.000	1.000	0.667	0.500	1.000	0.667	1.000
120	121	122	123	124	125	126	127	128	129
0.000	1.000	1.000	0.800	1.000	1.000	1.000	1.000	1.000	1.000
130	131	132	133	134	135	136	137	138	139
0.500	1.000	1.000	0.250	0.667	0.167	0.667	1.000	0.000	1.000
140	141	142	143	144	145	146	147	148	149
1.000	0.571	1.000	0.000	1.000	1.000	1.000	1.000	1.000	1.000
150	151	152	153	154	155	156	157	158	159
1.000	0.500	0.600	0.750	0.000	0.000	0.000	0.571	0.000	1.000
160	161								
1.000	0.333								

Tab. 3: Rescaled consistency index of all 162 characters

Rescaled Consistency Index of characters-tree 0

0	1	2	3	4	5	6	7	8	9
0.202	1.000	0.301	0.149	0.118	0.088	0.334	0.214	0.000	0.224
10	11	12	13	14	15	16	17	18	19
0.278	0.095	1.000	0.375	0.400	0.222	1.000	1.000	1.000	1.000
20	21	22	23	24	25	26	27	28	29
1.000	1.000	1.000	1.000	0.028	1.000	1.000	0.400	0.111	1.000
30	31	32	33	34	35	36	37	38	39
1.000	0.125	0.000	0.000	0.063	1.000	1.000	0.167	1.000	1.000
40	41	42	43	44	45	46	47	48	49
0.250	1.000	0.334	1.000	0.000	0.334	0.250	0.222	1.000	1.000
50	51	52	53	54	55	56	57	58	59
1.000	1.000	1.000	1.000	1.000	1.000	1.000	1.000	0.250	1.000
60	61	62	63	64	65	66	67	68	69
1.000	1.000	1.000	0.156	1.000	0.111	0.000	1.000	0.000	1.000
70	71	72	73	74	75	76	77	78	79
1.000	1.000	0.167	0.222	0.167	0.400	1.000	1.000	1.000	0.000
80	81	82	83	84	85	86	87	88	89
0.250	0.534	0.238	1.000	1.000	1.000	0.250	1.000	0.334	1.000
90	91	92	93	94	95	96	97	98	99
0.111	1.000	1.000	1.000	1.000	1.000	0.156	1.000	0.259	1.000
100	101	102	103	104	105	106	107	108	109
1.000	1.000	0.000	0.334	0.334	1.000	0.238	0.375	0.334	1.000
110	111	112	113	114	115	116	117	118	119
1.000	1.000	1.000	1.000	1.000	0.334	0.167	1.000	0.334	1.000
120	121	122	123	124	125	126	127	128	129
0.000	1.000	1.000	0.400	1.000	1.000	1.000	1.000	1.000	1.000
130	131	132	133	134	135	136	137	138	139
0.167	1.000	1.000	0.063	0.167	0.028	0.334	1.000	0.000	1.000
140	141	142	143	144	145	146	147	148	149
1.000	0.143	1.000	0.000	1.000	1.000	1.000	1.000	1.000	1.000
150	151	152	153	154	155	156	157	158	159
1.000	0.100	0.200	0.375	0.000	0.000	0.000	0.143	0.000	1.000
160	161								
1.000	0.067								

Tab. 4: Fitness of all 162 characters

Fitness of characters-tree 0 (conc 3)

0	1	2	3	4	5	6	7	8	9
0.685	1.000	0.820	0.622	0.545	0.686	0.857	0.792	0.901	0.746
10	11	12	13	14	15	16	17	18	19
0.787	0.576	1.000	0.750	0.750	0.600	1.000	1.000	1.000	1.000
20	21	22	23	24	25	26	27	28	29
1.000	1.000	1.000	1.000	0.375	1.000	1.000	0.750	0.600	1.000
30	31	32	33	34	35	36	37	38	39
1.000	0.500	0.600	0.500	0.500	1.000	1.000	0.600	1.000	1.000
40	41	42	43	44	45	46	47	48	49
0.750	1.000	0.750	1.000	0.750	0.750	0.600	0.600	1.000	1.000
50	51	52	53	54	55	56	57	58	59
1.000	1.000	1.000	1.000	1.000	1.000	1.000	1.000	0.600	1.000
60	61	62	63	64	65	66	67	68	69
1.000	1.000	1.000	0.500	1.000	0.600	0.750	1.000	0.750	1.000
70	71	72	73	74	75	76	77	78	79
1.000	1.000	0.500	0.600	0.600	0.750	1.000	1.000	1.000	0.750
80	81	82	83	84	85	86	87	88	89
0.750	0.750	0.600	1.000	1.000	1.000	0.600	1.000	0.750	1.000
90	91	92	93	94	95	96	97	98	99
0.600	1.000	1.000	1.000	1.000	1.000	0.500	1.000	0.600	1.000
100	101	102	103	104	105	106	107	108	109
1.000	1.000	0.750	0.750	0.750	1.000	0.600	0.750	0.750	1.000
110	111	112	113	114	115	116	117	118	119
1.000	1.000	1.000	1.000	1.000	0.750	0.429	1.000	0.750	1.000
120	121	122	123	124	125	126	127	128	129
0.750	1.000	1.000	0.750	1.000	1.000	1.000	1.000	1.000	1.000
130	131	132	133	134	135	136	137	138	139
0.600	1.000	1.000	0.500	0.500	0.375	0.750	1.000	0.600	1.000
140	141	142	143	144	145	146	147	148	149
1.000	0.500	1.000	0.750	1.000	1.000	1.000	1.000	1.000	1.000
150	151	152	153	154	155	156	157	158	159
1.000	0.429	0.600	0.750	0.600	0.750	0.750	0.500	0.750	1.000
160	161								
1.000	0.429								

DATA MATRIX: QUANTITATIVE CHARACTERS

Holocentrus adscencionis 0.140 0.670 1.000 ? 1.000 ? 1.000 0.090 1.000 0.000 0.000 0.100

Cynoscion striatus 0.180 1.000 0.000 1.000 1.000 ? 0.000 0.000 0.330 0.250 0.270 0.310

Eleutheronema tetradactylum 0.520 0.000 1.000 0.670 1.000 0.090 0.500 0.360 0.330 0.750 0.820 0.080

Eleutheronema tridactylum 0.580 0.000 1.000 0.330 1.000 0.000 0.500 0.360 0.330 0.750 0.820 0.000

Filimanus similis 0.110 0.000 0.670 0.170 0.500 0.360 0.500 0.180 0.330 0.670 0.730 0.920

Filimanus xanthonema 0.060 0.000 0.670 0.170 0.500 0.270 0.500 0.180 0.330 0.670 0.640 0.820

Galeoides decadactylus 0.000 0.000 0.670 0.330 0.000 0.640 0.500 0.000 0.330 0.670 0.730 0.540

Leptomelanosoma indicum 0.430 0.000 0.670 0.330 0.250 0.180 0.500 0.180 0.330 0.500 0.640 0.210

Parapolynemus verekeri 0.230 0.000 0.670 0.170 0.000 0.270 0.500 0.180 0.330 0.670 0.730 0.740

Pentanemus quinquarius 0.430 0.000 0.670 0.670 0.500 0.180 0.500 1.000 0.330 0.920 0.820 1.000

Polydactylus virginicus 0.280 0.000 0.670 0.170 0.750 0.360 0.500 0.270 0.330 0.580 0.640 0.460

Polydactylus oligodon 0.480 0.000 0.670 0.000 0.750 0.360 0.500 0.320 0.330 0.500 0.550 0.490

Polydactylus approximans 0.290 0.000 0.670 0.170 0.500 0.270 0.500 0.320 0.330 0.670 0.730 0.540

Polydactylus octonemus 0.290 0.000 0.670 0.000 0.750 0.450 0.500 0.270 0.330 0.580 0.640 0.720

Polydactylus microstomus 0.000 0.000 0.670 0.330 0.000 0.180 0.500 0.230 0.000 0.670 0.730 0.380

Polydactylus sextarius 0.030 0.000 0.670 0.170 0.500 0.270 0.500 0.230 0.330 0.670 0.730 0.490

Polydactylus opercularis 0.430 0.000 0.670 0.000 0.500 0.550 0.500 0.320 0.000 0.580 0.640 0.640

Polydactylus plebeius 0.290 0.000 0.670 0.330 0.750 0.180 0.500 0.180 0.330 0.500 0.550 0.380

Polydactylus sexfilis 0.310 0.000 0.670 0.170 0.500 0.270 0.500 0.180 0.330 0.670 0.730 0.490

Polynemus paradiseus 0.510 0.000 1.000 0.670 0.750 0.360 0.000 0.230 0.330 0.920 0.820 0.590

Polynemus multifilis 1.000 0.000 1.000 0.670 0.750 1.000 0.000 0.230 0.330 1.000 1.000 0.410

DATA MATRIX: QUALITATIVE CHARACTERS

Holocentrus adscencionis
0???00000??000100010110001100010??00000?0?000000?????????00000000?10?0000?00001000?0001000
???00000000??????00?00?001001000000000100?01000????000??00?

Cynoscion striatus

1010010110011010010000000100010??00000?0?11110100??0000?011100000?1100001010111100?0001000???10001000??????00?01?000000??0101001011010011100000011010?

Eleutheronema tetradactylum

1[01]0101111111001111101101011010010011110010111121110011111111100011010?01110101111100111101000001111011001001010020010101001101001011011021000000100110

Eleutheronema tridactylum

1001011111110011111011010110100100101100101111211100111111111000110 00?0111010111110011110100000111101100100101002001010100110100101101102100000011111 0

Filimanus similis

1010011111111010011111110111000100011100101111011101111111111101111111111010111011101110011110100000111101110001001002101010101001100111101102110110011 0111

Filimanus xanthonema

1010011111111010011111110111000100011100101111011101111111111101111111111010111011101110011110100000111101110001001002101010101001100111101102110110011 0111

Galeoides decadactylus

1100011111110010011010110010000100111100101111011100111111110011110110011111111111000101011001102110111020000100200101110000110010111110211010111001 10

Leptomelanosoma indicum

1001011111110110111111111110010100111100101111211101111111110111110112111111111110001010110001121101110101001002001011101001100101101102111001111011 0

Parapolynemus verekeri

1001011111110100011100011 00?0101110011111111110111001111011101111101121111111100?11101011101101111101111211011012011010111111101011011121111100110111

Pentanemus quinquarius

1010011111111011011100010110000111001100101111011100111101111011111100101011111111000110?1?1100111101111101011102101010101011110101101102111000011 0111

Polydactylus virginicus

1101011111111010011111010110000100111100101111011101111111111101111011001111111111110011110100001111101110001001012001010101111100111101102111000010 0110

Polydactylus oligodon

1101011111111010011111010110000100111100101111011101111111111101111011001111111111110011110
1000011111011100010010020010101010111001111011021110000110111

Polydactylus approximans

1101011111111010011111010110000100111100101111011101111111111101111011001111111111110011110
1000011111011101010010120010101010111001111011021110000101111

Polydactylus octonemus

1101011111111010011111010110000100111100101111011101111111111111111011001111111111110011110
1000011111011100010010120010101010111001111011021110000110110

Polydactylus microstomus

1001111111111010011011010010001100111100101111011100101111110111110111111111111111110011010
1000010111011100010010020010111011011001011111021100010100110

Polydactylus sextarius

1001111111111010011111010010001100111100101111011100100111110111110110111111111111110011010
1000010111011100010010020010101010111001011111021110000100110

Polydactylus opercularis

1001011111110011111111010110100100111100101111211101101111111001110010011111111111110001110
1000001111011101010010020010101011111111011011021110000100110

Polydactylus plebeius

1001011111111011011111010110000100111100101111011100111111110010110110011111111111110011110
1000001111011001010010020010101001111001011011021000000??110

Polydactylus sexfilis

1001011111111011011011010110000100011100101111011100111111110010110110011101111111110011010
1000011111011001000010020010101011111001111011021000000100110

Polynemus paradiseus

1010011111111100011111111110?01010100111110111111111111111111011111011211110111111110001010
1011011111111110110010120010111111011001011011121111100110111

Polynemus multifilis

1010011111111100011111101110?01010100111110111111110111111111011111011211110111111110001010
1011011111111110110010120010111111111001010011121111100110110

Chapter 3

Skeletal development in Polynemidae

1. INTRODUCTION

Marine fish eggs and larvae varies drastically and can have several different forms, morphological specializations and pigmentation patterns that act as important characters to identifying them (Moser, 1996). The study of larval ontogeny in systematic research has been a consistent tool to investigate the relationships among fishes and therefore trace homologies between structures (Cubbage and Mabee, 1996; Moser, 1996; Britz and Johnson, 2002; Warth *et al.*, 2017). The morphogenesis of skull, mandibular and hyoid arches are by far the most studied structures in fish development (Arratia and Schultze, 1991; Cubbage and Mabee, 1996; Adriaens and Verraes, 1998; Geerinckx *et al.*, 2005; 2007; Block and Mabee, 2012). Nonetheless, several others papers analyzed other structures such as pectoral girdle and branchial arches (Faustino and Power, 1999; Britz and Johnson, 2002; 2005; Warth *et al.*, 2017). Still, there are a lot of groups lacking information about larval development.

Polynemidae early stages descriptions are rare and can be found, in its majority, in larval identification guides such as Moser *et al.* (1984), Moser (1996), Leis and Carson-Ewart (2000) and Richards (2005). From the few species studied, most Polynemids are considered to be protandrous hermaphrodites, where eggs, larvae and juveniles are pelagic until they reach about 60 mm, in which they began to enter nearshore environments (Santerre and May, 1977; Sandknop and Watson, 1996; Motomura, 2004). In the study of Santerre and May (1977) the authors observed that *Polydactylus sexfilis* matures first as a male with around 200 to 290 mm of length and becomes a female by the time they reach approximately 300 to 400 mm of length. The pelagic eggs are spherical and transparent with approximately 0.79 to 0.99 mm (0.76 mm average) in diameter (De Sylva, 1984; Sandknop and Watson, 1996).

The larvae hatch with around 1.5 to 2 mm in which their mouth is yet not formed, the eye is unpigmented and they bear a large yolk sac ventrally that will nourish them during their early life history (Sandknop and Watson, 1996). The yolk sac is almost fully consumed by the time the larvae reach about 3 mm long (Santerre and May, 1977; Sandknop and Watson, 1996). Polynemidae larvae have a generally large head, with weak spination,

prominent eyes and a rounded snout – characteristic that is distinguishable during the postflexion stage – and a triangular coiled gut that extends about 44 – 62% of body length (Sandknop and Watson, 1996; Leis and Trnski, 2000; Motomura, 2004). During the preflexion stage, the main caudal fin rays are one of the first structures to develop in the larvae body. The flexion regularly occurs at 3.5 to 4.5 mm length, which, early in this stage, the anal and the second dorsal fin rays begin to simultaneously develop with about the same number of rays (Sandknop and Watson, 1996; Leis and Trnski, 2000; Richards, 2005). Small preopercular spines can be seen during flexion which become larger by settlement. These spines will later develop into the serrate preopercular margin of most of the adults (Leis and Trnski, 2000). Furthermore, still during chorda flexion, the pectoral fin rays and the spines of the first dorsal fin start to grow and at the end of the flexion process, pelvic and procurrent caudal fin rays commence to form (Sandknop and Watson, 1996).

Pectoral fin rays are usually leveled with the top of the gut in early flexion and during the postflexion stage they start to migrate ventrally, settling near the ventral margin of body by the time they reach approximately 12 mm, except for *Parapolynemus* and *Polynemus* species (Leis and Trnski, 2000; Motomura, 2004). The pectoral rays are added from top to bottom and as it moves, the fin becomes divided into two separate lobes. The lower lobe moves anteroventrally and present thicker rays in comparison to the upper lobe. As they develop, they become longer and the membrane connecting them starts to vanish (Sandknop and Watson, 1996; Leis and Trnski, 2000). The upper lobe rays are fully ossified at 6.5 mm, at which time the lower lobe rays start to ossify. By the time the larvae reach approximately 7 mm, all pectoral structures are ossified and with an extra 0.3 mm in length, all elements of second dorsal and anal fin are complete (Leis and Trnski, 2000; Motomura, 2004).

Larval polynemids are lightly to moderately pigmented, with melanophores distribution and density varying throughout the taxa (Leis and Trnski, 2000). The pigmented areas usually occur along the ventral midline of the tail and gut and on dorsal surfaces of the swimming bladder and head. Melanophores can also be present at the posterior margin of the articular or over the angular bone (Sandknop and Watson, 1996; Leis and Trnski, 2000). Finally, with 15 mm the scales are fully developed and so the adipose eyelid (Leis and Trnski, 2000; Motomura, 2004).

2. MATERIAL AND METHODS

Ontogenetic series of three polynemid species were assembled, *Polydactylus octonemus*, *P. approximans*, and *P.* sp. (due to lack of identification guides for larval polynemids, the identity of this species could not be confidently determined). The specimens analyzed were from the Southeast Area Monitoring and Assessment Program (SEAMAP) Archiving Center, which is managed in conjunction with Fish and Wildlife Research Institute (FWRI) in St. Petersburg, Florida (SEAMAP 10218, SEAMAP 10248, SEAMAP 10290, SEAMAP 10294, SEAMAP 10295), Natural History Museum of Los Angeles County (LACM 9789-2), and NMNH (USNM 181282). In total, 21 specimens were analyzed, cleared & double-stained, dissected and photographed: nine *Polydactylus octonemus*, eight *Polydactylus approximans* and four *Polydactylus* sp., assembling an ontogenetic series that ranged from 3.3 mm to 32.8 mm (Fig.1). All specimens were at the post-flexion stage and were measured from the anterior end of the maxilla to the posterior portion of the hypurals, therefore all measurements are in standard length.

The osteological terminology primarily followed Johnson and Patterson (1993). Specimens were cleared and double-stained for bone and cartilage following Taylor and Van Dyke (1985) and (Schnell *et al.* (2016)). Photographs were taken with a Zeiss SteREO Discovery.V12 stereomicroscope with attached Zeiss Axio-Cam HRc digital camera. During the analysis, the timing of ossification of each bone was recorded, described, and mapped into a diagram of ossification sequences following Cubbage and Mabee (1996: fig. 2) and Bird and Mabee (2003: fig. 3).

3. RESULTS

Neurocranium – olfactory region

Sequence of ossification: vomer – nasal and mesethmoid – lateral ethmoid

Vomer: The vomer starts to ossify between 3.50 and 4 mm as a dermal ossification on the ventral surface of the ethmoid plate (Fig. 2B). At around 4 mm the anterolateral projections of the bone are discernible and its posterior end is already articulating with the anterior portion of the parasphenoid. At 4.7 mm the anterolateral projections become thicker, and around 6 mm these structures are almost fully formed. The vomer continues to expand anterodorsally, and their teeth appear at approximately 9 mm. At 13.3 mm the vomer reaches the adult condition (Fig. 2E).

Nasal: At 8 mm the nasal starts to ossify as a thin line of dermal ossification dorsomedially to the nasal organ (Fig. 2C, 3B). Ossification expands laterally and anteroventrally. At 8.9 mm curls and flaps start to form and the bone is nearly fully ossified in its dorsoventral axis (Fig. 2D, 3C). At 13.3 mm the nasal articulates with the frontal (Fig. 2E, 3D) and, close to 17.9 mm, the adult condition can be recognized (Fig. 2F, 3E).

Mesethmoid: The first sign of ossification of the mesethmoid occurs at around 8 mm as a perichondral dot on the anterior portion of the ethmoid plate (Fig 2C, 3B). From this stage, ossification quickly expands ventrally and at 8.9 mm the bone reaches the ventral region in which the lateral ethmoid is beginning to form (Fig. 2D). At 13.3 mm the mesethmoid starts to articulate with the lateral ethmoid and is almost meeting the parasphenoid (Fig. 2E). At 21.3 mm the mesethmoid achieves the adult condition forming the dorsal region of the nasal cavity and articulating with the dorsal projection of the vomer.

Lateral ethmoid: The lateral ethmoid is the last bone to ossify in the olfactory region of the neurocranium. The bone first appears at 8.9 mm as a thin perichondral line on the ventrolateral margin of the *lamina orbitonasalis*, right on the articulation with the palatine

(Fig. 2D). Ossification expands dorsally towards the frontal and medially towards the mesethmoid, articulating with its posterior region. At 17.9 mm the adult condition is evident. In adults the lateral ethmoid is not completely ossified dorsally, leaving a cartilaginous gap between the lateral ethmoid and the frontal (Fig. 2F).

Neurocranium – orbital region

Sequence of ossification: parasphenoid – frontal and pterosphenoid – basisphenoid

Parasphenoid: The parasphenoid is the first bone to appear on the orbital region of the neurocranium. The dermal ossification starts very early in development along the *trabeculae* (Fig. 3A) and at 4 mm it is almost fully ossified on the anteroposterior axis, where it articulates anteriorly with the vomer and posteriorly with the basioccipital (Fig 2B). At this stage the dorsal projections are already forming and expanding towards the prootic. The posterior region of the parasphenoid is still lightly ossified at its median line and only the lateral borders of the bone articulate with the basioccipital. Ossification expands posteriorly, and at around 6.40 mm the sagittal region of the parasphenoid reaches the basioccipital. By the time the larva reaches 8 mm the anterodorsal projection starts to form (Fig. 2C), and at 17.5 mm the parasphenoid is fully ossified into the adult condition (Fig. 2F).

Frontal: The frontal was first observed at around 7.9 mm (Fig. 2C, 3B). At this stage, however, the bone is quite developed already, suggesting that it might have started to ossify earlier, at some stage between 6.4 mm and 7 mm (we were unable to obtain specimens within this interval). The ossification probably starts on the dorsal border of the orbital capsule and along the lateral margin of the *taenia marginalis*, at the level of the epiphyseal bar. The ossification then expands dorsomedially toward its counterpart and posteriorly towards the autosphenotic. At 7.9 mm the frontal is almost reaching the anterior region of the autosphenotic (Fig. 3B). The counterparts meet at the dorsalmost region of the neurocranium at around 8.9 mm (Fig. 3C). At this stage, the supraorbital canal starts to form immediately anterior to the autosphenotic and the posterior region of the frontal meets the anterior region of the supraoccipital and the parietal. At 13.3 mm the posterior margin of

the frontal starts to overlap the anterodorsal region of the autosphenotic (Fig. 3D) and, at around 17.5 mm, the frontal reaches the adult condition (Fig. 3E).

Pterosphenoid: The pterosphenoid is first recognizable at around 7.9 mm as a thin perichondral line on the ventral region of the *taenia marginalis posterior* (Fig. 2C). Ossification rapidly expands anterodorsally and, at 8.9 mm, it is almost articulating with the frontal (Fig. 2D). The two bones meet at 13.3 mm and the ossification now expands posteroventrally towards the otic region of the neurocranium. At 21.3 mm the pterosphenoid finally reaches the prootic and autosphenotic.

Basisphenoid: The basisphenoid is the last bone to ossify, being first visible around 17.5 mm (Fig. 2F). Its ossification probably starts earlier, around 17 mm, and expands dorsally towards its tip. At 17.5 mm the basisphenoid is still ossifying dorsally, but its base is almost fully formed. At 21.3 mm the bone is practically fully ossified reaching the level of the dorsal projection of the parasphenoid that articulates with the prootic.

Neurocranium – otic region

Sequence of ossification: autosphenotic, pterotic, and prootic – intercalar and epioccipital – parietal

Autosphenotic: The autosphenotic starts to ossify at 4 mm (Fig. 2B, 3A) as a concentrated perichondral dot on the anterodorsal region of the otic capsule, where it meets the posterior end of the *taenia marginalis posterior*, region in which the autosphenotic articulates with the hyosymplectic cartilage. Ossification expands dorsally and posteriorly. At 6.4 mm the initial ossification is much more robust and an anterior projection is visible. The posterior end of the autosphenotic meets the anterior portion of the pterotic at around 7.9 mm (Fig. 2C). The posterior region of the autosphenotic starts to be covered by the anterior region of the pterotic at around 8.9 mm (Fig. 2D, 3C) and at 13.3 mm the autosphenotic is covered dorsally by the portions of the frontal and dermopterotic traversed by the continuous supraorbital and otic canals (Fig. 2E, 3D). At this stage, the autosphenotic already presents the adult condition.

Pterotic (Dermopterotic + Autopterotic): The dermopterotic first appears at 4 mm as an extremely thin line along the dorsolateral region of the otic capsule, right at the articulation with the hyosymplectic cartilage (Fig. 3A). Ossification then expands quite quickly and at 4.7 mm the ossified dermopterotic is already larger than the autosphenotic (Fig. 2B). At this stage the dermopterotic is an ossified circle that irradiated dorsally from the line of the previous stage. At 7.9 mm the dermal portion of the pterotic reaches anteriorly the posterodorsal region of the autosphenotic (Fig. 2C), which marks the first step of the autosphenotic overlapping. At this same stage the chondral part of the pterotic starts to ossify at its posterior end, close to the region where the epioccipital and exoccipital are located (Fig. 2C, 3B). The autopterotic then expands anteriorly towards the dermopterotic and autosphenotic. At 8.9 mm the autopterotic is greatly expanded anteriorly while the dermopterotic is expanded posteriorly, so that the two portions meet each other at the level of the anterior region of the parietal (Fig. 2D, 3C). Around 13.3 mm the dermopterotic reaches the anteroventral region of parietal through a dorsal projection of membrane bone (Fig. 2E). Simultaneously, the posterior end of the dermopterotic reaches the posttemporal level and encloses the otic and postotic canals. At 32.8 mm there is no gap between the autosphenotic and autopterotic. At this stage the dermal and chondral portions of the pterotic are fully fused to each other and the bone achieves its adult condition.

Prootic: The prootic starts to ossify at 4 mm as a perichondral line around the *trigemino-facialis* foramen, at the anterior region of the otic capsule, ventral to the ossifying autosphenotic. The prootic ossification expands posteriorly and, at 4.7 mm, the posterior margin of the bone is leveled up with the anterior margin of the dermopterotic (Fib. 2B). At 6.4 mm the ossification starts to expand on the dorsoventral axis and medially towards its antimere, while still extending posteriorly. At 8.9 mm the anterior region of the prootic is almost fully ossified, including the area of all cranial-nerve foramina (Fig. 2D). At this size the anteroventral region of the prootic articulates with the dorsal projection of the parasphenoid, whereas the anterodorsal region of the same bone articulates with the autosphenotic. At this same stage the prootic is almost reaching the basioccipital, the autopterotic and the pterosphenoid. The prootic is fully formed at 32.8 mm.

Intercalar: The intercalar is a small membrane bone that ossifies on the tip of the ventral arm of the posttemporal and its first signs of ossification occur at 4.7 mm (Fig. 2B). Nevertheless at this stage the bone can only be seen on the right side of the skull. At 5.7 mm the ossification starts to expand anteroventrally towards the origin site of the future autopterotic. At 13.3 mm the intercalar achieves the adult condition (Fig. 2E).

Epioccipital: The epioccipital first appears at 4.7 mm, right below the articulation point between the neurocranium and the dorsal arm of the posttemporal (Fig. 2B). It starts as a thin perichondral line on the posterior vertical semicircular canal. The line-shaped morphology persists until 6.4 mm, when the bone expands anteriorly. At 7.9 mm the dorsal boundary encompasses the dorsal arm of the posttemporal and already articulates with the parietal (Fig. 2C, 3B). At 8.9 mm the ventral portion of the epioccipital meets the intercalar and almost reaches the posterior end of the autopterotic (Fig. 2D, 3C). At this same size, the epioccipital starts to be overlapped by the posterior region of the parietal and, at 17.5 mm, the dorsalmost region of the epioccipital contacts the supraoccipital (Fig. 3E). The epioccipital achieves the adult condition at 32.8 mm.

Parietal: The parietal starts to ossify at 8 mm and is the last otic bone to appear (Fig. 2C, 3B). The dermal ossification begins posterodorsally, between the supraoccipital and epioccipital. At 8.9 mm the dorsalmost region of the parietal articulates with the lateral projections of the supraoccipital and is starting to overlap it (Fig. 3C). At this size the epioccipital is also beneath the parietal and there is a small cartilaginous gap between the parietal and frontal. Close to 13.3 mm the anteroventral portion of the parietal meets the dorsal projection of the dermopterotic (Fig. 2E). At 17.5 mm the boundaries between the parietal and frontal are completely ossified (Fig. 3E) and, with 21.3 mm, the parietal is fully formed (Fig. 3F).

Neurocranium – occipital region

Sequence of ossification: basioccipital and exoccipital – supraoccipital

Basioccipital: The basioccipital is one of the earliest bones of the neurocranium to start to ossify. Its first unequivocal signs of perichondral ossification were observed at 4 mm (Fig. 3A). At this stage, the basioccipital is already quite developed along the anteroposterior axis and articulates anteriorly with the lateral margins of the parasphenoid. The whole neurocranial portion of the notochord is ossified at this stage, giving the basioccipital a strong triangular aspect in ventral view. Moreover, at this size the anterior portion of the basioccipital starts to extend anteriorly and laterally as thin membranous projections. The relatively large size and complex morphology of the basioccipital at 4 mm suggests that it might have started to ossify before this stage but not prior to 3.3 mm (the earliest stage analyzed with no clue of ossified basioccipital). At 6.4 mm the anterior membranous portion of the basioccipital is quite advanced and the bone articulates posterodorsally with the posteroventral region of the exoccipital. Around 17.5 mm the basioccipital reaches the adult condition (Fig. 2F).

Exoccipital: The exoccipital starts to ossify perichondrally around 4 mm (Fig. 3A) but, as in the case for the basioccipital (see above), it may have begun earlier, somewhere between 3.3 and 4 mm. The exoccipital at 4 mm is well developed on the dorsoventral axis, almost covering the whole occipital arch. At 4.7 mm the exoccipital greatly expands toward its contralateral portion (Fig. 2B) and, at 6.4 mm, the area of the notochord is completely ossified. At 17.5 mm the exoccipital meets the supraoccipital (Fig. 3E) and, with 21.3 mm, the bone reaches the epioccipital, fully ossifying the occipital arch and resembling the adult condition (Fig. 3F).

Supraoccipital: The supraoccipital first appears at 4.7 mm as a thin perichondral dorsal line on what will be the base of the supraoccipital spine (Fig. 2B). At around 8 mm the ossification starts to expand anteriorly and laterally to both sides (Fig. 2C, 3B) and, by 8.9 mm, the expanded bone articulates with the parietal and frontal (Fig. 3C). At this stage almost the whole dorsal region of the *tectum synoticum* is ossified. At 17.5 mm the lateral projections meet the epioccipitals on each side and the spine is almost fully formed (Fig. 3E). The supraoccipital is fully ossified around 21.3 mm (Fig. 3F).

Mandibular Arch

Sequence of ossification: dentary, premaxilla, maxilla, and articular – angular, retroarticular, and coronomeckelian

Dentary: Along with the premaxilla and maxilla, the dentary is one of the earliest bones to ossify. The first clue of ossification is at 3.3 mm where the dermal bone starts to form dorsally to Meckel's cartilage (Fig. 1A). Due to the relative large size of the dentary at this size, the bone probably starts its ossification in an earlier stage. Apparently no teeth are present at 3.3 mm. At 4 mm the dentary ossifies ventrally until the ventral margin of Meckel's cartilage and some minute teeth are present (Fig. 4B). The coronoid process base has already begun to form. At 6.4 mm the teeth become more prominent (Fig. 4C) and, the coronoid process starts to expand dorsally. At 8.9 mm the dentary ventral margin trespasses the ventral limits of Meckel's cartilage. The dentary reaches the adult condition at 17.5 mm.

Premaxilla: The premaxilla is a dermal bone detected in the smallest examined individual, with 3.3 mm (Fig. 1A). However, that bone probably starts to ossify earlier judging by its relatively advanced degree of ossification at that stage. At 3.3 mm the premaxilla is more strongly stained anteriorly and gradually fading toward posterior, thus suggesting and anteroposterior direction of ossification. No teeth are present at this stage. At 4 mm the posterior tip of the premaxilla is almost reaching the angulo-articular and the first teeth are distinguishable (Fig. 4B). At 4.7 mm the anterior region of the premaxilla is almost fully formed and a dorsal projection is beginning to ossify. This projection is very conspicuous at 6.4 mm and, at around 8.9 mm, the premaxilla resembles its adult morphology (Figs. 4E, F).

Maxilla: The maxilla is detected in the earliest analyzed stage, around 3.3 mm, and possibly had started its ossification earlier (Fig. 1A). At this stage the bone is still a thin line of dermal ossification and its posterior tip has yet not started to ossify. At 4 mm the posterior ossification becomes broader (Fig. 4B) and, at 6.4 mm, the posterior end reaches the level of the coronomeckelian bone (Fig. 4C). At 8 mm the anterior region is almost fully ossified (Fig. 4D). By the time the larva reaches 8.9 mm the maxilla has the adult condition (Figs. 4E, F).

Angulo-articular: The articular also ossifies early in development, with the first signs of perichondral ossification observed at 3.3 mm, right on the articulation of Meckel's cartilage with the quadrate (Fig. 1A). At 4 mm the articular and angular ossifications already seem to be fused (Fig. 4B). At this stage the angulo-articular is mostly dorsal to Meckel's cartilage and the posteroventral region of the compound bone is starting to expand ventrally towards the retroarticular. At 8 mm that posteroventral region reaches the retroarticular and starts to project anteriorly (Fig. 4D). At 8.9 mm the angulo-articular resembles the adult condition, except for a small hiatus between this bone and the dentary.

Retroarticular: The retroarticular starts to ossify at 4 mm as a small dot of chondral ossification on the posteroventral tip of Meckel's cartilage, right on the attachment site of interoperculo-mandibular ligament (Fig. 4B). Ossification expands dorsally until it reaches the angulo-articular that is expanding downward. The two structures meet at 8 mm and then the retroarticular expands anteriorly until contacts the ventral margin of the anteroventrally enlarged angulo-articular (Fig. 4D). At 17.5 mm the retroarticular meets the angulo-articular along its total perimeter thus resembling its adult morphology.

Coronomeckelian: The coronomeckelian is a small tendon bone located on the posterior end of Meckel's cartilage that starts to ossify from the insertion site of the meckelian tendon of the *pars stegalis* of the *adductor mandibulae*. The first appearance of this bone is quite early in development, being unequivocally identified at 4 mm (Fig. 4B). Across the ontogeny the coronomeckelian does not change drastically, only increasing in size. The analyzed size that is more similar to the adult condition is at 13.3 mm (Fig. 4E).

Hyopalatine Arch

Sequence of ossification: quadrate, hyomandibular, symplectic, metapterygoid, and ectopterygoid – dermopalatine – endopterygoid – autopalatine

Quadrate: The quadrate starts to ossify perichondrally at 4 mm on the ventral portion of the palatoquadrate cartilage, more specifically at its articulation with the lower jaw (Fig 4B). The posterior margin of the quadrate is ossified as a thin line. Ossification expands dorsally and,

at 6.4 mm, almost half of the quadrate is mineralized (Fig. 4C). The anterior margin is ossified in its full length as a thin line, similarly to the condition of the posterior margin. At 8.9 mm the quadrate greatly resembles the adult morphology (Fig. 4E), missing only the interdigitating suture with the metapterygoid (a putative synapomorphy for the clade Polynemidae + Sciaenidae). The larger analyzed specimen was 32.8 mm and, at this stage, a minute prominence probably representing the beginning of the interdigitation between the quadrate and metapterygoid is starting to form. This interdigitation will be fully formed in later stages (Fig. 4F).

Hyomandibular: The hyomandibular first develops at 4 mm ventral to the foramen for the *nervus facialis* on the dorsal region of the hyosymplectic cartilage (Fig. 4B). The perichondral ossification expands ventrally towards the ossifying symplectic. At this stage the opercular condyle of the hyomandibular is starting to ossify as a pair of thin lines along its dorsal and ventral margins. The anterior lamina of membrane bone is also starting to form. At 4.7 mm the anterior lamina is much more developed and the ventral border of the hyomandibular reaches the ventral limit of the opercle. At 6.4 mm the *nervus facialis* foramen is completely surrounded by bone and the ventral boundary of the hyomandibular is almost fully ossified (Fig. 4C). The opercular condyle is still ossifying, although its dorsal and ventral margins are almost fully mineralized. Ossification then expands mainly dorsally towards the autosphenotic and pterotic. At 8 mm the anterior lamina of membrane bone meets the posterodorsal region of the palatoquadrate cartilage, where the metapterygoid is forming (Fig. 4D). At this size the dorsal region is fully formed, and only the distal tip of the opercular condyle is ossifying. Around 13.3 mm the hyomandibular reaches its adult condition (Fig 4E).

Symplectic: The symplectic first arises at 4 mm as a perichondral ossification on the ventral region of the hyosymplectic cartilage (Fig. 4B). The ossification expands toward the extremities of the bone. The ventral portion of the symplectic forms before the posterior end and, at 6.4 mm, it is almost complete (Fig. 4C). Ossification continues dorsally and, at 8.9 mm, the symplectic resembles that of adults (Fig. 4E).

Metapterygoid: The metapterygoid is possibly one of the first bones to ossify. It starts to ossify very early in development but ends this process only after several other bones are fully formed. The adult condition was actually not achieved in the largest specimen analyzed (32.8 mm; see the quadrate description). The first signs of ossification are at 4 mm, when the metapterygoid is a tiny perichondral dot on the posterodorsal region of the palatoquadrate cartilage (Fig. 4B). Ossification expands ventrally. At 4.7 mm the dot develops into a pair of lines on each side of the dorsal tip of the palatoquadrate cartilage, forming a chevron-like structure. At 6.4 mm ossifications starts to fill the area between the chevron arms, and only at 8 mm a small triangle of bone can be distinguished on the dorsal tip of the cartilaginous palatoquadrate (Fig. 4C, D). At 8.9 mm the metapterygoid is more robust and is starting to acquire its adult shape, ossified at the level of the dorsal limit of the symplectic. On the subsequent sizes the metapterygoid expands ventrally towards the quadrate. On the larger analyzed specimen (32.8 mm) the metapterygoid is still ossifying and lacks the interdigitation with the quadrate (Fig.4F).

Ectopterygoid: The ectopterygoid starts to ossify at 4 mm as a dermal thin line on the ventral margin of the anterior region of the palatoquadrate cartilage (Fig. 4B). The ectopterygoid might have started to ossify prior to 4 mm, because at this stage the bone is quite ossified along its anteroposterior axis, extending from the mid-portion of the dentary to the dorsal region of the angulo-articular. At around 6 mm the posterior end of the ectopterygoid articulates with the anterior margin of the quadrate whilst its anterior extremity meets the posterior portion of the dermopalatine (Fig. 4C). At 8 mm the ossification expands laterally from the palatoquadrate cartilage and towards the adjoining area of the endopterygoid and metapterygoid, making the ectopterygoid thicker. At this same size, the anterior tip of the ectopterygoid is moving farther dorsally towards the dermopalatine and, at 8.9 mm, there is almost no cartilaginous gap between the ectopterygoid and both the dermopalatine and endopterygoid. At 13.3 mm the first tooth appears on the anterior region of the ectopterygoid (Fig. 4E). At 32.8 mm the bone resembles that of adults.

Palatine (Dermopalatine + Autopalatine): The dermo- and autopalatine have different timings of ossification. Similar to the pterotic development, the dermal component of the

palatine arises earlier than its chondral portion. The dermopalatine first appears at 4 mm as a thin line paralleling the anteroventral margin of the palatoquadrate cartilage, just posterior to its curved tip (Fig. 4B). At 6.4 mm it starts to become thicker and already articulates posteriorly with the anterior tip of the ectopterygoid (Fig. 4C). At 8 mm the first tooth appears on the anterior region of the dermopalatine. At the same time, the autopalatine starts to ossify perichondrally on the dorsal region of the curved tip of the anterior region of the palatoquadrate cartilage (Fig. 4D). The ossification of the autopalatine expands quite rapidly and, at 8.9 mm, it is almost fully formed and articulate posteriorly with the anterior region of the dermopalatine. This bone still bears a single tooth at this stage but is expanding away from the palatoquadrate cartilage. At 13.3 mm more teeth are added to the dermopalatine (Fig. 4E) and, at 21.3 mm, the dermo- and autopalatine are fused into a single palatine (Fig. 4F).

Endopterygoid: The endopterygoid commences its ossification at 6.4 mm as a dermal line on the anterodorsal margin of the palatoquadrate cartilage, at the middle of the orbital cavity (Fig. 4C). At 8 mm the posterior region of the endopterygoid meets the growing metapterygoid, whereas the anterior tip is ossified at the level of the posterior region of the dermopalatine (Fig. 4D). Ossification continues on the anteroposterior axis but also medially from the palatoquadrate cartilage. At 8.9 mm the bone articulates with the ectopterygoid along all its extent and, at 13.3 mm, the endopterygoid achieves the adult condition (Fig. 4E).

Opercular series

The first unequivocal signs of ossification of all bones of the opercular series are observed at 4 mm. These bones are quite developed at this stage and thus they probably began to ossify earlier, somewhere between 3.3 mm (with no trace of opercular series) and 4 mm. Based on the degree of ossification observed at 4 mm, the most likely sequence of ossification would be: opercle – interopercle – preopercle – and subopercle

Opercle: At 4 mm the adductor crest is starting to ossify from the articulation between the opercle and hyomandibular (Fig. 4B). The anteroventral margin of the opercle is already articulating with the anterodorsal margin of the subopercle. Ossification is expanding

posteriorly. At 4.7 mm the ossification starts to develop also dorsally, above the adductor crest. At 8 mm the adductor crest is almost fully formed and both the ventral and dorsal margins of the opercle are still ossifying (Fig. 4D). At 8.9 mm the dorsal region is almost completely mineralized and only the posteroventral region of the opercle is still expanding towards the subopercle. The opercle reaches the adult condition at 13.3 mm (Fig. 4E).

Interopercle: The interopercle was first observed at 4 mm and at this stage the bone is quite developed (Fig. 4B). Its posterior region is already articulating with the subopercle whilst the anterior region is still expanding towards the ossifying retroarticular. The interoperculo-mandibular ligament is already present. Ossification is expanding anteriorly and away from the preopercle. At 8 mm the anterior tip of the interopercle reaches the level of the anterior tip of the preopercle (Fig. 4D) and, at 13.3 mm, it achieves the adult form (Fig. 4E).

Preopercle: The preopercle at 4 mm is ossified along the edge of the convex margin of the hyosymplectic cartilage, where its dorsal end is even with the ventral limits of the opercular condyle of the ossifying hyomandibular (Fig. 4B). Ossification of the preopercle expands towards the remaining opercular bones and, at 6.4 mm, the horizontal arm of the preopercle meets the anterodorsal region of the interopercle (Fig. 4C). At this stage, the ventral tip extended to the level of the ventral end of the symplectic. At 8 mm the larger spine of the posterior margin of the preopercle starts to form (Fig. 4D). Moreover, at this size the vertical arm of the preopercle reaches the anterior regions of the opercle and subopercle. At 8.9 mm the dorsal tip surpasses the opercular condyle of the hyomandibular, almost reaching the articulation site between this bone and the pterotic. At 13.3 mm the ventral membrane of the preopercle starts to be formed (Fig. 4E) and, at 17.5 mm, the remaining spines of the serrated margin are ossifying. At 21.3 mm the preopercle reaches the adult condition (Fig. 4F).

Subopercle: The subopercle is most likely the last bone to start ossification in the opercular series. At 4 mm the bone starts to form in between the opercle and interopercle (Fig. 4B). Ossification of the subopercle expands posteriorly and, at 8 mm, the posterior extent is almost complete along the opercle margin (Fig. 4D). From that size the subopercle maintains

its general shape and only increases in size. At approximately 13.3 mm the subopercle reaches the adult condition (Fig. 4E).

Hyoid Arch

Sequence of ossification: branchiostegal rays, anterior ceratohyal, and posterior ceratohyal – urohyal – ventral hypohyal – dorsal hypohyal and interhyal – basihyal

Branchiostegal rays: The branchiostegal rays almost certainly started their ossifications prior to 4 mm (first ossification documented) but after 3.40 mm (no branchiostegal rays detected). Judging by the degree of development of the seven rays, their formations might have started posteriorly on the seventh ray (the single ray articulating with the posterior ceratohyal) and proceeded anteriorly until the first one. At 4 mm only the first three rays are poorly ossified, specially the first two (Fig. 5A). At 8.9 mm all branchiostegal rays are ossified and have the adult shape (Fig. 5C).

Anterior ceratohyal: The anterior ceratohyal is ossifying perichondrally at 4 mm, but this process may have started earlier. At this size, the anterior ceratohyal is ossifying approximately from its center, at the narrower portion of the ceratohyal cartilage (Fig. 5A). Ossification irradiates along the anteroposterior axis, at the same time that a lamellar outgrowth is forming ventrally. At 4.7 mm the ventral membrane bone is well developed into a triangular blade. Moreover, at this size the interdigitation between the ceratohyals is starting to form. At 6.4 mm almost the whole anterior, narrow portion of the anterior ceratohyal is ossified while its broader, posterior portion is almost still ossifying ventrally (Fig. 5B). At this same stage, the strong interdigitation between anterior and posterior ceratohyals are completely formed. At 13.3 mm the anterior ceratohyal resembles that of adults (Fig. 5D).

Posterior ceratohyal: The posterior ceratohyal starts to ossify at 4 mm on the posterodorsal region of the ceratohyal cartilage as a pair of perichondral dots (Fig. 5A). Ossification expands anteriorly towards the ossifying anterior ceratohyal. At 6.4 mm the first interdigitation with the posterior ceratohyal appears (Fig. 5B). At 8 mm the posteriormost

region of the posterior ceratohyal, where it articulates with the interhyal, is fully ossified (Fig. 5C). Ossification is still expanding anteroventrally. At 13.3 mm the posterior ceratohyal reaches the adult morphology (Fig. 5D).

Urohyal: The urohyal is a tendon bone that starts to ossify around 6.4 mm on the insertional tendon for the *sternohyoideus*, which at this stage attaches itself to the anteroventral end of the ceratohyal cartilage (Fig. 5B). Ossification expands posteriorly and, at 8.9 mm, the dorsal flange of the urohyal is well developed giving the bone its typical triangular shape in lateral view (Fig. 5C). At this size, the lateral projections of its ventral margin are in place and will grow in thickness along the development. At 17.5 mm the urohyal resembles that of adults (Fig. 5D).

Ventral hypohyal: The ventral hypohyal starts ossification at 6.4 mm as a small perichondral dot on the anteroventral margin of the ceratohyal cartilage (Fig. 5B). At 8 mm the ventral hypohyal is expanding posterodorsally. At 8.9 mm the dorsal limits of the ventral hypohyal align with the anterodorsal margin of the anterior ceratohyal, while its ventral border meets the first branchiostegal ray and the anterior ceratohyal (Fig. 5C). At 13.3 mm the dorsal region articulates with the anterior ceratohyal and, at 17.5 mm, the ventral projection seems to articulate with the anteroventral margin of the anterior ceratohyal. At this size the ventral hypohyal achieves the adult morphology (Fig. 5D).

Dorsal hypohyal: The dorsal hypohyal starts ossifying at 8 mm as a thin perichondral line on the triangular process of the anterodorsomedial surface of the ceratohyal cartilage. Ossification expands laterally and ventrally. At 8.9 mm the triangular process is practically fully ossified and, in the following stages, the dorsal hypohyal continues to increase in size towards the ventral hypohyal (Fig. 5C). At 32.8 mm the dorsal hypohyal resembles that of adults.

Interhyal: The interhyal starts to ossify perichondrally at 8 mm (not illustrated) on the mid-portion of the bone. Ossification expands rapidly towards the extremities and, at 8.9 mm,

the interhyal is fully ossified, except for its dorsal and ventral tips that remained cartilaginous (Fig. 5C).

Basihyal: The basihyal is the last bone to start ossification in the hyoid arch. The first signs of perichondral formation are observed at 8.9 mm on the posterior region of the basihyal cartilage (Fig. 5C). Ossification expands anteriorly. At 13.3 mm half of the anterior copula is ossified and, at 17.9 mm it reaches the adult condition, leaving a small anterior pad of cartilage (Fig. 5D).

Branchial Arches

Several bones from the branchial arches probably start to ossify earlier than in their first record at 4 mm. At this stage such bones are already quite developed, whereas at the immediately earlier stage, 3.3 mm, there is no sign of ossification. Thus many of these branchial bones might have begun to ossify in stages intermediate between these boundaries.

Sequence of ossification: tooth plates associated with ceratobranchial 5, pharyngobranchials 2 and 3, and pharyngobranchial 4 cartilage; ceratobranchials 1 to 5, gill rakers; epibranchials 1 to 4; and basibranchial 3 – hypobranchials 1, 2, and 3 – basibranchial 2 – basibranchial 1 and pharyngobranchial 1

Pharyngeal jaws: The pharyngeal jaws consist of dermal tooth plates associated with pharyngo- and ceratobranchials. The upper pharyngeal jaw comprises pharyngobranchials 2, 3, and 4, whereas the lower pharyngeal jaw comprises ceratobranchial 5. At 4 mm the tooth plate of ceratobranchial 5 is well developed and contains approximately four teeth (Fig. 6A). The tooth plates of the pharyngobranchials are similarly well developed, but less ossified than their ventral counterpart. The tooth plate of pharyngobranchial 3 is the larger one, with about four teeth (Fig. 7A). The plates associated with pharyngobranchial 4 and 2 bear, respectively, one and two teeth. The number of teeth gradually increases along the following stages. At 4.7 mm the tooth plate of ceratobranchial 5 almost double its teeth count (Fig. 6B) and, at 8 mm, the pharyngobranchial 3 tooth plate starts to expand towards the pharyngobranchial 2 tooth plate (Fig. 7C). At 8.9 mm these two tooth plates are articulating

with each other (Fig. 7D). At 17.5 mm the tooth plate of pharyngobranchial 4 exceeds the number of teeth present on the pharyngobranchial 3 plate and, at 17.9 mm, all tooth plates aforementioned achieve their adult condition (Fig. 7E).

Ceratobranchials: All the ceratobranchials are already in formation at 4 mm (Fig. 6A) and, judging by their degree of ossification, their most likely sequence of ossification would be: ceratobranchial 4 – ceratobranchial 1 – ceratobranchial 2 – ceratobranchial 3 – ceratobranchial 5. The perichondral ossification starts on the central portion of each ceratobranchial and expands along the anteroposterior axis and inside of each ceratobranchial during the development. At 4.7 mm ceratobranchial 4 is almost fully ossified on its anteroposterior extent (Fig. 6B). At this stage ceratobranchials 2 and 3 become thicker and acquire emergent membranous expansions. At 8.9 mm all five ceratobranchials reach the adult condition (Fig. 6E).

Gill rakers: At 4 mm the gill rakers can be seen as a sequence of small dots along the lateral margins of ceratobranchials 1 and 2 (Fig. 6A). At 4.7 mm the numbers of raker rudiments increase on the mentioned ceratobranchials and the first gill rakers of ceratobranchial 3 appear (Fig. 6B). Moreover, the gill rakers of ceratobranchial 1 start to get longer and the first gill rakers on the epibranchial 1 appear. At 6.4 mm the gill rakers of ceratobranchial 2 start to present teeth (Fig. 6C). At 8 mm the first gill rakers on the medial surface of ceratobranchials 1, 2, and 3, as well as the first gill rakers on the lateral surface of ceratobranchial 4, appear (Fig. 6D). At the same stage, epibranchial 2 presents its first gill rakers and, at 8.9 mm, gill rakers appear on epibranchial 3 and hypobranchials 1 and 2 (Fig. 6E). At 13.3 mm gill rakers start to develop on the third hypobranchials. At 17.5 mm the gill rakers of the first three ceratobranchials are very well developed and the medial surface of the fourth ceratobranchial starts to get its first gill rakers. At 17.9 mm all the gill rakers achieve the adult condition (Fig. 6F).

Epibranchials: All epibranchials are in process of ossification at 4 mm (Fig. 7A) and, judging by their degree of ossification, their probable sequence of ossification would be: epibranchial 1 - epibranchial 2 - epibranchial 3 - epibranchial 4. These ossifications start

perichondrally on the posterior end of each epibranchial cartilage, where they articulate with their respective ceratobranchials. Ossification then expands medially towards the pharyngobranchials. At 8 mm almost the whole body of each epibranchial is ossified (Fig. 7C) and, at 8.9 mm, they resemble the adult condition (Fig. 7D).

Basibranchials: The first basibranchial to appear is the third. At 4.7 mm it starts as a perichondral ossification on the posterior region of the anterior copula (Fig. 6B). Ossification then expands anteroposteriorly and laterally. At 8 mm the anterior region of basibranchial 3 reaches the posterior limits of hypobranchial 2, while the posterior end of the former bone aligns with the posterior end of hypobranchial 3 (Fig. 6D). At this stage lateral projections of membrane bones start to develop in basibranchial 3 and basibranchial 2 begins to ossify perichondrally on the mid-portion of the anterior copula, between the first and second ossifying hypobranchials (Fig. 6D). At 8.9 mm the anterior region of basibranchial 3 reaches the mid-portion of hypobranchial 2, a condition similar to that found on basibranchial 2, where its anterior end is aligned with the mid-portion of hypobranchial 1 (Fig. 6E). At this size, the first basibranchial starts to ossify perichondrally on the anterior region of the anterior copula. At 13.3 mm basibranchials 2 and 3 reach the adult condition (Fig. 6F). Basibranchial 1 is still ossifying in the largest specimen analyzed (32.8 mm).

Hypobranchials: hypobranchials 1 and 2 start to ossify perichondrally at 4.7 mm (Fig. 6B). The first hypobranchial starts to form as a thin line on the posterior margin of the hypobranchial 1 cartilage. The second hypobranchial starts ossifying, on the right side, as a couple of lines along the anterior and posterior margins of hypobranchial 2 cartilage; on the left side there is a thin line of ossification along the anterior margin of that cartilage. At 6.4 mm these ossifications expand towards their respective ceratobranchials, while the third hypobranchial starts to ossify as an extremely thin line of bone on the right counterpart only (Fig. 6C). At 8 mm more than half of each hypobranchials have ossified (Fig. 6D). At 8.9 mm all three hypobranchials reach the adult condition (Fig. 6E).

Pharyngobranchials: At 4 mm pharyngobranchial 3 starts to ossify anterior to the respective tooth plate (Fig. 7A). At 8 mm, pharyngobranchial 3 is further ossified, moving anteriorly

towards the second tooth plate, whereas pharyngobranchial 2 starts to ossify (Fig. 7C). Pharyngobranchial 1 starts to ossify perichondrally at 8.9 mm on the center of the pharyngobranchial 1 cartilage while the third pharyngobranchial is already in contact with the tooth plate associated with pharyngobranchial 2 (Fig. 7D). At 17.5 mm, most of the body of pharyngobranchial 1 is already ossified and pharyngobranchial 2 is fully ossified. At 17.9 mm pharyngobranchial 1 is fully formed, with only two small remnants of cartilage on its tips (Fig. 7E). The fourth pharyngobranchial remain cartilaginous on the adult.

Pectoral girdle

Sequence of ossification: cleithrum – supracleithrum, postcleithrum 1, postcleithrum 2, posttemporal – scapula, coracoid, pectoral radial 1, and pectoral-fin rays – pectoral filaments – pectoral radial 2 and propterygium – pectoral radial 3 and 4

Cleithrum: The cleithrum is one of the first bones to ossify. It is detected in the smallest analyzed size, at around 3.3 mm (Fig. 1A), and possibly has started to form earlier. At this size the dermal ossification is just a splint of bone extending from the level of the neurocranial floor to the level of the ventral limits of the branchial arches. At 4 mm the cleithrum starts to become thicker, especially at its dorsal region close to the articulation with postcleithrum 1 (Fig. 8A). At 8 mm the posterodorsal lamellar flange is well developed whereas the lateral projection starts to form (Fig. 8C). At 8.9 mm the dorsal portion of the bone is almost fully ossified and the ventral tip starts to bend ventrally to form the ventral process of the cleithrum (Fig. 8D). At 17.5 mm the lateral projection that houses several lateral pectoral muscles is fully formed and, at 21.3 mm, the ventral process is fully formed and the cleithrum resembles that of the adults (Fig. 8F).

Supracleithrum: The supracleithrum commences its ossification at 4 mm as a thin splint of bone and, at this stage, the bone already overlaps laterally the dorsal region of the cleithrum (Fig. 8A). At 4.50 mm the ventral tip of the supracleithrum is at the same level of the first vertebral centrum and, at 5.40 mm, this ventral tip surpasses ventrally the vertebral column. At 5.7 mm the ventral tip extends beyond the posterodorsal border of the cleithrum and, at

7.9 mm, the posterior expansion of the supracleithrum proceeds while the bone forms its anterior ridge (Fig. 8C). At 17.9 mm the supracleithrum achieves the adult condition (Fig. 8F).

Postcleithrum 1: The first postcleithrum starts to ossify at 4 mm as a thin dermal line medially to the pectoral girdle (Fig. 8A). The anterior tip already articulates with the posterodorsal region of the cleithrum. At 4.7 mm postcleithrum 1 becomes longer and, only at 8.9 mm, the posterior lamella starts to develop. At 13.3 mm postcleithrum 1 is almost fully ossified (Fig. 8E), achieving the adult condition at 17.5 mm.

Postcleithrum 2: The second postcleithrum starts to ossify at the same time of postcleithrum 1. At 4 mm postcleithrum 2 is a dermal thin line where its dorsal tip is at the level of the ventral tip of postcleithrum 1 (Fig. 8A). At this size, postcleithrum 2 is still a short splint of bone, not surpassing the pectoral radial plate. At 4.7 mm the bone becomes longer, trespassing the posterior limits of the pectoral-fin rays. At 8.9 mm postcleithrum 2 is well expanded, reaching the pelvic fin and, at 17.9 mm, the ossification is much thicker and resembles the adult morphology.

Posttemporal: The posttemporal starts to ossify at 4 mm as a dorsal dermal splint corresponding to the future dorsal arm of the bone. Ossification expands dorsally to the tip that articulates with the epioccipital and ventrally to the posteriormost region of the bone where it bifurcates into dorsal and ventral arms. At 4.7 mm the dorsal arm of the posttemporal is almost fully formed (Fig. 2B) and, at 5.7 mm, the ventral arm of the bone starts to ossify towards the intercalar. At 8.9 mm the ventral arm is almost fully ossified (Fig. 2D) and, at 13.3 mm, the ossified laterosensory canal appears laterally to the posttemporal (Fig. 2E). At 17.9 mm this canal fuses with the main body of the posttemporal, thus acquiring the condition found in adults (Fig. 2F).

Scapula: At 8 mm the scapula starts to ossify perichondrally on the posterodorsal region of the scapulocoracoid cartilage, dorsal to the scapular foramen where the first pectoral-fin ray articulates (Fig. 8C). Ossification expands anteroventrally and, at 8.9 mm, almost half of the

pars scapularis of the scapulocoracoid cartilage is ossified (Fig. 8D). At 13.3 mm the whole foramen is surrounded by bone (Fig. 8E) and at 17.5 mm the scapula resembles that of adults (Fig. 8F).

Coracoid: The coracoid commences its ossification at 8 mm as an extremely thin perichondral splint of bone on the anteroventral region of the scapulocoracoid cartilage, along the posterior margin of the cleithrum-coracoid fenestra (Fig. 8C). At 8.9 mm most of the ventral portion of the coracoid is ossified and ossification expands posterodorsally towards the scapula (Fig. 8D). At 13.3 mm the coracoid is almost fully ossified and the ventral projection of membrane bone starts to form medial to the fourth ossifying pectoral radial (Fig. 8E). At this same size, the first coracoid foramen appears. The ventral and dorsal portions of the coracoid meet the cleithrum at 17.5 mm and, at 17.9 mm, the coracoid reaches the adult condition, leaving a cartilaginous block in between the coracoid and scapula (Fig. 8F).

Pectoral radials: The pectoral radials have very distinct ossification timings during the ontogeny. All four pectoral radials begin to develop as a single cartilaginous pectoral radial plate visible at 4 mm (Fig. 8A). At around 4.6 mm the pectoral radial plate starts to divide itself to form each pectoral radial cartilage (Fig. 8B). The single pectoral radial plate first divides into a dorsal and a ventral subplate that will form the cartilages of pectoral radial 1-2 and 3-4, respectively. At this stage the cartilages of pectoral radials 1 and 2 start to separate from each other, whereas the ventral sub plate remains undivided. At approximately 8 mm, all four pectoral radials cartilages are distinguishable from one another and the first one starts to ossify along the anterior region of the cartilage, at its articulation with the scapulocoracoid cartilage (Fig. 8C). At this stage, the pectoral radial 3 cartilage starts to tilt and shift from horizontal to a more vertical position, and pectoral radial 4 starts to enlarge to support the pectoral filaments. At 8.9 mm almost the whole body of pectoral radial 1 is ossified, while the second pectoral radial starts to ossify on the anterodorsal region of its cartilage (Fig. 8D). At 13.3 mm the first pectoral radial cartilage is completely replaced by bone, whereas the second one is almost finishing its ossification (Fig. 8E). The third and the fourth pectoral radials start to ossify on their anterior regions, where they articulate with the

scapulocoracoid cartilage. At this same stage the third pectoral radial still supports the ventralmost pectoral-fin rays. At 17.5 mm the second pectoral radial achieves the adult condition while the two ventralmost radials are ossified along half of their extents. At this size, the third radial ceases to support any pectoral-fin ray or pectoral filament. At 17.9 mm the fourth pectoral radial form its first foramen and, at 32.8 mm, the third and fourth pectoral radial achieve a condition similar to the adult morphology. They probably ossify a little more in the subsequent stages of the ontogeny.

Pectoral-fin rays & pectoral filaments: The pectoral-fin rays start to ossify at around 8 m (Fig. 8C). Ossification starts on the uppermost fin ray and proceeds ventrally. At this stage no pectoral-fin rays have ossified to their total length, but almost all of them have started to ossify near the articulation with the pectoral radials. The ventralmost pectoral-fin rays start to migrate ventrally along with the fourth radial, marking the beginning of their differentiation into pectoral filaments. The early filaments are thicker and shorter than the pectoral rays. At 8.9 mm only the two ventralmost pectoral-fin rays are lightly ossified, whereas all remaining dorsalmost rays are well mineralized (Fig. 8D). At this size the pectoral filaments start to ossify from their bases towards their tips. At 13.3 mm the pectoral filaments reach the pectoral-fin rays length (Fig. 8E) and, at 17.5 mm, they trespass the posterior limit of the pectoral-fin rays. At 21.3 mm all pectoral-fin rays and pectoral filaments are fully ossified (Fig. 8F).

Propterygium: The propterygium starts to ossify at 8 mm on the posterior region of the propterygium cartilage (Fig. 8C). At 13.3 mm the propterygium is almost fully ossified and seems to fuse to the medial hemitrichium of the first pectoral-fin ray (Fig. 8E).

Supraneurals

The first and second supraneural cartilages first appear at 13.3 mm (Fig. 9A) and at 17.5 mm the third supraneural cartilage appears and already starts to ossify, as the second supraneural (Fig. 9B). Both ossifications occur from the dorsal region of each supraneural cartilage. At 17.9 mm the first supraneural starts to ossify while the second one is almost fully ossified (Fig. 9C). At 21.3 mm supraneural 2 is complete with only a small ventral

cartilaginous pad and the third supraneural is almost fully mineralized. At this size the first supraneural is nearly half ossified (Fig. 9D).

Vertebral column

The first signs of ossification of the vertebral column are visible on the first three centra on a 4 mm specimen (Fig. 1B, 10A). In this stage, the first two centra are already quite developed and centra 3 is starting to ossify from its dorsal region, close to the neural arch base. At 4.5 mm ossification continues posteriorly through the vertebrae and ventrally on each centra (Fig. 1C, 10B). Furthermore, in this stage, it is possible to observe that centra 4 follows the same pattern described for centra 3. At 5.4 mm almost the whole vertebral column is ossified, lacking only its posterior tip, preural centrum and urostyle (Fig. 1D). At 7.94 mm the whole vertebral column is formed (Fig. 1E) and achieves the adult condition at 13.3 mm (Fig. 1F). Ribs are formed only at 21.3 mm (Fig. 1H).

4. DISCUSSION

Ontogenetic studies are powerful tools to unravel homologies and provide novel morphological information for phylogenetic analyses (Britz and Johnson, 2002; 2005; Britz and Conway, 2009; Johnson *et al.*, 2009; Britz and Johnson, 2012; Johnson and Schnell, 2015; Kubicek and Conway, 2016). Ontogenetic studies usually focus on particular regions of the skeleton, such as neurocranium or axial skeleton, for example (Jardim and Santos, 1994; Adriaens and Verraes, 1998; Faustino and Power, 1999; Geerinckx *et al.*, 2005; 2007; Block and Mabee, 2012; Cardeira *et al.*, 2012). Nonetheless, there are few studies reporting full skeleton development of a given species. Up to date, there are only reports on *Danio rerio* (Cubbage and Mabee, 1996; Bird and Mabee, 2003; Britz and Conway, 2009), *Cheilopogon doederleinii* (Dasilao Jr and Yamaoka, 1998), *Salminus brasiliensis* (Mattox *et al.*, 2014), and *Sciaenops ocellatus* and *Cynoscion nebulosus* (Kubicek and Conway, 2016) that comprise the development of the whole skeleton.

The few studies on the early development of polynemids address only their external morphology (Kowtal, 1972; Moser *et al.*, 1984; Moser, 1996; Leis and Carson-Ewart, 2000; Richards, 2005) and larval behavior, physiology, and swimming performances (Santerre and May, 1977; Leis *et al.*, 2007; Leis, 2010). A complete survey on the skeletogenesis in polynemids has never been undertaken until the present study.

In general, the skeletal development of polynemids is a quite fast process in which almost all analyzed bony structures are present at around 9.0 mm (except the basisphenoid and pectoral radials 3 and 4; Fig. 1). In our analysis, the first signs of ossifications in polynemids are observable in 3.3 mm specimens (Fig. 1A), in which the cleithrum, maxilla, premaxilla, dentary, and articular have commenced to ossify. In the sciaenid *Sciaenops ocellatus*, the first bones to appear are the cleithrum, maxilla, anterior ceratohyal, dentary, opercle, and parasphenoid (Kubicek and Conway, 2016). Other perciforms (Dasilao Jr and Yamaoka, 1998) and even some distantly related ostariophysans (Mattox *et al.*, 2014), similarly have the cleithrum and jaw bones among the earliest elements to ossify. On the other hand, in *D. rerio* the first elements to ossify are the cleithrum, ceratobranchial 5,

opercle, and parasphenoid whilst the mandibular bones ossify later in development (Cubbage and Mabee, 1996; Bird and Mabee, 2003). This later ossification of the jaw apparatus in *D. rerio*, in comparison to the development of other teleosts might be related to the fact that premaxilla, maxilla, and dentary are toothless in all cypriniforms (Mattox *et al.*, 2014).

In contrast, the latter elements to start ossification in polynemids are the basisphenoid and the pectoral radials 3 and 4 at 17.50 mm and 13.30 mm, respectively (Figs. 2F, 8E). In the sciaenids *Sciaenops ocellatus* and *Cynoscion nebulosus* the basisphenoid also starts to ossify later, being one of the last bones to appear in development and, although pectoral radials 3 and 4 ossify earlier than some infraorbitals and some laterosensory canal ossifications not analyzed herein, they are the next two last elements to ossify (Kubicek and Conway, 2016). Jardim and Santos (1994) documented a slightly different pattern in the neurocranium of the sciaenid *Micropogonias furnieri*. According to the authors, the nasal and pterosphenoid were the last elements to start ossification whereas the basisphenoid ossified simultaneously with the autosphenotic and prootic. The two latter ossifications are among the earliest bones to appear in the *S. ocellatus* and *C. nebulosus* (Kubicek and Conway, 2016).

Cardeira *et al.* (2012) pointed out that in *Argyrosomus regius* (Sciaenidae) the first four vertebral centra start to ossify dorsally, close to their associated neural arches. Kubicek and Conway (2016) found this same pattern in *Sciaenops ocellatus* and *Cynoscion nebulosus* and named this type of ossification as a “saddle-like ossification” around the notochord and suggested that this type of ossification in vertebral centra 1-4 was conserved across Sciaenidae that is not commonly found elsewhere. Interestingly, a similar ossification pattern seems to be present in polynemids (Fig. 10). In one of the smallest analyzed specimens, with approximately 4 mm, it is possible to observe that centra 1 and 2 are well ossified whereas centrum 3 is starting to ossify exactly from its neural arch base as described for those three sciaenids. If this saddle-like ossification of the anteriormost vertebral centra proved to be widespread across Polynemidae, this condition might be an ontogenetic evidence supporting the closes relationship between polynemids and sciaenids.

Furthermore, Polynemidae and Sciaenidae are known to have a medial interdigitation connecting the quadrate and metapterygoid (Sasaki, 1989; Johnson, 1993; Kang *et al.*, 2017) and this intimate contact between bones is a characteristic that appear later in their development. Kubicek and Conway (2016) reported that 12.9 mm specimens of *Sciaenops ocellatus* present their quadrate and metapterygoid almost fully ossified and around 25.3 mm these bones have completely replaced the quadratometapterygoid portion of the palatoquadrate cartilage and yet no interdigitation have appeared. The interdigitation was only seen in specimens with approximately 43.2 mm although apparently not fully formed. The larger polynemid analyzed herein (32.8 mm) has the metapterygoid still ossifying and lacking an interdigitation with the quadrate (Fig. 4F). Therefore, the quadrate-metapterygoid contact might occurs in latter stages as in sciaenids.

In the examined polynemids, both the appearance of the first cartilages as the first ossifications of the supraneurals occur relatively later in the development, at 13.3 and 17.5 mm specimens, respectively (Figs. 9A, B). The delayed ossification of supraneurals in polynemids was not reported in *Sciaenops ocellatus* by Kubicek and Conway (2016). The first sign of presence of supraneural 1 and 2 cartilages in that sciaenid is at 5.1 mm specimens, while the third supraneural cartilage appears on 5.9 mm specimens. Although in the analyzed polynemids the first supraneural cartilages arise only on 13.3 mm specimens, the first two appear earlier than the third cartilage, as in *S. ocellatus*. In this sciaenid, the supraneural ossifications occur in following the sequence: supraneural 3 (8.3 mm), supraneural 2 (8.9 mm), and supraneural 1 (10 mm). In *C. nebulosus*, supraneural 2 starts to ossify (8.9 mm) prior to supraneural 3 (9.5 mm), while supraneural 1 is still the last one (20.8 mm). In our polynemids, supraneurals 2 and 3 started to ossify at the same time (17.5 mm) followed by the ossification of supraneural 1 (at 17.9 mm). At 17.9 mm (Fig. 9C) it is possible to see that supraneural 2 is far more developed in 17.9 mm specimen, suggesting that the polynemid probable sequence is 2>3>1. In any event, in both polynemids and sciaenids, supraneural 3 cartilage is the last one to appear and supraneural 1 is the last one to start its ossification. Contrastingly, Fritzsche and Johnson (1980) reported that in *Morone americana* and *M. saxatilis* (Moronidae, Perciformes) the supraneurals sequence of ossification follows

an anteroposterior path, where supraneural 1 ossifies first, followed by supraneural 2 and finally supraneural 3.

The pectoral-fin development is rather conservative among teleosts, in which the cleithrum is usually the first bony element to start ossification followed by supracleithrum, posttemporal and usually followed by the pectoral-fin rays (developing dorsoventrally), coracoid, scapula, mesocoracoid (if present), postcleithrum, and finally the pectoral proximal radials (Okiyama, 1981; Cubbage and Mabee, 1996; Dasilao Jr and Yamaoka, 1998; Faustino and Power, 1999; Mattox *et al.*, 2014; Kubicek and Conway, 2016). This pattern in known to have changed in the flying fish *Cheilopogon doederleinii* (Exocoetidae, Beloniformes). In this taxon, the pectoral-fin rays start to ossify earlier than the posttemporal and supracleithrum while all pectoral radials ossify almost at the same time as the coracoid and scapula (Dasilao Jr and Yamaoka, 1998). Such changes in the ossification timing are possibly related to accelerated formation of largely expanded pectoral fins that allow the gliding of these fishes in relatively earlier stages of the development (Dasilao Jr and Yamaoka, 1998). Yet, the pectoral radials of *C. doederleinii* ossify following a dorsoventral sequence (Dasilao Jr and Yamaoka, 1998).

This dorsoventral sequence of ossification of the pectoral radials (*i.e.* pectoral radial 1 is the first element to ossify whilst the fourth radial is the last one) is present in the most varied teleost lineages, such as *Danio rerio* (Cyprinidae, Cypriniformes; Cubbage and Mabee, 1996), *Sparus aurata* (Sparidae, Perciformes; Faustino and Power, 1999), *Salminus brasiliensis* (Bryconidae, Characiformes; Mattox *et al.*, 2014), and *Sciaenops ocellatus* and *Cynoscion nebulosus* (Sciaenidae, Perciformes; Kubicek and Conway, 2016). Moreover, this dorsoventral sequence of ossification occurs relatively fast. Cubbage and Mabee (1996) documented that in *D. rerio* the first pectoral radial starts to ossify in 8.0 mm specimens while the fourth starts to ossify in 9.2 mm specimens. Mattox *et al.* (2014) reported an interval of only 2 mm between the onset of ossification of the first and the fourth pectoral radial in *Salminus brasiliensis*. The same interval is also reported for the sciaenids *S. ocellatus* and *C. nebulosus* (Kubicek and Conway, 2016). Faustino and Power (1999) did not specified the separated timings of ossification for each proximal radial of *Sparus aurata*, stating only that the radials first appearance occurs on 10.5 mm and that they ossify dorsoventrally.

However, judging by their Fig. 1h (p. 1099), the difference in the ossification timing between radials 1 and 4 is very small. Contrastingly, the difference between the onset of ossification between radial 1 and 4 in polynemids is comparatively larger than in the other known teleosts (Fig. 8). The first pectoral radial starts to ossify in 7.94 mm specimens whereas the fourth radial starts its ossification around 13.30 mm, leaving an interval of 5.36 mm between these ossifications. This extended timing of radial ossification is probably related to the unique conformation of the polynemid pectoral skeleton in which the two ventralmost radials become mostly or entirely disassociated with the unmodified pectoral-fin rays. During the ontogeny, the third pectoral radial shifts from its original position to reach the adult condition, *i.e.* the distal portion which normally articulates with the pectoral distal radials (and consequently with the pectoral-fin rays), moves anterodorsally until it reaches the ventral portion of pectoral radial 2. The same occurs with the proximal region, which normally articulates with the scapulocoracoid, moves posteroventrally to articulate with the dorsal region of the enlarged fourth pectoral radial. As aforementioned, pectoral radial 4 is greatly enlarged in comparison with the other radials and this enlargement occurs almost at the same time as the shifting in position of the third radial.

5. CONCLUSIONS

Polynemids certainly present very distinct characteristics in the adult morphology, especially regarding their pectoral girdle, and the ontogeny of these unique morphological specializations has never been described. The study of a developmental series of threadfins larvae reveals ontogenetic patterns behind the formation of such specializations, such as the relatively slow sequence of ossifications of the pectoral radials, the shifting of radials 3 and 4 and the differentiation of the ventralmost pectoral rays into the tactile filaments that have vital functions during the threadfin life, such as foraging and avoiding predators. The late development of supraneurals of polynemids also possibly represents a unique pattern within Teleostei. The saddle-like pattern of ossifications in the first four vertebral centra is apparently only found in polynemids and sciaenids and this shared character may constitute an additional evidence of a closer relationship among these families.

REFERENCES

ADRIAENS, D.; VERRAES, W. Ontogeny of the osteocranium in the African catfish, Clarias gariepinus Burchell (1822)(Siluriformes: Clariidae): ossification sequence as a response to functional demands. **Journal of Morphology,** v. 235, n. 3, p. 183-237, 1998. ISSN 0362-2525.

ARRATIA, G.; SCHULTZE, H. P. Palatoquadrate and its ossifications: development and homology within osteichthyans. **Journal of morphology,** v. 208, n. 1, p. 1-81, 1991. ISSN 0362-2525.

BIRD, N. C.; MABEE, P. M. Developmental morphology of the axial skeleton of the zebrafish, Danio rerio (Ostariophysi: Cyprinidae). **Developmental dynamics: an official publication of the American Association of Anatomists,** v. 228, n. 3, p. 337-357, 2003. ISSN 1058-8388.

BLOCK, A.; MABEE, P. Development of the mandibular, hyoid arch and gill arch skeleton in the Chinese barb Puntius semifasciolatus: comparisons of ossification sequences among Cypriniformes. **Journal of fish biology,** v. 81, n. 1, p. 54-80, 2012. ISSN 1095-8649.

BRITZ, R.; CONWAY, K. Osteology of Paedocypris, a miniature and highly developmentally truncated fish (Teleostei: Ostariophysi: Cyprinidae). **Journal of Morphology,** v. 270, n. 4, p. 389-412, 2009. ISSN 0362-2525.

BRITZ, R.; JOHNSON, G. D. “Paradox lost”: skeletal ontogeny of Indostomus paradoxus and its significance for the phylogenetic relationships of Indostomidae (Teleostei, Gasterosteiformes). **American Museum Novitates**, p. 1-43, 2002. ISSN 0003-0082.

BRITZ, R.; JOHNSON, G. D. Leis' conundrum: Homology of the clavus of the ocean sunfishes. 1. Ontogeny of the median fins and axial skeleton of Monotrete leiurus (Teleostei, Tetraodontiformes, Tetraodontidae). **Journal of Morphology,** v. 266, n. 1, p. 1-10, 2005. ISSN 0362-2525.

BRITZ, R.; JOHNSON, G. D. Ontogeny and homology of the skeletal elements that form the sucking disc of remoras (Teleostei, Echeneoidei, Echeneidae). **Journal of Morphology,** v. 273, n. 12, p. 1353-1366, 2012. ISSN 0362-2525.

CARDEIRA, J. et al. Osteology of the axial and appendicular skeletons of the meagre Argyrosomus regius (Sciaenidae) and early skeletal development at two rearing facilities. **Journal of Applied Ichthyology,** v. 28, n. 3, p. 464-470, 2012. ISSN 0175-8659.

CUBBAGE, C. C.; MABEE, P. M. Development of the cranium and paired fins in the zebrafish Danio rerio (Ostariophysi, Cyprinidae). **Journal of Morphology,** v. 229, n. 2, p. 121-160, 1996. ISSN 1097-4687.

DASILAO JR, C. J.; YAMAOKA, K. Osteological and functional development of the flyingfish, Cypselurus heterurus doederleini (Teleostei: Exocoetidae). **Bulletin of Marine Sciences and Fisheries, Kochi University,** v. 18, p. 13-26, 1998. ISSN 0387-9763.

DE SYLVA, D. Polynemoidei: development and relationships. In: MOSER, H. G.;RICHARDS, W. J.*, et al* (Ed.). **Ontogeny and systematics of fishes**. Lawrence, Kansas: American Society of Ichthyologists and Herpetologists, v.Special Publication 1, 1984. p.540-541.

FAUSTINO, M.; POWER, D. Development of the pectoral, pelvic, dorsal and anal fins in cultured sea bream. **Journal of Fish Biology,** v. 54, n. 5, p. 1094-1110, 1999. ISSN 0022-1112.

FRITZSCHE, R. A.; JOHNSON, G. D. Early osteological development of white perch and striped bass with emphasis on identification of their larvae. **Transactions of the American Fisheries Society,** v. 109, n. 4, p. 387-406, 1980. ISSN 0002-8487.

GEERINCKX, T.; BRUNAIN, M.; ADRIAENS, D. Development of the chondrocranium in the suckermouth armored catfish Ancistrus cf. triradiatus (Loricariidae, Siluriformes). **Journal of Morphology,** v. 266, n. 3, p. 331-355, 2005. ISSN 0362-2525.

GEERINCKX, T.; BRUNAIN, M.; ADRIAENS, D. Development of the osteocranium in the suckermouth armored catfish Ancistrus cf. triradiatus (Loricariidae, Siluriformes). **Journal of Morphology,** v. 268, n. 3, p. 254-274, 2007. ISSN 0362-2525.

JARDIM, L. F. A.; SANTOS, F. K. Development of the neurocranium in Micropogonias furnieri (Perciformes: Sciaenidae). **Japanese Journal of Ichthyology,** v. 41, n. 2, p. 131-139, 1994. ISSN 0021-5090.

JOHNSON, D. G. Percomorph phylogeny: progress and problems. **Bulletin of marine Science,** v. 52, n. 1, p. 3-28, 1993. ISSN 0007-4977.

JOHNSON, G. D. et al. Deep-sea mystery solved: astonishing larval transformations and extreme sexual dimorphism unite three fish families. **Biology Letters,** v. 5, n. 2, p. 235-239, 2009. ISSN 1744-9561.

JOHNSON, D. G.; PATTERSON, C. Percomorph phylogeny: a survey of acanthomorphs and a new proposal. **Bulletin of Marine Science,** v. 52, n. 1, p. 554-626, 1993. ISSN 0007-4977.

JOHNSON, G. D.; SCHNELL, N. K. Development of the rostrum and upper jaws in Squirrelfishes and Soldierfishes (Beryciformes: Holocentridae): a unique ontogenetic trajectory. **Copeia,** v. 103, n. 4, p. 902-919, 2015. ISSN 0045-8511.

KANG, S.; IMAMURA, H.; KAWAI, T. Morphological evidence supporting the monophyly of the family Polynemidae (Teleostei: Perciformes) and its sister relationship with Sciaenidae. **Ichthyological Research,** v. 65, n. 1, p. 29-41, 2017. ISSN 1341-8998.

KOWTAL, G. V. Observations on the breeding and larval development of Chilka 'Sahal' Eleutheronema tetradactylum (Shaw). **Indian Journal of Fisheries,** v. 19, p. 70-75, 1972.

KUBICEK, K. M.; CONWAY, K. W. Developmental osteology of Sciaenops ocellatus and Cynoscion nebulosus (Teleostei: Sciaenidae), economically important sciaenids from the western Atlantic. **Acta Zoologica,** v. 97, n. 3, p. 267-301, 2016. ISSN 0001-7272.

LEIS, J.; TRNSKI, T. Polynemidae (Threadfin). In: LEIS, J. M. e CARSON-EWART, B. M. (Ed.). **The larvae of Indo-Pacific coastal fishes. An identification guide to marine fish larvae.** Brill, Leiden, v.2, 2000. p.435-440.

LEIS, J. M. Ontogeny of behaviour in larvae of marine demersal fishes. **Ichthyological Research,** v. 57, n. 4, p. 325-342, 2010. ISSN 1341-8998.

LEIS, J. M.; CARSON-EWART, B. M. **The larvae of Indo-Pacific coastal fishes: an identification guide to marine fish larvae**. Brill, 2000. 857 ISBN 9004115773.

LEIS, J. M. et al. Ontogeny of swimming speed in larvae of pelagic-spawning, tropical, marine fishes. **Marine Ecology Progress Series,** v. 349, p. 255-267, 2007. ISSN 0171-8630.

MATTOX, G. M.; BRITZ, R.; TOLEDO-PIZA, M. Skeletal development and ossification sequence of the characiform Salminus brasiliensis (Ostariophysi: Characidae). **Ichthyological Exploration of Freshwaters,** v. 25, n. 2, p. 103, 2014. ISSN 0936-9902.

MOSER, H. **The early stages of fishes in the California current region**. La Jolla, California: California Cooperative Oceanic Fisheries Investigations, 1996. 1505.

MOSER, H. G. et al. **Ontogeny and systematics of fishes**. Lawrence, Kansas: American Society of Ichthyologists and Herpetologists, 1984. 760.

MOTOMURA, H. **Threadfins of the world (Family Polynemidae): An annotated and illustrated catalogue of polynemid species known to date**. Food & Agriculture Org., 2004. ISBN 9251051283.

OKIYAMA, M. A larval Ipnops and its possible metamorphosing process. **Japanese Journal of Ichthyology,** v. 28, n. 3, p. 247-253, 1981. ISSN 0021-5090.

RICHARDS, W. J. **Early stages of Atlantic fishes: an identification guide for the western central north Atlantic, Two Volume Set**. CRC Press, 2005. 1696 ISBN 0203500210.

SANDKNOP, E.; WATSON, W. POLYNEMIDAE: Threadfins. In: MOSER, H. (Ed.). **The early stages of fishes in the California current region**. La Jolla, California: California Cooperative Oceanic Fisheries Investigations, v.Atlas no. 33, 1996. p.1082 - 1087.

SANTERRE, M. T.; MAY, R. C. Some effects of temperature and salinity on laboratory-reared eggs and larvae of Polydactylus sexfilis (Pisces: Polynemidae). **Aquaculture,** v. 10, n. 4, p. 341-351, 1977. ISSN 0044-8486.

SASAKI, K. Phylogeny of the family Sciaenidae, with notes on its zoogeography (Teleostei, Perciformes). **Memoirs of the Faculty of Fisheries Hokkaido University,** v. 36, n. 1-2, p. 1-137, 1989. ISSN 0018-3466.

SCHNELL, N. K.; KONSTANTINIDIS, P.; JOHNSON, G. D. High-proof Ethanol Fixation of Larval and Juvenile Fishes for Clearing and Double Staining. **Copeia,** v. 104, n. 3, p. 617-622, 2016. ISSN 0045-8511.

TAYLOR, W. R.; VAN DYKE, G. Revised procedures for staining and clearing small fishes and other vertebrates for bone and cartilage study. **Cybium,** v. 9, n. 2, p. 107-119, 1985. ISSN 0399-0974.

WARTH, P. et al. Development of the skull and pectoral girdle in S iberian sturgeon, Acipenser baerii, and R ussian sturgeon, Acipenser gueldenstaedtii (A cipenseriformes: A cipenseridae). **Journal of morphology,** v. 278, n. 3, p. 418-442, 2017. ISSN 0362-2525.

FIGURES

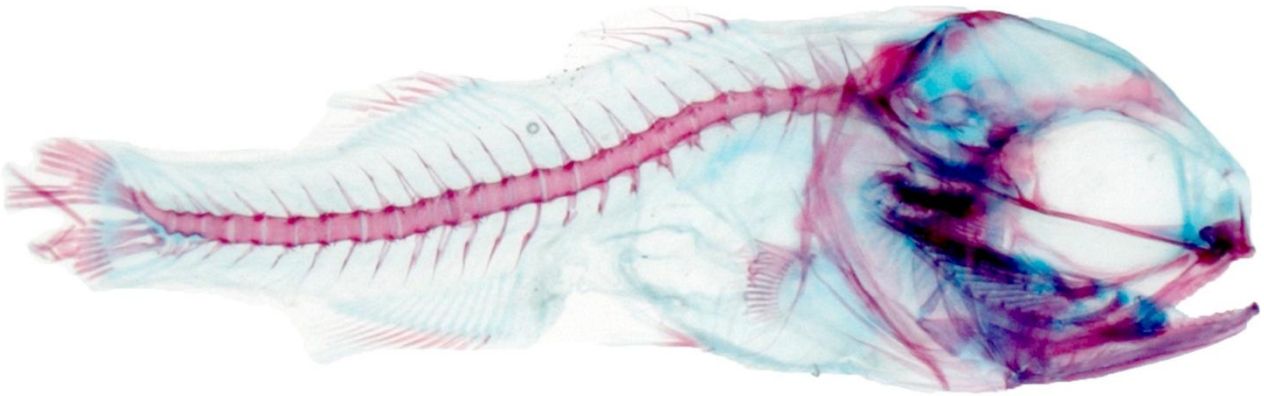

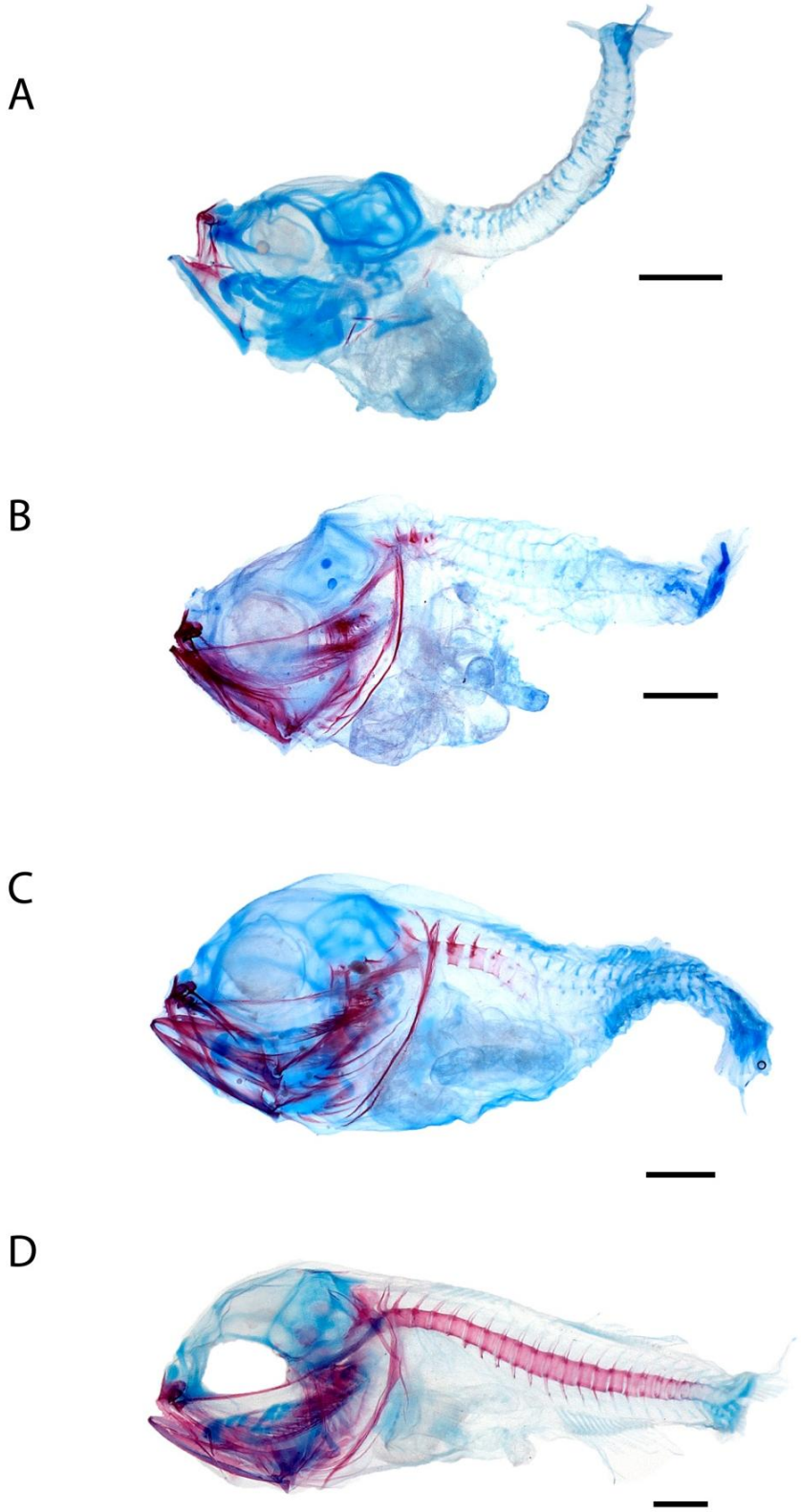

Fig. 1: Ontogeny. Whole body. *Polydactylus octonemus*; A: 3.3 mm. B: 4.0 mm. C: 4.5 mm. D: 5.7 mm. E: 7.94 mm. *Polydactylus approximans*; F: 13.3 mm. G: 17.5 mm. H: 21.3 mm. Scale bars: 0.5 mm (A-D); 1 mm (E-H).

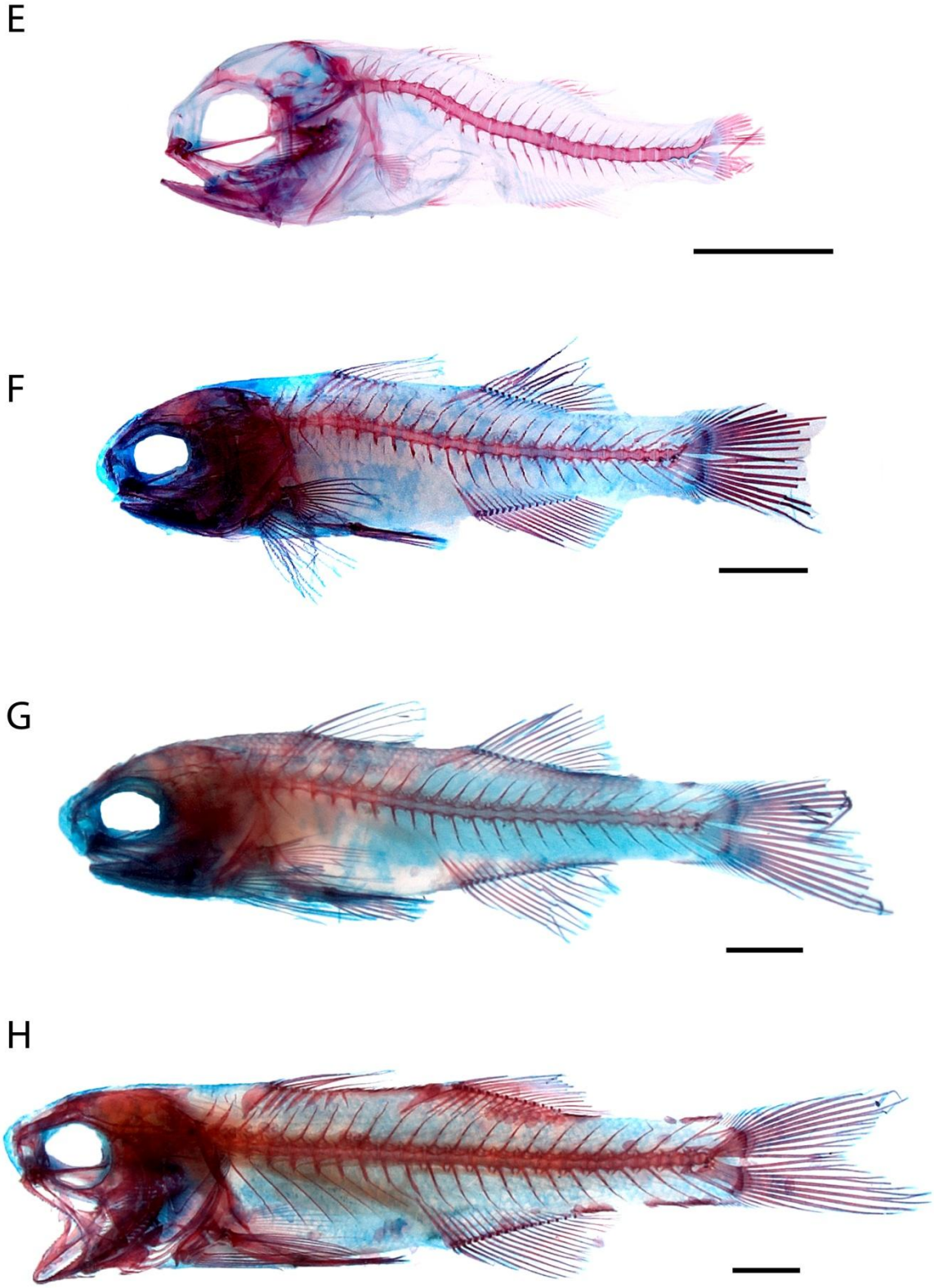

Fig. 1: Continued.

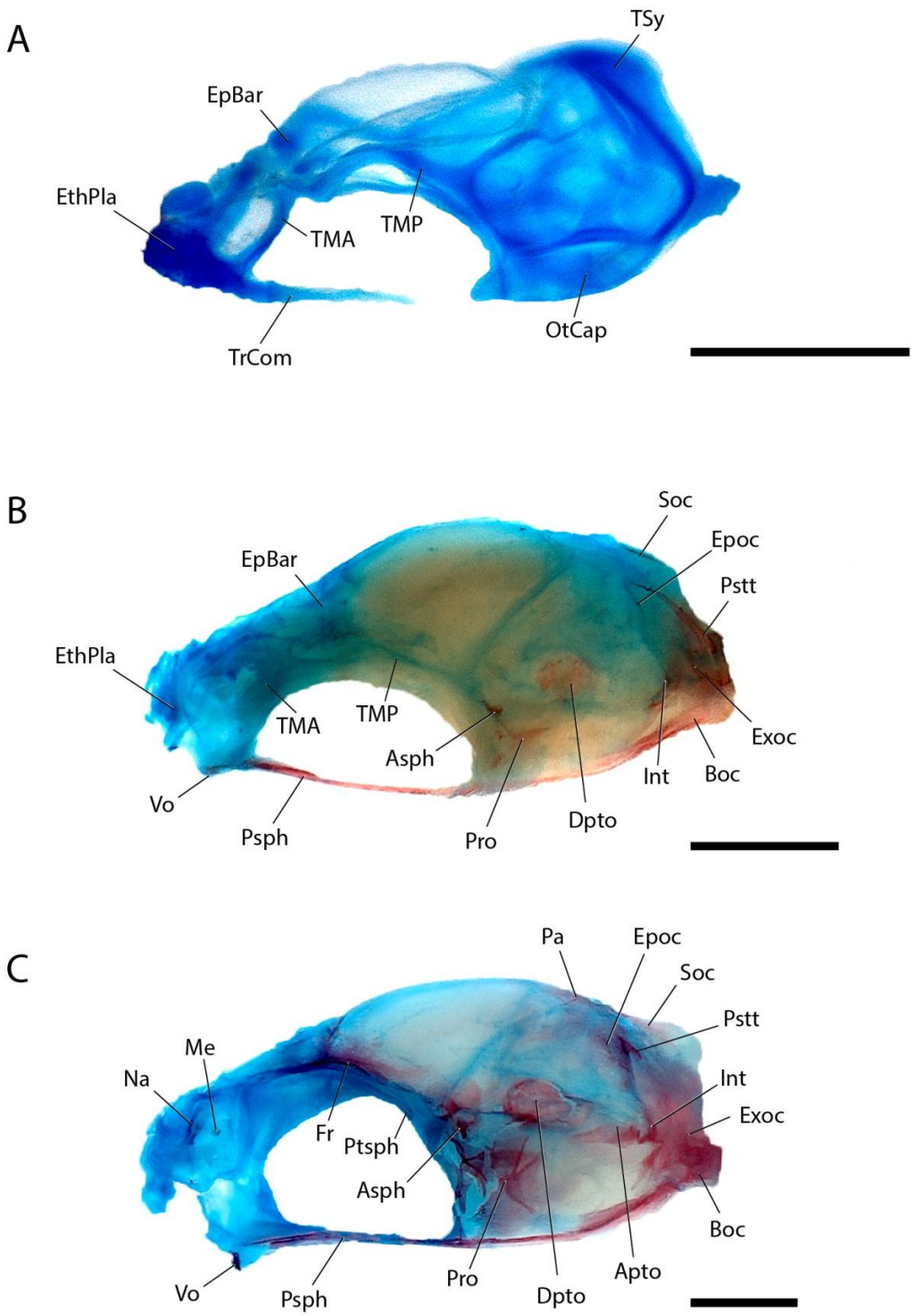

Fig. 2: Ontogeny. Neurocranium, lateral view. *Polydactylus octonemus*; A: 3.3 mm. *Polydactylus approximans*; B: 4.7 mm. C: 8.0 mm. D: 8.9 mm. E: 13.3 mm; F: 17.5 mm. Apto, autopterotic; Asph, autosphenotic; Boc, basioccipital; Bsph, basisphenoid; EpBar, epiphyseal bar; Epoc, epioccipital; EthPl, ethmoidal plate; Exoc, exoccipital; Fr, frontal; Int, intercalar; LEth, lateral ethmoid; Me, mesethmoid; Na, nasal; OtCap, otic capsule; Pa, parietal; Pro, prootic; Psph, parasphenoid; Pstt, posttemporal; Ptsph, pterosphenoid; Soc, supraoccipital; TMA, taenia marginalis anterior; TMP, taenia marginalis posterior; TrCom, trabeculae communis; TSy, tectum synoticum; Vo, vomer. Scale bars: 0.5 mm (A-C); 1 mm (D-F).

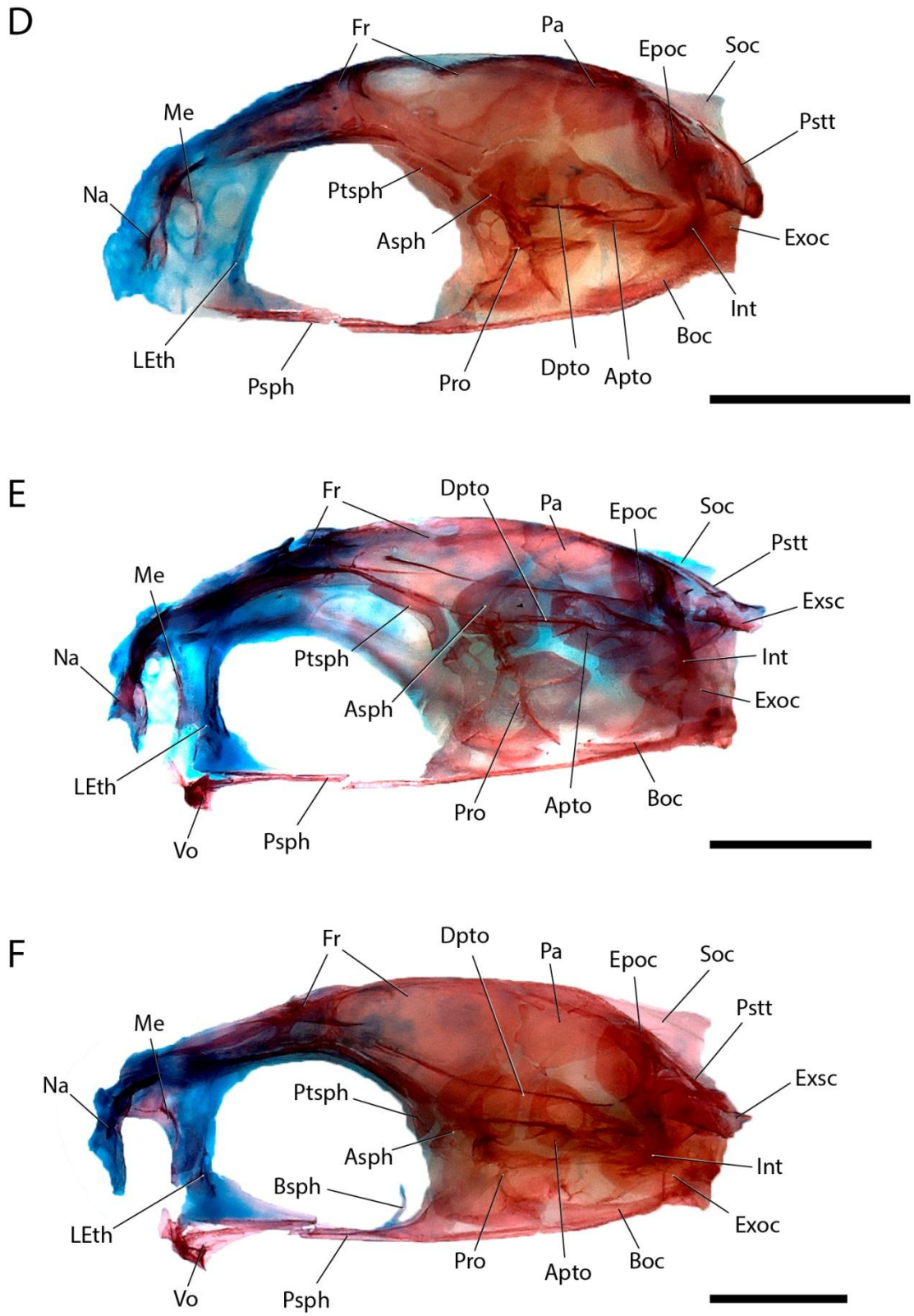

Fig. 2: Continued.

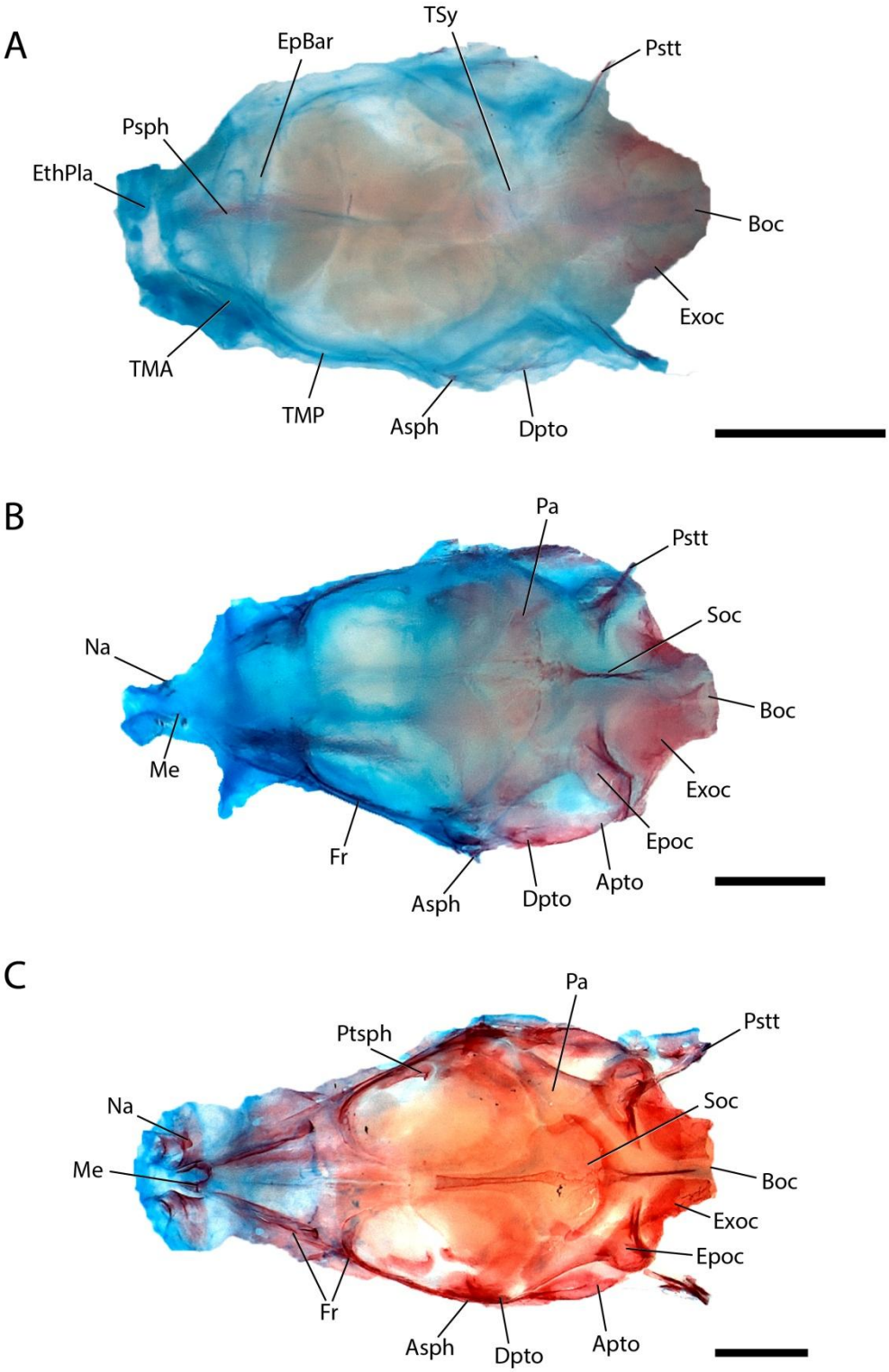

Fig. 3: Ontogeny. Neurocranium, dorsal view. *Polydactylus approximans*; A: 4.0 mm. B: 8.0 mm. C: 8.9 mm. D: 13.3 mm. E: 17.5 mm; F: 21.3 mm. Apto, autopterotic; Asph, autosphenotic; Boc, basioccipital; EpBar, epiphyseal bar; Epoc, epioccipital; EthPl, ethmoidal plate; Exoc, exoccipital; Fr, frontal; LEth, lateral ethmoid; Me, mesethmoid; Na, nasal; Pa, parietal; Psph, parasphenoid; Pstt, posttemporal; Ptsph, pterosphenoid; Soc, supraoccipital; TMA, taenia marginalis anterior; TMP, taenia marginalis posterior; TSy, tectum synoticum. Scale bars: 0.5 mm (A-C); 1 mm (D-F).

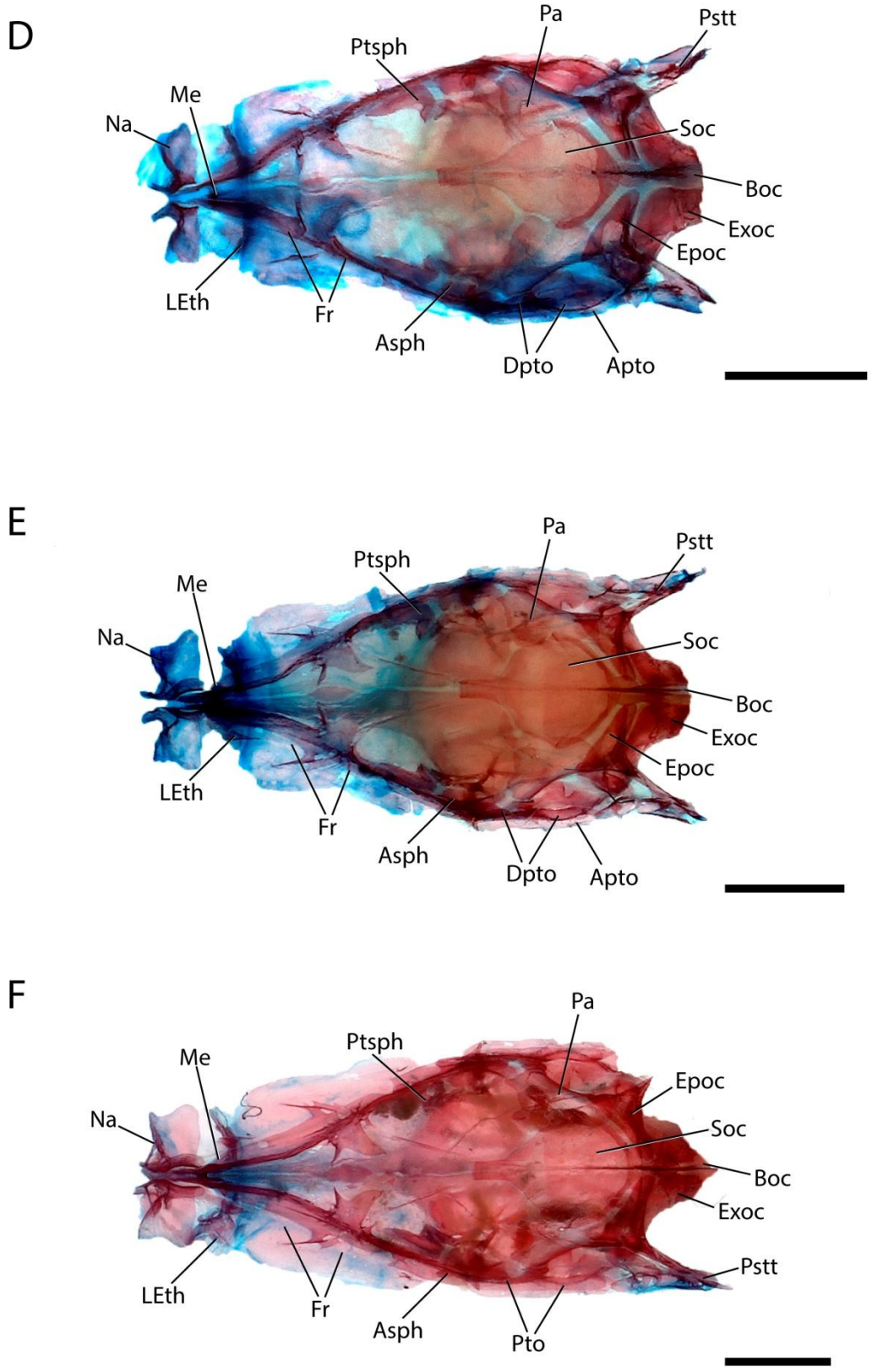

Fig. 3: Continued.

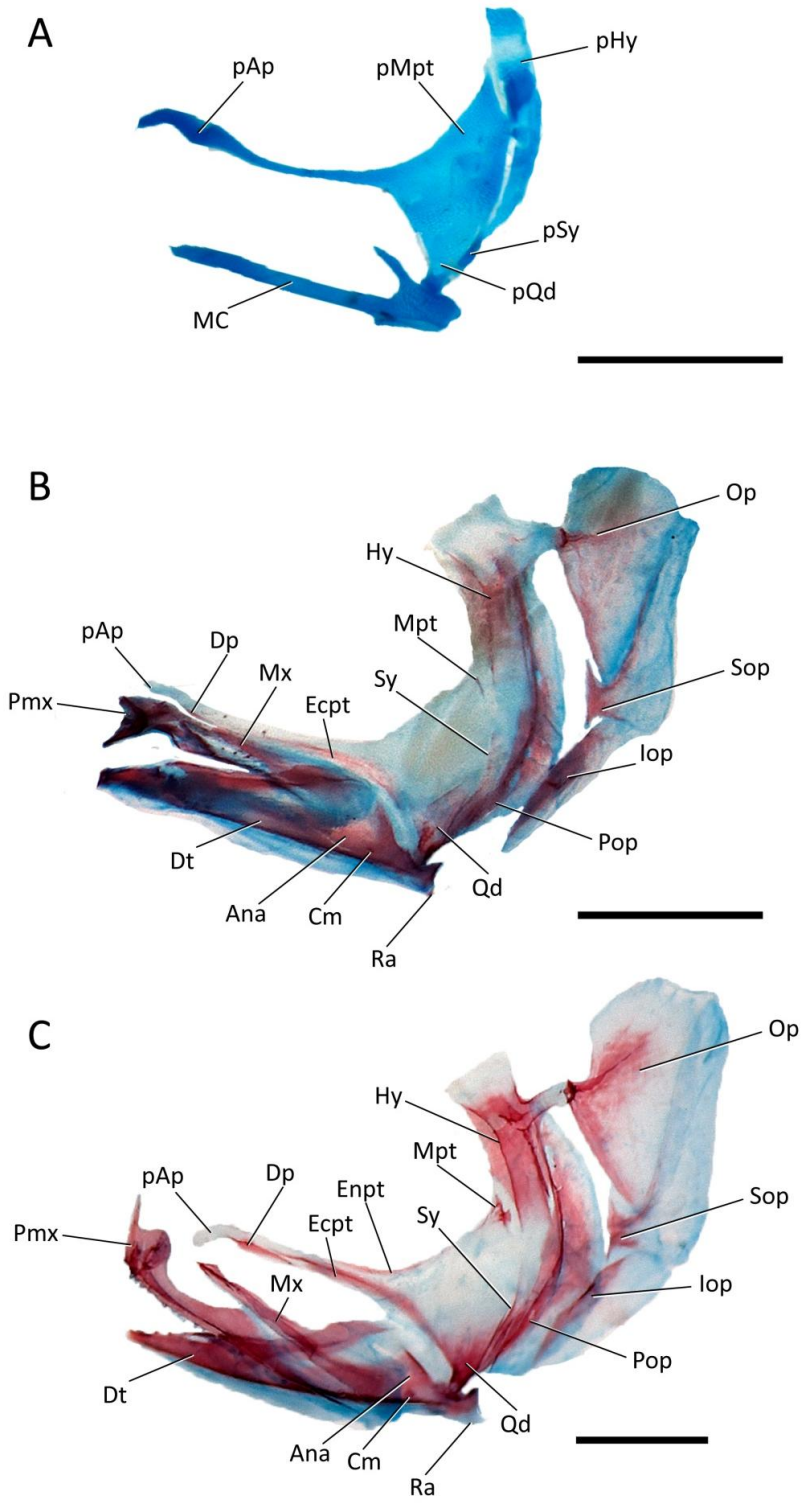

Fig. 4: Ontogeny. Jaws, hyopalatine arch, and opercular series. *Polydactylus octonemus*; A: 3 mm. *Polydactylus* sp.; C: 6.3 mm. *Polydactylus approximans*; B: 4.0 mm. D: 8.9 mm. E: 13.3 mm. F: 17.5 mm. Ana, angulo-articular; Cm, coronomeckelian; Dp, dermopalatine; Dt, dentary; Ecpt, ectopterygoid; Enpt, endopterygoid; Hy, hyomandibular; Iop, interopercle; MC, Meckel's cartilage; Mpt, metapterygoid; Mx, maxilla; Op, opercle; Pal, palatine; pAP, pars autopalatine; pHy, pars hyomandibularis; pMpt, pars metapterygoidea; Pmx, premaxilla; Pop, preopercle; pQd, pars quadrata; pSy, pars symplectica; Qd, quadrate; Ra, retroarticular; Sop, subopercle; Sy, symplectic. Scale bars: 0.5 mm (A-C); 1 mm (D-F).

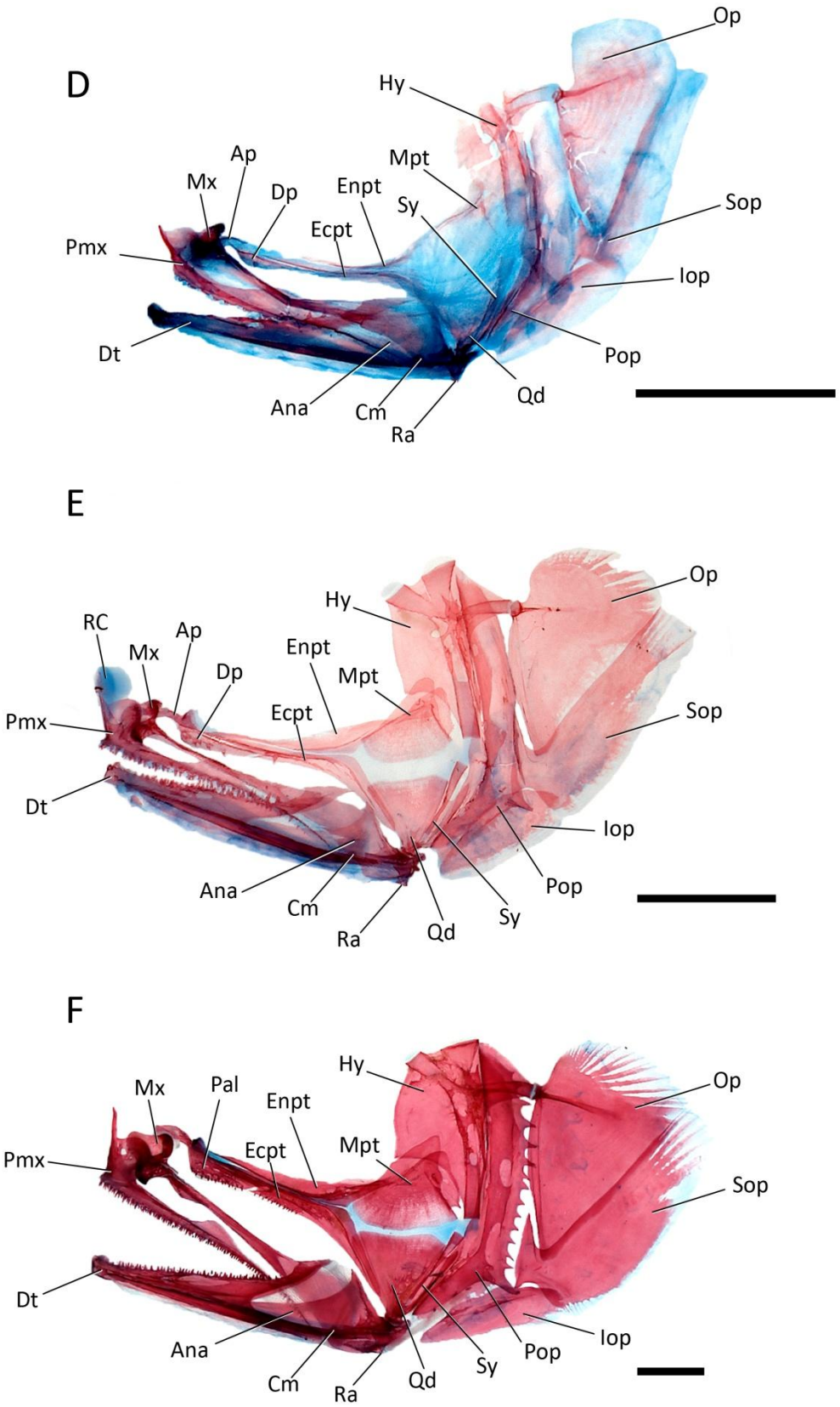

Fig. 4: Continued.

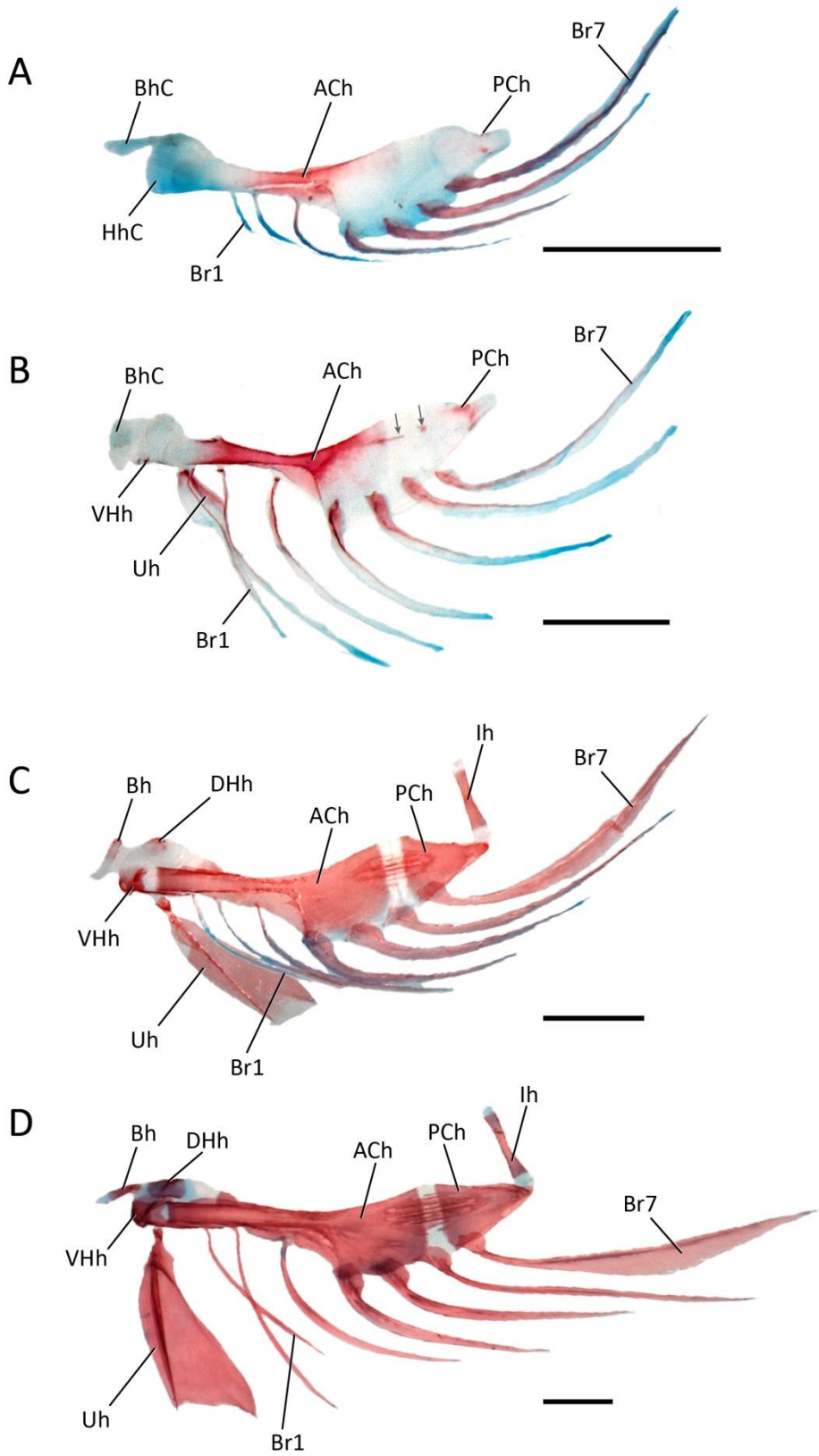

Fig. 5: Ontogeny. Hyoid arch. *Polydactylus* sp.; B: 6.3 mm. *Polydactylus approximans*; A: 4.0 mm. C: 8.9 mm. D: 17.9 mm. ACh, anterior ceratohyal; Bh, basihyal; BhC, basihyal cartilage; Br, branchiostegal ray; DHh, dorsal hypohyal; HhC, hypohyal cartilage; Ih, interhyal; PCh, posterior ceratohyal; Uh, urohyal; VHh, ventral hypohyal. Scale bars: 0.5 mm. Arrows indicate the beginning of interdigitation between ceratohyals.

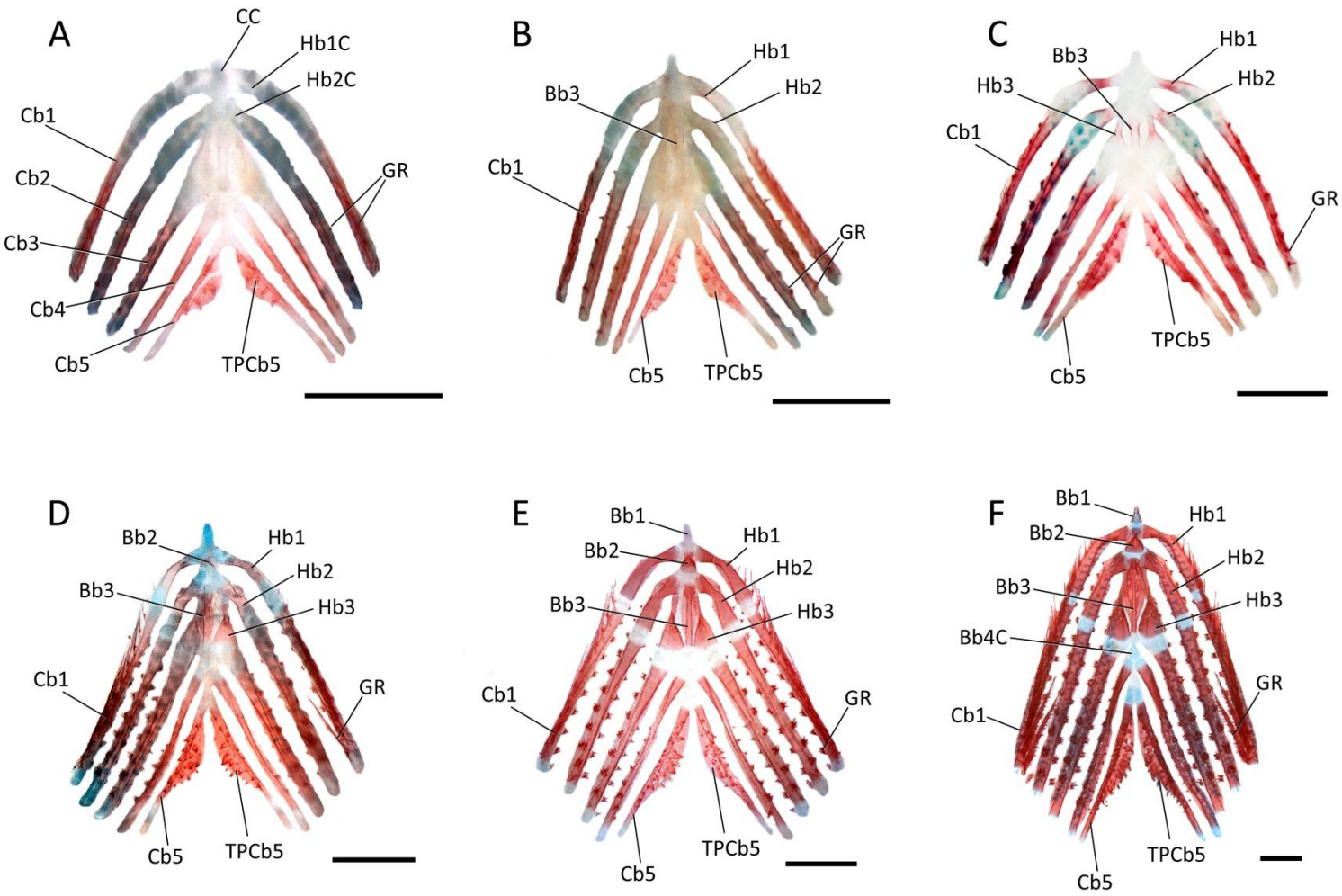

Fig. 6: Ontogeny. Gill arches, lower portion. *Polydactylus* sp.; C: 6.3 mm. *Polydactylus approximans*; A: 4.0 mm. B: 4.7 mm. D: 8.0 mm. E: 8.9 mm. F: 21.3 mm. Bb, basibranchial; BbC, basibranchial cartilage; Cb, ceratobranchial; CC, copula communis; GR, gill rakers; Hb, hypobranchial; TPCb, toothplate of ceratobranchial. Scale bars: 0.5 mm.

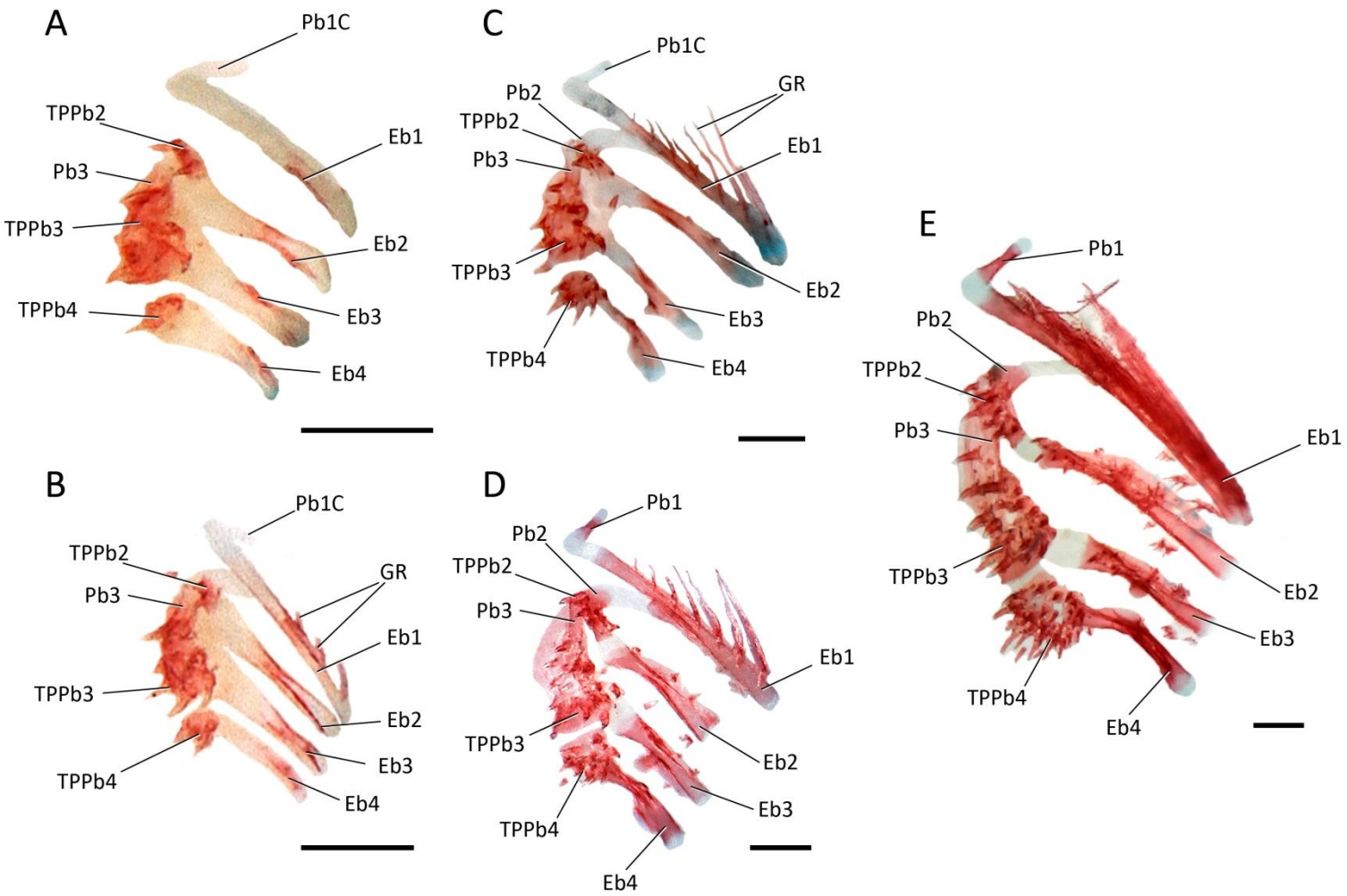

Fig. 7: Ontogeny. Gill arches, upper portion. *Polydactylus approximans*; A: 4.0 mm. B: 4.7 mm. C: 8.0 mm. E: 8.9 mm. F: 17.9 mm. Eb, epibranchial; GR, gill rakers; Pb, pharyngobranchial; PbC, pharyngobranchial cartilage; TPPb, toothplate of pharyngobranchial. Scale bars: 0.2 mm.

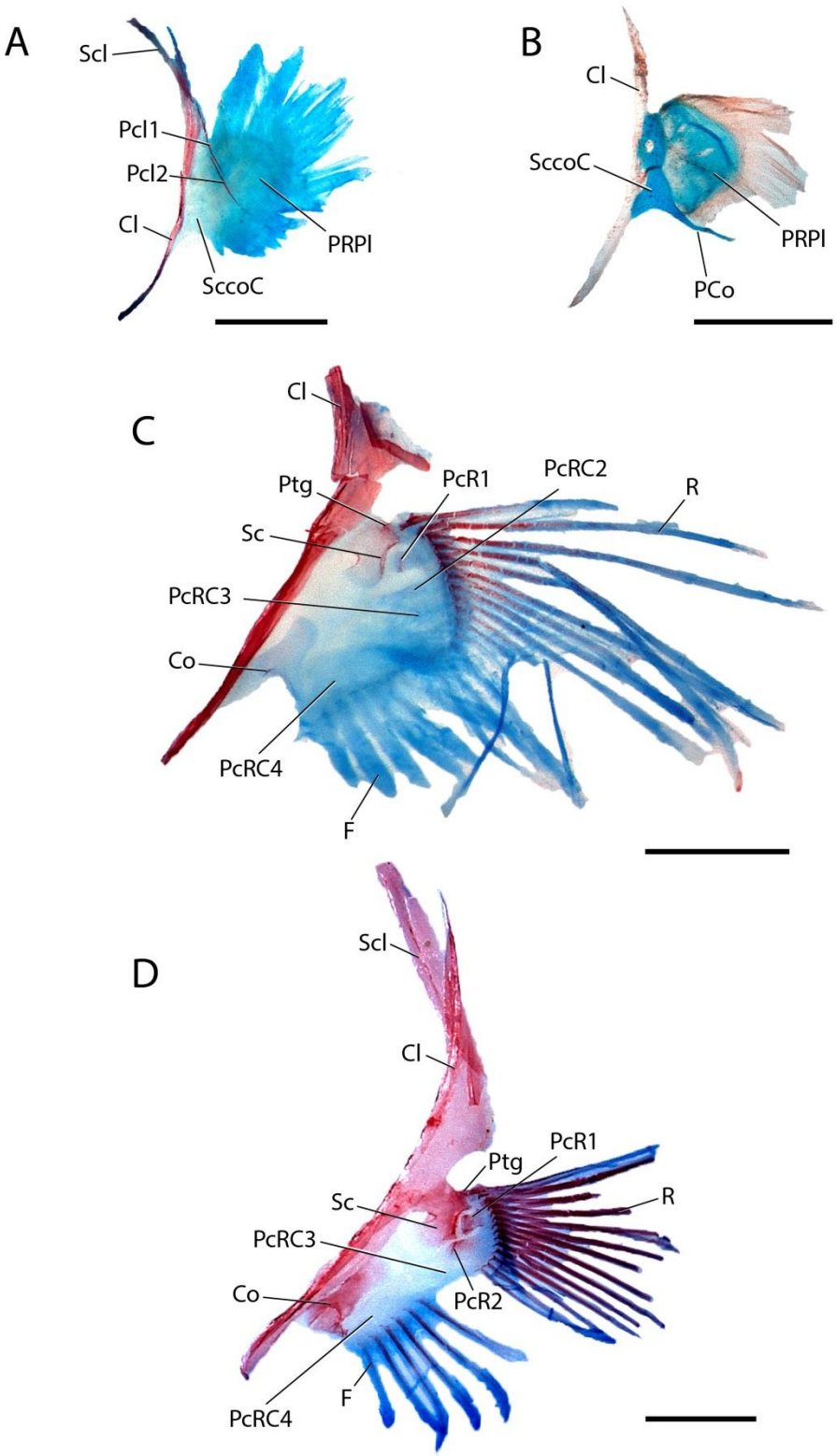

Fig. 8: Ontogeny. Pectoral girdle. *Polydactylus approximans*; A: 4.0 mm. B: 4.6 mm. C: 8.0 mm. D: 8.9 mm. E: 13.3 mm. F: 21.3 mm. Cl, cleithrum; Co, coracoid; F, pectoral filament; Pcl, postcleithrum; PCo, processus coracoideus; PcR, pectoral radial; PcRC, pectoral radial cartilage; PRPl, pectoral radial plate; Ptg, propterygium; R, pectoral-fin rays; Ra, retroarticular; Sc, scapula; SccoC, scapulocoracoid cartilage; Scl, supracleithrum. Scale bars: 0.5 mm (A-D); 1 mm (E-F).

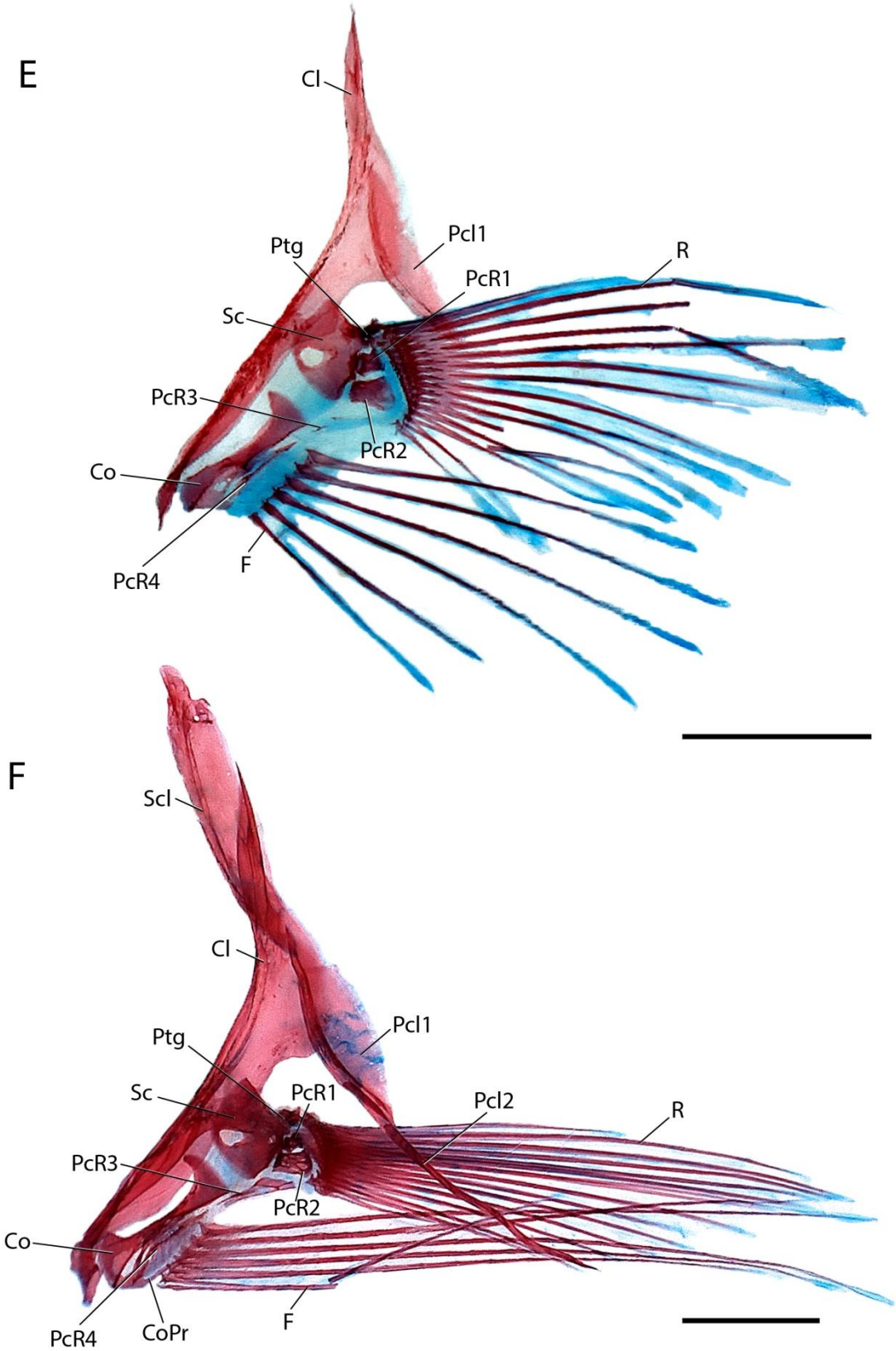

Fig. 8: Continued.

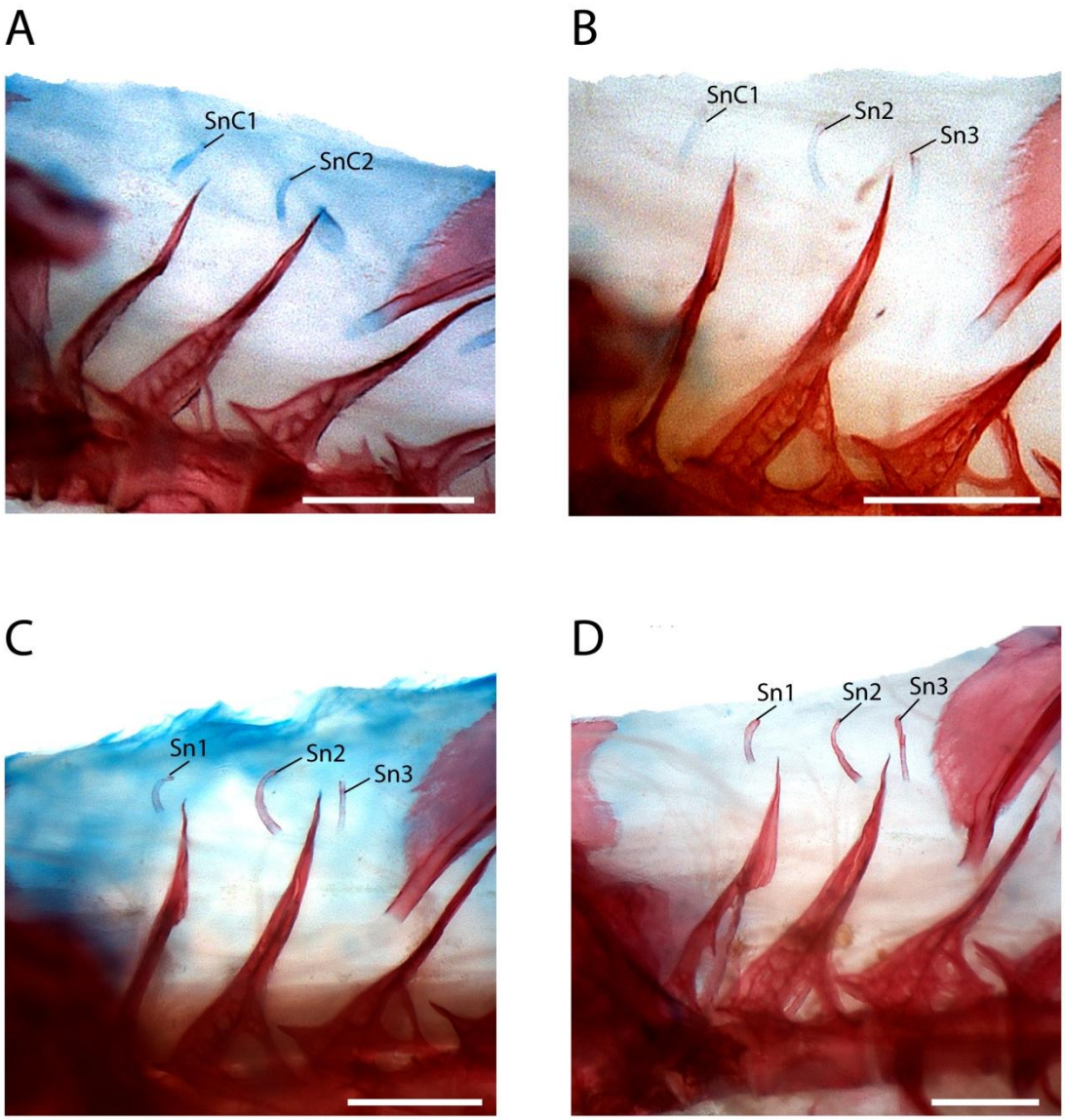

Fig. 9: Ontogeny. Supraneurals. *Polydactylus approximans*; A: 13.3 mm. B: 17.5 mm. C: 17.9 mm. D: 21.3 mm. Sn, supraneural. Scale bars: 0.5 mm.

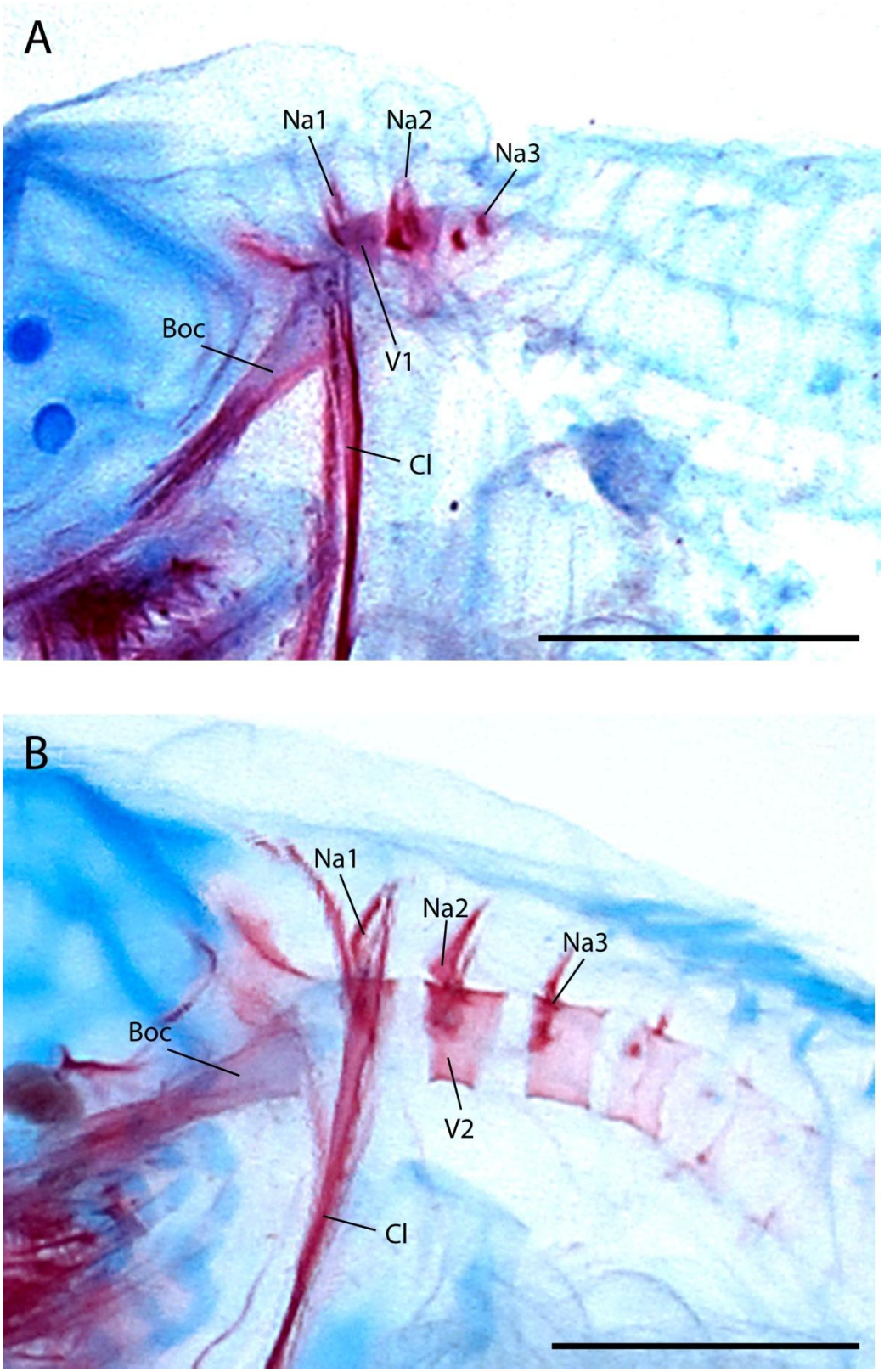

Fig. 10: Ontogeny. First vertebrae. *Polydactylus approximans*; A: 4.0 mm. B: 4.5 mm. Boc, basioccipital; Cl, cleithrum; Na, neural arch; V, vertebral centrum. Scale bars: 0.5 mm.

APPENDIX A

Tab. 1: Diagram of sequence of ossification of *Polydactylus* organized by anatomical complexes. First appearance of ossifications shown as thick horizontal line.

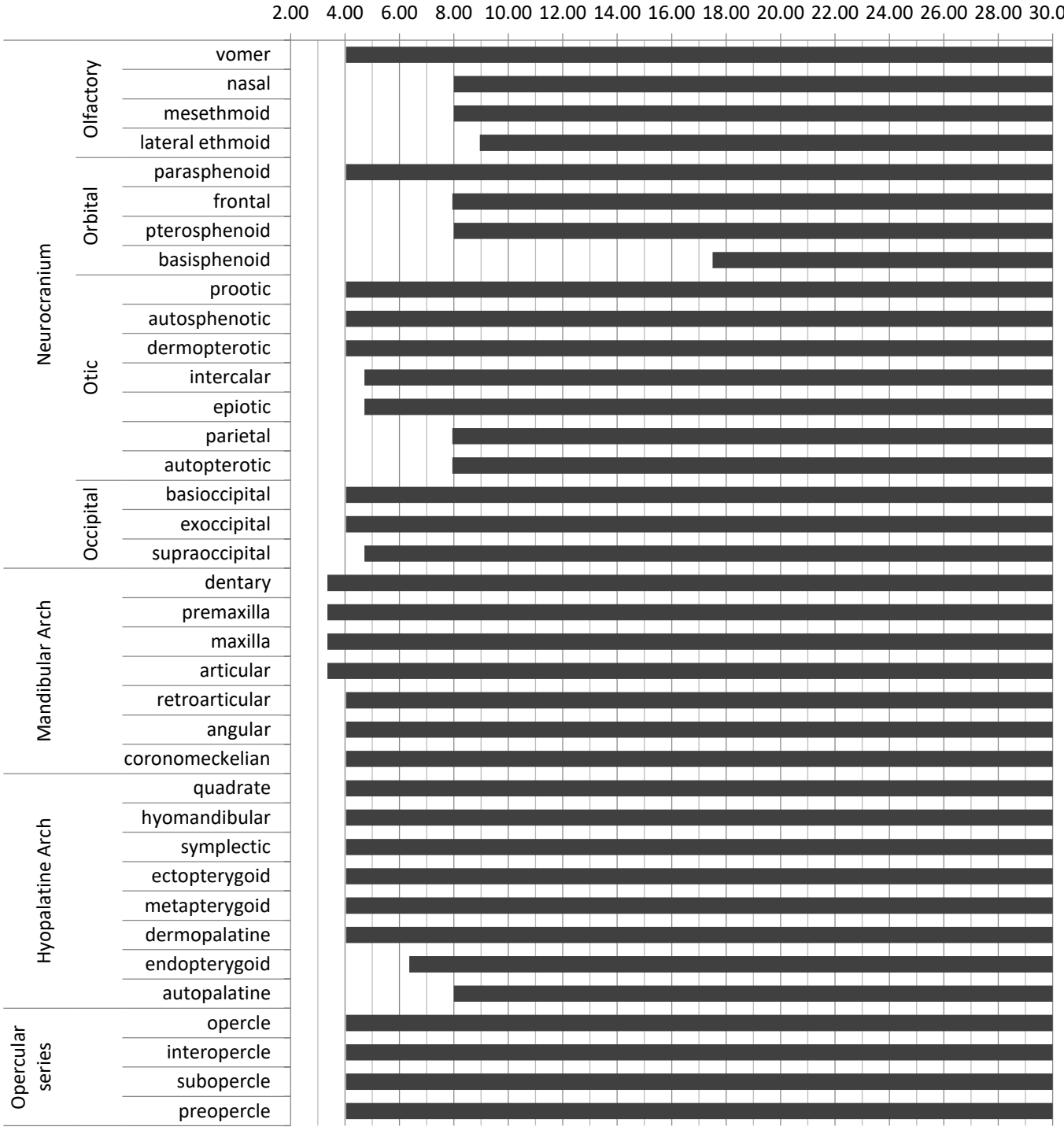

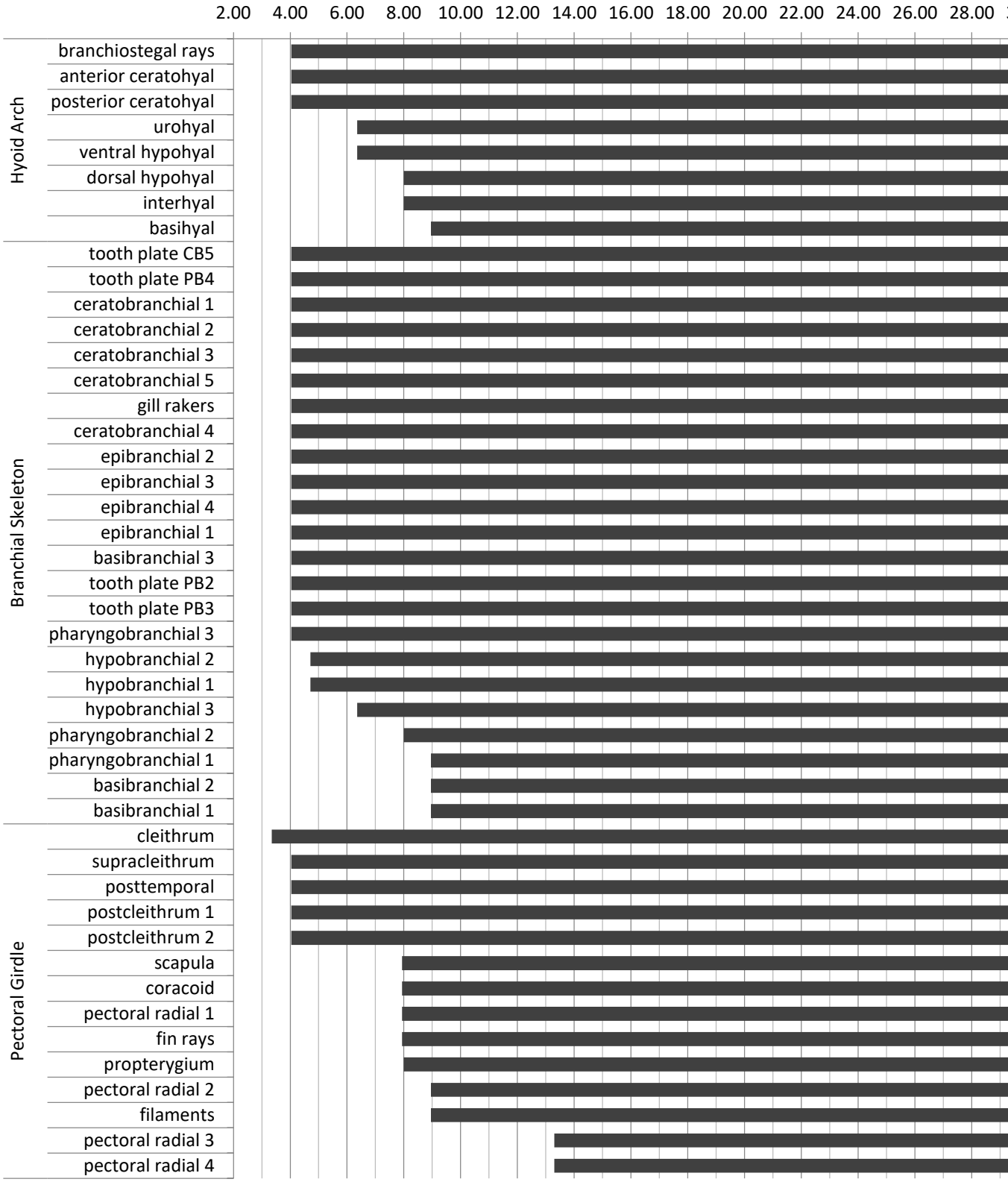
2.00
4.00
6.00
8.00
10.00
12.00
14.00
16.00
18.00
20.00
22.00
24.00
26.00
28.00
Hyoid Arch
branchiostegal rays
anterior ceratohyal
posterior ceratohyal
urohyal
ventral hypohyal
dorsal hypohyal
interhyal
basihyal
Branchial Skeleton
tooth plate CB5
tooth plate PB4
ceratobranchial 1
ceratobranchial 2
ceratobranchial 3
ceratobranchial 5
gill rakers
ceratobranchial 4
epibranchial 2
epibranchial 3
epibranchial 4
epibranchial 1
basibranchial 3
tooth plate PB2
tooth plate PB3
pharyngobranchial 3
hypobranchial 2
hypobranchial 1
hypobranchial 3
pharyngobranchial 2
pharyngobranchial 1
basibranchial 2
basibranchial 1
Pectoral Girdle
cleithrum
supracleithrum
posttemporal
postcleithrum 1
postcleithrum 2
scapula
coracoid
pectoral radial 1
fin rays
propterygium
pectoral radial 2
filaments
pectoral radial 3
pectoral radial 4